



---

# **Life-Cycle Management of Mission-Critical Systems through Certification, Commissioning, In-Service Maintenance, Remote Testing, and Risk Assessment**

*Final Project Report*

T-57HI

**Power Systems Engineering Research Center**  
*Empowering Minds to Engineer  
the Future Electric Energy System*



# **Life-Cycle Management of Mission-Critical Systems through Certification, Commissioning, In-Service Maintenance, Remote Testing, and Risk Assessment**

## **Final Project Report**

### **Project Team**

Mladen Kezunovic, Project Leader  
Tom Overbye  
Pratyasa Bhui, Jinfeng Ren  
Texas A&M University

Anurag K. Srivastava, David Bakken  
Param Banerjee, Pratim Kundu  
Washington State University

Sakis Meliopoulos, George Cokkinides  
Georgia Institute of Technology

### **Graduate Students**

Cheng Qian, Christoph Seidl, Ikponmwosa Idehen (Iyke)  
Texas A&M University

Ren Liu, Hyojong Lee, Zhijie Nie,  
Washington State University

Boqi Xie, Jiahao Xie, Yu Liu, Liangyi Sun  
Yuan Kong, Chiyang Zhong, Orestis Vasios  
Georgia Institute of Technology

### **Undergraduate Student**

Alex Askerman  
Washington State University

## **PSERC Publication 18-13**

September 2018

**For information about this project, contact:**

Mladen Kezunovic  
Texas A&M University  
Department of Electrical and Computer Engineering  
Wisnabaker Engineering Building 323C  
College Station, TX 77843  
Phone: 979-845-7509  
Email: kezunov@ece.tamu.edu

**Power Systems Engineering Research Center**

The Power Systems Engineering Research Center (PSERC) is a multi-university Center conducting research on challenges facing the electric power industry and educating the next generation of power engineers. More information about PSERC can be found at the Center's website: <http://www.pserc.org>.

**For additional information, contact:**

Power Systems Engineering Research Center  
Arizona State University  
527 Engineering Research Center  
Tempe, Arizona 85287-5706  
Phone: 480-965-1643  
Fax: 480-727-2052

**Notice Concerning Copyright Material**

PSERC members are given permission to copy without fee all or part of this publication for internal use if appropriate attribution is given to this document as the source material. This report is available for downloading from the PSERC website.

**© 2018 Texas A&M University. All rights reserved.**

## **Acknowledgements**

We wish to thank the following companies and their representatives for supporting the project over the years:

- Entergy (Floyd Galvan, Angela Nelson)
- Idaho Power Company (Dave Angel, Orlando Ciniglio, Milorad Papic, Erik Schellenberg)
- ISONE (Eugene Litvinov, Tongxin Zheng, Frankie (Qiang) Zhang, Xiaochuan Luo)
- MISO (Mark Westendorf, Kevin Frankeny)
- NYISO (Rana Mukerji, Michael Swider, Ed Cano, Muhammad Marwali)
- NYPA (Saman Babaei, George Stefopoulos, Bruce Fardanesh)
- PowerWorld (Mark Laufenberg)
- RTE (Patrick Panciatici, Thibault Prevost, Gabriel Bareux)

## Executive Summary

The overall research problem was to develop various tools and, methodologies to support life cycle management of mission-critical systems. The mission critical systems are represented with synchrophasor solutions, as well as the special protection schemes. The various evaluation stages included certification, commissioning, in-service maintenance, remote testing, and risk assessment. The tools have been developed for both laboratory and field-testing. The evaluation procedure assumed testing of individual components, as well as end-to-end system testing. With the developed tools, end-users will be able to maintain the system through the life-cycle from the initial selection of the system components and commissioning to the use throughout its life-time.

The project activities resulted in a PMU calibration lab developed at all participating universities, and other tools being developed as follows: a) Field test device and test protocols for device and system commissioning, acceptance, and in-service tests (M. Kezunovic, Texas A&M University), b) End-to-end remote testing of PMU and RAS (A. Srivastava and D. Bakken, WSU), c) PMU/MU Characterization and data validation via Substation Dynamic State Estimation, (Sakis Meliopoulos, GaTech), and d) Prototype algorithms and visualization for PMU data error identification and oscillation analysis (T. Overbye, Texas A&M University). The various tools have been tested mostly in the lab environment, and in some instances, actual utility data was used. The extension of this project in the future would be to use such tools and methodologies in specific utility applications.

### **Part I: Development of Field Test Devices and Test Protocols for Device and System Commissioning, Acceptance, and In-Service Tests**

In this part of the study we focused on development of the various testing and evaluation tools to meet the acceptance and commissioning of the synchrophasor systems. The research method was to gradually proceed with testing various components starting from PMUs, then adding the communication channel, and PDCs, and finally adding an application for a complete end-to-end test. This approach was designated as “nested testing” approach. To facilitate such evaluation, we engaged in three developments: PMU field calibrator, “Gold PMU”, and Fault Location assessment procedure. Besides that, we develop a PMU test and evaluation setup that may be used for future certification of PMU products.

The implication of our work is in the ability of end-users to utilize such devices and methodologies in evaluating performance of their synchrophasor system and its components. Such a capability was not readily available in the past resulting in inability of the end-user to verify performance of their synchrophasor system, particularly in the case when system components are showing some malfunction or even failure. The PMU certification lab may be used to evaluate future purchases and make sure they meet the IEEE standards. The Gold PMU may be used to verify that a commercial PMU meets its in-service performance requirements by comparing the outputs from an installed PMU and Gold PMU installed in parallel. To create test inputs for in-service evaluation of synchrophasor systems, the field calibrator has automated waveform replay features allowing the test plan to be executed automatically. The Fault Location application is used to illustrate how all the mentioned tools may be used to perform an in-service evaluation of performance of an application.

The next step in this research would be to utilize the mentioned tools extensively for utility uses and develop user manuals for the utilization.

## **Part II: End-to-End Remote Testing of PMU and RAS**

In addition to testing phasor measurement units before deployment following IEEE Test Suite Specification (TSS), it is important to test and validate PMU and associated real time critical applications in field. The proposed “PMU Performance Analyzer (PPA)” is capable of testing the PMU’s in field by integrating it with middleware called Erkios. The PPA is a software application that makes PMU testing effortless and highly accurate. It is capable of analyzing the performance of a PMU (under test) during steady state and dynamic conditions as specified in the IEEE Standard and guidelines. The PPA may also include some tests that are not in the standard based on utility specific requirements.

Erkios is developed with an objective to provide a solution for remote PMU testing and in-field testing of RAS. Erkios is a middleware framework and utilizes a number of fault-tolerance techniques to provide in-field testing of PMU and Remedial Action Scheme (RAS).

The first step in building such a tool is to set up a testbed that emulates the real-world scenario so that the tool can be validated. Development and integration of real time testbed with Erkios to facilitate cyber-physical simulation of end-to-end in-field testing of PMU and RAS are presented here. The testbed involves a real time power system simulator that has the capability to integrate with power system sensors and controllers in a closed loop. Also, the testbed has the communication channels and data flow closer to real world scenario.

This project resulted in updated PPA and Erkios software for remote PMU and RAS testing as well as a cyber-physical testbed to test and validate the developed tools.

## **Part III: PMU/MU Characterization and Data Validation via Substation Dynamic State Estimation**

Present day PMU and Merging Unit (MU) technologies offer the capability for better, accurate and faster monitoring of the power system. The data generated from these systems are utilized by many applications. These technologies are complex, and many things can cause deterioration of the performance of these systems. However, data from relays, PMUs, MUs, FDRs, and in general any IED in the substation are treated as separate entities without any tools to test their cross correlation and in general to provide automated checking of the validity of the data. If for some reason gaps and errors are generated in the data, these gaps/errors remain and propagate to higher level devices. Furthermore, if any physical anomalies occur (such as a blown fuse, a damaged wire, etc.) they will affect the quality and validity of the data, yet there is no mechanism to determine the root cause of these anomalies.

This project integrated technologies developed under previous projects into an integrated physical-and-protection co-model and analysis software that performs the following: (a) validate all data coming out of all relays, PMUs, and in general IEDs via the distributed state estimator, (b) detect anomalies and identify the root cause of these anomalies (hidden failures such as blown fuses, cut wires, etc. or human errors such as incorrect entry of system parameters such as CT and VT ratios, incorrect instrument transformer connection (delta/wye), etc.), (c) in case of temporary loss of

data, it creates the missing data from the state estimator and inserts the estimated data into the stream, and (d) it provides the validated data and the substation state up stream for further utilization, such as construction of the system wide real time model at the control center. These objectives have been achieved by a two parts process: (a) construction of a laboratory for the purpose of fully characterizing the individual components of the system, i.e. PMUs, merging units, digital fault recorders, etc. and (b) by constructing a laboratory that comprises the protective relaying scheme of a small substation, the substation automation infrastructure and a simulator to drive the system for the purpose of managing the data, identifying bad data and correcting bad data before the data are send upstream.

A field demonstration of the developed methods was planned. Specifically, the plan is to demonstrate these methods on the MARCY substation. Due to construction delays at MARCY substation, it was not possible to complete the demonstration before the end of the project. We do plan to complete this part of the project after the official completion of the project. Specifically, the required hardware at the substation for this demonstration will be installed in fall 2018 during a planned outage for the substation. Shortly after we plan to install the software at MARCY and test them in the field.

The work of this project will have substantial impact on future research activities. The developed methods and software will be critical components for many applications in the substation and control center. For example, we presently are extending these methods to be part of the protection and control system in the substation by making sure that all relays receive validated data. This application will solve a perennial problem in protection. Specifically, occasionally hidden failures occur in the instrumentation and data acquisition systems resulting in sending erroneous data to the relays and causing relay mis-operations. The data validation methods of this project can identify the hidden failures and correct data this avoiding relay mis-operations.

Another direction is to use the methods develop in this project to form the basic infrastructure of the next generation management systems. Note that a basic problem at control center operations is the accurate knowledge of the system in real time. The developed methods and software provide the validated data and model of each substation at speeds not possible before, specifically once per cycle. The validated data and validated real time model of each substation can be sent to the control center where the validated real time model of the entire system can be constructed by assembling the validated substation models at the same instant of time. This task can be achieved once per cycle. Thus, the control center can have the validated real time model of the entire system once per cycle and with a delay as short as much requires to stream the data from each substation, typically milliseconds. All the applications can now run on a validated real time model. In addition, the speed and accuracy open up a number of new applications such as full state feedback control of many fast responding resources in the power system such as universal power flow controller and other FACTS devises.

#### **Part IV: Prototype Algorithms and Visualization for PMU Data Error Identification and Oscillation Analysis**

An increased scale of power system interconnectivity and size poses challenges for operator visibility of the grid. Fast-measurement and high-reporting devices, known as phasor measurement unit (PMU) devices and used for monitoring grid health at high resolution scales, expand the

capabilities for grid data processing and analysis, whose results are then used to increase the awareness level of the power system. A growing interest in the use of these unique devices in large-scale systems prompts the development of newer, robust analysis methods fit enough to capture both local and holistic dynamic features of the system. For example, the integrity testing of huge amounts of data obtained from geo-spatially, distributed grid sensors prior to data usage by critical grid applications, such as stability monitoring, grid disturbance and oscillation monitoring, to assess the state of the system. In this report, the goal is to study mechanisms of PMU device failures, and prototype algorithms and visualizations for data error identification and oscillation analysis. A 2,000-bus synthetic large-scale system is used for the different case studies in this report.

Sections 2 and 3 present PMU device failure mechanism and data error analysis in large scale power systems. respectively Firstly, we ed error propagation models that allows for the study of different mechanisms of time issues associated with PMU device operation, which in turn affect the integrity of reported data measurements. Secondly, we developed an approach to measurement error analysis in large scale grids considering the spatial and temporal variations that could exist among device measurements. In addition, the use of a hybrid, multidimensional scaling (MDS) method is proposed for use to visualize all pairwise measurement error correlations among all buses in a test system. A Matlab user interface tool is developed to aid generation of artificial PMU data errors. Designed using the Matlab GUIDE program, the developed user interface accepts user input for a selected PMU error type. Also, a prototype visualization dashboard display designed in a rapid application development (RAD) studio, and using Delphi programming language, is developed for the presentation of PMU error information in the large-scale system. It uses MDS correlation plots, tables, trend and bar charts to present its information. To migrate these developed tools to an application level would require additional data processing modules (as some of the processes are still being implemented manually) and extensive debugging.

Sections 4 and 5 focus on methods for presenting information pertaining to system oscillation. This information is obtained from the processing of enormous amounts of PMU data measurements obtained from a large-scale power grid. The use of a one-line diagram of the 2,000-bus synthetic Texas system overlaid on a geographic map of Texas, small object representations (known as glyph objects) and a method in vector field visualization are used to visualize large-scale system oscillation information. A wide-area visualization method is intended to present large-scale system dynamics to an engineer in a condensed, easy-to-interpret, holistic view of the system. The proposed visualization method is currently implemented in the PowerWorld simulator software for field visualizations in geomagnetic disturbance (GMD) and oscillation monitoring studies.

In summary, the key contributions/takeaways from this project are:

- The formulation and use of model equations to explain some of the timing issues associated with PMU devices. In addition to other system dynamics, these model equations can be used to generate artificial data for research purposes.
- Assist engineers to better understand unique, PMU-reported data patterns attributable to timing issues in PMU device operation rather than supposedly actual events on the grid. This can help in the interpretation of data discrepancies, and further search for error source if patterns of time errors are observed in the data.

- Development of a hybrid, distributed analysis method to detect erroneous measurements from PMU data obtained from a large-scale power grid. The result of the proposed method shows a 100% accuracy, and greater improvement over a central error analysis method, in the detection of bad PMU data from measurements obtained from several measurement locations in a 2,000-bus, large-scale system.
- Implementation of data-layering techniques and vector field visualizations for the wide-area visualization of oscillation information obtained from the processing of large-scale system PMU data. Condensed and holistic views of system states will provide engineers with a better understanding of system dynamics.

### **Project Publications:**

- [1] C. Qian, M. Kezunovic. Dynamic Synchrophasor Estimation with Modified Hybrid Method. *2016 IEEE PES Conference on Innovative Smart Grid Technologies*, September 2016, Minneapolis, MN
- [2] C. Qian, M. Kezunovic, "Spectral Interpolation for Frequency Measurement at Off-Nominal Frequencies," *IEEE PES General Meeting, July 2017*, Chicago IL.
- [3] C. Qian, M. Kezunovic, "A Novel Time-Frequency Analysis for Power System Waveforms Based on "Pseudo-Wavelets," *IEEE PES T&D Conference and Exposition 2018*, Denver CO.
- [4] C. Qian, M. Kezunovic, "A Power Waveform Classification Method for Adaptive Synchrophasor Estimation," *IEEE Transactions on Instrumentation and Measurement*, vol. 67, no. 7, pp. 1646-1658, July 2018.
- [5] M. Zhou, Y. Wang, A. K. Srivastava, Y. Wu, P. Banerjee, "Ensemble based Algorithm for Synchrophasor Data. Anomaly Detection", *IEEE. Transactions on Smart Grid*, DOI 10.1109/TSG.2018.2816027,
- [6] P. Banerjee, S. Pandey and A. K. Srivastava "Testing and Validation of Synchrophasor Devices and Applications for Power Grid Operation", book chapter in "Power System Grid Operation Using Synchrophasor Technology", Springer, 2018
- [1] R. Liu, A. Srivastava, D. Bakken, A. Askerman, and P. Panciatici, "Decentralized State Estimation and Remedial Control Action for Minimum Wind Curtailment Using Distributed Computing Platform," *IEEE Transactions on Industry Applications*, 2017
- [2] H. Lee, P. Banerjee, and A. K. Srivastava, "Synchrophasor Applications for Load Estimation and Stability Analysis", *IET Power and Energy Series, Synchronized Phasor Measurements for Smart Grids*, 2017
- [3] H. Lee Tushar, P. Banerjee, and A. K. Srivastava, "Synchrophasor Applications for Load Estimation and Stability Analysis", *IET Power and Energy Series, Synchronized Phasor Measurements for Smart Grids*, 2017
- [4] A. Srivastava and P. Banerjee, "Wide Area Close Loop Control in Smart Electric Grid", *Power and Energy Automation Conference*, Spokane, WA, March, 2016
- [5] A. P.Meliopoulos, "Legacy SE to Distributed Dynamic State Estimators: Evolution and Experience," *Proceedings of the IEEE-PES 2015 General Meeting*, Denver, CO, July 26-30, 2015.
- [6] A. P.Meliopoulos, "Dynamic State Estimation-Based Diagnostic Systems: Evolution and Experience," *Proceedings of the IEEE-PES 2015 General Meeting*, Denver, CO, July 26-30, 2015.

- [7] H. Albinali and A. P. Meliopoulos, "Centralized Substation Protection Scheme to Detect Hidden Failures", Accepted, *Proceedings of the IEEE-PES 2016 General Meeting*, Boston, MA, July 17-21, 2016.
- [8] H. F. Albinali and A. P. S. Meliopoulos, "Resilient Protection System Through Centralized Substation Protection," in *IEEE Transactions on Power Delivery*, vol. 33, no. 3, pp. 1418-1427, June 2018.
- [9] A. P. Meliopoulos, "Legacy SE to Distributed Dynamic State Estimators: Evolution and Experience," *Proceedings of the IEEE-PES 2015 General Meeting*, Denver, CO, July 26-30, 2015.
- [10] A. P. Meliopoulos, "Dynamic State Estimation-Based Diagnostic Systems: Evolution and Experience," *Proceedings of the IEEE-PES 2015 General Meeting*, Denver, CO, July 26-30, 2015.
- [11] H. Albinali and A. P. Meliopoulos, "Centralized Substation Protection Scheme to Detect Hidden Failures", Accepted, *Proceedings of the IEEE-PES 2016 General Meeting*, Boston, MA, July 17-21, 2016.
- [12] R. Fan, A. P. S. Meliopoulos, G. J. Cokkinides, L. Sun and Yu Liu, "Dynamic state estimation-based protection of power transformers," *2015 IEEE Power & Energy Society General Meeting*, Denver, CO, 2015, pp. 1-5.
- [13] S. Meliopoulos, G. J. Cokkinides, P. Myrda, Y. Liu, R. Fan, L. Sun, R. Huang and Z. Tan, "Dynamic State Estimation Based Protection: Status and Promise", *IEEE Transactions on Power Delivery*, vol. 32, no. 1, pp 320-330, Feb. 2017.
- [14] Y. Liu; A. P. Meliopoulos; R. Fan; L. Sun; Z. Tan, "Dynamic State Estimation Based Protection on Series Compensated Transmission Lines," *IEEE Transactions on Power Delivery* 32.5 (2017): 2199-2209.
- [15] Y. Liu, S. Meliopoulos, L. Sun and R. Fan, "Dynamic State Estimation Based Protection on Mutually Coupled Transmission Lines", *CSEE Journal of Power and Energy Systems*, vol.2, no.4, pp 6- 14, Dec. 2016.
- [16] Y. Liu, S. Meliopoulos, Z. Tan, L. Sun and R. Fan, "Dynamic State Estimation Based Fault Locating in Transmission Lines", *IET Generation, Transmission & Distribution*, in press.
- [17] S. Meliopoulos, R. Huang, E. Polymeneas and G. Cokkinides, "Distributed dynamic state estimation: Fundamental building block for the smart grid," *2015 IEEE Power & Energy Society General Meeting*, Denver, CO, 2015, pp. 1-6.
- [18] R. Huang, G. Cokkinides, C. Hendrington, and A. P. Meliopoulos, "Distribution System Distributed Quasi-Dynamic State Estimator", *IEEE Transactions on Smart Grid*, Volume 7, No. 6, pp 2761-2770, November 2016
- [19] Xie, A. P. S. Meliopoulos, Y. Liu and L. Sun, "Distributed quasi-dynamic state estimation with both GPS-synchronized and non-synchronized data," *2017 North American Power Symposium (NAPS)*, Morgantown, WV, 2017, pp. 1-6.
- [20] L. Sun, A. P. S. Meliopoulos, Y. Liu and B. Xie, "Dynamic state estimation based synchronous generator model calibration using PMU data," *2017 IEEE Power & Energy Society General Meeting*, Chicago, IL, 2017, pp. 1-5.
- [21] Xie, A. P. S. Meliopoulos, C. Zhong, Y. Liu, L. Sun, and J. Xie "Distributed Quasi-Dynamic State Estimation Incorporating Distributed Energy Resources," *2018 North American Power Symposium (NAPS)*, Fargo, ND, 2018, pp. 1-6.
- [22] Idehen, T. Xu, and T. J. Overbye, "Subsequence dynamic time warping in the detection of PMU time errors," *IEEE Transactions on Smart Grid*, in preparation.

- [23] Idehen, B. Wang, K. Shetye and T.J. Overbye, "Visualization of large-scale electric grid oscillation modes," *2018 North American Power Symposium (NAPS)*, accepted.
- [24] Idehen and T. J. Overbye, "A similarity-based PMU error detection technique," in *2017 19th International Conference on Intelligent System Application to Power Systems (ISAP)*, 2017, pp. 1-6.
- [25] Idehen, Z. Mao, and T. J. Overbye, "An emulation environment for prototyping PMU data errors," in *2016 North American Power Symposium (NAPS)*, 2016, pp. 1-6.

#### **Student Theses:**

- [1] Cheng Qian. *Phasor Parameter Modeling and Time-Synchronized Calculation for Representation of Power System Dynamics*, PhD Dissertation, Texas A&M University.
- [2] Christoph Seidl. *A comparison of end-to-end testing techniques for Synchrophasor Systems*, Master's Thesis. Texas A&M University.
- [3] Ren Liu. *Cyber Physical Security Analysis for Synchrophasor Applications*, PhD Dissertation, Washington State University, December 2017.
- [4] Hyojong Lee. *Development, Modeling, and Applications of PMUs*, PhD Dissertation, Washington State University, December 2017.
- [5] Ikponmwosa Idehen. *Data Analytics and Wide-Area-Visualization Associated with Power Systems Using Phasor Measurement*. PhD Dissertation, Texas A&M University, July 2019 (expected).

## **Part I**

# **Development of Field Devices and Test Protocols for Device and System Commissioning, Acceptance, and In-Service Tests**

Mladen Kezunovic

Pratyasa Bhui

Jinfeng Ren

Cheng Qian, Graduate Student

Christoph Seidl, Graduate Student

Texas A&M University

**For information about this project, contact**

Mladen Kezunovic  
Texas A&M University  
Department of Electrical and Computer Engineering  
Wisnabaker Engineering Building 323C  
College Station, TX 77843  
Phone: 979-845-7509  
Email: kezunov@ece.tamu.edu

**Power Systems Engineering Research Center**

The Power Systems Engineering Research Center (PSERC) is a multi-university Center conducting research on challenges facing the electric power industry and educating the next generation of power engineers. More information about PSERC can be found at the Center's website: <http://www.pserc.org>.

**For additional information, contact:**

Power Systems Engineering Research Center  
Arizona State University  
527 Engineering Research Center  
Tempe, Arizona 85287-5706  
Phone: 480-965-1643  
Fax: 480-727-2052

**Notice Concerning Copyright Material**

PSERC members are given permission to copy without fee all or part of this publication for internal use if appropriate attribution is given to this document as the source material. This report is available for downloading from the PSERC website.

**© 2018 Texas A&M University. All rights reserved**

## Table of Contents

1. Introduction.....	1
1.1 Background.....	1
1.2 Summary of Chapters .....	1
2. PMU Calibration and Certification Lab.....	3
2.1 Introduction.....	3
2.2 Design Specification .....	3
2.2.1 Calibration System Functional Requirements .....	3
2.2.2 Calibration System Hardware Specifications.....	4
2.3 Implementation Features.....	6
2.3.1 Calibration System Overview .....	6
2.3.2 PMU Type Test and Application Test.....	7
2.4 Use in Testing .....	12
2.4.1 Acceptance Testing and Certification of PMUs Using Laboratory Environment .....	12
3. Gold PMU.....	14
3.1 Introduction.....	14
3.2 Design Specification .....	15
3.2.1 Functionality Requirement Specification .....	15
3.2.2 Definition of Gold PMU Algorithm.....	15
3.3 Implementation Features.....	16
3.3.1 Implementation of Hardware Functionality .....	16
3.3.2 Implementation of Software Functionality.....	17
3.3.3 Implementation of Gold PMU Algorithm.....	18
3.4 Use in Testing .....	18
4. Field End-to-End Calibrator .....	20
4.1 Introduction.....	20
4.2 Design Specification .....	20
4.2.1 Objectives.....	20
4.2.2 Functional Overview .....	21
4.2.3 Additional Settings and Instructions for Periodic Maintenance Test Set.....	21
4.2.4 Timing Reference .....	21

4.2.5	Signal Source(s)	22
4.2.5.1	Signal Sources for Steady-State Tests	22
4.2.5.2	Signal Sources for Dynamic Tests	23
4.2.6	PMU Measurement Receiver	23
4.3	User Interface Specification	23
4.3.1	Common setting for all offered tests that are provided to the user	24
4.3.1.1	Communication Settings	24
4.3.1.2	PMU Settings	24
4.3.1.3	Amplifier Settings (needs to be set according to data sheet)	24
4.3.1.4	Test Settings	24
4.3.2	Additional settings for in-service testing and instructions	25
4.4	Implementation Features	25
4.4.1	Hardware Modules	26
4.5	Use in Testing	26
5.	Integration of Gold PMU and In-Service Calibrator	29
5.1	Introduction	29
5.1.1	General	29
5.1.2	Continuum Modeling of Power System	31
5.2	Design Specification	32
5.2.1	Functional Requirement	32
5.3	Implementation Features	33
5.3.1	IPC Model Calibration	33
5.3.2	Implementation of Fault Location Algorithm	34
5.4	Use in Testing	35
6.	Conclusions	37
	References	38

## List of Figures

Figure 1. PMU Calibration System Platform.....	7
Figure 2. Calibration Lab Implementation.....	8
Figure 3. Synchrophasor applications in real world .....	10
Figure 4. Synchrophasor-based test-bed setup.....	11
Figure 5. Functionality specification diagram of Gold PMU .....	14
Figure 6. Use of Gold PMU as synchrophasor reference source in commercial PMU evaluation.....	14
Figure 7. Gold PMU algorithm structure.....	16
Figure 8. Overall hierarchy of Gold PMU software .....	17
Figure 9. Hierarchy of FPGA implementation of synchronized voltage and current waveform sampling.....	18
Figure 10. Gold PMU used in end-to-end application test .....	19
Figure 11. Using Gold PMU to perform troubleshooting test in a substation .....	19
Figure 12. Module representation of TEES development with type/application test waveforms	27
Figure 13. Exemplary test setup for End-to-end testing in synchrophasor applications .....	28
Figure 14. Understanding electromechanical-wave propagation. (a) 64-generator ring system, (b) Bus angle modulation following a fault at bus 16.....	30
Figure 15. Incremental system used for continuum modeling of system .....	32
Figure 16. Fault location and the configuration of midpoint substation.....	33
Figure 17. Comparison between measured and simulated results .....	34
Figure 18. Block diagram for binary search method .....	35
Figure 19. One-line diagram for IPC test system .....	35
Figure 20. Diagram for End-to-End Application Test.....	36

## **List of Tables**

Table 1. PMU Steady State Type-Test .....	8
Table 2. PMU Dynamic State Type-Test.....	9
Table 3. Gold PMU Functionality Description.....	15
Table 4. Voltage/Current Data Acquisition Modules for Gold PMU .....	16
Table 5. Proposed Timing I/O Module of Gold PMU .....	16
Table 6. Proposed Embedded Controller Module of Gold PMU.....	17

## Nomenclature

<i>FPGA</i>	Field programmable gate array
<i>GPS</i>	Global positioning system
<i>IED</i>	Intelligent electronic device
<i>IPC</i>	Idaho power company
<i>PDC</i>	Phasor data concentrator
<i>PMU</i>	Phasor measurement unit
<i>ROCOF</i>	Rate of change of frequency
<i>SCADA</i>	Supervisory control and data acquisition
<i>TSS</i>	Test suite specifications
<i>TVE</i>	Total vector error
<i>WAMPAC</i>	Wide-area measurement, protection, and control
<i>WAMS</i>	Wide-area measurement system

# **1. Introduction**

---

## **1.1 Background**

Synchronized phasor measurement systems are becoming increasingly important in the modern power grid. Synchrophasor-based wide-area monitoring, protection, and control (WAMPAC) strategies have proven to be beneficial to the early detection and timely mitigation of emergencies in the power system. Despite the vital role of synchrophasor systems in the modern power grid, no standard tools for certification, commissioning, in-service maintenance, and risk assessment are available for synchrophasor infrastructure, which is composed of phasor measurement units (PMUs), intelligent electronic devices (IEDs), phasor data concentrators (PDCs), and end-use applications.

The mission-critical synchrophasor components are introduced to improve monitoring and control performances and are expected to operator correctly each time they are triggered. Because their design complexities, the components may have hidden design defects and imperfections that may cause trouble at any unpredictable time. As a result, it is crucial to closely monitor the performances of synchrophasor devices throughout their entire life-cycle. Especially, when the synchrophasor components are initially commissioned, when the components have been in-service for a long time, and when a potential abnormal operation is detected. In those cases, rigorous test procedures, reliable test tools to test different aspects of hardware and software design, from the individual synchrophasor component level, to overall end-to-end system level are the only solution to assure more reliable and robust operation of the mission-critical system. In order to test various levels of synchrophasor tools, a reference infrastructure is needed, which provides the reference operating conditions that the devices under test are tested against.

In Part I of the project, PMU calibration and certification lab, reference PMU, field calibrator test set, the integration tool for testing end-to-end synchrophasor system, as well as the test procedure for synchrophasor component testing are designed and implemented. The developed solutions can be used to perform lab acceptance, as well as field commissioning and in-service tests on the components of the synchrophasor systems, and the end-to-end system.

## **1.2 Summary of Chapters**

This report is structured as follows. In chapter 2, the PMU calibration and certification lab is introduced. The lab is used to perform PMU performance testing according to standardized procedures.

Chapter 3 presents Gold PMU. Gold PMU is a device which is designed to provide accurate reference synchrophasor streams. Gold PMU hardware platform and accurate Gold PMU algorithm are implemented.

Chapter 4 discusses the development of a calibrator designed to perform PMU and end-to-end synchrophasor system calibration in the field.

Chapter 5 evaluates the integration of Gold PMU and field calibrator, where nested testing on synchrophasor system, including PMU, PDC, and end-use application can be performed and evaluated.

## **2. PMU Calibration and Certification Lab**

---

### **2.1 Introduction**

The Phasor Measurement Unit (PMU), introduced in the 80s, is an instrument capable of measuring amplitude and phase angle of voltage and current phasors, as well as the frequency and rate of change of frequency. Phasor angle is defined as a relative displacement at a given location compared to the reference cosine signal at another location, both synchronized to the Coordinated Universal Time. The synchronization is usually accomplished using the time reference signal from Global Positioning System of satellites. Fast calculation and reporting of the PMU data helps capture and track high-resolution real-time information for new advanced applications and improves situational awareness of the grid states.

PMU measurements can be employed in a large number of power system applications often implemented as Wide Area Monitoring, Protection and Control (WAMPAC) systems. PMU measurements are also applied in the model validation processes and are widely utilized in the system protection applications such as fault detection and location, out-of-step protection, oscillation detection, etc. To ensure the reliability and security of the infrastructure for synchrophasor-based end-use applications, good synchronization (better than 1 us), fast reliable communication network, and precise phase angle and magnitude measurements are needed.

Performance requirements of a PMU are specified in IEEE standards C37.118.1-2011 and C37.118.1a-2014 [1] [2]. Two classes of PMUs, namely the P and M performance class, are defined in the standards. The protection (P) class is focused more on the fast response rather than high precision. The opposite is required by the measurement (M) class PMUs. Each synchrophasor-capable Intelligent Electronic Device (IED) has to conform to at least one performance class. IEEE standard C37.118.1 specifies the type of the tests (i.e. steady state and dynamic state) and the maximum allowed measurements error, e.g., Total Vector Error (TVE), Frequency Error (FE) and Rate of Change of Frequency Error (ROCOF), which is defined for each reporting rate and performance class. The procedures and requirements for test equipment, e.g., timing reference, signal sources, calibration devices, and environmental conditions are specified in the IEEE Synchrophasor Measurement Test Suite Specification (TSS) report [3].

### **2.2 Design Specification**

#### **2.2.1 Calibration System Functional Requirements**

According to IEEE TSS, a PMU Calibration System should have the following functions:

#### **2.2.2 Signal generation/HIL system: generating test signals**

- Timing reference: providing UTC-traceable timing signals (GPS, PSS, IRIG-B, etc.) to the calibration system.
- Receiver: to receive the synchrophasor measurement data from PMUs under test.

- Synchrophasor reference source: provide high precision reference synchrophasor to the system.
- Accuracy analysis: by comparing reference synchrophasor with PMU measurements, the calibration system performs calculations for total vector error (TVE), phasor magnitude error, phase angle error, frequency error, rate of change of frequency error, and additional calculations for dynamic step test results.
- The calibration system is able to determine the time of arrival of PMU data messages and comparing that time against the message timestamp. (Reporting latency test)
- The calibration system is able to document test result.

### 2.2.3 Calibration System Hardware Specifications

The specification includes:

- Hardware Specification for Timing Reference
- PMU under test may require various components to create the timing signals:
- GPS antenna
- IRIG-B (sometimes with 1 pps) (DC level or AM)
- Possibly with the addition of IEEE Std. 1344 extension
- Possibly with the IEEE Std. C37.118.1-2011 extension to the IEEE Std. 1344 extension.
- IEEE Std. 1588

For the purpose of the project three GPS antennas were located on the roof of the TAMU building where the PMU calibration lab is located. The PMU under test can be connected directly to either a GPS antenna or timing signal, that can be generated using available receivers (SEL-2407, Tektron TCG02-G, NI PXI 6683H module). A NI PXI 6683H is used as a synchronization PXI module to provide a synchronization signal for the signal generator as well as a timing reference for the acquisition module. The NI PXI-6683H has a GPS receiver which powers an active GPS antenna and receives and processes the RF signals (1.575 GHz) from the satellites. The GPS receiver then generates a very precise pulse-per-second (PPS) that the NI PXI-6683H uses to achieve sub-microsecond synchronization. This module is also capable of generating IRIG-B timing signal for the tested device.

In addition, two more devices are available for the purpose of generating timing reference:

- SEL-2407, Satellite-Synchronized Clock, provides time display, reliability, durability and high-accuracy timing to  $\pm 100$  nanoseconds.
- The TCG 02-G is a highly accurate fully featured GPS and GLONASS (GNSS) clock, offering multiple oscillator options, Time Code and Frequency outputs.

All three devices comply with the requirements defined in the IEEE standards.

## 1. Hardware Specification for Signal Source

The requirement of the signal source for a PMU Calibration System is:

- PMU calibrator shall provide three-phase voltage and current input signals to PMUs under test. The signals shall comply with both steady-state and dynamic test requirements.
- Total harmonic distortion plus noise of the input signal shall be less than 0.2% of the fundamental
- PMU calibrator shall be capable of supplying at least 120% of the selected nominal voltage (typically 84 V rms for  $V_{nom} = 70$  V rms) and 200% of the selected nominal current per phase (10 A rms).
- Signal sources shall be capable of providing signal frequencies ranging from 45 Hz to 65 Hz.
- Bandwidth of the signal source should be at least 3 kHz. (down-limit is DC)

The available signal generator module in the PMU Calibration Lab at TAMU comprises of the NI PXI 7854R module as well as the power amplifiers.

The NI PXI 7845R module consists of:

- 8 analog inputs, independent sampling rates up to 750 kHz, 16-bit resolution,  $\pm 10$  V
- 8 analog outputs, independent update rates up to 1 MHz, 16-bit resolution,  $\pm 10$  V
- 96 digital lines configurable as inputs, outputs, counters, or custom logic at rates up to 40 MHz
- Virtex-5 LX110 FPGA programmable with the LabVIEW FPGA Module
- 3 DMA channels for high-speed data streaming

For generating voltage signals in range  $\pm 10$  V, 6 analog outputs of NI PXI 7845R are used.

In order to amplify the generated signals from NI PXI 7854R, voltage and current amplifiers from AE Techron model TEC3600 and 7224 are selected and calibrated. Their performance meets the aforementioned standard requirements.

## 2. Hardware Specification for Receiver

PMUs may transmit their measurements over a variety of physical media (Ethernet via twisted pair copper using RG45 connector, or optimal Ethernet using ST or LC connectors, RS-232) using a variety of protocols (IEEE Std. C37.118-2005, IEEE Std. C37.118.2).

The NI PXI 6683H is equipped with the Gigabit 10/100/1000 Ethernet port used as the receiver interface for the stream of the device under test. In case that the Serial communication is required, NI PXIe-8105 embedded Controller can be used for interfacing the device under test. Our calibration lab is not equipped with ST or LC connectors.

### 3. Analyzer Tool

True (reference) values of the phasors are calculated in the course of time while being generated, and the tool for calculating the required errors (TVE, PE, ME, FE, RFE) is developed using NI LabVIEW software package and it is running on the NI PXIe-8105 embedded controller. All modules described above are parts of the NI PXIe1062Q chassis.

## 2.3 Implementation Features

### 2.3.1 Calibration System Overview

A PMU test and calibration platform used to verify the conformance of the evaluated PMUs under various static and dynamic tests according to the IEEE standards is shown in Figure 1. As shown in Figure 1, the PMU test system consists of a timing reference (GPS receiver), signal generator, power amplifier, and data management and results analytics tools. The timing reference provides GPS clock and time-code information to the calibration equipment and to the device under test so that the entire system is synchronized and time-stamped. Test signals are generated by the signal generator according to test types determined by the IEEE TSS [3]. The calculated and theoretical reference synchrophasor can be, hence, used for the comparison, and then followed by a result analysis and documentation.

The PMU test and calibration platform is implemented using National Instruments (NI) hardware as shown in Figure 1. The entire system consists of the PXI virtual instrument system with embedded Controller NI PXIe-8105, a user-programmable FPGA which is a part of NI PXI-7854R multifunctional reconfigurable I/O module to generate the required waveforms, and power amplifiers to generate 3-phase voltage and current signals feeding the PMU device under the test. As a part of the system, software based Phasor Data Concentrator (PDC) module that receives and parses the data is running on the PXI system. Measurements from the tested PMU are acquired through fast speed Ethernet communication ports, analyzed, and the reported using the NI LabVIEW software interface. Reports consist of all data reported by tested PMU as well as true values of phasors sent to the device, which allows extensive post-analysis of the collected results.

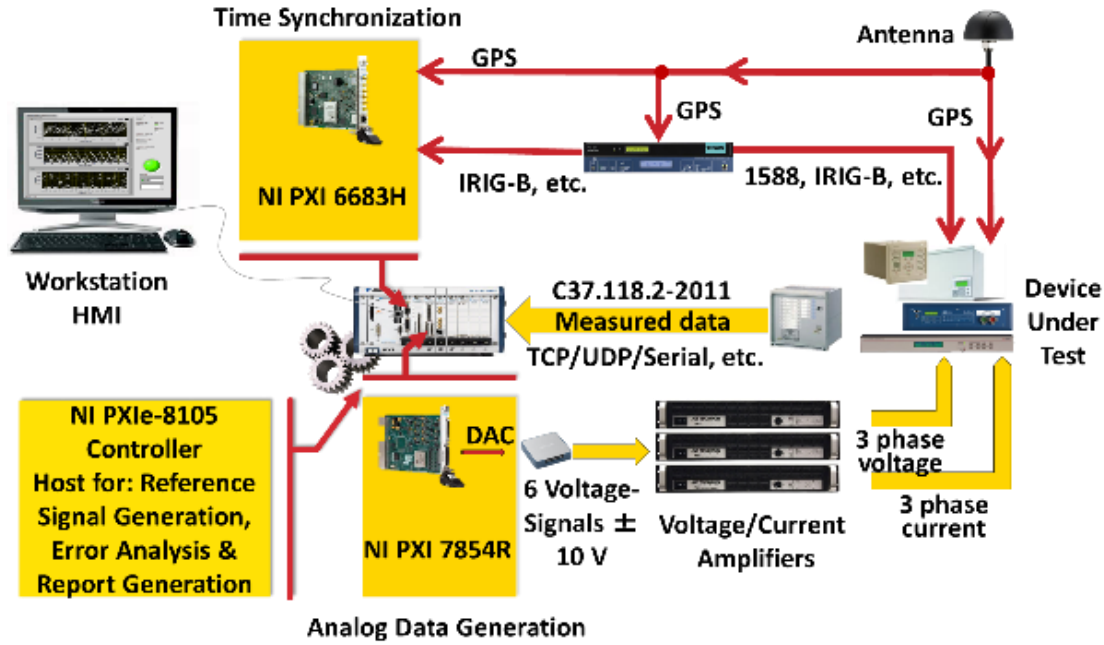


Figure 1. PMU Calibration System Platform

### 2.3.2 PMU Type Test and Application Test

- Type Test

PMUs provide different types of calculated values such as voltage and current magnitude, angle, frequency, rate of change of frequency, etc. According to the IEEE standard C37 118.1, each device that is capable of providing GPS synchronized measurements has to undergo various steady state and dynamic test scenarios while being calibrated. During the steady state tests, PMUs are exposed to various type-test scenarios where all variables are kept unchanged during each test and the measurements are captured according to the standard procedure. Such static type-tests include performance evaluation of PMUs over a range of frequency values, voltage/current amplitudes as well as influence of harmonic and inter-harmonic interferences. Dynamic type-tests involve testing PMUs with the modulated signals, checking their performance during the step occurrence in amplitude and angle, as well as testing the PMU response to the frequency ramp events. As a part of the standard requirements, latency of a PMU device has to be measured too (see Table 1). Table 2 shows a graphical representation of how the calibration lab at Texas A&M University for PMU calibration and testing is implemented.



Figure 2. Calibration Lab Implementation

Table 1. PMU Steady State Type-Test

Steady state tests					
Test subtype	Step	P (Protection) class		M (Measurement) class	
		Range	Error Requirements	Range	Error Requirements
Signal Frequency Range (test applied nominal + deviation $f_0 \pm f_{dev}$ ) Three temperatures (0,23,50)	0.1 Hz	$f_0 \pm 2$ Hz	1% TVE 0.005 Hz FE 0.44 Hz/s RFE	$f_0 \pm 2.0$ Hz for $F_s < 10$ $\pm F_s/5$ for $10 \leq F_s < 25$ $\pm 5.0$ Hz for $F_s \geq 25$	1% TVE 0.005 Hz FE 0.1 Hz/s RFE
Signal Magnitude—Voltage	10% of nominal value	80 to 120 % of nominal	1% TVE	10 to 120 % of nominal	1% TVE
Signal Magnitude—Current	10% of nominal value	10 to 200 % of nominal	1% TVE	10 to 200 % of nominal	1% TVE
Phase Angle	No need for testing*	$\pm \pi$ radians (+/- 180°)	1% TVE	$\pm \pi$ radians (+/- 180°)	1% TVE
* The requirements of the phase angle test are satisfied by the signal frequency range test when the input frequency is nominal frequency $\pm 0.2$ Hz and the test duration is 5 seconds. Therefore, no separate phase test need be performed.					
Harmonic distortion (single harmonic)	50 measurements (each time just one harmonic)	1%, each harmonic up to 50th	1% TVE 0.005 Hz FE 0.44 Hz/s RFE	10%, each harmonic up to 50th	1% TVE ( $F_s \leq 20$ ) 0.005 Hz FE ( $F_s > 20$ ) 0.025 Hz FE Limit suspended RFE
the harmonic sequence shall NOT be positive sequence for all harmonics but shall be in-phase with the fundamental frequency for all three phases					
Out-of-Band Interference	Form min In-Band to 10 Hz decrease fi exponentially (+0.1 Hz, +0.2 Hz, +0.4 Hz, +0.8 Hz...) From max In-Band to 120 Hz increase fi exponentially (+0.1 Hz, +0.2 Hz, +0.4 Hz, +0.8 Hz...)	/	/	10% of input signal magnitude, 10 Hz to 120 Hz	1.3% TVE 0.01 Hz FE Limit suspended RFE
Out-of-band compliance is to be checked with the frequency of the fundamental power signal at the nominal system frequency and also at nominal frequency $\pm 10\%$ of the Nyquist frequency of the reporting rate ( $F_s$ ) (test shall be repeated three times)					

Table 2. PMU Dynamic State Type-Test

Dynamic state tests									
Test subtype		P (Protection) class				M (Measurement) class			
		Range		Error Requirements		Range		Error Requirements	
$f_m = \omega/2\pi$ is the modulation frequency in Hz, $k_x$ is the amplitude modulation factor, and $k_a$ is the phase angle modulation factor The modulation frequency shall be varied in steps of 0.2 Hz or smaller over the range specified in the table									
Measurement Bandwidth—phase modulation $k_x = 0$ $k_a = 0.1$ radian	0.2 Hz	Fs	Modulation frequency (Fr)	3% TVE		Fs	Modulation frequency (Fr)	3% TVE	
				Max FE Hz	Max RFE Hz/s			Max FE Hz	Max RF E Hz/s
10	1	0.03	0.6	10	2	0.12	2.3		
12	1.2	0.04	0.8	12	2.4	0.14	3.3		
15	1.5	0.05	1.3	15	3	0.18	5.1		
20	2	0.06	2.3	20	4	0.24	9		
Measurement Bandwidth—amplitude modulation $k_x = 0.1$ $k_a = 0$ radian	0.2 Hz	25	2	0.06	2.3	25	5	0.3	14
		30	2	0.06	2.3	30	5	0.3	14
		50	2	0.06	2.3	50	5	0.3	14
		60	2	0.06	2.3	60	5	0.3	14
			min(Fs/10,2)	$0.03 \times Fr$	$0.18 \times \pi \times Fr^2$		min(Fs/5,5)	$0.06 \times Fr$	$0.18 \times \pi \times Fr^2$
Ramp of System Frequency Ramp rate = $\pm 1.0$ Hz/s	More details in	$\pm 2$ Hz Exclusion interval = $2/F_s$		1% TVE 0.01 Hz FE 0.4 Hz/s RFE		Lesser of $\pm (F_s/5)$ or $\pm 5$ Hz Exclusion interval = $7/F_s$		1% TVE 0.01 Hz FE 0.2 Hz/s RFE	
Step Change in Phase $k_x = 0$ , $k_a = \pm \pi/18$		$\pm 10^\circ$ from nominal		Response time (s) Response delay (s) Overshoot (%) Frequency response time (s) ROCOF response time (s) See Error! Reference source not found.		$\pm 10^\circ$ from nominal		Response time (s) Response delay (s) Overshoot (%) Frequency response time (s) ROCOF response time (s) See Error! Reference source not found.	
Step Change in Magnitude $k_x = \pm 0.1$ , $k_a = 0$		$\pm 10\%$ of nominal				$\pm 10\%$ of nominal		Response time (s) Response delay (s) Overshoot (%) Frequency response time (s) ROCOF response time (s) See Error! Reference source not found.	
PMU Reporting Latency		2 / Frequency of data reporting		0.002 second		7 / Frequency of data reporting		0.002 second	

- Application Test

Various applications for power system protection have different sensitivities to the data errors in the input measurements. Various PMU algorithms for synchrophasor estimations may have different responses to the input signals experienced during different protection application disturbances. The impacts of such input signal uncertainties and related application errors are largely unknown to the end-users and need to be fully investigated.

Even though the IEEE standards define the basic type-tests that PMUs have to undergo with certain precision, the test procedure does not reveal the impact of such results on the system-wide applications. In addition, the error impacts of the signal components present at the time of a specific protection event are not known. The performance is further affected by different requirements in terms of calculation speed, accuracy of estimated frequency, angle and magnitude measurements, etc., which are different for different protection applications. Hence, making meaningful trade-offs between such performance indicators to reduce the error impact is imperative. Since such decisions are made at the time of the PMU design, the user is primarily interested in evaluating the performance under various application scenarios. In order to build a trustworthy mindset for the protection end-users, the first step is to recognize the critical parameters of interest for a given application and then evaluate how the estimation algorithm matches the application requirements using the results acquired from the calibration tests. Such analyses could build the confidence about the quality of the synchrophasor application outputs. Figure 3 and Figure 4. demonstrate the end-to-end synchrophasor system and how it looks in real world scenarios as well as its implementation in Texas A&M University in the form of a synchrophasor-based test-bed.

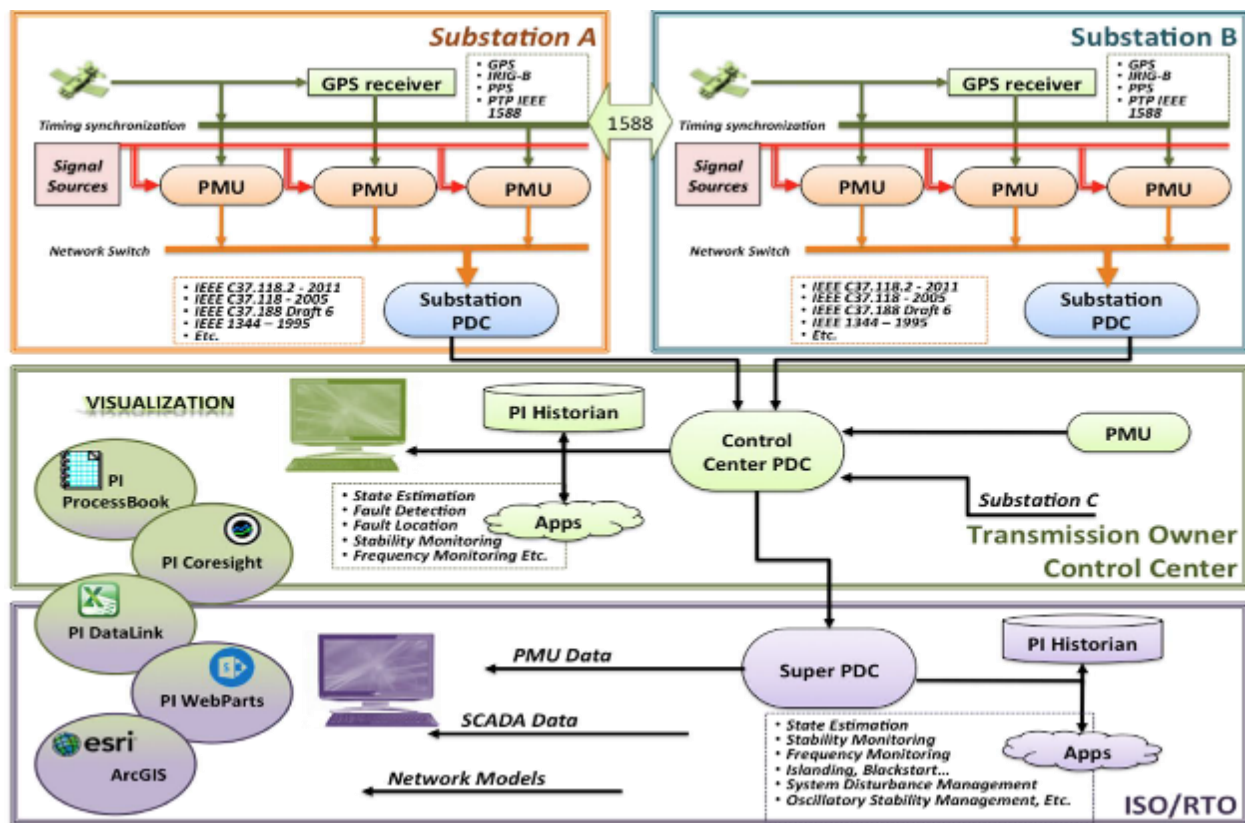


Figure 3. Synchrophasor applications in real world

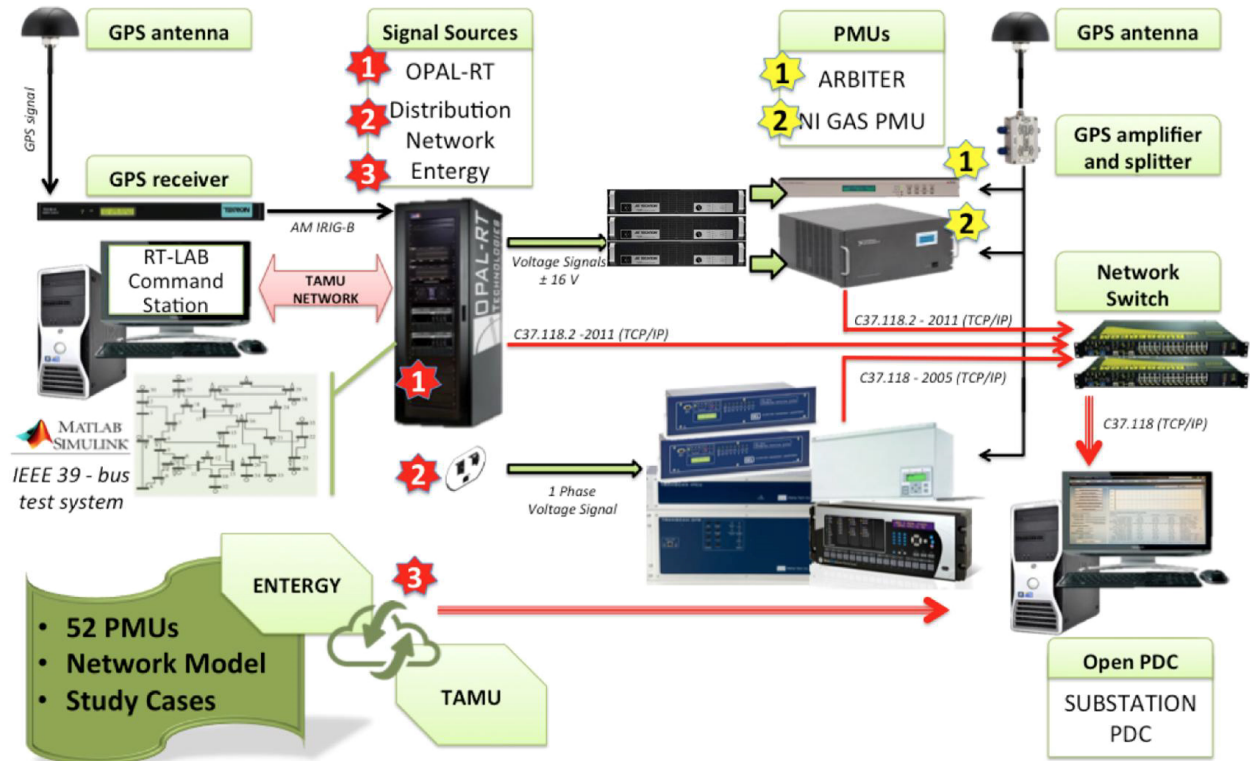


Figure 4. Synchrophasor-based test-bed setup

The test-bed platform used for characterizing the PMU response under fault (or other prevailing) conditions and evaluating the impact of the PMU errors on the end-use application outcome is implemented at Texas A&M University. The developed infrastructure is generic enough to be employed not only for quantifying the impact of PMU errors on fault scenarios, but also performing studies on trustworthy assessment of any end-use power system application that uses PMU measurements. General structure of the test setup is depicted in Figure 4. As shown in Figure 4, the synchrophasor system consists of timing references, signal generator, power amplifiers, and data management and analytic tools. Timing reference provides GPS clock reference to the PMUs so that measurements from different devices are synchronized and time-stamped. Model of the network under evaluation is built in the ATP-EMTP software package environment or from the digital simulators (OPAL-RT). Various fault (or other prevailing) scenario use cases can be simulated, and waveforms are generated using low voltage simulators. In order to have realistic measurements from the PMU, the applied signals must conform to the nominal level defined by the PMU device (i.e., normally 70 V rms and 5 A rms for voltage and current, respectively). Signals from the simulators are amplified to the nominal level using power amplifiers. Each PMU is connected to the GPS antenna for the synchronization purposes and measured data streams from the devices are collected and fed to a desired application algorithm for further evaluation purposes.

## **2.4 Use in Testing**

### **2.4.1 Acceptance Testing and Certification of PMUs Using Laboratory Environment**

A use case is identified when testing PMU devices and IEDs with synchrophasor capabilities in the Calibration Laboratory to check their compliance with latest IEEE Std. C37.118.1a-2014 and issuing of ICAP certificate if complied with the IEEE Standards.

1. The main scenario and implementation procedure is given below:
2. PMU testing is requested by the PMU manufacturer or owner (user).
3. Connect inputs of the PMU to the signal generator
4. Establish communication between tested device and calibration collector device through Ethernet interface.
5. Acquire the target IP address and PDC port (target port) from the PMU under test in case that UDP protocol is tested or acquire the PMU port number (host port) where the stream is sent.
6. Set the communication parameters on the local port of the calibrator system to match those of the PMU under test (the same net mask; and IP in the allowed range but different from the PMU's).
7. Ping the PMU under test in order to verify the communication connectivity.
8. Connect timing source to the PMU device (GPS antenna connection or IRIG-B signal generated by calibration equipment).
9. Wait until the tested PMU is synchronized to UTC and "Locked".
10. Set the communication protocol parameters, such as PDC port number and PMU IP address in the calibration PDC software.
11. Verify whether the communication is established between PMU and the calibration system using the PDC software.
12. Run the PDC software and obtain the phasors reporting order, and corresponding channel indices.
13. Set input parameters for the calibration software (PMU settings: nominal voltage, performance class, reporting rate, standard version; communication settings: PDC port, IP address of the PMU under test, communication protocol (UDP/TCP); phasor channel indices).
14. Run the calibration software.
15. When the tests are done, navigate to report folder and print the results.

The variations in this use case include:

- 2a. PMU device can be replaced with any synchrophasor-capable device that supports C37.118-2005 or C37.118.2-2011 communication protocols such as DFR, DPR, etc.;

- 3a. Establish communication between tested device and calibration collector device through RS-232 serial interface. (If the device under test does not have an Ethernet interface);
- 4a. Acquire information from PMU such as baud rate, data bits, parity, stop bits, and flow control;
- 5a. Update communication port (COM1 parameters) in the calibration system to match those of the PMU under test.

### 3. Gold PMU

#### 3.1 Introduction

Gold PMU is defined as an absolutely accurate PMU. The functionality of Gold PMU can be described as a “Reference PMU”. This PMU will be utilized to compare performance of the field PMU for the same inputs provided to the PMU under evaluation and the Gold PMU. A logical diagram of Gold PMU is shown in Figure 5 below.

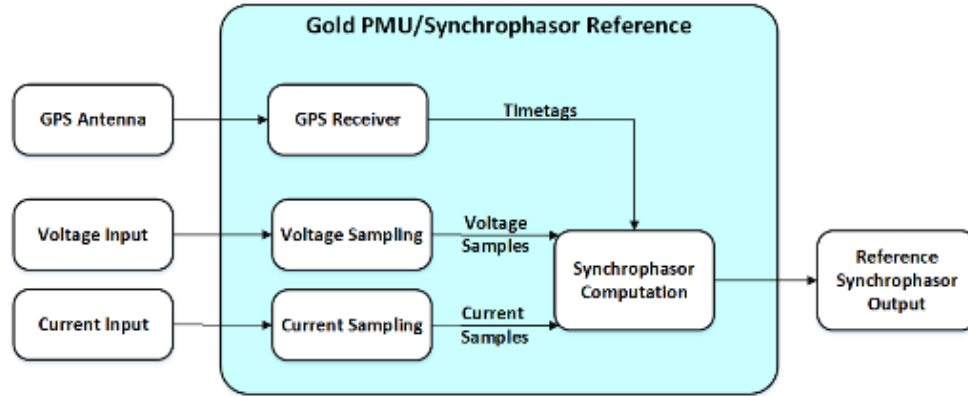


Figure 5. Functionality specification diagram of Gold PMU

The internal functionality specification of Gold PMU, marked in shaded blue block, is similar to a commercial PMU device. When used to test a commercial PMU, Gold PMU and PMU under evaluation will be connected in parallel, and both connected to the same signal generation source and GPS source, and the synchrophasor estimation results will be compared at embedded controller. This schematic is shown in Figure 6 below.

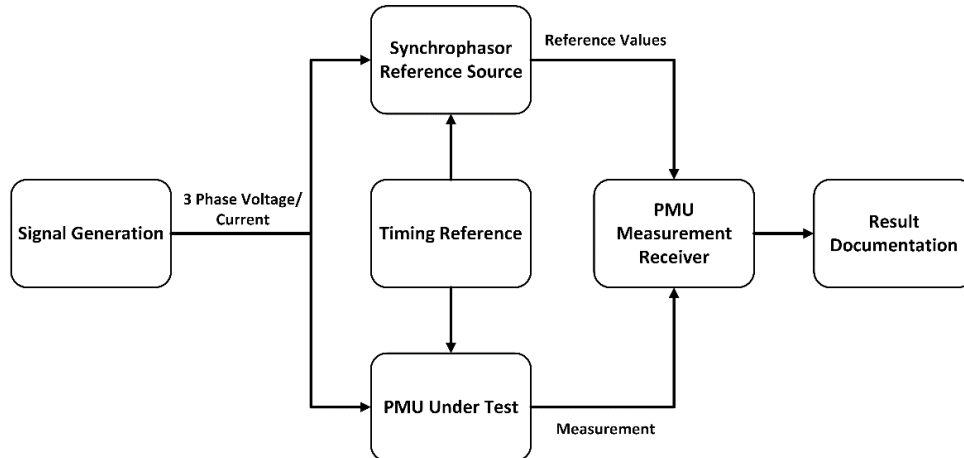


Figure 6. Use of Gold PMU as synchrophasor reference source in commercial PMU evaluation

## 3.2 Design Specification

### 3.2.1 Functionality Requirement Specification

As previously discussed, Gold PMU is designed as a more accurate PMU device, and thus should be equipped with the same hardware components that enable the same functionality of a commercial PMU device. The structure of Gold PMU functionality is shown in Figure 5, and a detailed description is listed in Table 3.

Table 3. Gold PMU Functionality Description

Functionality	Requirement Specification
Operating system, user interface, computation	CPU, hard drive, memory: in order to perform phasor estimation Control programs and user interface: enabling time-synchronized waveform sampling and user control
Phasor parameter calculation	Measurement algorithms for phasor parameters: the accuracy should be higher than IEEE standards.
Synchrophasor data transfer	Communication ports: streaming of calculated phasor.
Synchronized voltage waveform sampling	Voltage data acquisition module and synchronization of voltage samples
Synchronized current waveform sampling	Current data acquisition module and synchronization of current samples
Attenuators	When applicable, attenuate voltage and current inputs to acceptable level to data acquisition modules
Timing input	GPS antenna to receive timing signal from GPS satellites. Module/Program that decodes raw timing input signal (GPS, IRIG-B, etc.) Necessary peripheral cables to distribute timing information to voltage and current sampling modules.

### 3.2.2 Definition of Gold PMU Algorithm

At the core of the embedded controller lie Gold PMU algorithms, which ultimately enable the high synchrophasor estimation accuracy of Gold PMU.

A thorough literature survey has been performed to review available commonly used synchrophasor estimation algorithms. Synchrophasor estimation algorithms calculate phasor parameters from a vector of time-stamped samples. Benefited from interdisciplinary efforts such as signal processing technology, control theory, estimation theory, literature regarding synchrophasor estimation algorithms have proliferated since its inception three decades ago. A detailed literature survey document can be found on project website. And the basic scheme of Gold PMU algorithm to achieve high accuracy is shown in Figure 7.

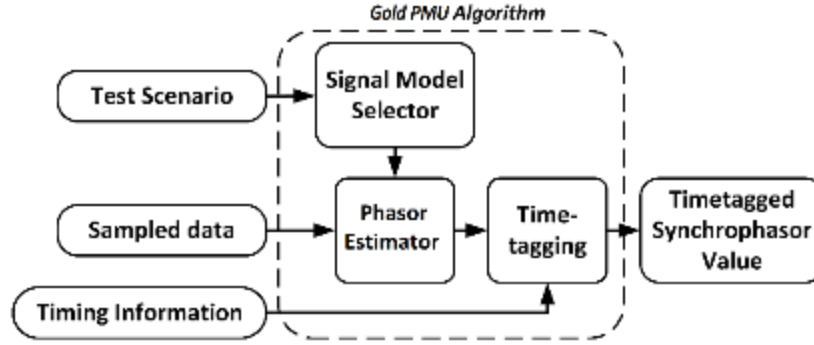


Figure 7. Gold PMU algorithm structure

From literature survey, it is concluded that none of the prior contributions in synchrophasor algorithms is able to be accurate for all types of input waveforms. Therefore, in this project, it is proposed that a “signal type classifier” be designed so that the “Test Scenario” can be identified. Then, in “Signal Model Selector”, the fittest algorithm form will be selected to perform phasor parameter estimation. The fittest algorithm may be from current literature, or maybe a newly designed algorithm.

### 3.3 Implementation Features

#### 3.3.1 Implementation of Hardware Functionality

The Gold PMU is implemented in National Instruments platform, which is composed of a chassis (embedded controller), and separate modules that can be inserted into the chassis slots.

The overall implementation strategy is shown from Table 4 to

Table 6.

Table 4. Voltage/Current Data Acquisition Modules for Gold PMU

Requirement	Design	Hardware Specification		
		Analog Input Level	Sampling Rate	Resolution
Voltage Input	NI 9225	300Vrms line to neutral	Max 50kHz/Ch,-3 channel	24-bit
Current Input	NI 9227	5Arms	Max 50kHz/Ch, 4-channel	24-bit

Table 5. Proposed Timing I/O Module of Gold PMU

Requirement	Implementation	Hardware Specification	
		Accuracy	Voltage Level
Timing I/O	NI 9467	$\pm 100\text{ns}$	5VDC

Table 6. Proposed Embedded Controller Module of Gold PMU

Requirement	Implementation	Hardware Specification
Embedded Controller (CPU, hard drive, memory)	NI cRIO-9039 <sup>[11]</sup>	1.91 GHz Quad-core CPU, 2GB DRAM, 16GB hard drive
Communication I/O	NI cRIO-9039	2 Ethernet, 2 serial ports

### 3.3.2 Implementation of Software Functionality

Gold PMU software, including user's interface, Gold PMU algorithms, data acquisition, timing acquisition, communication. All Gold PMU software is coded in NI LabVIEW for convenient implementation on NI hardware platform. The Gold PMU software hierarchy is shown in Figure 8.

The code that requires stable and efficient execution are programmed on the FPGA chip of NI 9039. Programs for data manipulation, signal processing, communication, and users' interface are coded in the Host Computer of NI 9039. The key is simultaneous acquisition of voltage waveform samples, current waveform samples, and absolute UTC time. The flowchart to achieve synchronized sampling is shown in Figure 9.

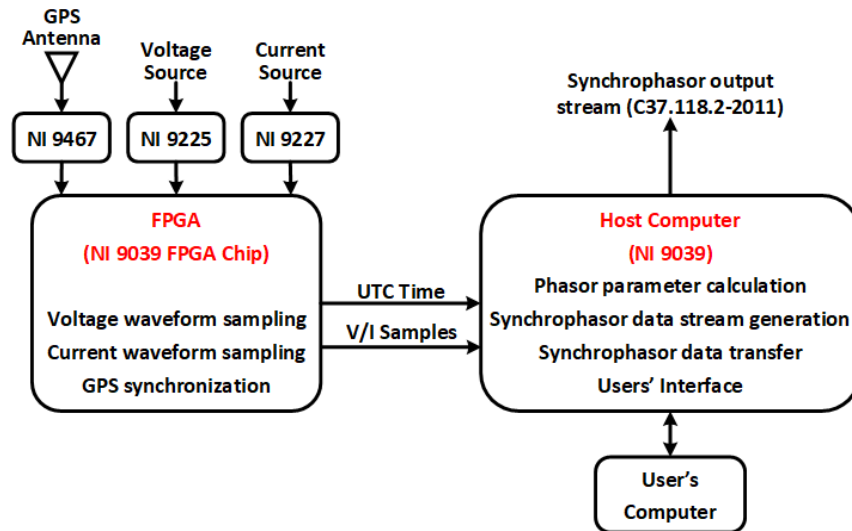


Figure 8. Overall hierarchy of Gold PMU software

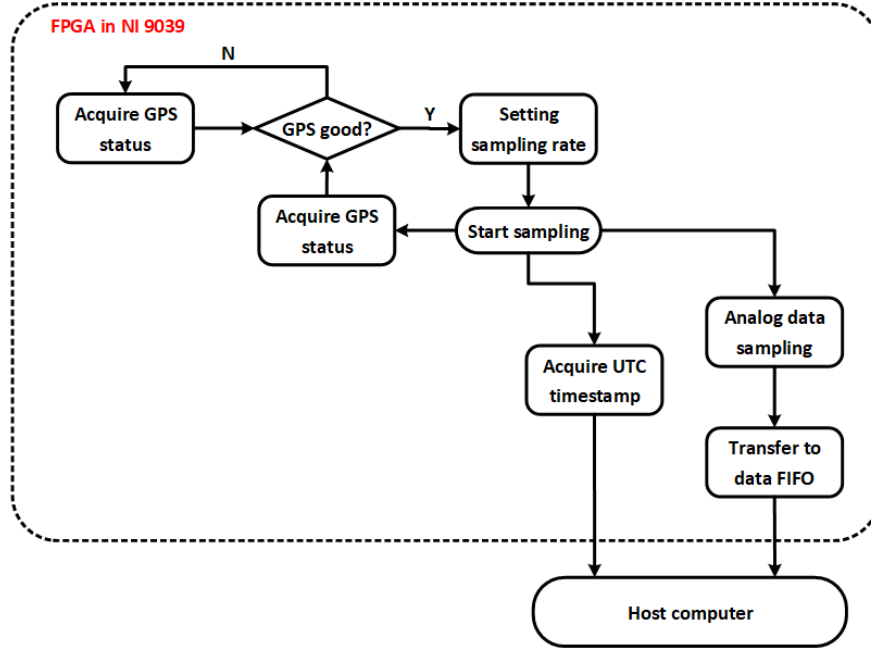


Figure 9. Hierarchy of FPGA implementation of synchronized voltage and current waveform sampling

### 3.3.3 Implementation of Gold PMU Algorithm

The approach for accurate synchrophasor estimation is discussed in Section 3.2.2. The input waveform type is first identified according to paper [4], which categorized input waveforms into steady-state, dynamic amplitude and frequency oscillations, and dynamic frequency ramping test scenarios.

For steady-state signals, frequency-domain algorithms, which are generally based on discrete Fourier transform (DFT) will be used. The fundamental frequency of a signal is first estimated [5], in an effort to reduce spectrum leakage, which is commonly observed in DFT-based methods when subjected to off-nominal frequency input. A typical DFT-based method, known as interpolated DFT (IpDFT) [6], is used to estimate synchrophasors from steady-state signals.

For dynamic waveforms with oscillatory phasor parameters, algorithm [7] is used. This algorithm is adopted to estimate the slow changing movement of magnitude and frequency, while effectively eliminating the impact of harmonic infiltration. For dynamic waveforms with non-oscillatory behaviors, noticeably frequency ramping up or down, algorithm [8] is used.

### 3.4 Use in Testing

Gold PMU is essentially used to provide synchrophasor reference. The input of Gold PMU, i.e. the test waveforms designed to evaluate commercial PMU performance, can be either be from standardized waveforms, or be generated by electromagnetic/electromechanical dynamic simulation software. In this project, the Gold PMU is intended to be used with Field End-to-End Calibrator to perform end-to-end application testing, shown in Figure 10. The accuracy of

commercial PMU is evaluated by comparing the synchrophasor estimation results from both the commercial PMU and Gold PMU; the performance of a given synchrophasor application is assessed by comparing the application results using the synchrophasor streams from both commercial PMU and Gold PMU. The details of “nested testing” strategy will be introduced in Section 4 along with Field End-to-End Calibrator.

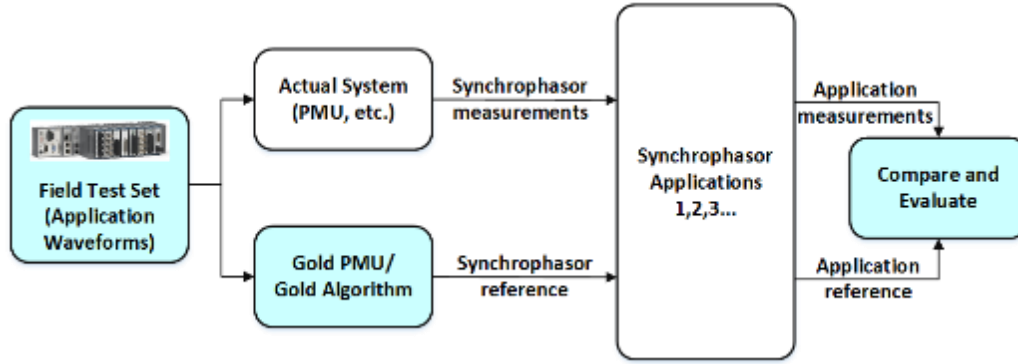


Figure 10. Gold PMU used in end-to-end application test

Gold PMU may be installed in a substation to perform troubleshooting test, as shown in Figure 11. In this approach, Gold PMU is permanently installed in a substation. When detection schemes trigger a troubleshooting command, a test switch will connect the Gold PMU, which will perform a reference synchrophasor estimation. In the meantime, phasor data streams from both PMU in field and Gold PMU will be collected by a field calibrator test set, where the performance of field PMU will be evaluated.

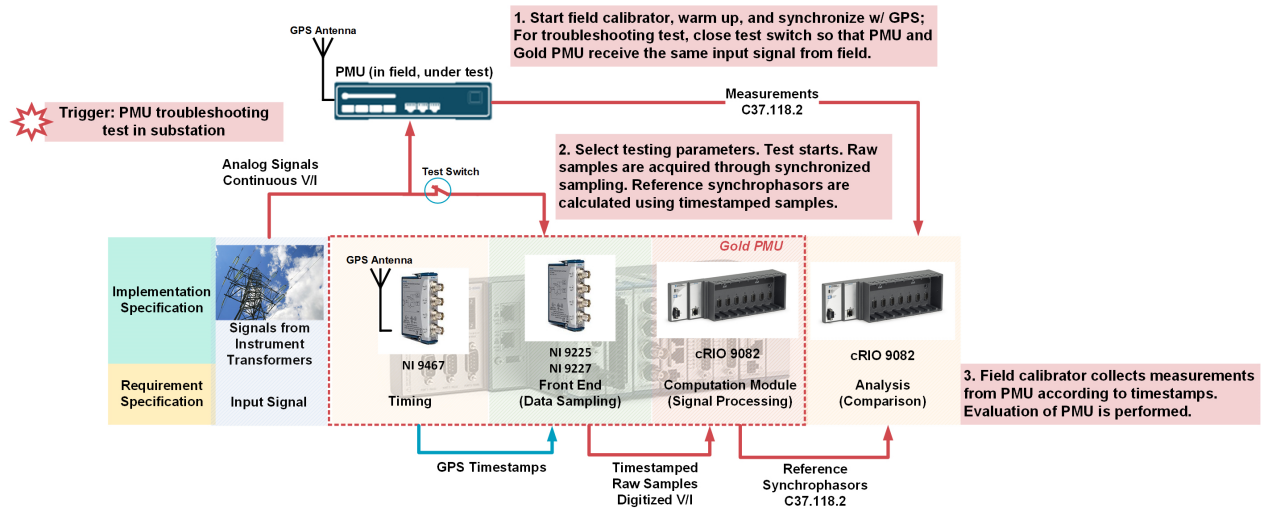


Figure 11. Using Gold PMU to perform troubleshooting test in a substation

## 4. Field Calibrator

---

### 4.1 Introduction

The entire synchrophasor system consists of multiple layers (see Figure 3): PMU devices, communication subsystem, applications and visualization. To evaluate synchrophasor systems as a complete solution it is necessary to confirm that all pieces work properly once they are connected. Even if all components pass the laboratory tests, there is no guaranty that everything will work properly after installation in the system. During the validation of PMU in a laboratory environment it is practically impossible to simulate conditions of a real network. Errors caused by instrumentation channel, cabling, GPS equipment, and cyber security solutions have to be studied and taken into account.

Field calibration consists of two sets of tests: field acceptance tests (commissioning tests) and periodic maintenance tests. PMU field commissioning tests include PMU calibration and basic system functionality check. It also verifies the correct phase sequence, GPS signal strength and correct interfacing, data sending/receiving sequences, and the communication link between PMUs and PDCs. As a part of the portable calibration system, a calibrated and accurate Gold PMU algorithm is used to provide a reference for testing. The output results from the reference PMU and PMU under test are compared so that corrective measures can be taken.

The Field Calibrator is a device capable of characterizing, calibrating and optimizing the performance of a given synchrophasor system and performing the aforementioned actions. Through performing a variety of standardized, so called *type tests*, as well as *application tests* based on simulated or observed power system data, the portable device captures and analyzes the behavior of Phasor Measurement Units (PMUs) and Phasor Data Concentrators (PDCs). By looping back the output streams of those devices and comparing them to the known generated input signals, various characteristics like time delay, fault uncertainty and design quality can be determined. This information may then be used for calibration to improve overall system performance and accuracy.

The procedure associated with the use of the Field Calibrator may be performed during initial calibration, periodic maintenance or trouble shooting when issues have already become apparent.

### 4.2 Design Specification

#### 4.2.1 Objectives

- Provide field calibration tools for periodic maintenance tests
- Support end-to-end calibration of synchrophasor systems
- Enable in-service application testing using advanced synchrophasor algorithms
- Serve as a testbed for evaluation of new synchrophasor algorithms

### 4.2.2 Functional Overview

The following functions are required for the field calibrator purpose of periodic maintenance of a PMU in the field:

- Shall be run off an accurate timing source (IRIG-B/GPS/1PPS).
- Shall provide voltage and current input signals [Signal source(s)]
- Shall receive measurements from PMU under test (Receiver).
- Shall compare phasor magnitude and phase angle, frequency and rate of change of frequency (ROCOF) measurements from PMU to “true” (reference) phasor magnitude and phase angle, frequency and ROCOF represented by the signal source input to the PMU.
- Shall perform calculations for total vector error (TVE), phasor magnitude error (ME) and phase angle error (PE), frequency error (FE) and rate of change of frequency error (RFE), and additional calculations for the dynamic step test results.
- Shall have a means of determining the time of arrival of PMU data messages and comparing that time against the message timestamp.
- Shall provide test result documentation.

In addition, the following functions are required for end-to-end testing of the synchrophasor system:

- Required very accurate, with high precision measurements PMU algorithm – Gold PMU, as a reference measurement unit in case of unknown input signals.
- Shall provide an interface to analog voltage and current signals from the substation CTs and VTs (A/D converters).

### 4.2.3 Additional Settings and Instructions for Periodic Maintenance Test Set

For the purpose of maintenance testing, the inputs of the device under test must be de-energized from the substation signal source and connected to calibrator. The field calibrator performs testing by generating test signals based on the end-user preference that can be customized and analyzing the response to the generated signals using various software tools integrated in the calibrator. All the test signals are generated according to the user choice and sent to the amplifier (if applicable) and then to the PMU under test. Stream from the tested PMU is sent back to the field calibrator for further analysis.

### 4.2.4 Timing Reference

PMU under test may require one of the timing signals:

- GPS antenna
- IRIG-B (sometimes with 1 PPS) (DC level or AM)
  - Possibly with the addition of IEEE Std 1344 extension.

- Possibly with the IEEE Std C37.118.1-2011 extension to the IEEE Std 1344 extension.
- IEEE Std 1588 The timing reference shall have an uncertainty  $\leq 1$  microsecond ( $\mu\text{s}$ ).

The calibration system need only provide one instance of each type of timing source accepted by the PMU being tested

#### **4.2.5 Signal Source(s)**

This functionality is required only for periodic maintenance.

- PMU calibrator shall provide three-phase voltage and current input signals to PMUs under test. The signals shall comply with both steady-state and dynamic test requirements as specified in the IEEE C37.118.1 standard.
- Total harmonic distortion plus noise of the input signal shall be less than 0.2% of the fundamental harmonic (except where otherwise specified by harmonic distortion or out-of-band interference tests)
- The voltage and current amplitudes must be at “nominal” value (except where specified in signal magnitude tests, and dynamic step tests).
- A common nominal voltage for testing PMUs is 70 V rms and current 5 A rms (except for small signal testing which is 5V for both cases).
- PMU calibrator shall be capable of supplying at least 120% of the selected nominal voltage (84 V for  $V_{\text{nom}} = 70$  V) and 200% of the selected nominal current per phase (10 A).

##### **4.2.5.1 Signal Sources for Steady-State Tests**

- Signal frequency range test – signal sources shall be capable of providing signal frequencies from 45 Hz to 65 Hz.
- Signal magnitude tests – Voltage levels from 10% nominal level to 120% nominal level, and current levels from 10% nominal level to 200% nominal level shall be available from the signal source.
- Phase angle tests – constant phase at  $\pm\pi$  radians or a “slowly varying” phase angle with the input frequency  $\leq 0.25$  Hz from the nominal frequency for a duration that allows at least  $360^\circ$  of phase rotation.
- Harmonic distortion tests – required harmonics from the second harmonic up to the 50th harmonic of the nominal frequency.
- Out-of-band interference test – require interfering signals from 10 Hz up to twice nominal frequency.

#### **4.2.6 Signal Sources for Dynamic Tests**

- Measurement bandwidth tests – require modulation of the input signals in phase and in amplitude individually.
- The modulation frequency range from 0.1 HZ to 5 Hz and the index of modulation is 0.10. Frequency ramp tests – require sweep (chirp) of frequency from up to 5 Hz below to 5 Hz above the nominal frequency at rates of  $\pm 1$  Hz per second.
- Step tests – require steps  $\pm 10\%$  nominal magnitude and  $\pm 10^\circ$  of phase.

##### **4.2.6.1 PMU Measurement Receiver**

For PMUs that are able to use multiple protocols and over a variety of physical media full testing at all reporting rates shall be conducted using one protocol and limited testing shall be conducted at one reporting rate using the other protocol or protocols. The limited testing shall consist of the following:

- Dynamic step changes in phase and magnitude
- PMU latency

Protocols:

- IEEE Std C37.118-2005
- IEEE Std C37.118.2-2011

Physical media:

- TCP, UDP, or combined UDP/TCP Ethernet via:
  - twisted pair copper using RG45 connector
  - optical Ethernet using ST or LC connectors
- RS-232 (obsolete and may not be required for modern PMU calibration systems)

#### **4.3 User Interface Specification**

For the purpose of testing the entire synchrophasor system in the field environment, two different use cases were defined:

1. Test set for the periodic maintenance of PMU device employed in the field
2. Test set for testing the PMU device in-service

After the user has made a choice regarding the desired calibration procedure through the developed user interface, a short description of the procedure will pop-up including the required follow-up steps.

### **4.3.1 Common setting for all offered tests that are provided to the user**

#### **4.3.1.1 Communication Settings**

- Communication protocol (TCP, UDP, Serial)
- PMU port (default value for TCP is 4712, and for UDP is 4713, but it can be customized based on the PMU internal settings)
- PMU address (IP address of the tested device; recommended to be a Static IP address)

#### **4.3.1.2 PMU Settings**

- Nominal frequency of the tested device (50 Hz/60 Hz; default value is 60 Hz)
- Performance class (M/P class)
- Reporting rate (all possible value defined in the standard are available; 60 is set as default value)
- Standard version (2011; for the old PMU devices 2005 standard version is also available)
- Nominal voltage and current values (default for voltage is 70 Vrms and for current is 5 Arms)

#### **4.3.1.3 Amplifier Settings (needs to be set according to data sheet)**

The following parameters need to be configured to meet the nominal output values:

- Voltage Amplification Factor
- Current Amplification Factor
- Phase shift/delay of the amplifier

#### **4.3.1.4 Test Settings**

User can choose to either run one test, a group of tests or all tests.

Group 1 – Steady State Tests

- Steady Magnitude
- Steady Frequency
- Harmonic Distortion
- Out-of-band interference
- Latency

## Group 2 – Dynamic Tests

- Amplitude Modulation
- Phase Modulation
- Frequency Ramp
- Amplitude Step
- Phase Step

## Non-standard Tests

- Application Test

After choosing the desired settings, the communication between the portable calibrator and the PMU under test has to be established; all information about channel indices has to be gathered and updated in order to start the calibration procedure.

Subsequently, when tests are done, the user will get a notification on the screen and the reports will be generated in a pre-defined folder location.

### **4.3.2 Additional settings for in-service testing and instructions**

For the purpose of in-service PMU testing and evaluation of the entire synchrophasor system as a whole, the Field Calibrator input needs to be connected to the Gold PMU, which references the substation signal source, and test PMU data for analysis and comparison. Multilayer testing of in-service PMUs consists of testing the timing reference, PMU device, communication layer, PDC and the application layer with visualization tools. For each level, separate groups of tests, for which selection options are provided, can be performed.

#### Test Set:

- Timing reference testing
- PMU basic performance test
- PDC test with the communication layer
- Application test with the visualization tools

### **4.4 Implementation Features**

- 19” Rack mount capability
- Portable device
- In-service testing capability
- Periodic maintenance testing capability
- Standardized Type/Design testing capability

- Application testing capability
- PMU testing capability
- PDC testing capability
- Supports GPS/IRIG-B/1PPS
- Graphical User Interface

#### **4.4.1 Hardware Modules**

NI cRIO 9082:

- Controller Type: High Performance
- Number of Slots: 8
- Operating Temperature: 0..55°C
- CPU Clock Frequency: 1.33 GHz
- FPGA: Spartan-6 • Spartan-6 LX150

I/O slots: 6

- NI 9225 (Current Simultaneous Analog Input, 5 Arms, 50 kS/s, 4 Ch Module)

Current input for reference Gold PMU:

- NI 9225 (Voltage Simultaneous Analog Input, 300 Vrms, 50 kS/s, 3 Ch Module)

Voltage input for reference Gold PMU:

- NI 9263 x 2 (Analog Outputs: 4 DIFF • 100000 S/s/ch • 16 bits Measurement Type: Voltage range +-10V)

Output I/O cards for signals generated by portable calibrator: NI 9402 x 2 (Digital I/O: 4 DIO • 20 MHz Counter/Timers: 4 Measurement Type: Digital)

- Used as input for receiving IRIG-B/1 PPS

Digital I/O for control signals:

- NI 9467 (GPS Timestamping and Synchronization Module)

#### **4.5 Use in Testing**

Figure 12 shows the development and its functionality to replay simulated waveforms as well as standardized type tests [2] with respect to the module outputs on the enclosure as a synchronized analog waveform. The graphs in this figure show the 1PPS signal (green) extracted from an IRIG-B signal in sync with two exemplary waveforms for both type and application waveform.

The Field Calibrator is used to fully evaluate a systems performance under predefined situations and test scenarios. An exemplary test setup can be observed in Figure 13. The Field Calibrator as well as the reference PMU (Gold PMU) are connected to an accurate timing source (IRIG-B connection) to ensure synchronous testing. The generated waveforms are distributed to all modules involved in the test circuit (U5 -> U3/U4/U6). As can be seen, for larger networks and test applications the Synchrophasor Comparison is being computed in a separate module (U11) that is capable of consolidating a multitude of synchrophasor data streams tapped at the outputs of the various PMUs and PDCs in the system (ET3 – ET8).

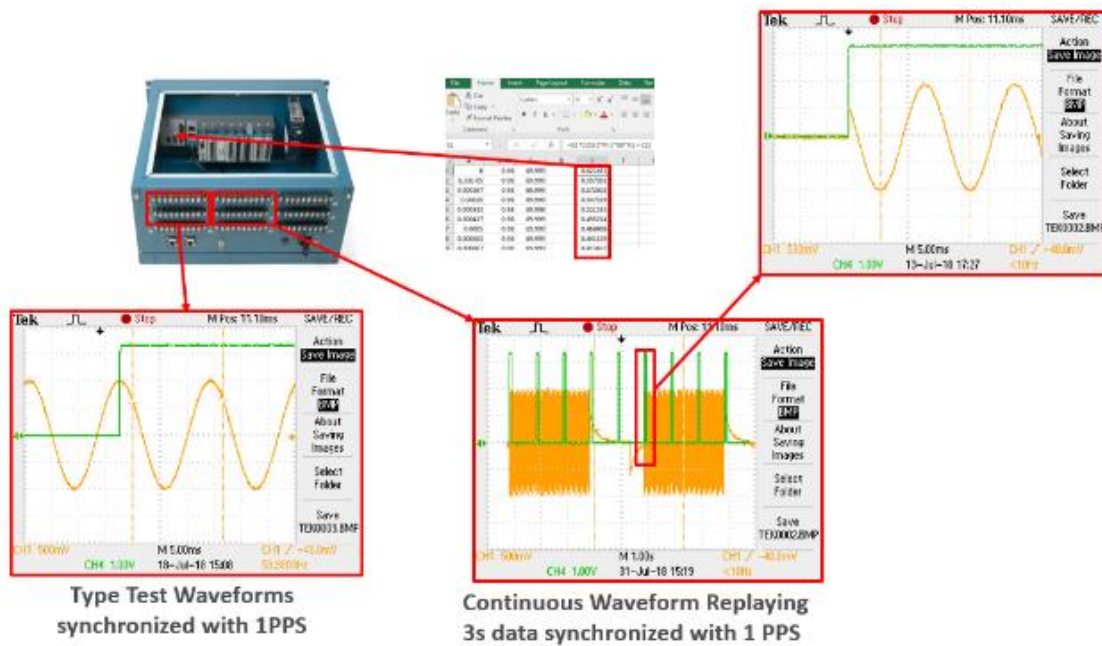


Figure 12. Module representation of TEES development with type/application test waveforms

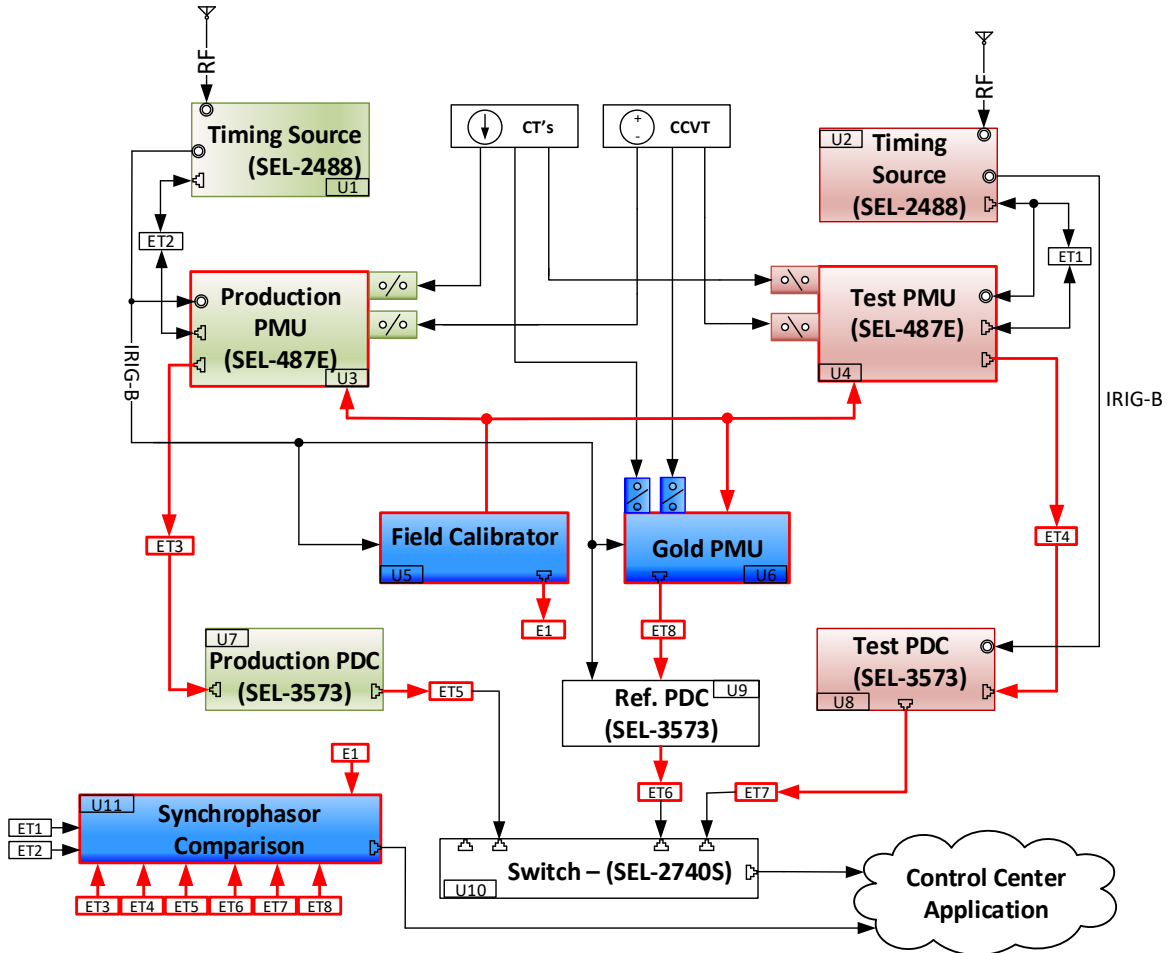


Figure 13. Exemplary test setup for End-to-end testing in synchrophasor applications

## 5. Integration of Gold PMU and In-Service Calibrator

---

### 5.1 Introduction

#### 5.1.1 General

Power system is subjected to faults caused by various reasons such as different weather condition, animal or human contacts, vegetation contacts, etc. Once circuit breakers clear the fault following relays trip command, the fault point must be determined and proper action taken to expedite troubleshooting and minimize repair time [4]. Various fault location methods have been proposed in literature [5]–[11]. Single-end impedance based fault location methods are considered the most conventional scheme [5]–[11]. These methods utilize power frequency component of single-end voltage and (or) current measurements to locate faults on transmission lines. The main advantage of such methods is the simplicity and low cost of implementation. However, their accuracy might be affected by different factors, such as infeed current from remote end, fault resistance, variation of source impedance, loading conditions or fault incidence angle. Several methods were developed using unsynchronized two-end measurements [12]–[16]. In [12], post fault voltage and current phasor measurements are used to locate faults. The method is applicable even if line parameters are unknown. In [13], symmetrical components theory is used to formulate fault location scheme.

The method proposed in [14] is based on voltage magnitude at fault point and does not require phase angles. In [17], a time-domain method based on synchronized sampling of the voltage and current data from the two ends of the line is proposed. The line model equations are then solved to build the voltage and current profiles to accurately locate the fault. Improving the line model considering distributed line parameters led to more accurate results in [18]. In [19], the method proposed in [18] was modified to reduce the sampling rate from 20 kHz to 1 kHz. The main advantage of the mentioned two-end fault location methods comparing to single-end methods is their higher accuracy in locating faults. However, availability of measurements through the entire network might not be feasible due to the cost and installation concerns for foreseeable future [4]. Hence, a sparse measurement-based fault location method could be more practical due to its low implementation cost. In recent decades, development of phasor measurement units (PMUs) introduced various synchrophasor based methods [20]–[23]. In [20], [21], Clarke transformation is applied to the synchronized voltage and current phasors aligned with a discrete Fourier transform-based algorithm to calculate the location of fault.

Another fault detection/location technique is presented in [22], [23] with consideration of arcing fault discrimination based on synchronized fundamental phasor measurements. In [24], a bus-impedance matrix was utilized to calculate fault point with access to limited synchronized measurements at two remote buses in the network. Several methods utilize electromagnetic transient propagation in power system and are known as travelling wave based methods [25]–[28]. The method proposed in [25], [26] is based on measuring time of arrival (ToA) of electromagnetic traveling waves which propagate from the fault point to sparsely located synchronized measurement devices. Then, an optimization method is applied to calculate the location of fault. In [27], a wide area traveling wave-based method is proposed which determines faulty line and distance to fault by analyzing the traveling wave propagation times using the extended double end method. In [28], a traveling wave principle along with two graph theory-based lemmas is deployed

to sectionalize power system and locate faults within suspected sections. Despite the high accuracy of travelling wave-based methods, they require measurement device with high sampling rate to capture electromagnetic transient which increase cost of implementation.

Power system experiences electromechanical oscillations after fault clearing. The oscillation propagates through the system with certain speed based on network parameter, generator inertia etc. The time of arrival of oscillations at different measurement buses can be used to locate faults. A brief theory on electromechanical oscillation propagation has been given below.

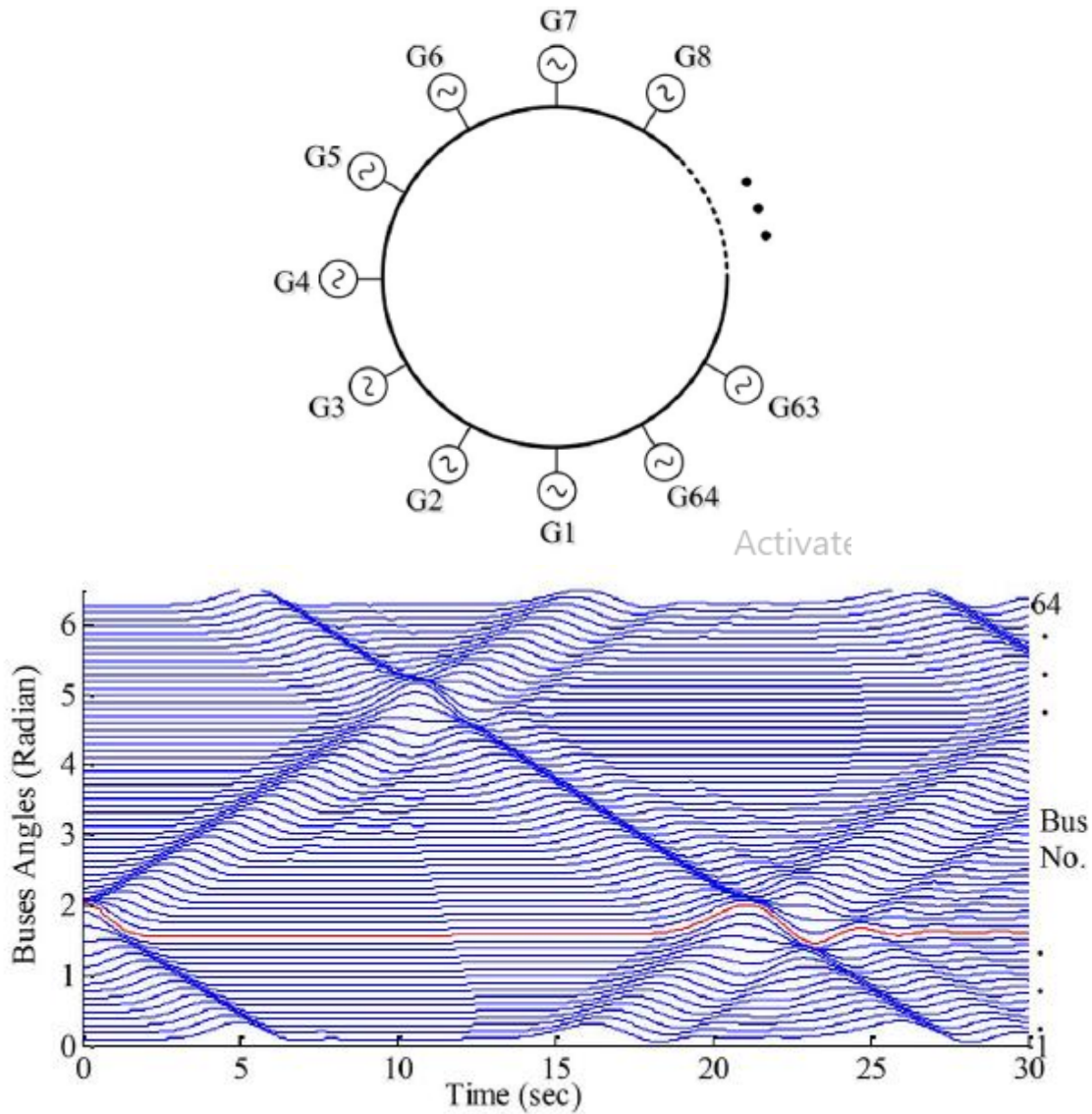


Figure 14. Understanding electromechanical-wave propagation. (a) 64-generator ring system, (b) Bus angle modulation following a fault at bus 16.

### 5.1.2 Continuum Modeling of Power System

#### A. Electromechanical-Wave Propagation Phenomena

When a disturbance occurs on a transmission line, electrical power flow changes in the network. This leads to a mismatch between electrical and mechanical torque of generators located in the vicinity. Therefore, each generator rotor angle changes to compensate the mismatch. Following the generators' rotor angle oscillations, the adjacent buses also encounter changes in their generators' rotor angle which again causes a mismatch in the electrical torque of the adjacent generators. In this fashion, the oscillation known as the electromechanical-wave propagation is “seen” throughout the entire network. Electromechanical oscillations could be detected by monitoring phasor angle of bus voltages and characterized with much lower frequency (0.1–10.0 Hz) than electromagnetic transients (kHz) [29]. To illustrate the concept, a simple power-system model in the form of a ring is used. Figure 14(a) shows the 64-generator ring system introduced in [29], which comprises 64 identical serially connected generators through identical transmission lines, forming a ring. The initial bus angles are evenly distributed from 0 to 360 degrees by steps equal to degrees. Due to homogeneity and ring shape of the 64-bus system, it is well-suited to study basic aspects of electromechanical-wave propagation phenomena. Figure 14(b) shows the phasor angle of 64-buses (in radian) with respect to time of a given disturbance occurring at bus 16 at. Following the change in the angle of bus 16 shown by the dashed line in Figure 14(b), the other generators react in a similar fashion, but with a certain time delay. Plotting all the bus angles together, this time delay can be represented as a wave modulated on buses' phasor angles, which travels away from the disturbance source into the network at a finite speed.

#### B. Continuum Modeling

Applying differential algebraic equations (DAEs) is the conventional way of modeling electromechanical-wave propagation in power system. Due to complexity, this approach could be time consuming and the result would be hard to analyze for large networks. Therefore, researchers introduced a much simpler method which embeds the effect of electromechanical wave propagation into power system behavior [29]–[33].

The so called continuum model, considers power system with spatially distributed parameters. The continuum model is based on applying partial differential equations (PDEs) describing the power systems to the infinitesimal element distributed along the power system. Due to generators rotor inertia, the timescale of electromechanical oscillations is large compared to the power system frequency. Therefore, the variables in continuum model can be considered as phasor parameters [33].

In the context of continuum modeling, any point in a power system could be represented by the incremental system as shown in Figure 15.

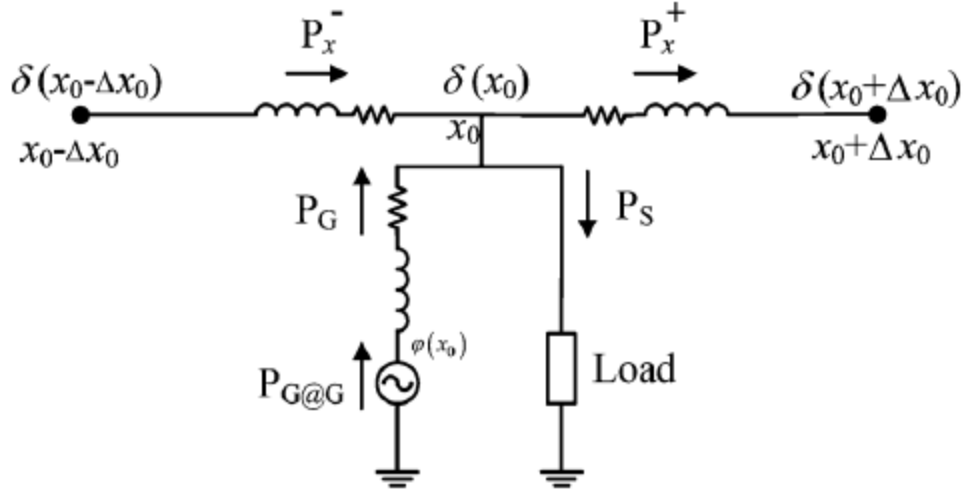


Figure 15. Incremental system used for continuum modeling of system

The model allows for representation of lines with different per-unit impedances, shunt reactances, generators and loads. The flexibility of the incremental model allows any arbitrary network topology to be modeled with continuum approach. Following is a brief summary of continuum formulation.

After several simplifications, the power flow and the swing equation for the continuum model can be obtained as:

$$G \left( \frac{\partial \delta(x_0)}{\partial x} \right)^2 - \frac{B \partial^2 \delta(x_0)}{\partial x^2} = G_{int} [\cos(\delta(x_0) - \varphi(x_0)) - 1] - B_{int} \sin(\delta(x_0) - \varphi(x_0)) - G_s \quad (1)$$

$$m(x_0) \frac{\partial^2 \varphi(x_0, t)}{\partial t^2} + d(x_0) \frac{\partial \varphi(x_0, t)}{\partial t} = P_m(x_0) + B_{int} \sin(\delta(x_0) - \varphi(x_0)) - G_{int} [1 - \cos(\delta(x_0) - \varphi(x_0))] \quad (2)$$

Where  $G, B, m, P_m$  represent the conductance, susceptance, inertia and the mechanical power of elementary length.

## 5.2 Design Specification

### 5.2.1 Functional Requirement

- The simulation model, used for generating offline fault data base, should accurately represent the system and the operating condition during faults.
- Accurate phasors of voltage and angle from different buses in the network

## 5.3 Implementation Features

### 5.3.1 IPC Model Calibration

The purpose of this task is to calibrate the model of Idaho Power Company power system data with field measurements. The detailed descriptions of the field measurement and the validation of the simulation model is given below:

**Field Measurement:** The measurements were recorded during a L-G fault on a series compensated line Hemingway (HMWY) – Midpoint (MPSN). Recording from the SEL relay (400 samples/s) and the DFR (12000 samples/s) were collected in COMTRADE ASCII 2005 format. The fault location and the midpoint substation configuration are shown in Figure 16.

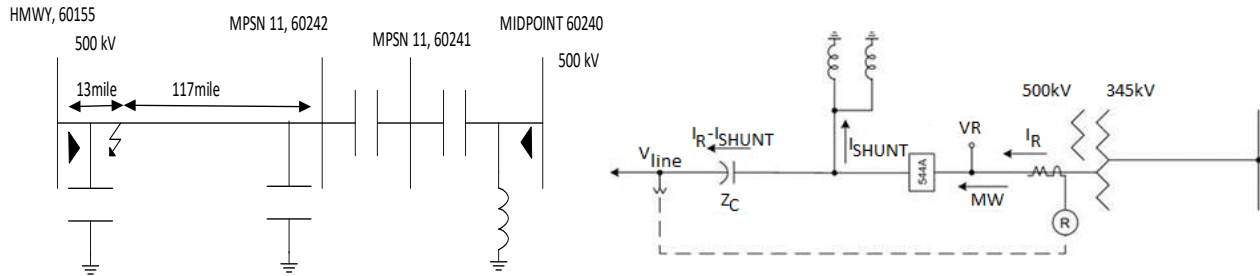


Figure 16. Fault location and the configuration of midpoint substation

**Simplification the IPC Model:** Original model collected from IPC was in PSS/E format which was obtained by converting the system model in PSLF format. There were several simplifications done to the model before it could be used for comparing with field measurements, as follows:

- Removed shunt compensation in few buses to converge power flow,
- Wind generators (only few MW) were converted to conventional generator as no suitable dynamic data was available,
- System external to IPC was considered classical model while detail modelling of IPC was retained,
- Net negative and zero sequence impedances were considered as equal and 1.5 times of positive sequence impedance.

**Model Calibration:** As PSS/E can provide only positive sequence measurement, positive sequence currents were computed from the SEL relay measurements using DFT. The comparison is shown Figure 17.

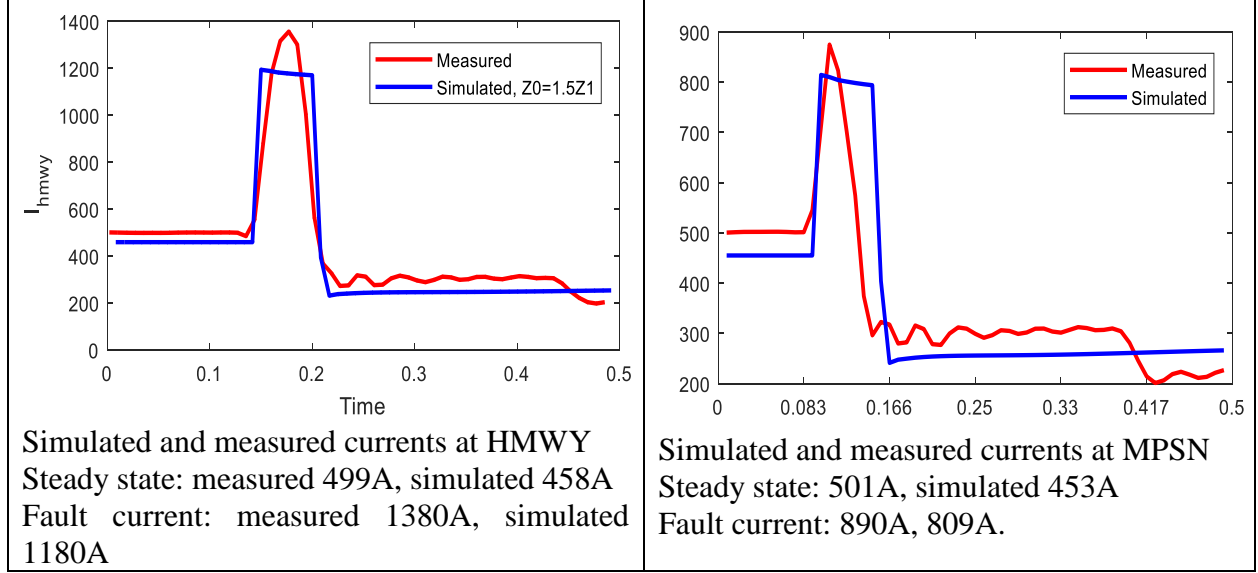


Figure 17. Comparison between measured and simulated results

The difference between measured and simulated waveforms may be because of a) difference in operating condition, b) error in zero sequence impedance, c) smoothing effect of DFT in measured current, d) different fault clearing instances at two ends, e) neglecting L-C transients, sub-synchronous resonance (25 Hz oscillations in measured waveforms) in simulation in PSS/E.

### 5.3.2 Implementation of Fault Location Algorithm

The method works on the basic principle that electromechanical oscillations propagate in power system with certain speed depending on the generator inertia and line reactance. Time of arrival of oscillation at a location may be approximated using continuum modeling,  $toa = \frac{distance}{velocity} = \frac{d}{\sqrt{\frac{\omega}{2h|z|}}}$

second, where  $d$ =distance from the fault location in mile,  $\omega = 377 \text{ rad/s}$ ,  $h = \text{inertia/mile}$ ,  $z = \text{line reactance per mile}$ . A decision tree is trained with four predictors ( $v, \theta, \dot{\theta}$  and  $\ddot{\theta}$ ) where  $v = \text{bus voltage}$ ,  $\theta = \text{bus angle}$ . Calculated  $toa$  as per the equation above is used for the target value in the decision tree training. When any fault occurs a 3second window is selected starting from one second before the fault and ( $v, \theta, \dot{\theta}$  and  $\ddot{\theta}$ ) are computed. This is used in the trained decision tree to measure the  $toa$  of the oscillations. For each measurement locations (3 buses considered here), separate decision tree is used.

Minimum difference between measured  $toa$  and calculated  $toa$  indicates the fault location. It can be obtained with binary search method as shown in Figure 18.

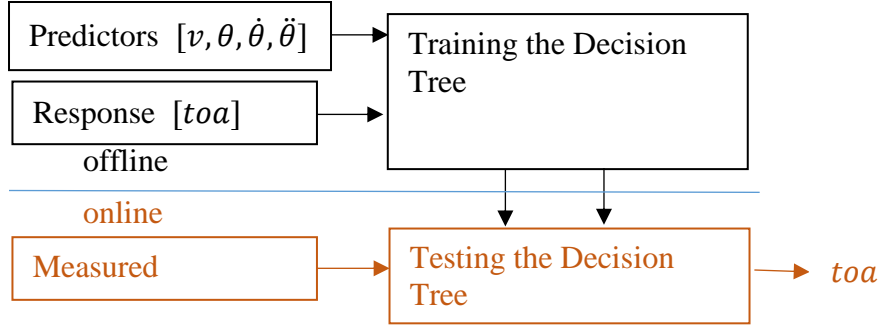


Figure 18. Block diagram for binary search method

The IPC Test System one-line diagram and parameters are given in Figure 19.

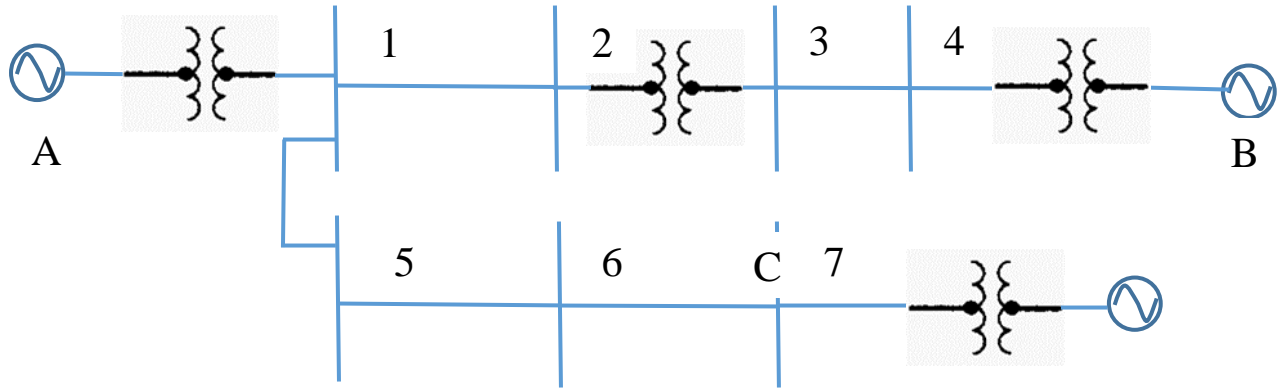


Figure 19. One-line diagram for IPC test system

Original bus number as per PSS/E is given within bracket as follows:

From Bus	To Bus	Branch number	Branch Data
1 (60215)	2 (60250)	1	$0.0481+j0.1518$
2 (60250)	3 (61805)	2	$0.00667+j0.07303$
3 (61805)	4 (61800)	3	$0.036818+j0.109717$
1 (60215)	5 (61223)	4	$0.0481+j0.1518$
5 (61223)	6 (60225)	5	$0.00014+j0.00117$
6 (60225)	7 (60040)	6	$0.00198+j0.01138$

Inertia of generators is 6s for each generator.

Transformer reactance of each generator: A:  $0.0025+j0.1798$ , B:  $0.0147+j0.4363$ , C:  $0.0037+j0.1363$

## 5.4 Use in Testing

The complete connection diagram for the end to end application test has been shown in Figure 20. PSSE has been used to simulate faults and store voltage phasors and angles of different buses. A field calibrator may be used to generate analog waveforms which is used in the PMU to compute

phasors. Phasors are passed through the synchrophasor systems and finally the FL algorithm is run in the control center. The fault location obtained from the WAMS based algorithm can be compared with the actual location obtained from manual inspection or any highly accurate reference fault location algorithm.

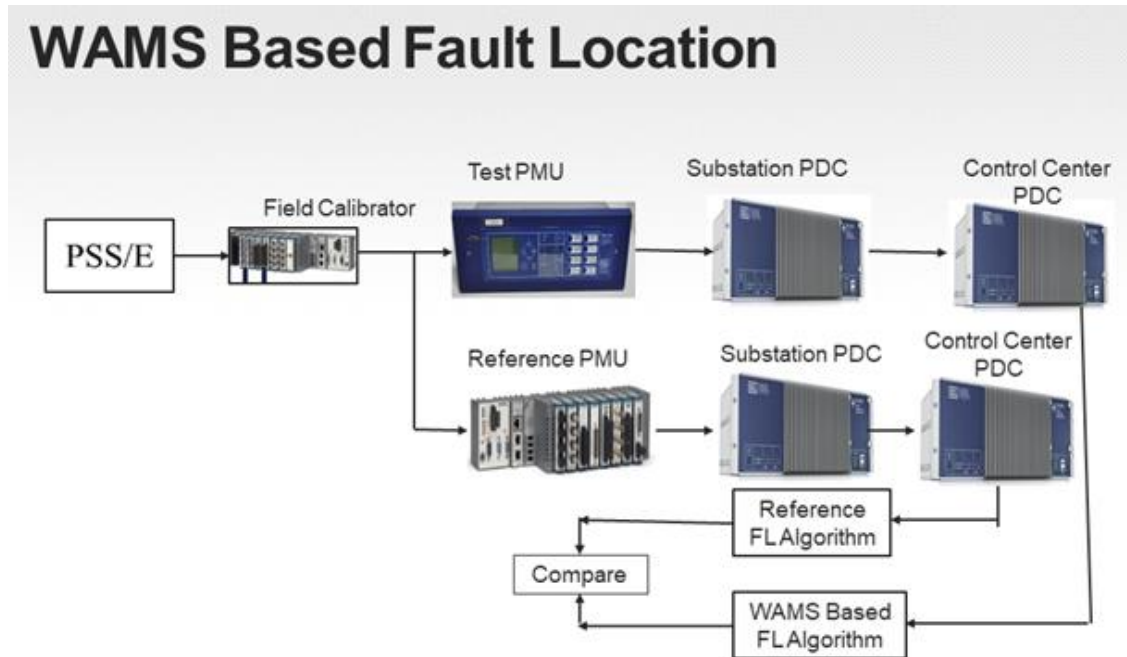


Figure 20. Diagram for End-to-End Application Test

## 6. Conclusions

---

The development of field test devices and protocols for commissioning, acceptance, and in-service testing procedures of synchrophasor devices and systems has been achieved. In particular, the PMU calibration and certification lab is constructed to perform standardized PMU acceptance tests; Field Calibrator performs commissioning and in-service testing on PMUs, PDCs, as well as synchrophasor applications, where Gold PMU is used as a reference synchrophasor source. The performance of Gold PMU is achieved by both robust physical hardware module selection, and accurate Gold PMU algorithms. The notion of nested testing is introduced so that the performance of synchrophasor system is tested device by device, and layer by layer. Then, the evaluation of a particular synchrophasor application, i.e. fault locations, is used as an example of the integration of Gold PMU and in-service field calibrator. The methodology is verified using IPC system data.

## References

---

- [1] "IEEE Standard for Synchrophasor Measurements for Power System, IEEE Std. C37.118.1-2011".
- [2] "IEEE Standard for Synchrophasor Measurements for Power System, Amendment 1: Modification of Selected Performance Requirements, IEEE Std. C37.118.1a-2014".
- [3] "IEEE Synchrophasor Measurement Test Suite Specification (TSS), version 2, 2015".
- [4] C. Qian, M. Kezunovic. "A Power Waveform Classification Method for Adaptive Synchrophasor Estimation," in *IEEE Transactions on Instrumentation and Measurement*, vol. 67, no. 7, pp. 1646-1658, July 2018.
- [5] C. Qian, M. Kezunovic, "Spectral Interpolation for Frequency Measurement at Off-Nominal Frequencies," in *IEEE PES General Meeting*, Chicago IL, July 2017.
- [6] D. Macii, D. Petri and A. Zorat, "Accuracy Analysis and Enhancement of DFT-Based Synchrophasor Estimators in Off-Nominal Conditions," in *IEEE Transactions on Instrumentation and Measurement*, vol. 61, no. 10, pp. 2653-2664, Oct. 2012.
- [7] C. Qian, M. Kezunovic, "Dynamic Synchrophasor Estimation with Modified Hybrid Method.," in *2016 IEEE PES Conference on Innovative Smart Grid Technologies North America*, Minneapolis, MN, September 2016.
- [8] C. Qian, M. Kezunovic, "Synchrophasor Reference Algorithm for PMU Calibration System," in *2016 IEEE PES Transmission & Distribution Conference and Exposition*, Dallas, TX, May 2016.
- [9] Z. Galijasevic and A. Abur, "Fault location using voltage measurements," *IEEE Trans. Power Del.*, vol. 17, no. 2, pp. 441-445, Apr. 2002.
- [10] M. S. Sachdev and M. A. Baribeau, "A new algorithm for digital impedance relays," *IEEE Trans. Power App. Syst.*, vol. PAS-98, no. 6, pp. 2232-2239, Dec. 1979.
- [11] A. A. Girgis, "A new Kalman filtering based digital distance relay," *IEEE Trans. Power App. Syst.*, vol. PAS-101, no. 9, pp. 3471-3480, Sep. 1982.
- [12] T. Kawady and J. Stenzel, "A practical fault location approach for double circuit transmission lines using single end data," *IEEE Trans. Power Del.*, vol. 18, no. 4, pp. 1166-1173, Oct. 2003.
- [13] H. Ha, B. H. Zhang, and Z. L. Lv, "A novel principle of single-ended fault location technique for EHV transmission lines," *IEEE Trans. Power Del.*, vol. 18, no. 4, pp. 1147-1151, Oct. 2003.
- [14] C. E. M. Pereira and L. C. Zanetta, "Fault location in transmission lines using one-terminal post-fault voltage data," *IEEE Trans. Power Del.*, vol. 19, no. 2, pp. 570-575, Apr. 2004.
- [15] Z. Qingchao et al., "Fault location of two-parallel transmission line for non-earth fault using one-terminal data," *IEEE Trans. Power Del.*, vol. 14, no. 3, pp. 863-867, Jul. 1999.
- [16] M. Farshad and J. Sadeh, "Accurate single-phase fault-location method for transmission lines based on k-nearest neighbor algorithm using one-end voltage," *IEEE Trans. Power Del.*, vol. 27, no. 4, pp. 2360-2367, Oct. 2012.
- [17] Y. Liao and S. Elangovan, "Unsynchronized two-terminal transmission- line fault-location without using line parameters," *Proc. Inst. Elect. Eng., Gen. Transm. Distrib.*, vol. 153, no. 6, pp. 639-643, Nov. 2006.
- [18] J. Izykowski et al., "Accurate noniterative fault location algorithm utilizing two-end unsynchronized measurements," *IEEE Trans. Power Del.*, vol. 25, no. 1, pp. 72-80, Jan. 2010.

- [19] E. G. Silveira and C. Pereira, "Transmission line fault location using two-terminal data without time synchronization," *IEEE Trans. Power Del.*, vol. 22, no. 1, pp. 498–499, Feb. 2007.
- [20] M. Davoudi, J. Sadeh, and E. Kamyab, "Parameter-free fault location for transmission lines based on optimization," *IET Gen., Transm. Distrib.*, vol. 9, no. 11, pp. 1061–1068, Aug. 2015.
- [21] M. Davoudi, J. Sadeh, and E. Kamyab, "Time domain fault location on transmission lines using genetic algorithm," in *Proc. 11th Int. Conf. Environment Elect. Eng.*, May 2012, pp. 1087–1092.
- [22] M. Kezunovic and B. Perunicic, "Automated transmission line fault analysis using synchronized sampling at two ends," *IEEE Trans. Power Syst.*, vol. 11, no. 1, pp. 441–447, Feb. 1996.
- [23] A. Gopalakrishnan et al., "Fault location using the distributed parameter transmission line model," *IEEE Trans. Power Del.*, vol. 15, no. 4, pp. 1169–1174, Oct. 2000.
- [24] P. Dutta, A. Esmaeilian, and M. Kezunovic, "Transmission-line fault analysis using synchronized sampling," *IEEE Trans. Power Del.*, vol. 29, no. 2, pp. 942–950, Apr. 2014.
- [25] J. A. Jiang et al., "An adaptive PMU based fault detection/location technique for transmission lines part I: Theory and algorithms," *IEEE Trans. Power Del.*, vol. 15, no. 2, pp. 486–493, Apr. 2000.
- [26] J. A. Jiang et al., "An adaptive PMU based fault detection/location technique for transmission lines. II. PMU implementation and performance evaluation," *IEEE Trans. Power Del.*, vol. 15, no. 4, pp. 1136–1146, Oct. 2000.
- [27] Y. H. Lin et al., "A new PMU-based fault detection/location technique for transmission lines with consideration of arcing fault discrimination— Part I: Theory and algorithms," *IEEE Trans. Power Del.*, vol. 19, no. 4, pp. 1587–1593, Oct. 2004.
- [28] Y. H. Lin et al., "A new PMU-based fault detection/location technique for transmission lines with consideration of arcing fault discrimination—Part I: Theory and algorithms," *IEEE Trans. Power Del.*, vol. 19, no. 4, pp. 1594–1601, Oct. 2004.
- [29] Y. Liao, "Fault location for single-circuit line based on bus-impedance matrix utilizing voltage measurements," *IEEE Trans. Power Del.*, vol. 23, no. 2, pp. 609–617, Apr. 2008.
- [30] M. Korkali, H. Lev-Ari, and A. Abur, "Traveling-wave-based fault location technique for transmission grids via wide-area synchronized voltage measurements," *IEEE Trans. Power Syst.*, vol. 27, no. 2, pp. 1003–1011, May 2012.
- [31] M. Korkali and A. Abur, "Optimal deployment of wide-area synchronized measurements for fault-location observability," *IEEE Trans. Power Syst.*, vol. 28, no. 1, pp. 482–489, Feb. 2013.
- [32] Y. Chen, D. Liu, and B. Xu, "Wide-area traveling wave fault location system based on IEC61850," *IEEE Trans. Smart Grid*, vol. 4, no. 2, pp. 1207–1215, Jun. 2013.
- [33] S. Azizi et al., "A traveling-wave-based methodology for wide-area fault location in multi-terminal DC systems," *IEEE Trans. Power Del.*, vol. 14, no. 3, pp. 863–867, Jul. 1999.
- [34] J. S. Thorp et al., "Electromechanical wave propagation in large electric power systems," *IEEE Trans. Circuits Syst. I, Fundam. Theory Appl.*, vol. 45, no. 6, pp. 614–622, Jun. 1998.
- [35] A. Semlyen, "Analysis of disturbance propagation in power systems based on a homogeneous dynamic model," *IEEE Trans. Power App. Syst.*, vol. PAS-93, no. 2, pp. 676–684, Mar. 1974.

- [36] P. Dersin and A. Levis, "Feasibility sets for steady-state loads in electric power networks," IEEE Trans. Power App. Syst., vol. PAS-101, no. 1, pp. 60–70, Jan. 1982.
- [37] A. J. Arana, "Analysis of electromechanical phenomena in the power-angle domain," Ph.D. dissertation, Elect. Eng. Dept., Virginia Polytechnic Institute and State University, Blacksburg, VA, USA, Dec. 2009.
- [38] M. Parashar et al., "Continuum modeling of electromechanical dynamics in large-scale power systems," IEEE Trans. Circuits Syst. I, Reg. Papers, vol. 51, no. 9, pp. 1848–1858, Sep. 2004.

## **Part II**

### **End-to-End Remote Testing of PMU and RAS**

Anurag K. Srivastava

David Bakken

Param Banerjee

Pratim Kundu

Ren Liu, Graduate Student

Hyojong Lee, Graduate Student

Zhijie Nie, Graduate Student

Alex Askerman, Undergraduate Student

Washington State University

**For information about this project, contact**

Anurag K. Srivastava  
Washington State University  
School of Electrical Engineer and Computer Science  
Pullman, WA 99164  
Phone: 5093352348  
Email: anurag.k.srivastava@wsu.edu

**Power Systems Engineering Research Center**

The Power Systems Engineering Research Center (PSERC) is a multi-university Center conducting research on challenges facing the electric power industry and educating the next generation of power engineers. More information about PSERC can be found at the Center's website: <http://www.pserc.org>.

**For additional information, contact:**

Power Systems Engineering Research Center  
Arizona State University  
527 Engineering Research Center  
Tempe, Arizona 85287-5706  
Phone: 480-965-1643  
Fax: 480-727-2052

**Notice Concerning Copyright Material**

PSERC members are given permission to copy without fee all or part of this publication for internal use if appropriate attribution is given to this document as the source material. This report is available for downloading from the PSERC website.

**© 2018 Washington State University. All rights reserved**

## Table of Contents

1. Introduction .....	1
1.1 Background .....	1
2. PMU Lab development .....	4
2.1 Background .....	4
2.2 Purpose.....	5
2.3 Summary of the Test cases .....	6
2.4 Specification of the Equipment for PMU testing lab .....	7
2.5 Results .....	11
2.6 Summary .....	12
3. PMU Lab testing using the PMU Performance Analyzer .....	13
3.1 Background .....	13
3.2 Required features of PPA .....	13
3.3 Validity Checking .....	14
3.4 Interface Requirements .....	14
3.5 “About” window .....	14
3.6 Pre-Production Splash Screen.....	14
3.7 Test Plan.....	15
3.8 Installation.....	15
3.9 Highlights .....	17
3.10 Test Results .....	18
3.11 Summary .....	19
4. COMTRADE Module .....	20
4.1 Introduction of COMTRADE Module.....	20
4.2 Work Statement of Host Computer VI.....	21
4.3 CompactRIO System and FPGA VI .....	23
4.4 Error Correction by GPS .....	25
4.5 Results .....	26
4.6 Summary .....	29
5. Erkios Middleware Software.....	30
5.1 Erkios software for end-to-end testing .....	30
5.2 Functional Requirements for ERKIOS .....	31

5.3	Validity checking .....	32
5.4	Interface Requirements .....	32
5.5	Security, Availability, Reliability, Recoverability and Business Continuity .....	32
5.6	Maintenance and Support.....	32
5.7	Quality Plan.....	32
5.8	Test Plan.....	33
5.9	Installation.....	33
5.10	Purpose.....	33
5.11	Need for this specification.....	33
5.12	Related Standard .....	33
5.13	Assumptions .....	34
5.14	General System Description.....	34
5.14.1	System Context .....	34
5.14.2	System Environments and Modes .....	34
5.14.3	User Characteristics.....	34
5.14.4	Operational Scenarios .....	34
5.15	Functional Requirements for ERKIOS .....	34
6.	Remote PMU testing .....	36
6.1	Integration of PMU Performance Analyzer and Erkios Software .....	36
6.2	Purpose.....	36
6.3	System Environments and Modes.....	36
6.4	User Characteristics .....	36
6.5	Substation Specification.....	36
6.6	Results.....	38
6.7	Summary .....	39
7.	Remote RAS Testing.....	41
7.1	Introduction .....	41
7.2	Test plans of wind curtailment RAS .....	43
7.3	Idaho Power RAS .....	48
7.4	Summary .....	52
8.	Conclusions .....	53
	Appendix A.....	54
	References.....	63

## List of Figures

Figure 2.1: Parameters for step response .....	5
Figure 2.2a: Test Suite: A software application for testing PMU using NI device. ....	8
Figure 2.2b: Test Suite: A software application for testing PMU using RTDS. ....	9
Figure 2.3: SNR of the “Sine Wave Generator Express VI” block in NI-cRIO platform .....	10
Figure 2.4: Phase angle difference resulted due to the slight difference in frequency. ....	11
Figure 3.1 Installation and results reporting of the PMU performance analyzer.....	17
Figure 3.2: PMU Testing Lab .....	18
Figure 3.3: Magnitude Change for balanced system .....	19
Figure 4.1: COMTRADE Module Algorithm Architecture .....	20
Figure 4.2: DMA FIFO Working Diagram.....	21
Figure 4.3: Local Host VI Example.....	21
Figure 4.4: Host VI Flowchart .....	22
Figure 4.5: Assembled compactRIO System .....	23
Figure 4.6: FPGA VI Flowchart .....	24
Figure 4.7: FPGA VI Block Diagram .....	24
Figure 4.8: GPS Correction Algorithm.....	26
Figure 4.9: Spectral estimation of fundamental component .....	28
Figure 4.10 Spectral estimation of harmonic frequencies .....	28
Figure 5.1: Erkios architecture for remote resting .....	31
Figure 5.2: ERKIOS Middleware based Remote Testing of PMU and RAS .....	35
Figure 6.1: ERKIOS Architecture.....	37
Figure 6.2: FILE command in TELNET session .....	39
Figure 6.3: SCP command to transfer configuration file using SSH session .....	39
Figure 6.4: File command to send a configuration file from LTS to target PMU .....	39
Figure 7.1: Interfacing Architecture with RAS at Substation.....	42
Figure 7.2: Real-Time Implementation Testbed.....	44
Figure 7.3: One Line Diagram of IEEE 14-Bus Test System with 3 Wind Farms.....	45
Figure 7.4: OPAL-RT SLD Idaho RAS geographic area involved .....	49
Figure 7.5: Power flow in the monitored line .....	49
Figure 7.6: 345kV line outage .....	50
Figure 7.7: Monitored power flow during line outage.....	50

Figure 7.8: RAS control action by adding shunt capacitor during line outage.....	51
Figure 7.9: Power flow after RAS control action .....	51
Figure A1.1: PPA test for balanced system with angle change. ....	62

## **List of Tables**

Table 1.1: Summary of PMU testing results.....	11
Table 7.1: Facts on Wind Curtailment Issues .....	43
Table 7.2: Test Plan Objectives of Wind Curtailment Ras .....	44
Table 7.3 Descriptions of Base Case .....	45

# 1. Introduction

---

## 1.1 Background

The critical component in Wide Area Measurement System (WAMS) is the Phasor Measurement Unit (PMU), which converts the point on wave signal of voltage and current to corresponding magnitude and phase angle. The magnitude and phase angle of voltage and current are time stamped using Global Positioning System (GPS) synchronized clock. The phase angle of voltage and current at a bus or a line are evaluated with reference to GPS synchronized sinusoid. The time stamped magnitude and angle (collectively called phasors) of voltage and current are transmitted to successive hierarchical archival mechanism using Phasor Data Concentrator (PDC), super PDC and control center PDC, where the end application retrieves the phasor for computation [1-4].

The PMUs installed in the field are subject to drift in performance, inaccurate wiring due to scheduled maintenance in the substation and inconsistent anomalies in settings due to human interaction. Hence, PMUs installed in the field are required to be calibrated in a scheduled manner (every 2 years or after major substation upgrade suggested). The extension of the local PMU testing in the lab is performing calibration and testing of PMUs installed at the substation. The task of uninstalling all the PMUs and transporting them to a PMU testing lab, performing testing and reinstall them in the field, discourage utilities to perform regular calibration. It is Imperative to develop a framework for testing the PMUs installed in a substation remotely for which tools are being developed in this work.

The synchrophasor application or wide area application mainly undergoes three stages before field deployment. The first stage is the algorithm development based on Differential and Algebraic Equation (DAE) model of the power system. In this stage, the validation of the application is performed using offline simulators. The offline simulators provide same simulation time increment for both the system and the controller model in the same simulation framework. The second stage is real-time testing and validation using hardware in the loop (HIL) test bed. The application or the controller implemented in hardware setup, cannot be validated using offline simulators. The simulation time of the system model in the offline simulators are not synchronized with the actual time used by the hardware controller, resulting in time skew of the controller output to the system or system response to the controller. The real-time simulators using HIL test bed simulate the test system in real-time and synchronization with the actual time of the hardware controller is guaranteed. The real-time HIL test bed emulated input output equivalent of the true power system. The synchrophasor based control application consists of a large number of interacting components in the power system network. The overall application can degrade the system performance, even if one or more devices are individually tested and validated. Even each device may be validated satisfactorily, there are chances that the system consisting of one or more devices may fail to achieve the desired objective. Validation and testing of the application with one or more devices as a single entity are also desirable before field deployment. The requirement of end-to-end testing of such control application is discussed in this chapter. The Remedial Action Schemes (RAS) are considered as an example synchrophasor based control application for performing end-to-end testing. The requirements of a RAS test bed are enlisted and architecture of middleware called Erkios for RAS testing developed at WSU. The developed testbed is evaluated for single substation and multiple substations RAS.

Validation and conformance testing of PMU performed at South California Edison (SCE) using the PMU Performance Analyzer (PPA), a software tool developed at WSU is presented as a part of device testing. The specification of testing equipment and architecture of a testbed for the PMU testing and associated applications is also presented in this chapter. Validation of PMU based anomaly detection and PMU based event detection are the two monitoring application presented in this chapter.

The phasors estimated using different PMUs might have variation in accuracy depending on the type of signal. This variation affects the performance of WAMS based monitoring and control applications running in the control centers. In view of this, a set of test scenarios and error metrics are enlisted in IEEE standard C37.118.1 for synchrophasors [3], amended in C37.118.1a.2014. PMU vendors are expected to provide compliance testing of their PMUs accuracy before deploying them in the field. However, PMU testing is carried out by limited agencies as it is expensive and requires a significant amount of manual labor.

Remedial Action Scheme (RAS) is a special control action that minimizes the impact of contingencies that cannot be constrained in time with normal protection and control devices. They are typically designed to stop events that would lead to cascading effects and cause a major blackout. The Western Electricity Coordinating Council (WECC) and North American Electric Reliability Corporation (NERC) have adopted certain standards for implementation, operation and performance of RAS. The standards are listed for various aspects like RAS logic, hardware involved, arming, detection and initiating devices, logic processing, transfer trip equipment, test switches, etc. Based on these standards, the following aspects of the RAS and standard have to be incorporated into the real time testbed to emulate real world scenario.

1. **Maximum Allowable Time:** The response time depends basically on the type of scenario. For angular stability, short-term voltage stability and other similar problems, the response time should be from a few cycles to a second. For slow stability problems, the response time can be up to several seconds. For thermal overloading of transmission lines, the response time can range from several seconds to minutes based on the line rating and operating state. The testbed should make sure that the delay caused by the test process and test network is not included in the evaluation. Further, the testing should also note the fact that the time taken for the actuator to react is not being included in the process. The RAS system could include more than one utility and so the response time for the action can includes the time taken to communicate between different utilities. To handle this, issue the NERC and WECC standards clearly state the starting point to evaluate the performance of the RAS.
2. **Communication Channels:** The standards state that the requirements should meet the "Communication Systems Performance Guide for Protective Relaying Applications" and "Critical Communications Circuits-Guidelines for Design". The main requirement is that the scheme logic should be designed so that the loss of the channel, noise or other failure will not result in a false operation of the scheme. This necessitates the need for a similar communication design in the testbed.
3. **Cyber Security:** The NERC adopted the standards CIP-002-1 through CIP-009-1 to address both physical and electronic security for critical assets. Erkios should abide these standards when doing an end-to-end in-field testing

4. Redundancy: This is a very important standard for implementing RAS as it addresses failure and maintenance issues. The WECC standard illustrates all scenarios and requirements in depth. The standard states that, except for a few components like substation batteries, PT/CTs (potential transformer/current transformer), breaker, and communication towers, all other equipment involved in RAS implementation should be redundant and especially the RAS logic. Also, the standard states that any mis-operation of RAS should not have an adverse effect on the power grid at the system level.

Results demonstrate that testing and validation of synchrophasor devices and applications is an iterative process to keep improving the performance of devices and applications involving all the stakeholders before the field deployment and even after field deployments for maintenance.

The mentioned tools will be demonstrated on synchrophasor WAMPAC solutions, but the mentioned test protocols and equipment/software will be made available in a modular design that can be utilized for a full evaluation and testing of any mission-critical systems including SPS and EMS. The testbeds are:

- Synchrophasor system
- EMS/SCADA
- SPS/ RAS for a given application

The testbed should resemble actual system displacement where the measurement equipment may be in substations, data concentrators in a control center, and displays at ISOs and/or TOs, and everything is connected through a communication network.

## 2. PMU Lab development

---

### 2.1 Background

Large deployment of PMUs in the field mandates that they are tested for compliance with IEEE TSS. The PMUs are tested for different parameters subject to different testing scenario for voltage and current. The PMU testing lab aims to provide all the necessary hardware and software infrastructure for carrying out the performance evaluation of PMUs under test. The Real Time Digital Simulator from RTDS is used for generating the time stamped analog signals which accurately follow the test cases mentioned in IEEE TSS. The RSCAD model controls the analog signal generation by RTDS and transmits the GPS time stamp of the signal events to the PMU Performance Analyzer (PPA) software. The PPA reconstructs the true value of the phasor for comparing with the PMU phasors using the GPS time stamps. The analog signals generated by the RTDS are amplified using voltage and current amplifiers and given to the PMU under test. The PMU under test estimate the time stamped voltage and current phasors using the GPS clock for the amplified signal given as input. The time stamped phasors from the PMU are archived by the Phasor Data Concentrator (PDC) and fed to the PPA for comparison with the time stamped true phasor. The PPA generates a detailed report for all the test cases performed by the user.

The test scenario listed requires generation of sinusoidal test signal with specific values of amplitude, frequency and harmonics. The signal generated by the test equipment needs to be validated for parameter accuracy before performing PMU testing using those signals. In this work, PMU testing using low cost NI-cRIO is proposed. The investigation demonstrates that the built-in signal generation using Labview is not suitable for PMU testing application.

The IEEE standard for synchrophasors mentions Total Vector Error (TVE) for comparing the accuracy of PMUs from different vendors. The TVE is the vector difference of the estimated phasor and the actual phasor, expressed as the percentage of the actual phasor. Apart from TVE, several other error metrics are also used for compliance testing of PMU. These include Frequency Error (FE) and Rate of Change of Frequency Error (RFE) [5-7].

The static test scenario mentioned in includes off-nominal frequency, static variation in magnitude and phase, and harmonic distortion along with out of band interference. The synchrophasor standard C37.118.1 mention different sets of tests for P and M class PMUs. The P- class PMUs utilize a shorter window length (in the range of one or two cycles) and provide less filtering of the phasors. P class PMUs are typically used for faster operation with limited accuracy of the phasor measurements during dynamic and transients. The M- class PMUs uses larger data window and larger filters to eliminate aliased signal from the fundamental component and, hence, out of band interference test is required to be performed for M class PMUs. To filter out interference signals from the fundamental, the required length of the data window is typically greater than 5 cycles of the fundamental component, which results in larger reporting delays but more accurate phasor measurements. The Frequency Error (FE) and Rate of Change of Frequency Error (RFE) are the additional performance criteria mentioned in this standard for the performance evaluation of the PMUs. The dynamic signal variation added for testing the PMUs are amplitude and phase modulation, frequency ramp and step change of amplitude and phase. The response time, delay time and overshoot for a typical step response test case are shown in Figure 2.1. The maximum

TVE specified for different test cases includes a summation of time synchronization error, instrumentation error and processing error. The response time of FE and RFE for the PMUs of different classes are also separately specified for each of the test cases in the standard [8, 9].

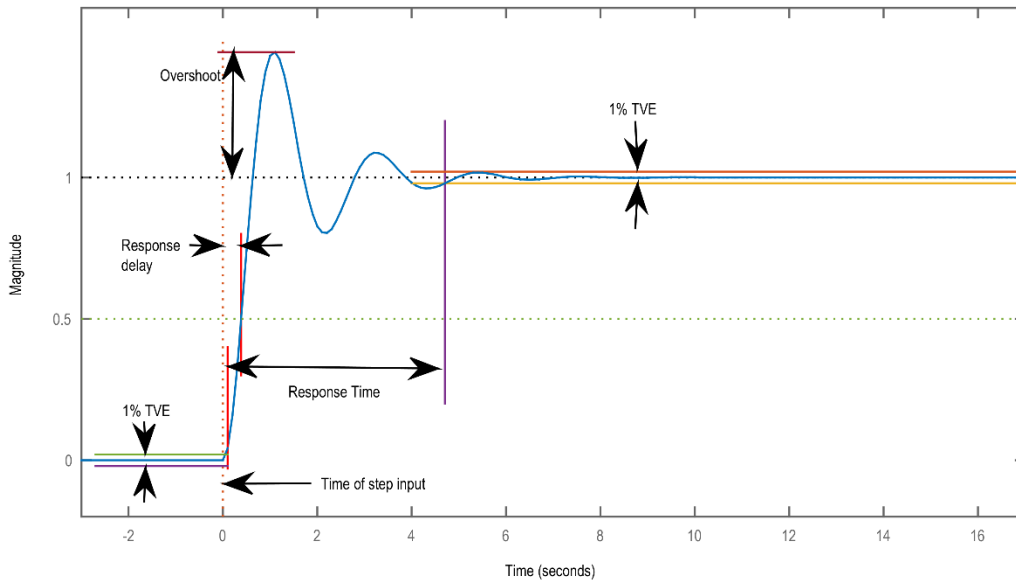


Figure 2.1 Parameters for step response

The IEEE synchrophasor standard was further amended in C37.118.1a.2014, in which the RFE values for most of the test cases are revised. The oscillation test signal, which was previously carried out by using a signal having joint amplitude and phase oscillation, has been changed to two separate signals for the amplitude and phase oscillations in the revised version of the standard. The reporting latency of the M- class PMUs has also been increased in the revised version of the standard.

The PMU estimates the magnitude and angle of the voltage and current signal samples buffered for a window length. The PMU uses the GPS time stamp at the center of the data window to report the magnitude and angle. The true value of phasor at the center of the data window is required to report the accuracy of the estimated phasor by the PMU. The magnitude and angle of the voltage and current signal mandated for PMU testing, may be constant with respect to time for static test cases or may be a simple function of time for dynamic test cases. In view of this, the PMU testing setup should have mechanism to obtain the GPS time and establish the true value of magnitude and phase, which may be dependent on GPS time stamp, particularly in the dynamic test cases. This specification is for testing Phasor Measurement Unit (PMU) according to IEEE TSS. It describes the specification of equipment required for setting up a PMU testing lab.

## 2.2 Purpose

The testing procedure of PMU for different static and dynamic scenarios is presented in this specification document. The PMU under test is given analog input of voltage and current with different parameters. The phasor outputs of the PMU are compared with the true phasors to obtain

different metrics and check for compliance with the limits mentioned in the IEEE C37.118.1-2011 standard.

## **2.3 Summary of the Test cases**

The IEEE TSS specifies the detail of the testing procedure for different test cases carried out for testing a Phasor Measurement Unit (PMU).

The procedure for PMU testing for magnitude range test:

- a) Start the voltage and current at a lower magnitude at a nominal frequency for 5sec.
- b) Increase the input magnitudes by 10% of the nominal value and wait for 5sec.
- c) Repeat step 2 till the upper magnitude limit is reached.

The procedure for PMU testing for frequency range test:

- a) Start the voltage and current at rated magnitude at the lower frequency limit for 5sec.
- b) Increase the input frequency by 0.1Hz of the nominal value and wait for 5sec.
- c) Repeat step 2 till the upper frequency limit is reached.

The procedure for PMU testing for harmonic distortion test:

- a) Start the voltage and current at rated magnitude with 1% (for P Class) or 10% (for M Class) second harmonic at rated frequency for 5sec.
- b) Increase the harmonic number by 1 and wait for 5sec.
- c) Repeat step 2 till the upper harmonic limit is reached.

The procedure for PMU testing for out of band interfering test:

- a) Start the voltage and current at rated magnitude at rated frequency with 10% rated magnitude of the first lower frequency limit of interfering signal for 5sec.
- b) Increase the interfering signal frequency in exponential steps and wait for 5sec.
- c) Repeat step 2 till the interfering signal frequency reaches the first upper out of band limit.
- d) Change the interfering signal frequency to second lowest out of band limit and wait for 5sec.
- e) Increase the interfering signal frequency in exponential steps and wait for 5sec.
- f) Repeat step 5 till the interfering signal frequency reaches the second upper out of band limit.
- g) Repeat steps 1-6 for input signal frequency at a nominal frequency plus and minus 10% of the PMU reporting rate divided by two.

The procedure for PMU testing for step change of magnitude and phase test:

- a) Start the voltage and current at rated magnitude and phase at a nominal frequency for 5sec.

- b) The voltage and current magnitude are changed to +10% and -10% of the initial value and remain for 1 sec.
- c) The voltage and current magnitude are changed to nominal value after 1 sec.
- d) The step 2 and 3 are repeated 10 times with the starting of the step shifted by PMU reporting time interval divided by ten w.r.t to the first step instant.
- e) The steps 1-4 are repeated for +10deg and -10deg phase change keeping the magnitude of rated value.

The procedure for PMU testing of positive and negative frequency ramp test:

- a) Start the voltage and current at rated magnitude at the lower frequency limit for 5sec.
- b) The frequency of the voltage and current are changed from the lower limit to the upper limit at 1Hz/s.
- c) Wait for 5sec at the upper frequency limit
- d) Decrease the frequency from the upper limit to lower frequency limit at -1Hz/s.

The procedure for PMU testing for AM, PM and Joint AM-PM test:

- a) Start the voltage and current with a modulation magnitude of 10% of nominal and modulation frequency of 0.1Hz for 5sec.
- b) Increase the modulation frequency of 0.2Hz and wait for 5sec.
- c) Repeat step 2 till the upper modulation frequency limit is reached.
- d) Repeat steps 1-3 for phase modulation keeping the magnitude of rated value.

Repeat steps 1-3 for combined magnitude and phase modulation.

## **2.4 Specification of the Equipment for PMU testing lab**

Signal source: The PMU should be given input from a programmable voltage and current signal source.

- a) The Signal source should have at least 1 three phase output for voltage and 1 three phase output for the current.
- b) The voltage magnitude range of the Signal source should be in the range of 12V to 600V.
- c) The current magnitude range of the Signal source should be in the range of 1A to 15A.
- d) The Signal source should generate the fundamental signal frequency from 45Hz to 65Hz.
- e) The magnitude of the voltage and current signal should be controllable using mathematical functions like level shifter, trigonometric functions and algebraic equations.
- f) The phase of the voltage and current signal should be controllable using mathematical functions like level shifter, trigonometric functions and algebraic equations.

- g) The Signal Source should also be able to inject at least one harmonics with 10% of the rated voltage and current magnitude. The single harmonic frequency should be variable from 100Hz to 3000Hz.
- h) The Signal source should be controllable at required instances of the GPS pulses.

GPS time source: The time input to the PMU and the Signal source.

- a) The GPS time source should be obtained from a GPS antenna.
- b) The option to generate 1PPS, IRIG-B through copper or fiber should be present in the GPS clock receiver.

PMU measurement receiver: The Phasor Data Concentrator (PDC) is typically used for archiving the C37.118 phasor data from a PMU

- a) The PDC should be configurable to receive C37.118 phasor data from Ethernet port or Serial port.
- b) The PDC should have sufficient memory to archive three phase voltage, current, frequency and rate of change of frequency data.
- c) The PDC should be able to export the archived phasor data in computer processing data file like .xlsx or .csv files.

Ethernet Switch: Connecting PMU, PDC and test report generator.

Calibrator: PMU are designed to calibrate before commissioning.

- a) The calibrator should be able to remove any magnitude error in the reading of the PMU at rated voltage, current, and frequency.
- b) The calibrator should be able to remove any angle error in the reading of the PMU at rated voltage, current, and frequency.

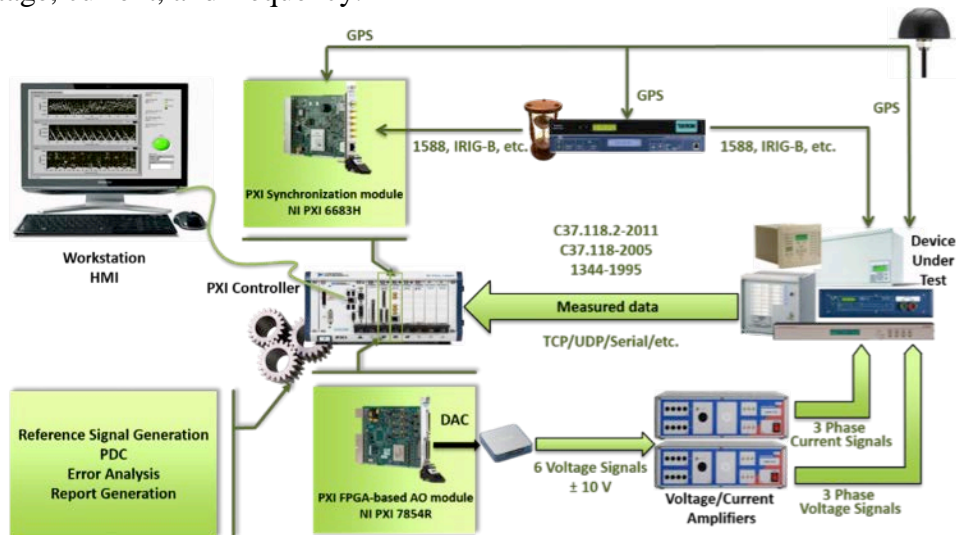


Figure 2.2a Test Suite: A software application for testing PMU using NI device.

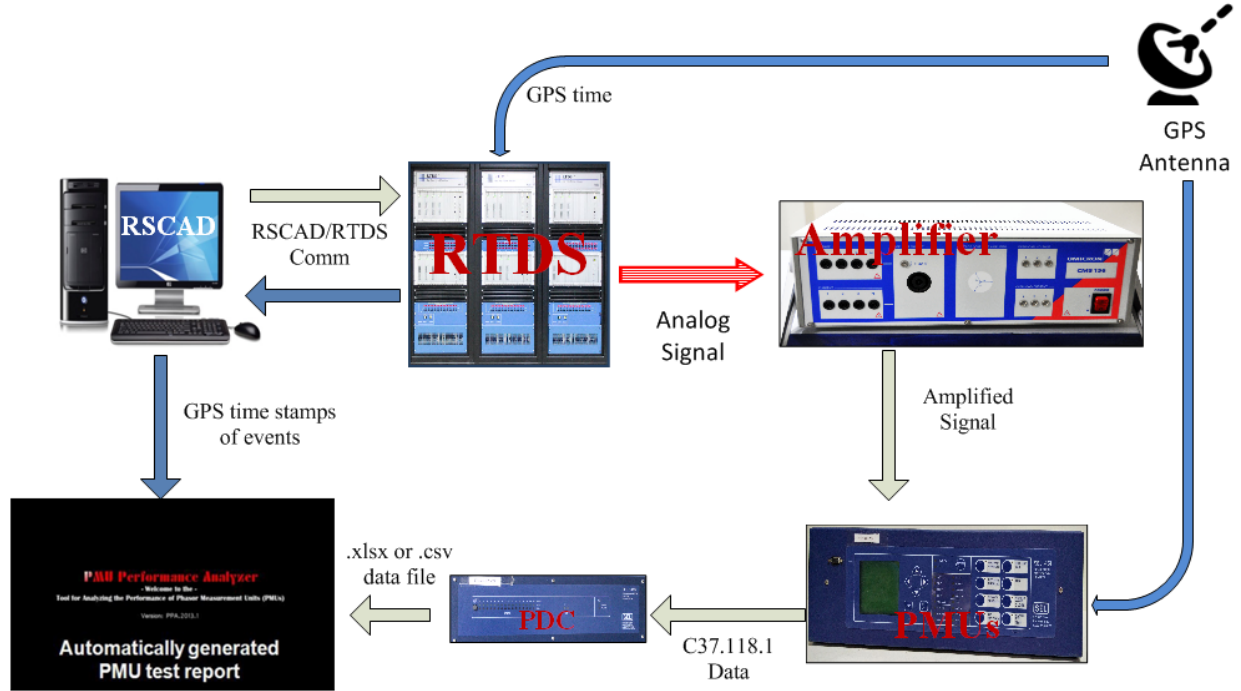


Figure 2.2b. Test Suite: A software application for testing PMU using RTDS.

The PMU testing lab development involves the implementation procedure for PMU testing mentioned in IEEE TSS. The list of equipment required for PMU testing is decided based on the previous document “Review of the IEEE TSS test plan requirements and lab specification requirements”. The different scenario mentioned in the IEEE TSS for PMU testing are required to be implemented in RSCAD/RTDS for generating the analog test signal having changing parameters at known GPS time stamps. The test PMU is to be put in a setup consisting of RTDS, signal amplifier, PDC and communication network. The testing procedure is evaluated by loop back testing of the GPS time stamp generated analog signals. The analog signals generated by the analog output channels are connected to the analog input channels. The analog outputs generated are transferred back inside the RSCAD simulation and is compared with the digital signal generated using arithmetic components undergoing similar parameter change. Close similarity between these two signals validates the PMU testing procedure. The amplifier is a source of noise and non-linearity in the setup for PMU testing lab. The amplifier is validated using the NI Compact Rio platform. The analog (RTDS, amplifier and PMU) and networking connections (PMU, PDC and PPA) are finalized for the prototype testing. The amplifier is tested using the analog output and input modules available in the NI Compact Rio platform. The DC voltage at different values is provided to the input of the amplifier and the amplifier outputs are recorded using the analog input of the NI Compact Rio. The standard deviation of the recorded output gives the noise uncertainty of the amplifier. In this test the uncertainty of the analog input of the NI Compact Rio is assumed to be negligible. The linearity and step test are also carried out using the signals similar to the PMU testing, mentioned in the IEEE TSS document. The standard deviation of the power amplifier for static test is obtained for few DC voltage values. They are compared with standard deviation of the analog output module of the NI Compact Rio at low voltage. A typical result shows that the standard deviation of the amplifier for 50 V output is 0.0026v and that of the NI

Compact Rio is 0.0017v at 1V output. Large difference in the standard deviation of the amplifier and NI Compact Rio indicates higher noise injected by the amplifier. The response of step and dynamic test signals are also acquired and compared with the mathematically generated signals by super imposition.

The different modules of the NI-cRIO platform are tested for linearity, noise and frequency accuracy for PMU calibration application. The NI-cRIO platform uses “Sine Wave Generator Express VI” for generating dynamic sine wave with varying magnitude, phase and frequency. As the phase and frequency are related to each other (phase is the integration of frequency deviation), hence, the frequency error largely affects the phasor estimation accuracy.

The linearity study reveals that the NI-cRIO platform is largely linear within the working precision up to 4 decimal places. The given settings resulted in typical SNR below 160dB as shown in Figure 2.3.

The phase angle plot of RTDS signal with different frequency and NI-cRIO is shown in Figure 2.4. The target frequency from NI-cRIO platform is 59.9958Hz. The phase angle of the GT-NET PMU, which matches with the NI-cRIO angle (green curve) is RTDS signal having frequency 59.9957568Hz (purple curve). This resulted that the frequency accuracy of the NI-cRIO is accurate upto third decimal place. This frequency accuracy is not sufficient for PMU calibration application and we are actively coordinating with NI to solve this issue.

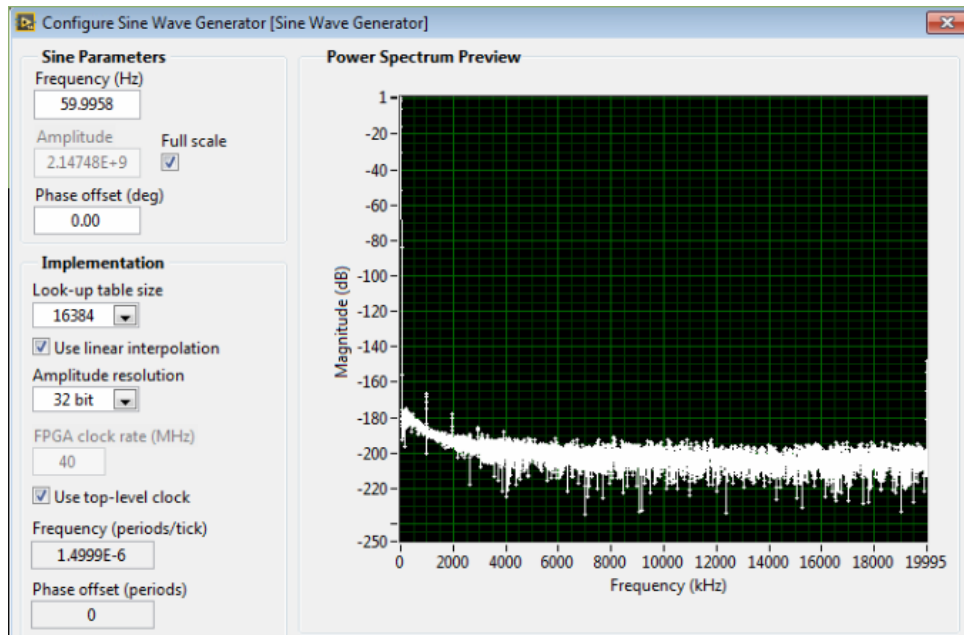


Figure 2.3: SNR of the “Sine Wave Generator Express VI” block in NI-cRIO platform

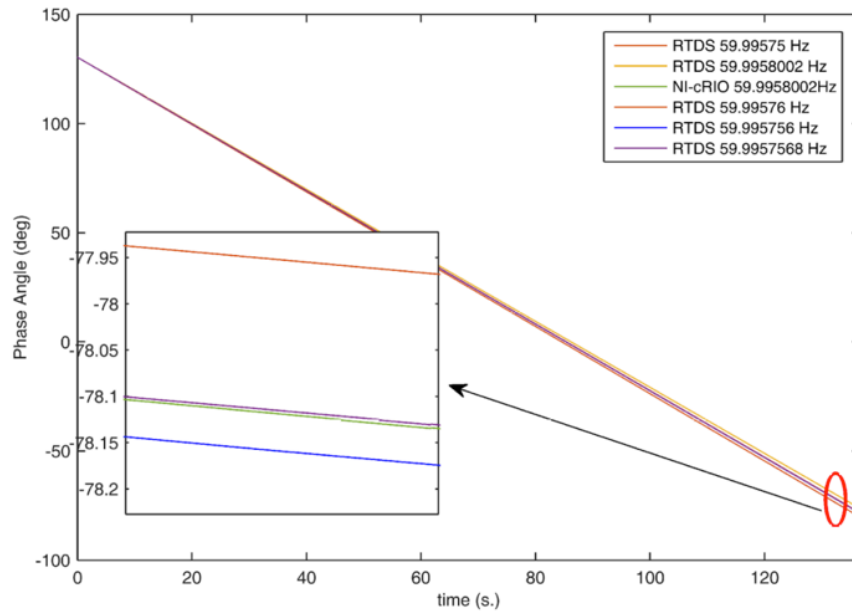


Figure 2.4: Phase angle difference resulted due to the slight difference in frequency.

## 2.5 Results

A DFR PMU is tested according to the error metric mentioned in for P class PMU. The testing is performed for different PMU phasor reporting rates of 30fps and 60fps. The results of the PMU testing are shown in Table I.

Table 1.1: Summary of PMU testing results

Static Tests				
Error	Magnitude Change (30/60 fps)	Angle Change (30/60 fps)	Signal Frequency Change (30/60 fps)	Harmonic Distortion (30/60 fps)
V Phasor TVE	P	P	F	P
I Phasor TVE	P	P	F	P
FE	P	P	F	F
RFE	P	P	F	F
Test Results (30/60 fps)				
# of Tests	16			
# of Test Passed	10			
Success Rate	62.50%			

The static state test of magnitude change and angle change are complied by the PMU for all the error metric for both 30 and 60 fps. The frequency change test is not complied by the PMU for all the error metric at 30fps and 60 fps. The harmonic distortion test is complied by voltage and current TVE for both 30 and 60fps. The FE and RFE for 30 and 60 fps are also not complied for the harmonic distortion test. The Dynamic test are also performed, but not presented due to space limitation.

The frequency uncertainty of the built-in function is observed to be more resulting in incorrect TVE evaluation. The frequency uncertainty of the generated signal is minimized using the combination of LUT and CORDIC blocks and hence, generating more accurate signals for PMU testing. The harmonic content of the signal generated using proposed method is also observed to be less than the threshold mentioned in the standard. The TVE, FE and RFE of a PMU for static tests are also performed using the proposed method. The proposed method demonstrates that a low-cost computing platform can be used for PMU calibration. The COMTRADE module section presents an alternative method of sinusoid signal generation for PMU calibration for static tests. The accurate signal will be generated by NI module using method provided by the COMTRADE module.

## **2.6 Summary**

The PPA is used for testing PMU using various test signals as mentioned in the IEEE TSS specification. The PPA is used to perform steady state and dynamic testing of the PMU following IEEE TSS and IEEE C37.118.1-2011. The PPA generates the testing sequence and compares the error of the measurement obtained from PMU. The installer of the PPA is launched to deploy the tool in a system and all the steady state and dynamic test sequence are selected to perform the testing. The PPA is expected to perform the testing and generate the report for the magnitude error, phase error, total vector error, frequency error and rate of change of frequency error for all the steady state test. The TVE response time and overshoot under shoot are tested for the step change test of magnitude and phase. The magnitude error, phase error, total vector error, frequency error and rate of change of frequency error are tested for other dynamic test case, which are frequency ramp and amplitude and phase modulation test case.

The error metrics presented in the test report are obtained by running all the static and dynamic test case on a commercial PMU. The error metrics consist of Total Vector Error of voltage signal, Total vector error of current signal, Frequency error and Rate of change of frequency error for all the phase and positive sequence component of voltage and current signal. The TVE response time and magnitude and phase overshoot of voltage signal for magnitude and phase step change test case is also presented in the test report.

### 3. PMU Lab testing using the PMU Performance Analyzer

---

#### 3.1 Background

The phasors obtained for different test scenario from the PMU under test is compared with the true phasor using PPA. The PPA gets the time stamps of all the events, which are associated with the change in parameters of analog signals. The PPA calculates the true value of the phasor for the corresponding variation in the analog signal and stores them internally. The user is expected to provide the time stamped phasor from the PDC in a specified .xlsx or .csv data format. The user specifies the PMU class (P or M class) and the PMU reporting rate in the PPA. The user also mentions the list of test cases for which the PMU under test is required to be evaluated. The PPA imports the test PMU phasors from the .xlsx or .csv file and generates the plots of total vector error (TVE), phasor magnitude error (ME) and phase angle error (PE), frequency error (FE) and rate of change of frequency error (RFE), and additional metrics for the dynamic step test results. The PPA also generates the PDF report for all the test cases conducted by the user [11,12].

The purpose of the software is to evaluate the percentage of conformity of the test PMU with the metrics mentioned for different scenario in Standard IEEE-C37.118.1. This process consists of the following steps:

1. The user selects a group of phasor data pertaining to different test cases under which the PMU is tested.
2. The user selects the PMU class and reporting rate for which the test is to be carried out.
3. The user selects the list of tests that has to be conducted from the all the test cases mentioned in Standard IEEE-C37.118.1.
4. The PPA scans the phasor data and reports if it is useable and free of any synchronization errors.
5. The PPA is expected to give the results in the final step.

#### 3.2 Required features of PPA

- a) True Value: It is assumed that the test PMU is provided with time synchronized analog signal having parameter variation at different time instants. The signal generator changes one analog signal parameter at a known time instants and continue that parameter for a fixed time interval. The PPA should be able to generate true value of the phasor using the GPS time stamps of the phasor data.
- b) The PPA should be able to process the exported.xlsx or .csv data file from the PDC.
- c) The PPA should be able to calculate the total vector error (TVE), phasor magnitude error (ME) and phase angle error (PE), frequency error (FE) and rate of change of frequency error (RFE), and additional calculations for the dynamic step test results.
- d) The PPA shall have a means of determining the time of arrival of PMU data messages and comparing that time against the message timestamp.

- e) The PPA should be able to generate test result documentation and pie-charts of the success rates of the PMU testing

### 3.3 Validity Checking

If errors are found in the input values, the program should provide an error message to the user that gives the reason for the error and its location in the input file. The locations can be recorded in either a log file or an on-screen window for the user's reference.

### 3.4 Interface Requirements

Users will interact with the program via a graphical user interface. To use the program, a user selects the data files using the **Browse** button. The file is then checked to determine the valid time range of the data.

The user is expected to either load the pre-saved configuration file or manually change the test configuration and PMU settings (PMU type, and the PMU reporting rate).

Next, the user selects a folder where the output results should be placed. Clicking on the **Compute Results** button causes the analysis to run, during which time the status bar at the bottom of the screen is updated to provide the user with some idea of what the program is doing. Once the analysis has completed, the list of results available for plotting becomes enabled, and the first test result is plotted automatically. The user can then click the **Save plot** button to enter a filename for the exported image [13-16].

Before exiting the program, the user can save the configuration settings used in the analysis process. This file can be loaded in the future, if the user wishes to repeat the analysis with different data sets from different PMU.

### 3.5 “About” window

An “About” screen is also required, which must display the copyright and contact information.

### 3.6 Pre-Production Splash Screen

This screen shows, the releases of the software with a disclaimer. It also allows the user to accept or decline the terms contained therein. Acceptance of the terms allows the software to continue launching; declining the terms causes the program to exit.

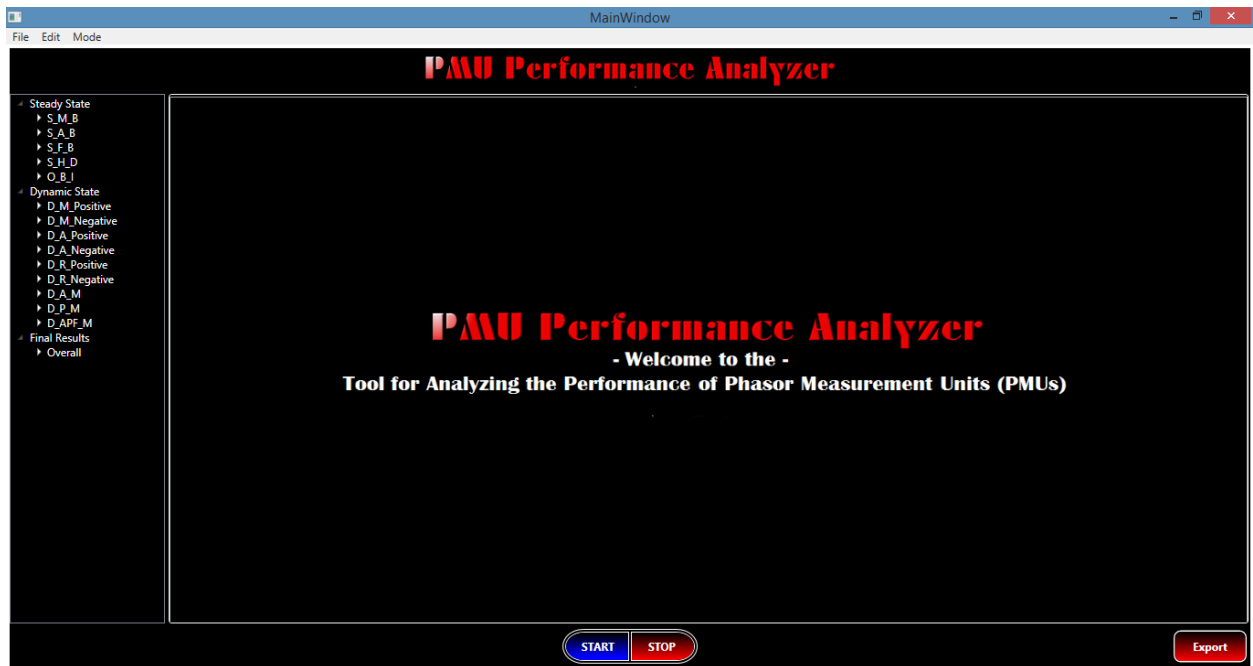
- **Configuration Management:** Software source code must be stored in a suitable revision control system, such as git or Team Foundation Server. (Note: Source code **cannot** be placed on a publicly available server, such as GitHub.)

### 3.7 Test Plan

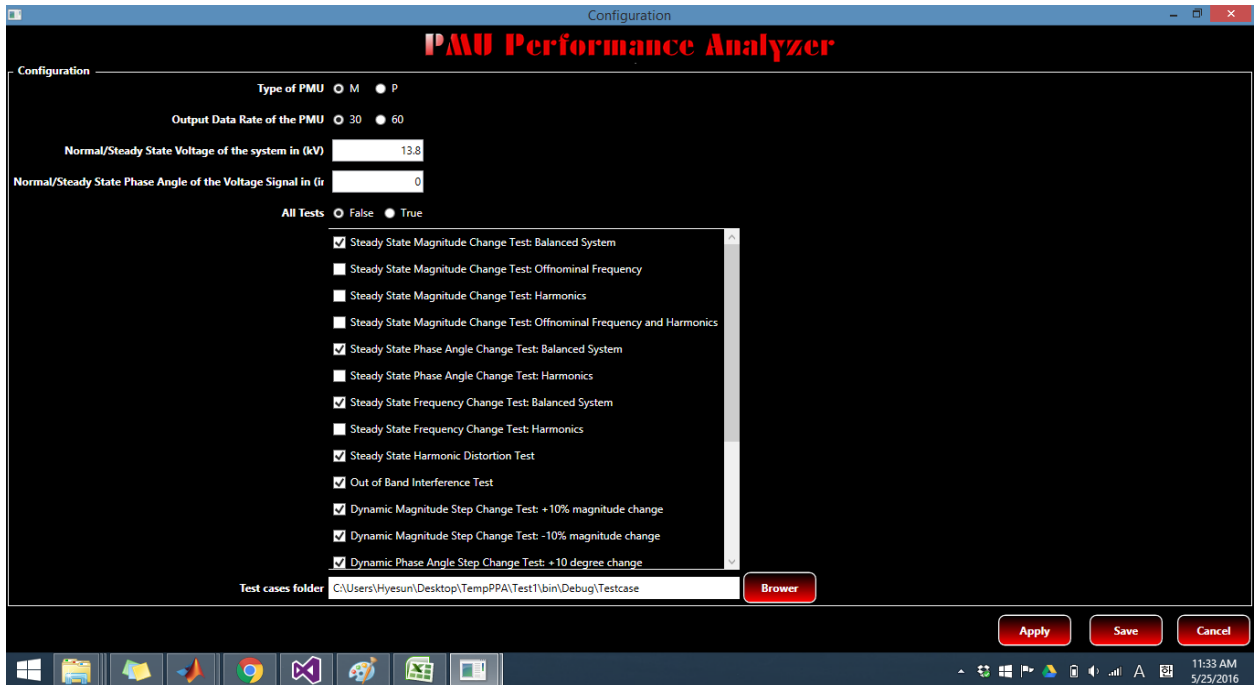
- **Testing Approach:**
  - **Input validity** – Ensure that data files exist before trying to open them. Test program with input files that are improperly formatted, missing required columns, or that contain invalid entries. The user must be provided with a meaningful error message that describes the type and location of the error in the file.
  - **Output validity** – PPA will be tested using RTDS-produced results of GTNET-PMU and compared with the known test results. Documents from Inter Lab Comparison report may be referred for output testing.

### 3.8 Installation

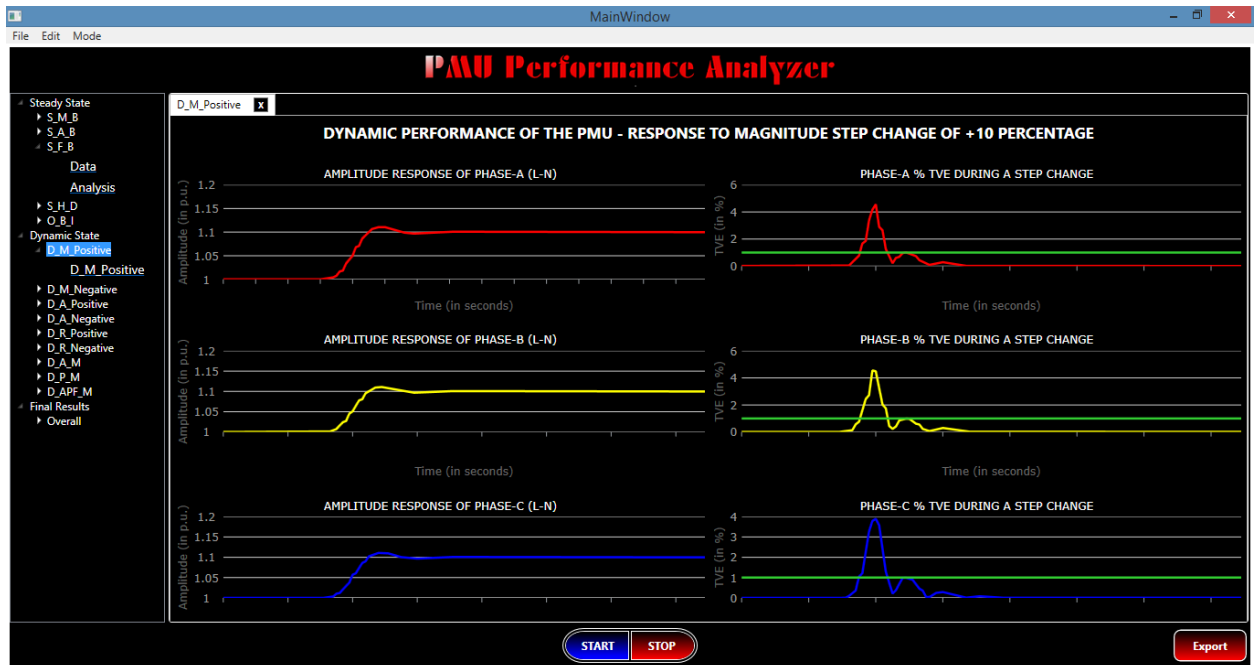
The software must include an installer executable that installs the program in the user's desired location. In addition, the installer must also check for any missing required prerequisites and prompt the user to install them prior to beginning the installation process.



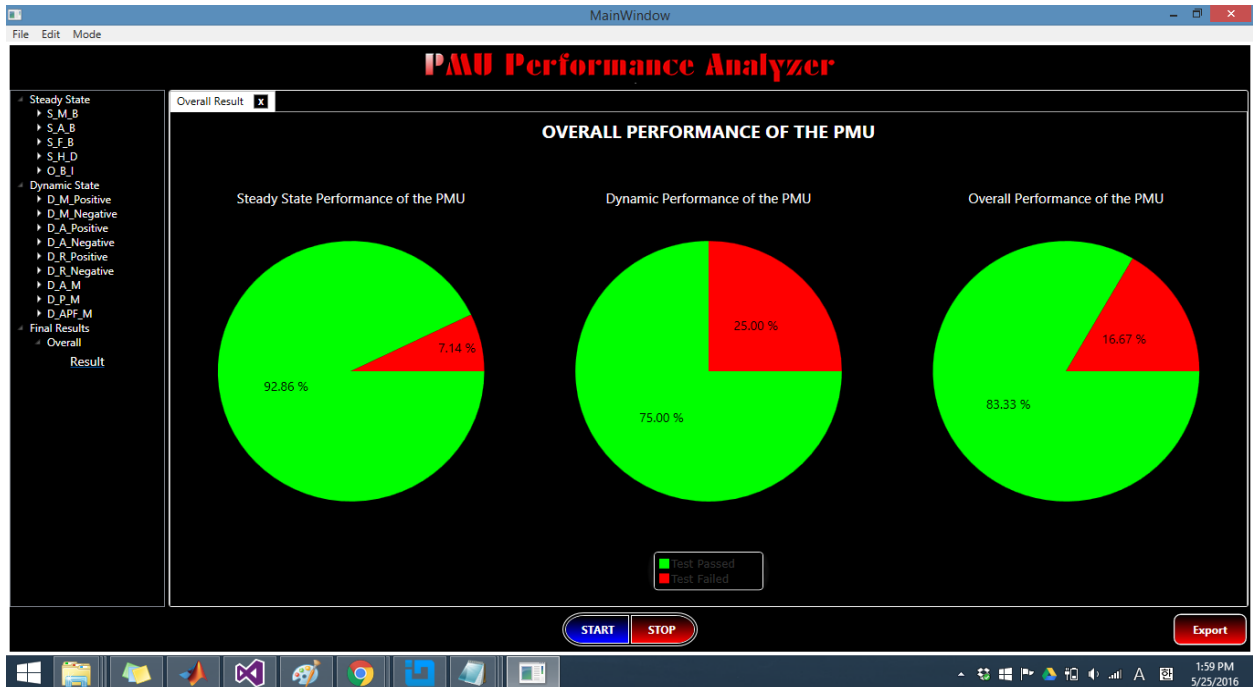
(a)



(b)



(c)



(d)

Figure 3.1 Installation and results reporting of the PMU performance analyzer

### 3.9 Highlights

- IEEE C37.118.1-2011 compliance test for P (Protection)-type PMU has been carried out for a 2 PMU device using PPA (PMU Performance Analyzer) s/w developed by WSU (Washington State University).
- The delay time, frequency response time and ROCOF in *dynamic* step change tests are carried out using multiple simulations run.
- For *steady-state* signal magnitude (voltage and current) tests, FE and RFE values were recorded for additional measures, although they are not required for IEEE compliance tests. DFR\_PMU passed all of those additional tests.
- Test Procedures:
  - The PPA internally generates the true phasor and also utilizes PDC (Phasor Data Concentrator) to store the PMU data during the simulation of test cases. The PMU data collected from the PDC are in turn to be run and analyzed by PPA s/w and graphs and report are auto-generated instantly.

#### Interfacing PPA with NI CRIO platform

The time stamp of the change in signal parameter in NI-cRIO platform is required by the PPA for generating the true phasor.

The overall architecture of the lab with NI-cRIO and PPA is shown in Figure 3.2. The Labview system generates a log file, which contains the time stamp of the instances when signal parameter changes. The PPA read this log file and internally generates the true phasor.

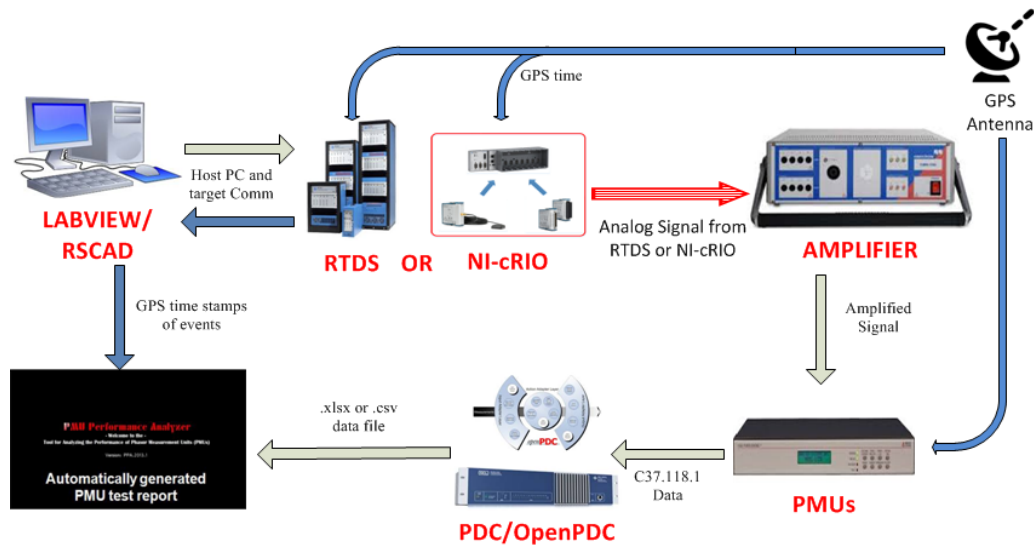


Figure 3.2: PMU Testing Lab

### 3.10 Test Results

Results of steady state performance of PMU - magnitude change: balanced system

Status of time synchronization of the ideal pmu & the test pmu: The test pmu is in perfect time synchronization with the ideal pmu.

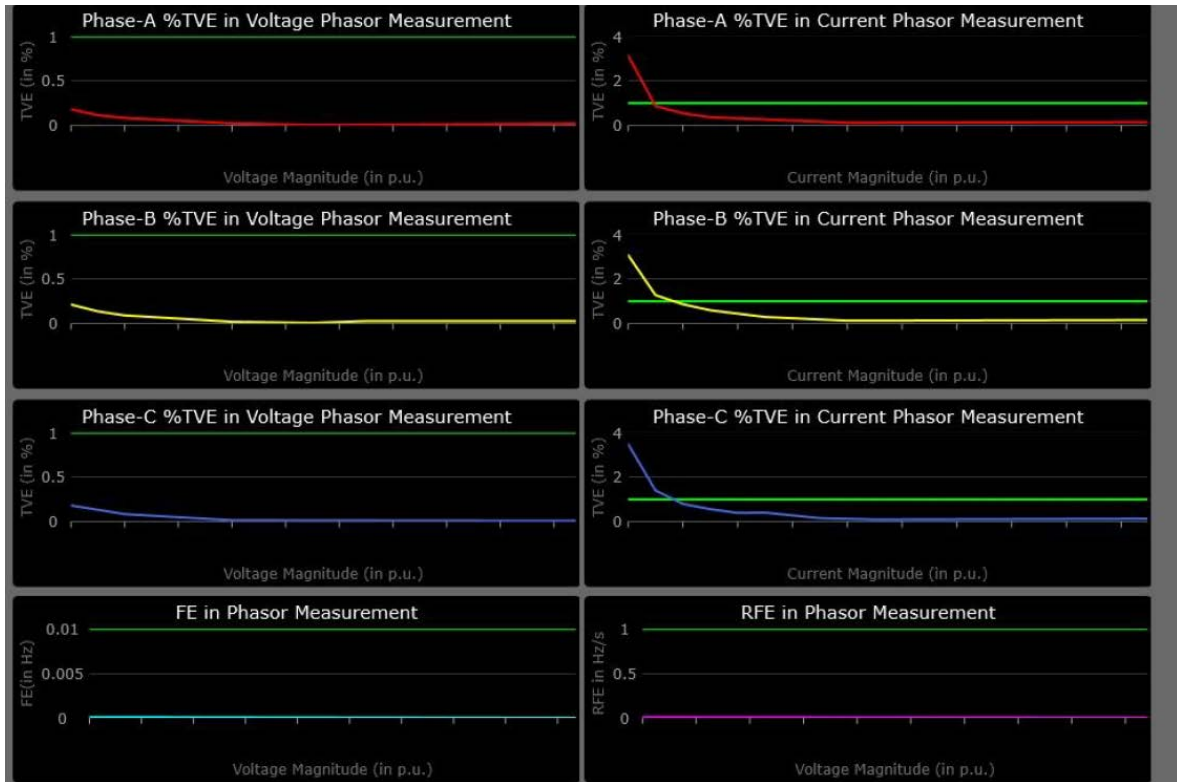


Figure 3.3: Magnitude Change for balanced system

Additional results are available in Appendix A.

### 3.11 Summary

This chapter presents the need and procedure for testing synchrophasor devices and applications before the field deployment. The specification of the testing equipment required for the PMU testing lab is discussed in detail. The architecture of the test bed and the features of the software called PPA used for automatic PMU testing is presented. The successful implementation of PMU testing performed in the Southern California Edison (SCE) using PPA is presented. The result of the PMU testing shows that the compliance of the standard for 30 fps and 60 fps can be different for some of the test scenarios.

## 4. COMTRADE Module

### 4.1 Introduction of COMTRADE Module

The COMMon format for TRAnsient Data Exchange for power systems (COMTRADE) module is a set of integrated equipment, which includes a local host computer, compactRIO system, and amplifier. The local host computer has faster data processing rate, which responses for reading, scaling and preparing a large amount of data. The cRIO system is made up of a low cost National Instrument cRIO with a GPS that is used to generate accurate analog output signals. Using the COMTRADE input module is a suitable algorithm, that can convert digital data source to accurate and stable analog output signal for further use by PMU testing, remotely PMU testing or further remotely RAS testing. An amplifier in the system is used to amplify and restore the voltage amplitude to original scale. The architecture of system algorithm is shown in Figure 4.1.

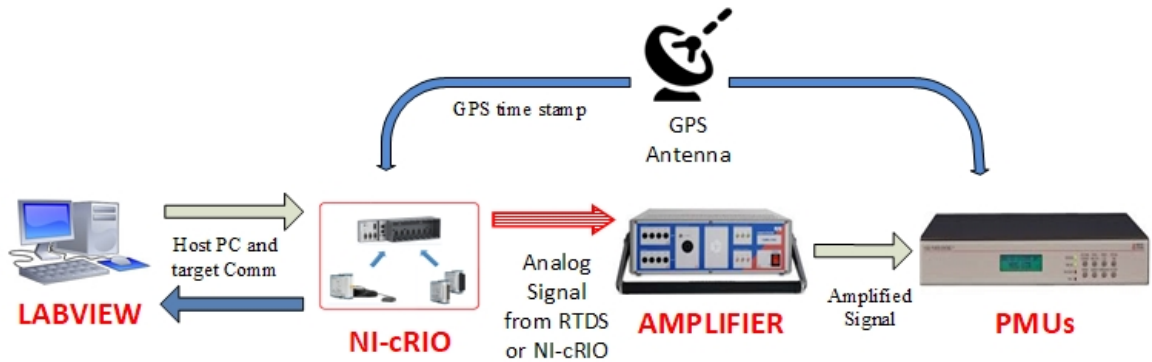


Figure 4.1: COMTRADE Module Algorithm Architecture

The analog output signal is generated using a reference COMTRADE file by Direct Memory Access (DMA) First In First Out (FIFO) method with GPS PPS correction for increased accuracy. A DMA channel consists of two FIFO buffers: one on the host computer and one on the Field-Programmable Gate Array (FPGA) target. After creating the DMA FIFO, the data can be read from COMTRADE file and write into buffer, depending on programming block diagram code on the host PC side, transfer using DMA channel to FPGA side, then read and processed by the FPGA. The DMA FIFO working illustration is shown as below.

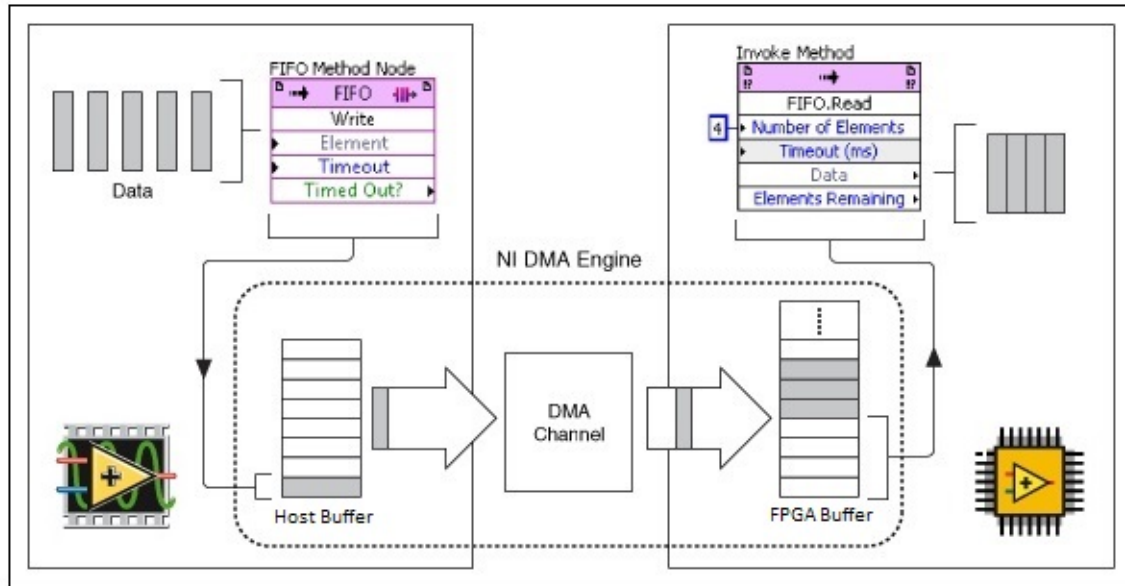


Figure 4.2: DMA FIFO Working Diagram

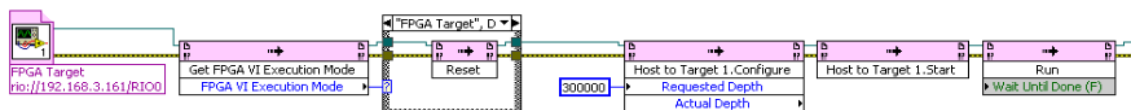
## 4.2 Work Statement of Host Computer VI

COMTRADE file includes digitally sampling measurement DATA file (.dat) and signal information ConFiGuration file (.cfg). On the Host computer side, 20 second length buffer is created depends on data sampling rate by using an invoke method. Labview host VI firstly reads data file from assigned path, shrinks the data amplitude, and shifts to FiXed Point (FXP) ( $\pm$ , 20, 5) that is FPGA specify available resolution. The FXP notation representation indicates (Sign, Bit length, Integer length) and allows for minimal approximation error. Then transfers prepared data through the DMA channel to cRIO-9068. A local host VI example is shown in Figure 4.3.

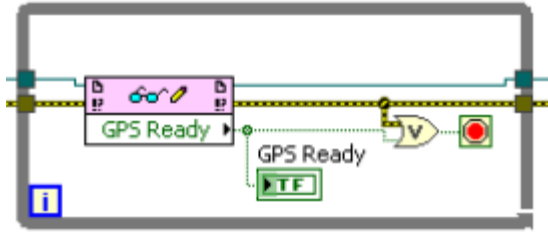


Figure 4.3: Local Host VI Example

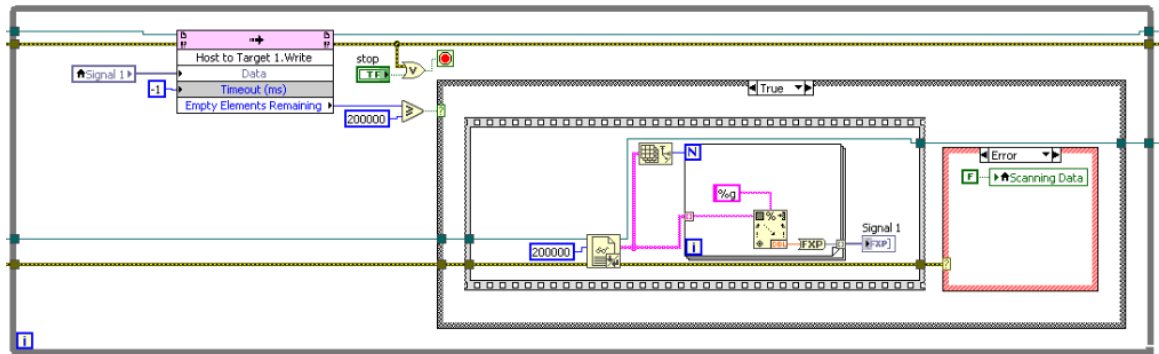
In Figure 4.3, highlight blocks are:



\*Block1: Initialize FPGA VI and Create Host Buffer Using Invoke Method



\*Block2: Check GPS Status



\*Block3: Invoke Method Write and Transfer Data to DMA

The host VI is communicating with FPGA VI continuously. In this example host VI, it firstly initialized the FPGA VI, and then prepared host buffer for DMA transferring as \*Block1. When the host VI checked that GPS signal was ready and stable from FPGA VI as \*Block2, it would immediately warp data in buffer and send them to the FPGA by DMA channel using invoke method as \*Block3. A logic flow chart of host VI work is shown as below.

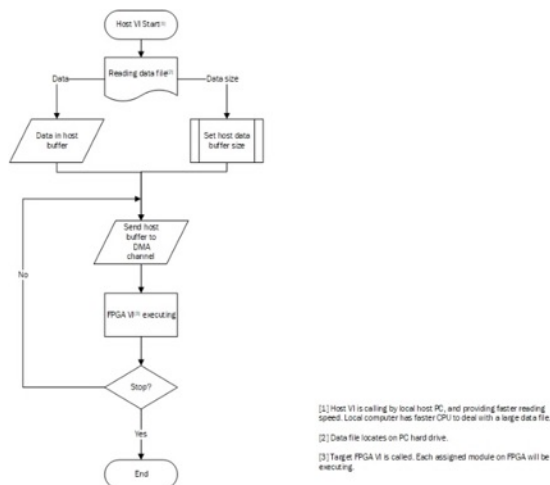


Figure 4.4: Host VI Flowchart

### 4.3 CompactRIO System and FPGA VI

CompactRIO System is one important part of the COMTRADE module, which important, it includes a cRIO-9068 compactRIO controller, NI-9467 GPS C series synchronization module, and a NI-9264 C series voltage output module. The assembled entity compactRIO system is shown in Figure 4.5.

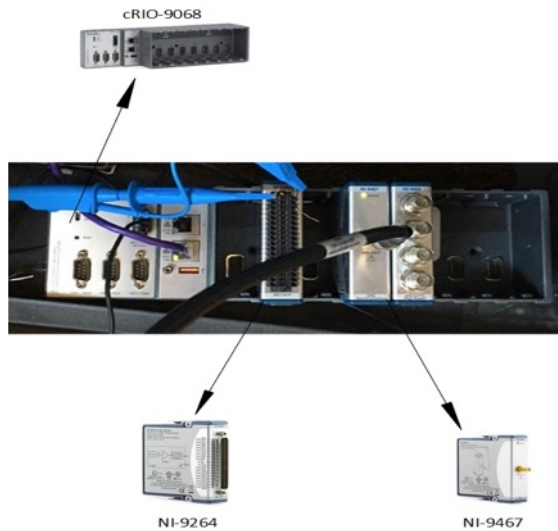


Figure 4.5: Assembled compactRIO System

In this part of the system, cRIO-9068 is embedded controller that contains a programmable Zynq-7020 FPGA that provides 2 slots for a GPS module and a digital-to-analog converter (DAC) module. The NI-9467 module provides accurate time synchronization for the compactRIO system, which be used for calibration of FPGA oscillator in every GPS Pulse-per-second signal (PPS), and accurate data time stamping, thus to get reliable analog signal output. The NI-9264 is a simultaneously updating analog output module. It contains 16 DAC channels, which can be used to generate  $\pm 10$  V voltage.

The programmed embedded FPGA is based on Labview FPGA VI to read data from DMA buffers. The NI-9264 analog output (AO) module then samples the resulting values at an assigned update rate to match the AO module at a base 60 Hz frequency. Meanwhile, the GPS will correct the oscillator depends on its time stamp. A Labview FPGA VI logic flowchart is shown in Figure 4.6, and an FPGA VI Block diagram is shown in Figure 4.7.

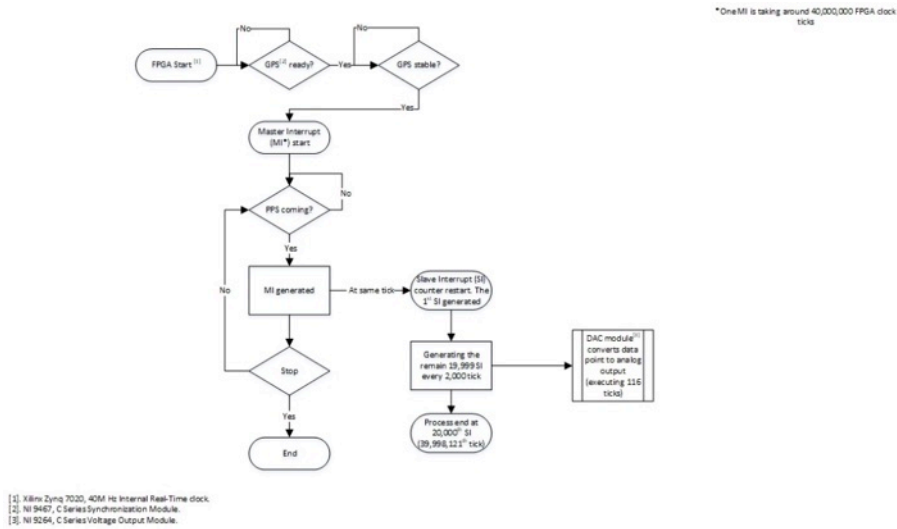


Figure 4.6: FPGA VI Flowchart

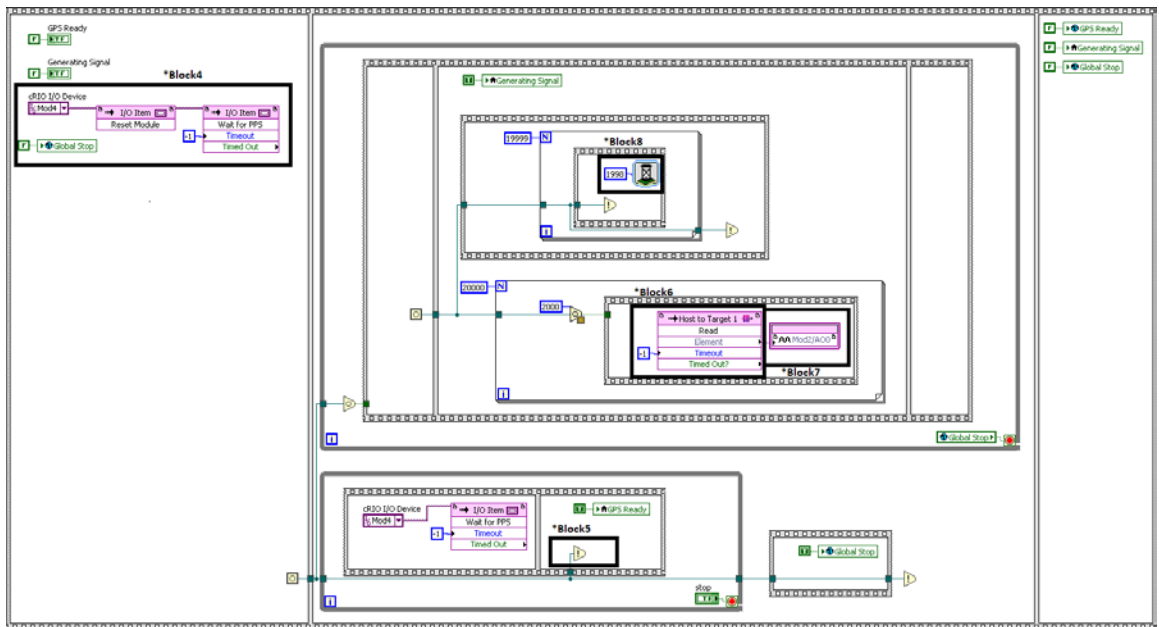


Figure 4.7: FPGA VI Block Diagram

In Figure 4.7, highlight blocks are:



\*Block4: Initialize GPS Module by FPGA I/O Method Node (NI-9467)



\*Block5: Generate Interrupt & Waiting for Interrupt



\*Block6: Read FIFO Method Read Data from DMA Channel



\*Block7: FPGA I/O Node - Analog Output (DAC NI-9264)



\*Block8: Wait Express VI (Unit: ticks)

After data buffer transfer to FPGA target, the FPGA waits for GPS initialize as \*Block4, and then generates interrupt as \*Block5 to nested loop to read an element from buffer one by one in every 2,000 ticks. Labview FPGA VI read data buffer from the DMA channel using read FIFO method as \*Block6, and send each element to the DAC module to generate analog output by the FPGA I/O Node function as \*Block7. In this example, data sampling rate was 20,000 Hz. According to the 40 MHz top-level clock, to generate 60Hz frequency signal, the buffer-reading rate was ideally set at 2,000 ticks per element. Actually, the reading, executing speed of FPGA is one tick per element, and for loop executing speed is one tick per cycle. Therefore, wait clock VI was set to 1,998 ticks (\*Block8) to get appropriate performance. Since the first PPS generated by I/O item function has deviated, and will cost a tiny oscillator error, the GPS module reset and initialized at beginning, thus to skip those errors and get further steady time stamps.

#### 4.4 Error Correction by GPS

The NI cRIO-9068 has a 40MHz top level clock. According to tests, the internal clock cannot generate a constant number of ticks during each GPS PPS, since the instability of FPGA oscillator. The top-level clock has a timing accuracy of 5ppm. The missed or additional tick, causes a potential drift of 0.000299998 Hz. Therefore, adding GPS PPS interrupt during the signal generating can help to increase the signal accuracy. The algorithm and FPGA working time line is shown in Figure 4.8 as below.

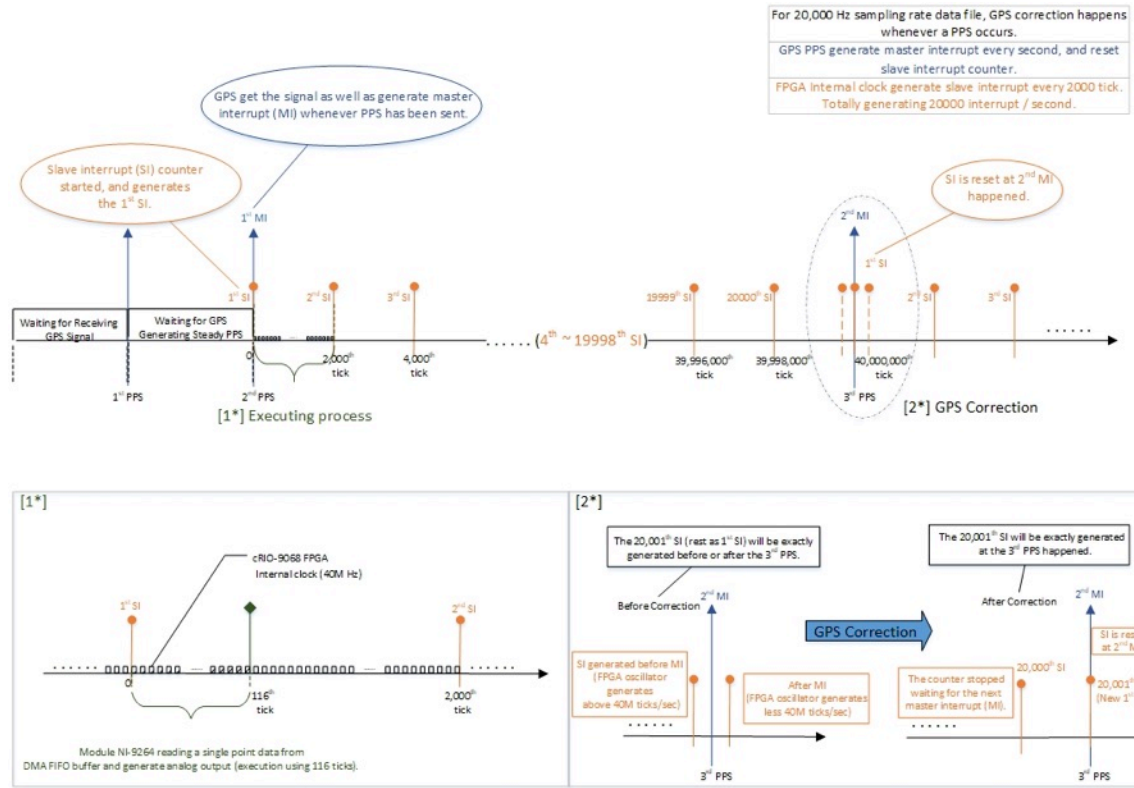


Figure 4.8: GPS Correction Algorithm

## 4.5 Results

The synchrophasor standard C37.118.1-2011 mention that phase error of 0.01 radian results in 1% TVE provided there is no error in the magnitude. The standard C37.118.1a-2014 also mentions that the test uncertainty ratio (TUR) of the calibrator must be greater than 10, which implies that the phase angle of the calibrator must be at least 10 times more accurate than the threshold value of 0.01 radian. The IEEE TSS mentions that most of the static test is 5 sec long along. On this basis, the frequency accuracy of the calibrator must be greater than  $0.01 / (2\pi \cdot 10) = 0.000159$  Hz. The measuring frequency accuracy of a sinusoidal signal in the range of 0.00015 Hz, require a spectral resolution of 0.00007Hz. The frequency of interest of the sinusoid is 50Hz or 60Hz, which mandates that the sampling frequency must be more than the Nyquist rate. The sampling frequency for this study is fixed at 200Hz and the spectral resolution selected is 0.00001Hz. The length of the sinusoid required for this study is given by

$$L = F_s / R = 200 / 0.00001 = 20000000$$

Where  $F_s$  is the sampling frequency of the oscilloscope,  $R$  is required frequency resolution and  $L$  is the length of signal required for spectral estimation. The signal length required is around 27 hours of data at 200Hz sampling frequency.

The lower limit of FE specified for static state tests in C37.118.1-2011 and C37.118.1a-2014 is 0.005Hz, which require the calibrator to be accurate up to 0.0005 Hz, with a TUR of 10. The

spectral resolution of 0.00001 Hz is also sufficient to measure the frequency accuracy of the calibrator at 0.0005 Hz range.

The synchrophasor standard C37.118.1-2011 also mentions that the Total Harmonic Distortion (THD) of the calibrator must be less than 0.2% of the fundamental. The upper limit of frequency used for evaluating THD is not specified in C37.118.1-2011, which is limited to 50xbase freq, where base frequency is the fundamental frequency in Hz.

The step change test mentioned in C37.118.1-2011 requires the magnitude of the signal to change by 10% of the nominal value each step. The magnitude of the calibrator need to be accurate up to 1% with a TUR of 10. This demands that the minimum magnitude resolution of the analog output of the calibrator is accurate up to 0.5% at around 50% of the range of the calibrator output. For a calibrator output of  $\pm 10$  volt and 16-bit resolution, the magnitude resolution at 50% of the output is 0.0015%, which is sufficient to detect accuracy of 0.5%.

The frequency accuracy of the proposed method is demonstrated in Figure 4.9, in which the spectral estimation of the fundamental component is shown. The spectral resolution for the fundamental component is fixed at 0.00001 Hz, which is obtained using 27hours of data using the Yokogawa DL850 ScopeCorder. The fundamental frequency of the sinusoid evaluated using Labview built-in function is 59.99538Hz and that of the CORLUT method from previous work is 60.00211Hz and proposed method is 59.99971946 Hz with error of  $\pm 0.00001$ Hz. However, the bandwidth of the fundamental component having magnitude more than 0.002 p.u. using CORLUT is 0.000222Hz, while that of Labview built-in function 0.00273Hz and proposed method is 0.00066Hz. This means that the fundamental frequency using Labview built-in function varies over a wide range over cycle to cycle, whereas the clock correction using CORLUT and the proposed method reduces the swing of the fundamental frequency component to a narrow band and improves the frequency uncertainty of the fundamental component over each cycle.

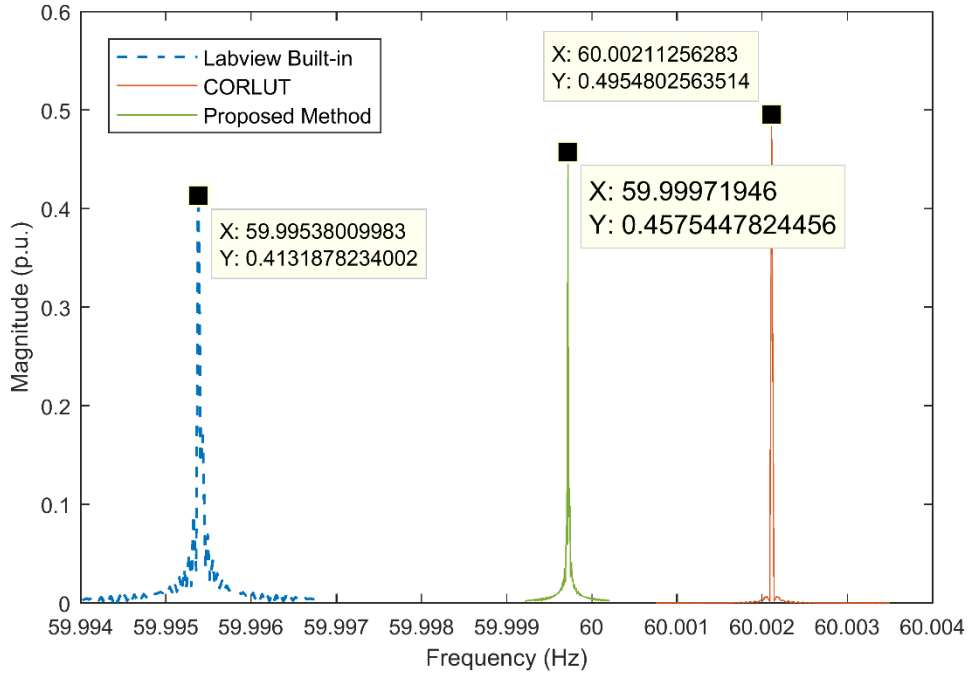


Figure 4.9: Spectral estimation of fundamental component

The spectral estimation of harmonic component of the proposed method is shown in Figure 4.10. The THD of the proposed method is evaluated as  $8.8228 \times 10^{-7}\%$ , which is less than the threshold value of 0.2% mentioned in the standard.

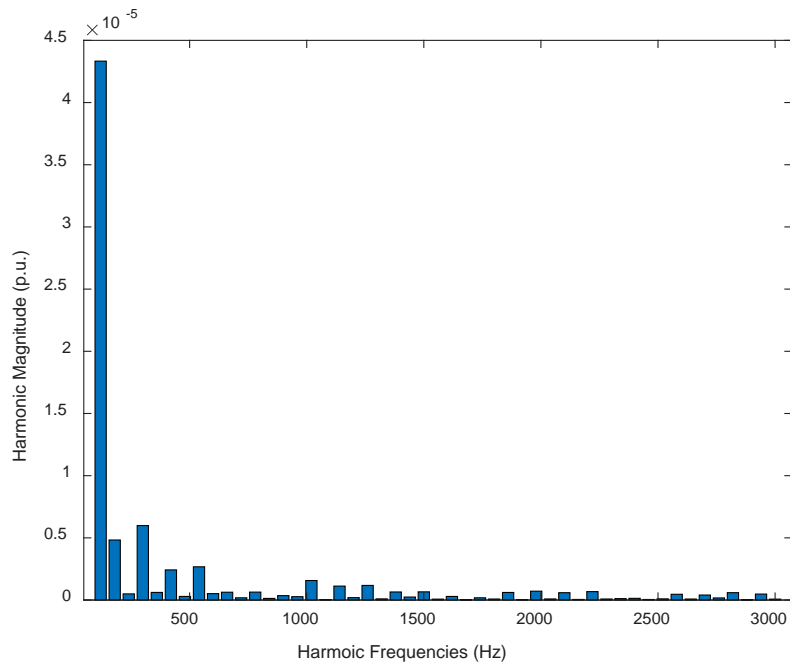


Figure 4.10 Spectral estimation of harmonic frequencies

## 4.6 Summary

The PMU testing system is developed to ensure the security, accuracy, and reliability of synchrophasor based applications in the power grids. The PMU testing method aims at a better solution for PMU calibration, and involves the implementation procedure for PMU testing, which mentioned in IEEE TSS. The necessary devices can be used for PMU testing includes analog signal generated by RTDS, GPS time stamps, low cost NI-cRIO, Phasor Analyzer (PPA) software. According to the simulation, analog output from RTDS, the time stamped phasors from the PMU are archived by the Phasor Data Concentrator (PDC), and then fed to the PPA software for comparison with the time stamped true phasor. Then the PPA generates a detailed report for all the test cases performed by the user. The Frequency Error (FE) and Rate of Change of Frequency Error (RFE) are the additional performance criteria mentioned in this standard for the performance evaluation of the PMUs.

For the PMU Testing Lab, outcome was all the necessary hardware and software infrastructure for carrying out the performance evaluation of PMUs under test, and details of the PMU testing lab setup.

For the PMU Lab testing using the PMU Performance Analyzer (PPA), the developed software evaluates the percentage of conformity of the test PMU with the metrics mentioned for different scenario in Standard IEEE-C37.118.1.

For the Comtrade Module part, it is one update and accurate method for NI-cRIO setup for PMU testing lab.

## 5. Erkios Middleware Software

---

### 5.1 Erkios software for end-to-end testing

The regular testing of equipment installed in the field is desirable because no more testing is carried out during the lifetime after initial testing and installation. Hence, correct working of these equipment's in case of a triggering event is uncertain after 5-10 years of commissioning. Therefore, in-field remote testing of equipment's becomes necessary to guarantee that they perform accurately at all times and will not be affected by any sort of software/hardware error that develop with time or hidden failure that was not captured before commissioning. In view of this, Erkios is developed for end-to-end and in-field testing of mission critical systems and equipment. The Erkios is a middleware, which is currently developed for in field-testing of PMUs and Remedial Action Schemes (RAS). The Erkios is capable of testing the field equipment, communication network and control logic without the need for de-commissioning. The Erkios is capable of remotely managing such test over a large number of substations [17-18].

In the Erkios architecture as depicted by Figure 5.1, there are four important modules or building blocks: Central Test System (CTS), Local Test System-Initiator (LTI), Local Test System-Collector (LTC) and Operation Wide-Area Network (or Op WAN). The CTS plays the role of a coordinator during tests. It is responsible for the creation of a test signal that consists of data regarding the test, transmitted to other modules. LTI is responsible for disabling the PT/CT inputs to sensor and disabling the actuator (or breakers) before the testing starts. After the testing is complete, it enables the sensor and actuator for normal operation. LTC is responsible for collecting the control actions and measurement data, and forwards it to the CTS. Op WAN transmits data between CTS, LTI, and LTC. Signal Generator and Amplifier are used to convert the digital signal sent out by LTI into analog signals suitable for the sensor inputs.

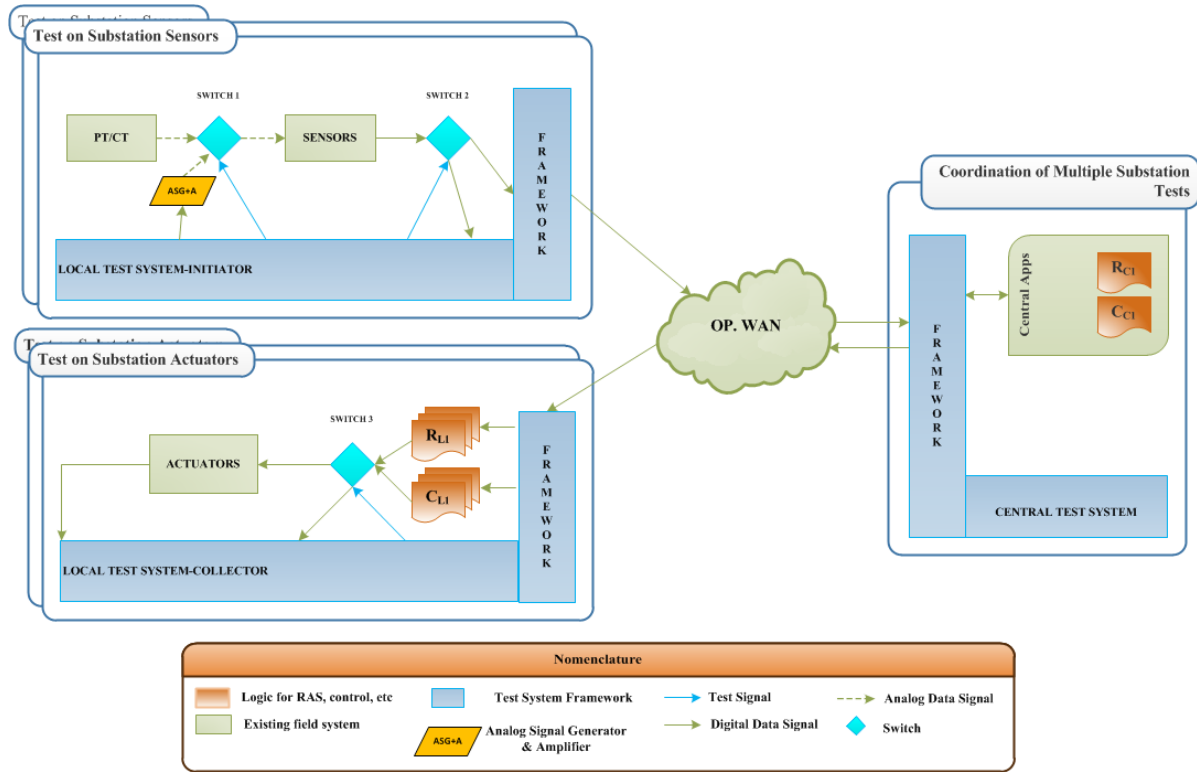


Figure 5.1: Erkios architecture for remote testing

Remote PMU testing is done by the middleware ERKIOS, which consists of several modules. This document provides some requirements for having a middleware glue layer to perform PMU testing. To ensure that the requirements for performing IEEE standardized tests on PMUs are met by ERKIOS. This document specifies the salient features required for designing middleware to test PMUs in a standard compliant manner. The lists of modules required in the substation for remote PMU testing are mentioned in “Specification and Middleware Requirements for Substation implementation with PMU”. It is assumed that device specific requirements will be known and understood by the operator, and will subsequently be entered correctly at configuration time. The ERKIOS substation located modules, in specific the LTS initiator and collector will interact with PMUs.

## 5.2 Functional Requirements for ERKIOS

The following features need to be incorporated in the middleware to carry out the remote PMU testing:

- Maximum Allowable time- The time taken by the test process and the test network should not be included in the PMU latency reporting
- Break time between two tests- There are several tests mentioned in the IEEE Synchrophasor TSS, which takes sufficiently long time (in the range of minutes). The starting of such test will affect the performance of the EMS software running in the control centers. It is possible to break longer test scenario in multiple parts such that the LTI and Programmable Router can be coordinated to transmit some measurements from CT/PT to

make least effect on the EMS software. The EMS software takes several seconds to update the screen. Hence, the switching between PMU inputs from CT/PT to Signal Generator could be optimized to make the PMU testing process transparent to the EMS software in the Control center.

- c) Authentication- The different modules in the middleware should communicate with the test PMU, Programmable Router and other modules using secure communication protocol.
- d) Fault Tolerant- The middleware should have fault tolerant features within its own modules and the test bed. The crashing of any client and servers of the different components in the substation need to be handled during testing by abort, restart or notifying operators for human intervention.
- e) Database management- The middleware is designed to test PMUs installed in multiple substations. The CTS interaction with the database for archiving the test results of multiple PMU and maintains a log of the testing carried out at each PMU.
- f) Mask heterogeneity – The middleware should abstract many of the procedural steps of testing a device down with a uniform interface independent of device types. Once an LTS is setup for the devices in a substation an operator should be able to test any of them by following a simple process.

### **5.3 Validity checking**

If errors are found in the input values, the program should provide an error message to the user that gives the reason for the error and its location in the input file. The locations can be recorded in either a log file or an on-screen window for the user's reference. ERKIOS should be able to check that the settings are within an expected sane interval of values.

### **5.4 Interface Requirements**

An operator should be able to enter required information through a configuration window. A complete list of device types and necessary rules for each specific device as well as the overarching type should be enterable by the operator and validated by the ERKIOS central test system.

### **5.5 Security, Availability, Reliability, Recoverability and Business Continuity**

Components should communicate only to authenticated ERKIOS modules. Only an authorized trained operator should be able to update device specific settings.

### **5.6 Maintenance and Support**

It is anticipated that WSU personnel will maintain the software for the next two years.

### **5.7 Quality Plan**

- **Change Control:** Changes in the ERKIOS architecture are to be done based on the feedback of the PSERC industry members.

- **Configuration Management:** Software source code must be stored in a suitable revision control system, such as git or subversion or Team Foundation Server. (Note: Source code **cannot** be placed on a publicly available server, such as GitHub.)

## 5.8 Test Plan

- **Testing Approach:**
  - **Input validity** – Ensure that data files exist before trying to open them. Test program with input that is improperly formatted, missing required variables, or that contain invalid entries. The user must be provided with a meaningful error message that describes the type and location of the error.
  - **Output validity** – Devices should be confirmed to function with the settings applied.

## 5.9 Installation

The software must include an installer executable that installs the program in the user's desired location or be able to run as a portable app from any location. In addition, the installer must also check for any missing required prerequisites and prompt the user to install them prior to beginning the installation process.

This document is the specification for the ERKIOS signal interface. It describes the requirements for data input from RAS test suites. ERKIOS v0.2 supports data interfacing from a user to the internal RAS simulator. Going forward, ERKIOS will interface with third party RAS test suites.

## 5.10 Purpose

To provide an outline on how ERKIOS will be designed to connect into existing simulation tools aware of the grid's network of devices. By using a third party tool, the feature set of ERKIOS is instead focused on the distributed test initiation and collection process.

## 5.11 Need for this specification

An operator will use the RAS test suite to generate analog or digital signals that is expected to trigger a specific action from a RAS controller deployed into a substation. This standard action and signal will be passed to ERKIOS, along with a source of the signal. The information required for ERKIOS to formulate the test cases is listed under this section of the specification.

## 5.12 Related Standard

The requirements for specific devices such as PMU and PPA testing can be found under the respective sections. Usage of this data at the substation is mentioned in "Requirement specification for alternative interfacing architecture with RAS at Substation"

### **5.13 Assumptions**

A standalone test suite exists with knowledge of the grid assets that can accurately simulate the complete impact of specific signals when measured at any given device. The RAS test suite should be able to output, either directly to ERKIOS or through the actions of an operator.

### **5.14 General System Description**

#### **5.14.1 System Context**

The software is non-self-contained; it must interact with test suites or provide contextually clear prompts for an operator to bridge the gap.

#### **5.14.2 System Environments and Modes**

The prototype software will be used in a research environment under normal operating conditions.

#### **5.14.3 User Characteristics**

It is assumed that users will be comfortable performing basic computer tasks such as locating and selecting files saved on disk. In addition, users are assumed to be capable of operating the testing utility with a high level of proficiency, so as to be able to incite actions at specific devices desired to be tested.

#### **5.14.4 Operational Scenarios**

Only a “normal” operational mode needs to be supported.

### **5.15 Functional Requirements for ERKIOS**

The ERKIOS local test system should be able to transfer a signal representation into an appropriate analog or digital signal generator for the destination device in the substation via the Local Test System Initiator (LTS-initiator)

Device designations are common names recognized by ERKIOS to map to a specific device located at the substation, for example by hostnames. Additionally, ERKIOS local test systems must understand devices common names and possess knowledge of the device type and input format so as to be able to perform the appropriate signal switchover from real to test signals.

ERKIOS should seamlessly transition from the specified origin, source input on the destination test device and pass the test signal.

The ERKIOS local test system collector can intercept the resulting action before it is performed and can compare it to the expected resulting action.

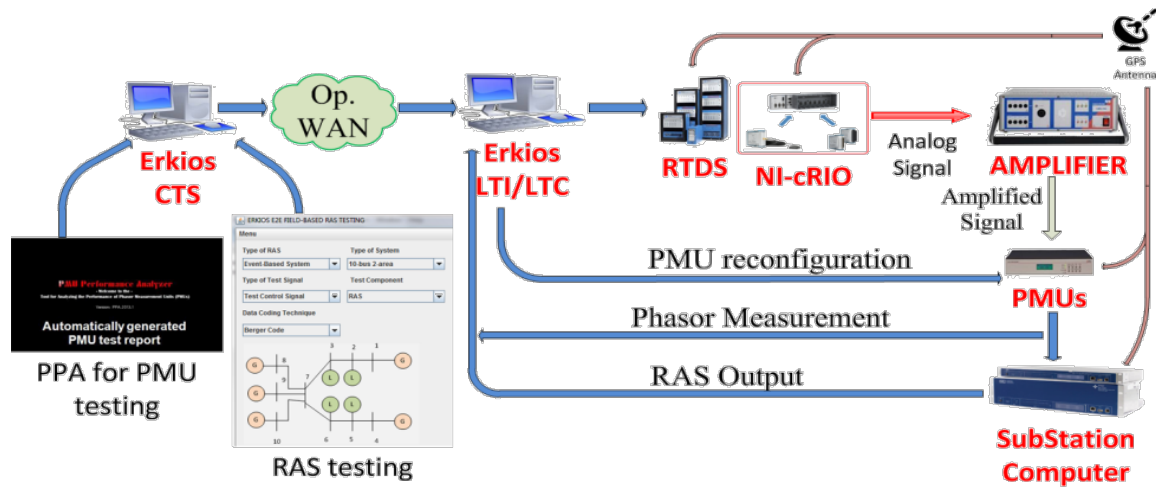


Figure 5.2: ERKIOS Middleware based Remote Testing of PMU and RAS

## **6. Remote PMU testing**

---

### **6.1 Integration of PMU Performance Analyzer and Erkios Software**

The Erkios can be used for remotely testing the PMUs in the field as shown in Figure 6.1, without the need to remove them from service and bring them in the PMU testing lab. The PMU testing lab is primarily designed for testing the new PMU before commissioning in the field. However, periodic testing of large number of PMUs, which are already in service is a difficult task. The proposed solution to this problem is integrating Erkios and PPA for carrying out remote testing of the PMUs installed in the substations. The PPA establishes the connection with the Erkios CTS and sends the lists of the test cases need to be performed on the remote PMU. The LTI generates the analog signal using the GPS time stamps and send the GPS time stamps to the LTC. The LTC also receives the time stamped phasor data from the test PMU through the programmable router. The GPS time stamps of the events and the time stamped phasor data in .xlsx or .csv format are transmitted to the PPA via CTS. The PPA generates the true phasor for all the testing scenarios and compares with the test PMU phasors.

The testing of PMUs installed at the substation is carried out using the middleware ERKIOS. The different modules of ERKIOS are mentioned in this specification.

### **6.2 Purpose**

The remote testing of PMUs is carried out using the ERKIOS middleware. The limits given in the IEEE C37.118.1-2011 and sequence of parameters varied to the voltage and current signal for System Context

The remote PMU testing infrastructure consists of different modules of the middleware ERKIOS and the PMU Performance Analyzer (PPA). The modules of ERKIOS communicate with each other through Ethernet network using server client architecture.

### **6.3 System Environments and Modes**

The remote PMU testing is required to work in unreliable communication network over long distances. The normal operating condition involves fault tolerant features of ERKIOS for reliable operation.

### **6.4 User Characteristics**

It is assumed that users will be comfortable performing basic computer tasks such as locating and selecting files saved on disk. In addition, users are assumed to be capable of manipulating the layout of a spreadsheet using Excel or a similar tool. The middleware typically takes care of the underlying communication and switching function for remote PMU testing.

### **6.5 Substation Specification**

The specification of the substation capable of remote PMU testing are briefly described as follows



The PMU installed at the substation may require recalibration following maintenance of other equipment in the substation. Apart from that, PMU may also require calibration in the interval of 2-3 years due to drifting of parameters resulting from temperature variations. The expansion of power system may also require the PMU installed at the substation to recalibrate.

The Erkios consists of different modules, which communicate with each other for achieving the goal of in-service and end-to-end testing of synchrophasor equipment and RAS schemes. The Erkios module communicates with each other over insecure networks, which demands robust algorithms for handling delays, data drop and data corruption. The issue of security is also needed to be addressed for communication of Erkios modules. The different methodology available for timing coordination, data drop and security are reviewed and are under implementation stage. These algorithms can be tested using cyber physical test bed consisting of NS3 network simulator for communication and RTDS, PMUs and relays for power system. The statistical metrics are required for evaluating the methods implemented in Erkios for handling delays, drop and corruption of the data packets. The “Requirement specification for timing coordination, data dropped and other issues” is prepared for implementation in Erkios tool. The different failure models are identified in the specification document with the details of each Erkios modules that may be associated with some kind of failures. The specification also mentions different failures and security handling mechanisms, which are required to be implemented in the Erkios. The procedure for interfacing PPA with Erkios is explored in this deliverable. The remote testing of PMU is carried out using Erkios middleware. The PPA has interface for local testing and remote testing of PMUs installed at the substation. The protocol, authentication and error detection features are discussed in this specification document. The procedure for remote testing of PMU is done by transmitting the test signals to the Erkios PC in the substation known as Local Test System Initiator. The LTI plays back the test signals following the IEEE TSS guidelines and captures the result as data files. The Erkios transfer the data file to the PPA for performance evaluation of the remote PMU. The communication of the PPA and Erkios is finalized by following server client architecture with authentication and implementing error detection mechanism. The infield calibration of PMU either requires a physical switch or configuration change for providing a test signal to the PMU. The physical connection requires an extra switch to change the connection between the real system and testing system. However, the configuration change only requires access of PMU via communication layer. The configuration change uses the software of the PMU to switch the signal for phasor estimation from the grid to the signal generator. By changing PMU configuration setting, the PMU data packet is redirected to ERKIOS system. The ERKIOS system transfers the collected PMU data and sends to the PPA system for testing. The configuration of PMU can change using either configuration software provided by manufacture or TELNET communication. To integrate with ERKIOS, locally TELNET commands are being used to transfer new configuration parameters for in-field PMU calibration.

## **6.6 Results**

The PMU from one vendor is tested for changing the configuration using the TELNET command. The TELNET command is generated by ERKIOS Local Test System Initiator and verifies the transfer of the configuration files to the target PMU.

Using the FILE command in TELNET session, the PMU configuration file can transfer between test PMU and ERKIOS as shown in Figure 6.1 to back up the pre-test configuration.

```

=>File Read CFG.TXT
#000 Ready to send file
#001 Transfer Complete

=>

=>

=>

=>

=>File Read SETTINGS\SET_S1.TXT
#000 Ready to send file
#001 Transfer Complete

=>

=>

=>File Read SETTINGS\SET_S2.TXT
#000 Ready to send file
#001 Transfer Complete

```

Figure 6.2: FILE command in TELNET session

The ERKIOS system is a general remote testing platform catering to both PMU and RAS remote testing by controlling substation equipment. The ERKIOS can control substation equipment to enable/disable testing mode for remote PMU testing. Most of the substations are unmanned substation that is not controlled manually. The ERKIOS uses TELNET session to redirect PMU data using a local testing system (LTS) for the PMU Performance Analyzer. The configuration files of controlling substation devices are updated by control command from ERKIOS master computer via TELNET session. The redirecting data are most important step for security point of view. The ERKIOS also uses secure communication layer such as SSH to transfer the configuration file. The SEL PMU used to test ERKIOS system for controlling substation equipment as shown in Figure 6.2.

```
$ scp ERKIOS@/conf/SEL421/SET_S5.txt LTS@conf/SEL/SET_S5.txt
```

Figure 6.3: SCP command to transfer configuration file using SSH session

Once the configuration file is transferred in the LTS, it sends the configuration file to target PMU locally via TELNET session as shown in Figure 6.3.

```

=>>File Write SETTINGS\SET_S5.TXT
CCC#001 Transfer Complete

=>>

```

Figure 6.4: File command to send a configuration file from LTS to target PMU

## 6.7 Summary

ERKIOS is developed to test RAS systems in the field. Its deployment has the potential to enhance the reliability of RAS systems, which can possibly avoid power blackouts if they work properly. The given approach was applied as a middleware framework prototype; which goal is to detect the

existence of hidden or dormant failures to verify the correct operation in the field of the power grid system. The analysis focused on Self-Testing coding techniques and Remedial Action Schemes: Impacts on the System and Input Variables Schemes. The approach proposed was applied at different levels to hardware and/or software of the End-to-End composition of modules to improve robustness.

## 7. Remote RAS Testing

---

### 7.1 Introduction

Remedial Action Scheme (RAS) is an automatic control mechanism designed to detect the abnormal system conditions and take fast control action for maintaining the system reliability. A new RAS is developed to minimize the wind power curtailment and protect the transmission lines from overload/ congestion problems, which can be easily extended for voltage stability or other related problems. Distributing this RAS logic to multiple computers located near the edge improves the robustness and remedial action response times. To highlight this, how we run RAS logic in the testbed will evolve through a variety of configurations. Initially curtailment logic is run in a standard single, centralized style as a baseline comparison point. Distributed schemes, each have unique redundancy and fault-tolerance capabilities compared to a centralized system, often with measurable performance tradeoffs [19-23].

The specifications of the RAS test suite are briefly listed:

- The RAS test suite should be able to test Relays, Instrument transformers, and communication network, PMU, and RAS controller for the end-to-end remote testing.
- The RAS test suite should be able to generate appropriate testing signals based on the test target.
- The data format of packets, which transmit from the control center to the substation, should contain a time stamp, voltage phasor values, current phasor value, frequency values, and couple reserved bits.
- The ERKIOS should be able to send the testing signals from the control center to substations and send the control actions back to control center from the substation.
- The ERKIOS should be able to control the signal switch based on the test signal.
- The Analog Signal Generator and Amplifier should be able to receive the testing signals from the ERKIOS substation PC and convert them to appropriate testing power signal.
- The RAS test suite should be able to intercept the control actions from relays.
- All the signals should have the time stamps, which can utilize for analyzing communication latency, possible packet drop and the speed of the RAS.
- The RAS test suite should be able to generate the test result report based on the received control actions and the related time stamps.

The test result report should contain 1) Whether the RAS give the correct control action 2) How is the performance of communication network 3) Whether the Instrument transformers work well 4) Whether the PMU/PDC work well 5) Whether the RAS controller works as expected 6) Whether the relays work correctly

In the normal operation mode, the PMU measures voltage and current phasors based on the signal from CT/PT, which connects on the power grids. Then, PMU sends the measurements to substation computer, which is implementing the RAS algorithm. In the RAS testing mode, the input signal

must be generated before the PMU by an Analog Signal Generator and Amplifier, which generate the test analog signal based on the trigger signal from ERKIOS. The analog signal is delivered to an amplifier, which will convert it into a high-power analog signal to replicate a standard grid measurement. The high-power analog signal will be measured by PMU and the PMU measurements will be sent to the substation computer, which is then the same with the normal operation mode.

The interface of the RAS output should also be controlled by another signal switch. In the normal operation mode, the signal switch should connect to the RAS action performing actuator, which is the circuit breaker in the power grid. In the RAS testing mode, the signal is switched to connect to the ERKIOS local test system collector, which can collect the control actions from the substation computer and send them back to ERKIOS Master Computer. This switching can be a physical switch or a network switch performing the collection.

An operator setting up an ERKIOS local test system must establish a device specific connection, either with analog switched connectors, alternative connection, or digital network traffic rerouting. In addition to a device's specific input connections general requirements, such as device maximum allowable time for testing should be specified along with device types. Specific details about timing and test requirements can be found under the IEEE TSS review sections.

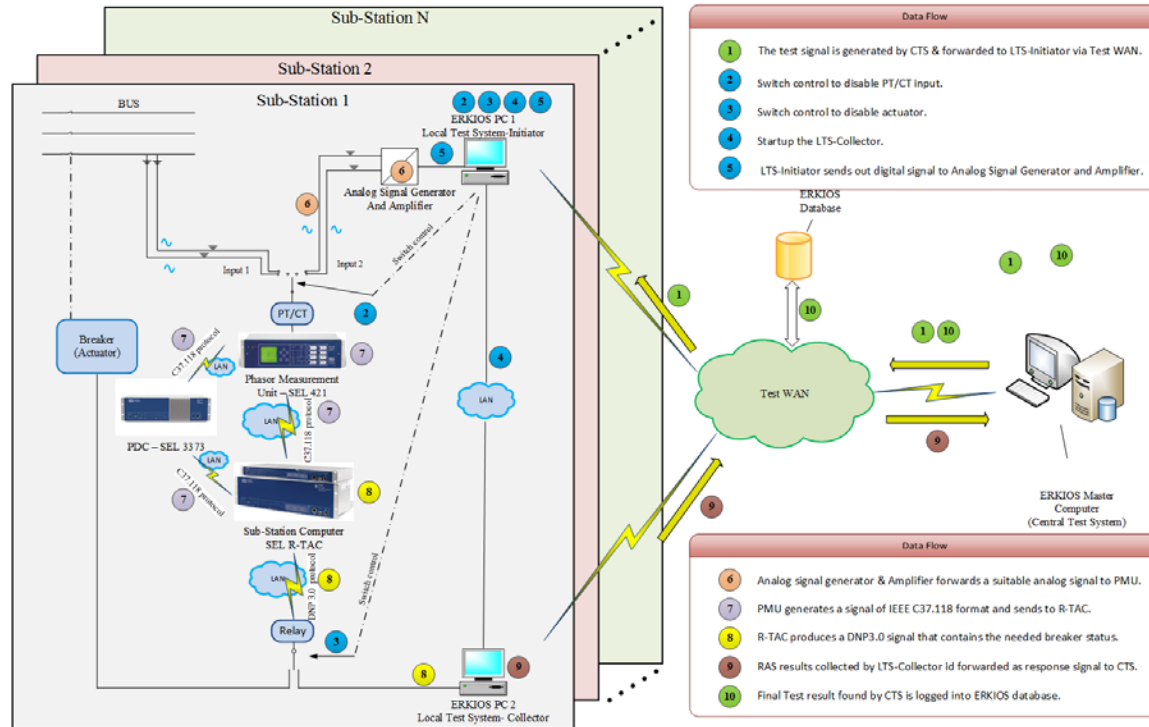


Figure 7.1: Interfacing Architecture with RAS at Substation

In order to enable the end-to-end and in field remote testing for RAS, a middleware framework called ERKIOS is developed. ERKIOS was designed to test a very wide range of RAS schemes in the field in order to ensure that the distributed components in a RAS scheme are functioning property. ERKIOS also supports a very wide range of failure models, handling failures of both

grid components as well as pieces of ERKIOS itself. The architecture of end-to-end in-field testing of RAS by ERKIOS is shown in the Figure 7.1. There are two different operation modes for this architecture: 1) Normal Operation 2) RAS testing.

In the Normal Operation mode, all the substations are connected to the rest of the power grid through the transmission lines. The sensor, which is Phasor Measurement Unit in this case, measures the different parameters, such as voltage and current phasors, in all the substations. The measurements are delivered to the substation computer, which implements the RAS algorithm, based on C37.118 communication protocol. The substation computer runs the RAS algorithm and generates the appropriate control actions, which is sent to the respective relay, breaker, or actuator. The control actions are transmitted by DNP 3.0 communication protocol.

In the RAS testing mode, ERKIOS is involved as a middleware framework for RAS testing. There are five main components for the RAS testing mode: 1) ERKIOS Master Computer 2) LTS-Initiator 3) Analog Signal Generator and Amplifier 4) Sensor and Substation Computer 5) LTS-Collector.

## 7.2 Test plans of wind curtailment RAS

Since the installation of wind farm is increasing rapidly, wind power has become an important renewable source of power generation in smart grids. Based on <sup>[1]</sup>, the wind energy consumption occupies 19% of the total renewable energy consumption in 2015, and the percentage is keeping increasing. However, the wind generation highly depends on local weather condition. Intermittency and uncertainty in wind generation may cause exceeding the line ratings of the low voltage transmission lines, which requires wind generation curtailment to protect the transmission line from overload conditions.

Table 7.1: Facts on Wind Curtailment Issues

Regions	Curtailment Facts
ERCOT, US	Wind generation is curtailed approximately 45-50% of the days from Jan. to Aug. 2008. From Dec. 2008 to Dec. 2009, daily wind curtailment is between 500MW and 2000MW, sometimes up to 3900 MW. Monthly averages ranged from about 24-28% of potential wind generation.
Midwest ISO, US	About 200,000 MWh wind energy were curtailed in 2009.
SCE, US	About 3-4 hours curtailment every two days (or 6-8% of the time).
China	30% of installed wind capacity hasn't been connected to the grid by end-2011. Moreover, according to data from China Electricity Council (CEC), approximately 11% of wind power generated in China was not procured by grid operators.
Alberta, Canada	From Jan. to Dec. 2010: 3055 hours of wind curtailment period and 155 facilities were affected.
Spain	In 2010, wind curtailment totaled 315,230 MWh. Between Jan. 2011 and Apr. 2011, wind curtailment totaled 23,994 MWh

Table 7.1 shows some of the wind curtailment conditions all over the world. In order to keep increasing the integration of wind renewable energy and maintain the reliability and stability of power system, innovative automation and information technologies need to be deployed for the power system operation and control.

This demonstration includes eight test-plan for the wind curtailment remedial action scheme (RAS). These RAS tests are conducted based on the measurements collected from PMUs. The optimal RAS solution is calculated for the minimal curtailment of wind generation based on DC power flow model. The RAS controllers should be able to collect measurement data, analyze the system status, propose control strategy, and execute control actions of wind farm generation curtailment. For implementation, this project deploys a real-time hardware-in-the-loop (HIL) testbed, which involves with RTDS as a power system simulator, BeagleBone programmed controller, SEL-421 hardware PMU, and GTNET software PMU.

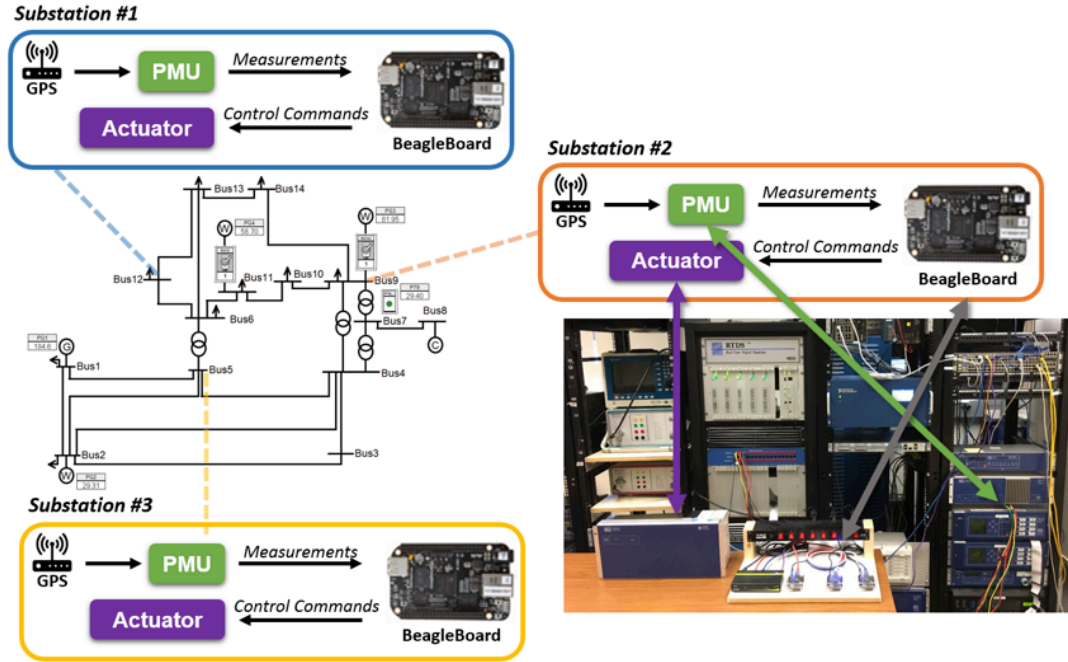


Figure 7.2: Real-Time Implementation Testbed

Table 7.2: Test Plan Objectives of Wind Curtailment Ras

Test	Operating Condition	Objectives
1	Normal	Verify if the RAS controller can remain stable when there is no operational violation detected
2	Alert	Verify if the RAS controller can execute RAS control action of wind curtailment when there exists <i>one</i> transmission line violating the preset line ratings
3	Alert	Verify if the RAS controller can execute RAS control action of wind curtailment when there exists <i>one</i> transmission line violating the modified line ratings

Verify if the RAS controller can execute RAS control action of wind curtailment when there exists *two* transmission line violating the modified line ratings

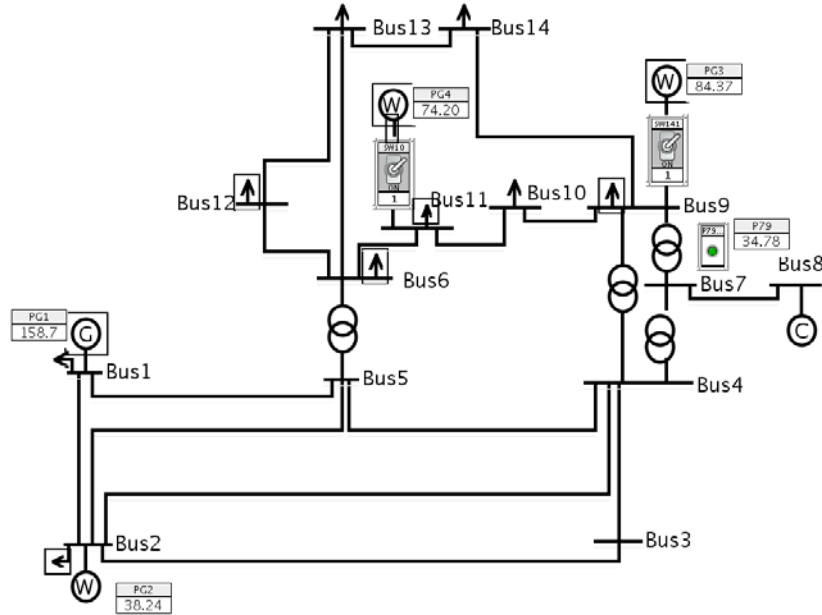


Figure 7.3: One Line Diagram of IEEE 14-Bus Test System with 3 Wind Farms

Table 7.3 demonstrates the basic information of the Ras testing system in details.

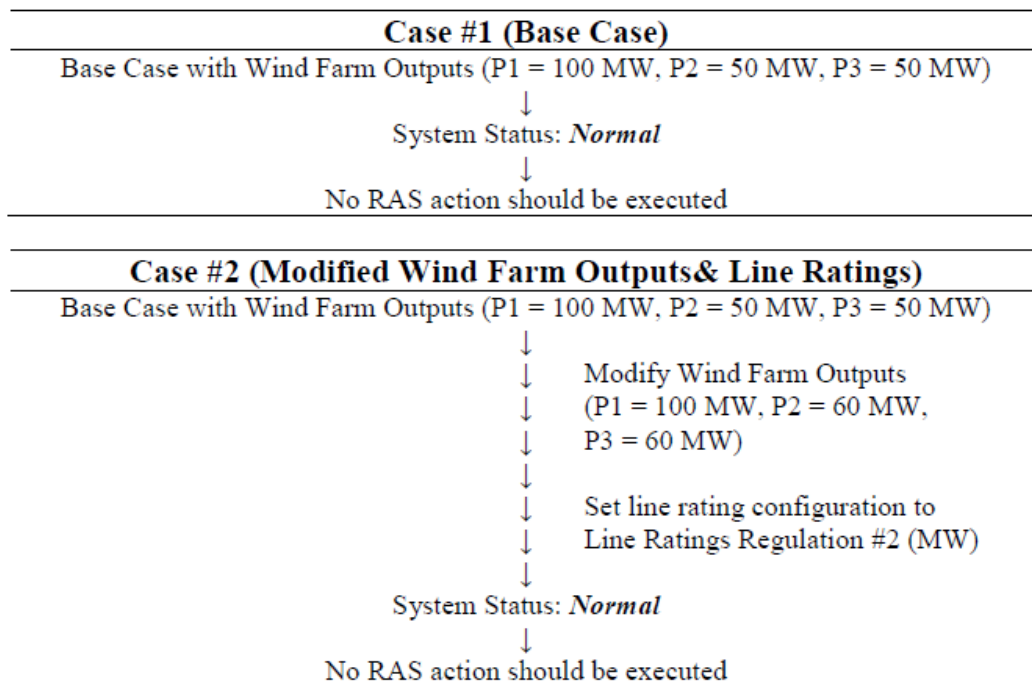
Table 7.3 Descriptions of Base Case

Property	Configurations
Test System Model	Extended IEEE 14-Bus System
Total Load for Base Case	347.8 MW
Number of Wind Farms	3
Wind Farm Locations	Bus #2, #9 and #11
Preset Slack Bus Generator Output	$P_S = 148.7$ MW
Preset Wind Farm Output	$P_1 = 100$ MW, $P_2 = 50$ MW, $P_3 = 50$ MW
Number of Regulated Transmission Lines	20
Preset Line Ratings (MW)	[100, 50, 100, 35, 50, 50, 50, 50, 50, 50, 70, 50, 50, 50, 35, 30, 50, 70, 30, 30]
Line Ratings Regulation #1 (MW)	[100, 50, 100, 35, 50, 50, 50, 50, 50, 50, 70, 50, 50, 50, 35, 30, 50, 70, 30, 30]
Line Ratings Regulation #2 (MW)	[100, 50, 100, 35, 50, 50, 50, 50, 50, 50, 70, 50, 50, 50, 30, 30, 50, 70, 30, 30]
Line Ratings Regulation #3 (MW)	[100, 50, 100, 35, 50, 45, 50, 50, 50, 50, 70, 50, 50, 50, 35, 30, 50, 70, 30, 30]

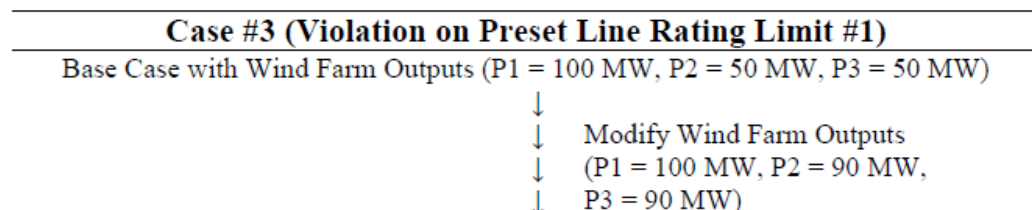
Line Ratings Regulation #4 (MW)	[100, 50, 100, 35, 50, 45, 50, 50, 50, 50, 70, 50, 50, 50, 30, 30, 50, 70, 30, 30]
---------------------------------	--

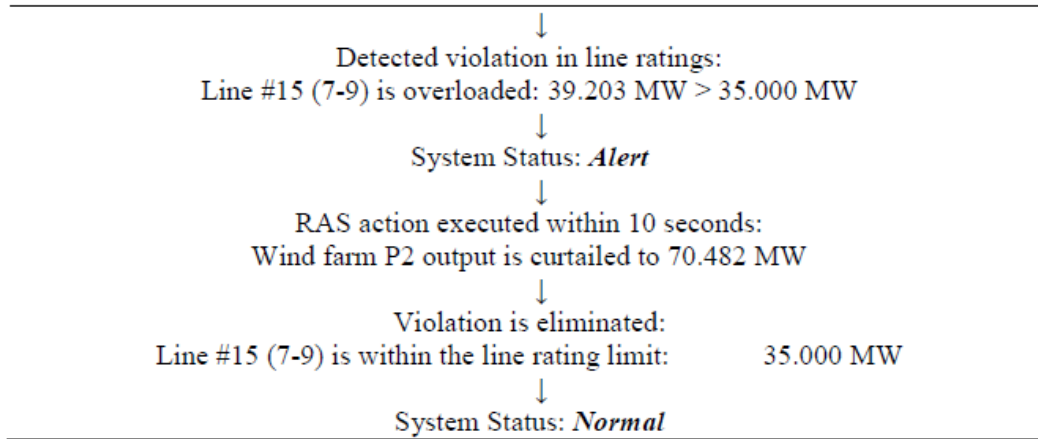
## **Demonstration of Test Plans**

*Test 1: Verify if the RAS controller can remain stable when there is no operational violation detected*

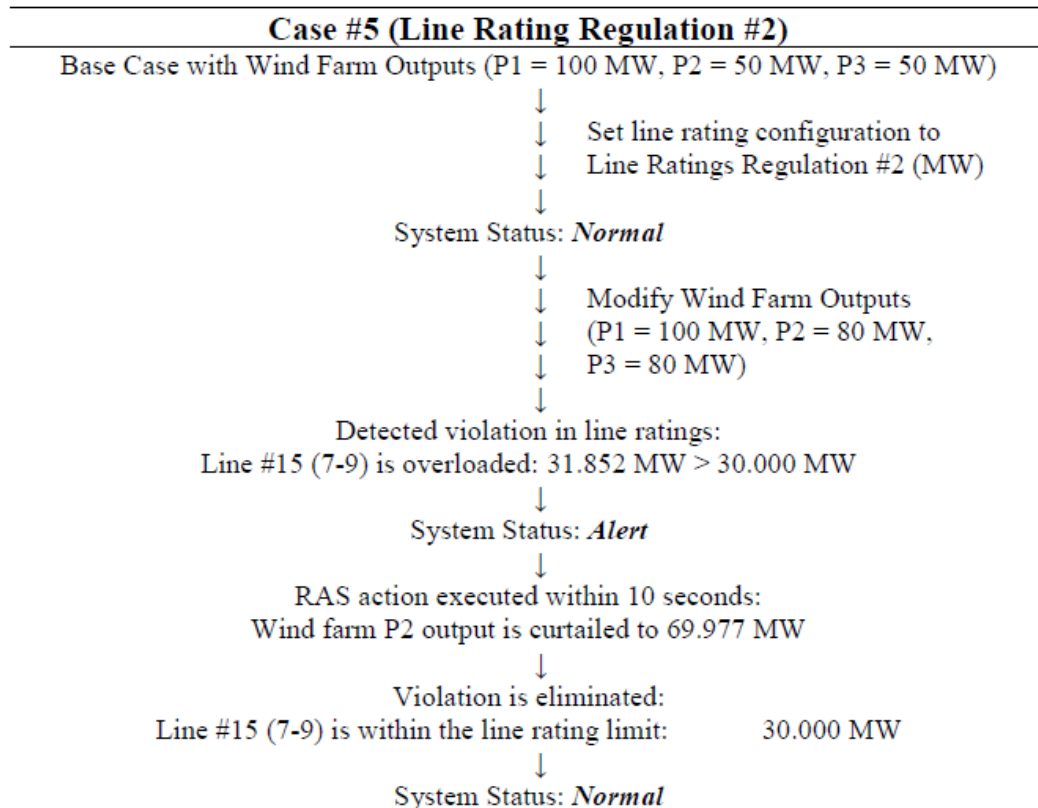


*Test 2: Verify if the RAS controller can execute RAS control action of wind curtailment when there exists **one** transmission line violating the preset line ratings*

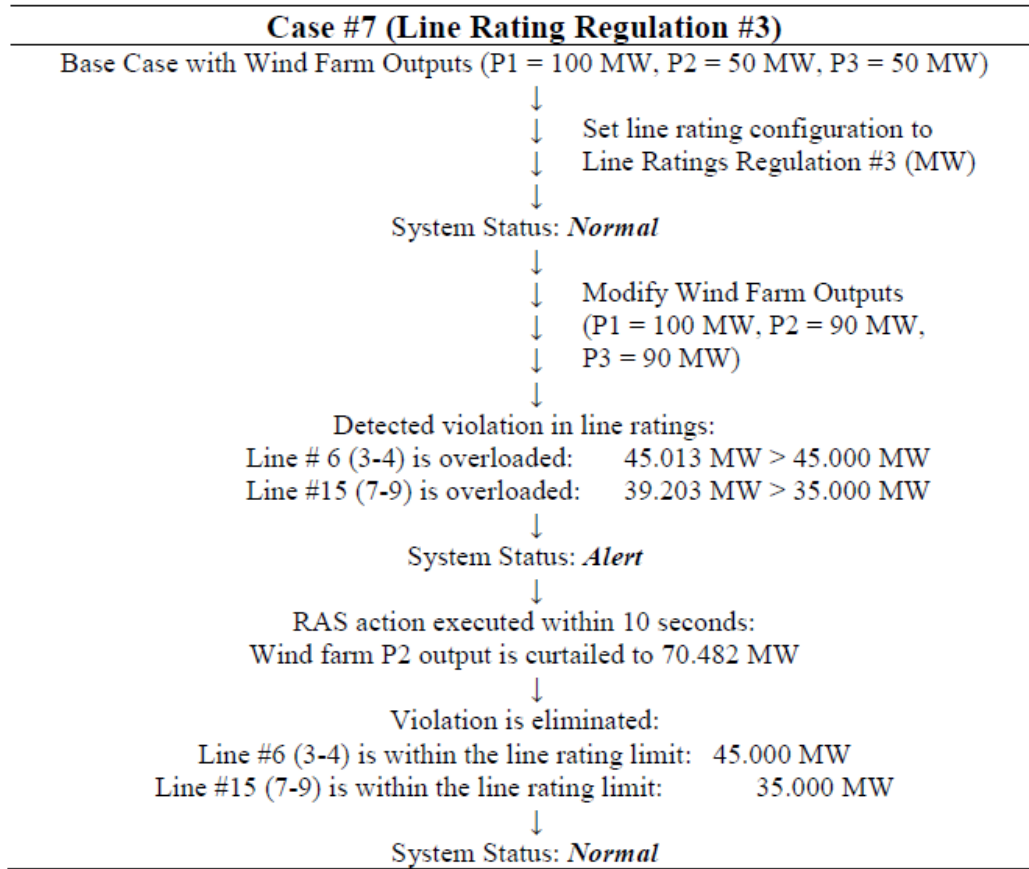




*Test 3:* Verify if the RAS controller can execute RAS control action of wind curtailment when there exists **one** transmission line violating the modified line ratings



*Test 4:* Verify if the RAS controller can execute RAS control action of wind curtailment when there exists *two* transmission lines violating the modified line ratings



### 7.3 Idaho Power RAS

The 179 bus WECC system was modified to include the geographical area involved in one of the RAS scheme implemented by Idaho Power. The model was built on Opal-RT to study the test cases for the implemented RAS. The primary function of the RAS is to prevent thermal damages to the lines following any contingency or if a line is removed for maintenance activities. It also helps to optimize the transfer along critical corridors.

This simulation considers an event where remediation is being taken by the RAS. A 345 kV line outage is considered. The power flow monitored at another line gets overloaded during this line outage. The RAS takes control action by adding a shunt capacitor, which limits the line flow in the overloaded line as shown in the simulation results below.

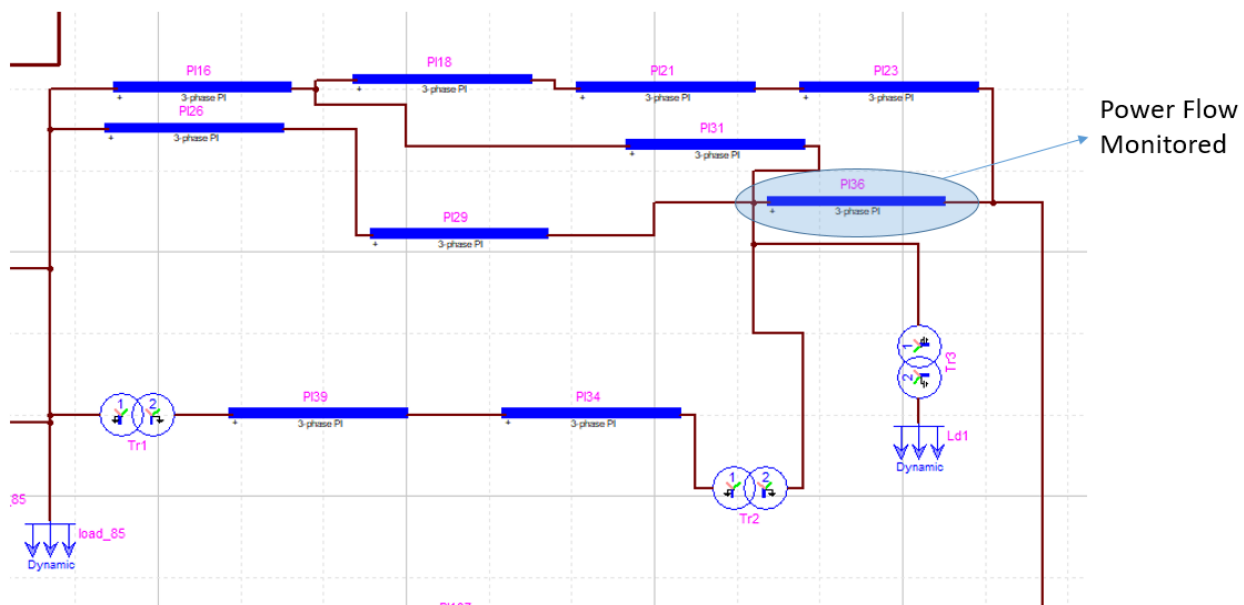


Figure 7.4: OPAL-RT SLD Idaho RAS geographic area involved

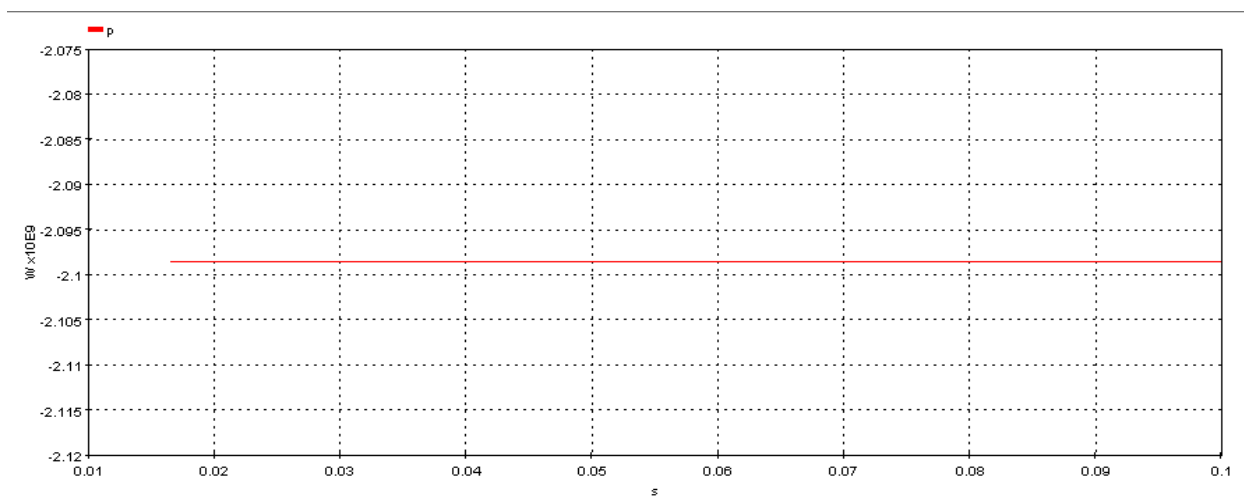


Figure 7.5: Power flow in the monitored line

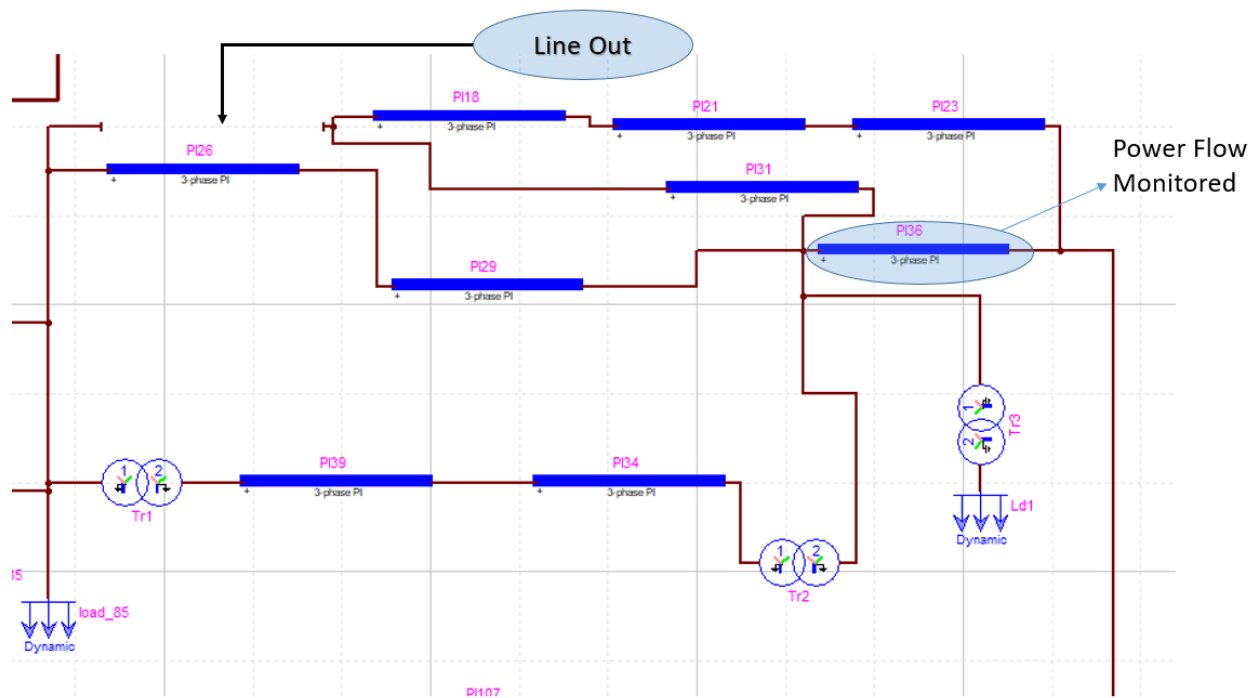


Figure 7.6: 345kV line outage

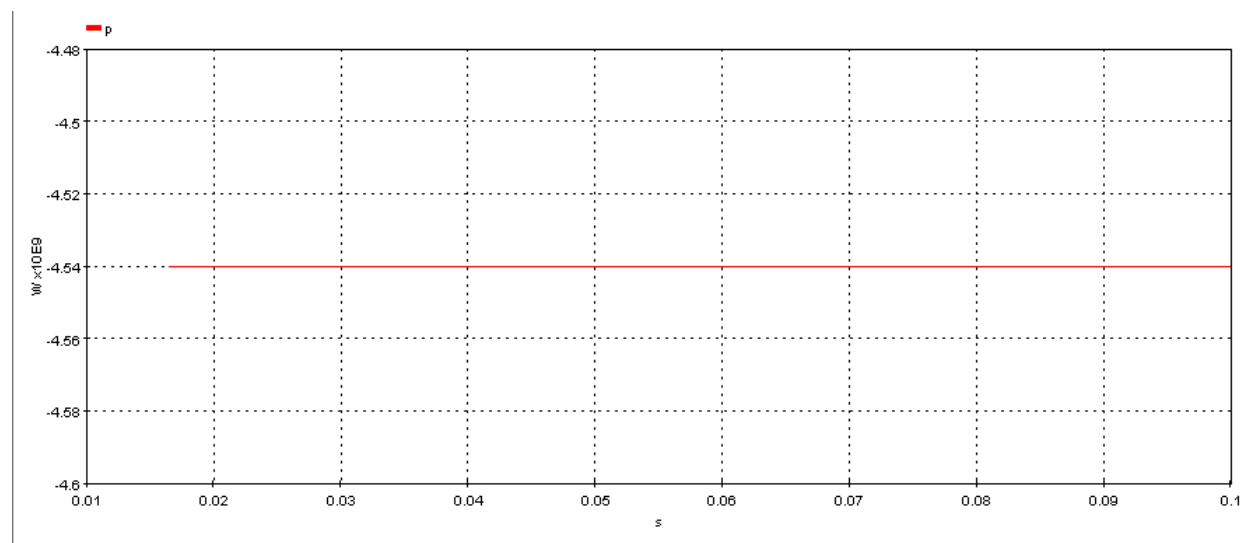


Figure 7.7: Monitored power flow during line outage

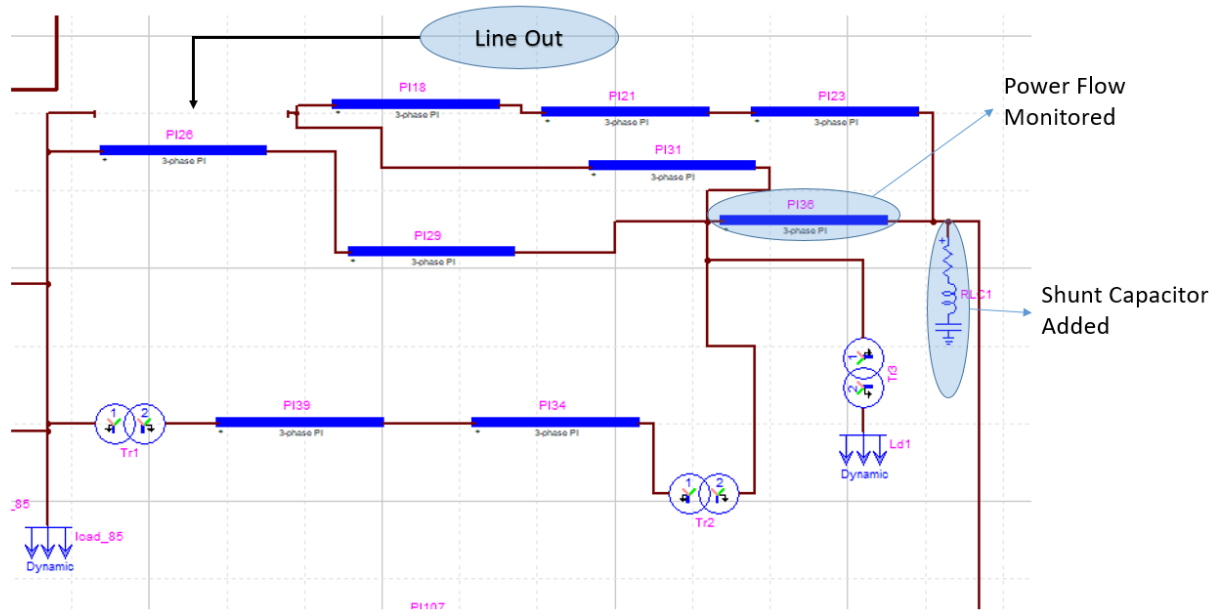


Figure 7.8: RAS control action by adding shunt capacitor during line outage

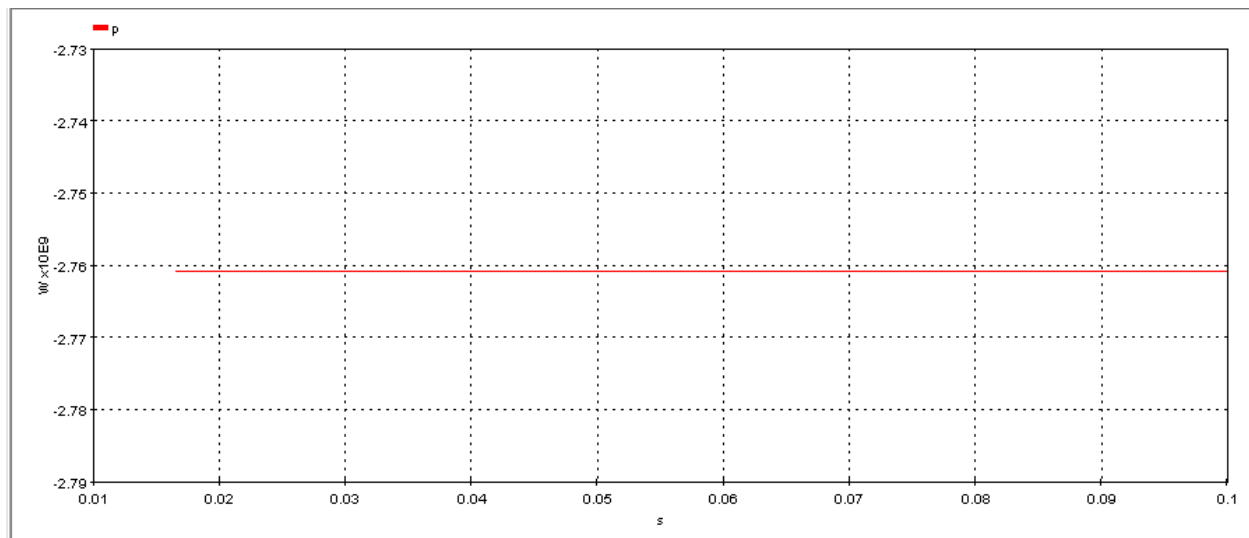


Figure 7.9: Power flow after RAS control action

### Future Testing

Future testing involves validating the remediation taken by RAS for contingencies, which include loss of line from service and overload condition in monitored lines and transformers. The control actions implemented by RAS include adding of shunt capacitors, bypassing series capacitors and shedding of generation at the power plants.

## 7.4 Summary

The RAS test suite is a software & hardware hybrid platform, which is designed for remote testing the specific RAS. The standalone RAS test suite is integrated with ERKIOS middleware for the data management of RAS testing and communication between the substation and control center. Erkios is developed to provide in-field and end-to-end testing of RAS system. The RAS test suite and ERKIOS is capable of end-to-end remote testing in-field RAS without interrupting them from operation for a long time. The operation of the setup will prove the feasibility and reliability of the Erkios framework in a real power grid. Further, it will enrich Erkios by helping to build functionality and libraries to test different RAS. The testbed also paves the niche for implementing other in-field testing applications like PMU and relay testing.

## 8. Conclusions

---

The specification of the testing equipment required for the PMU testing lab is discussed in this report. The architecture of the test bed and the features of the software called PPA used for automatic PMU testing are presented. The successful implementation of PMU testing performed at the Southern California Edison (SCE) using PPA is presented. The result of the PMU testing shows that the compliance of the standard for 30 fps and 60 fps can be different for some of the test scenarios. The process of integrating a middleware like Erkios for Remedial Action Scheme (RAS) testing with the simulated power grid and connected hardware in the loop is discussed. The infrastructure and other requisites to build such an integration and data management are clearly described with the implementation of the testbed. The operation of the prototype testbed integration provides the insight for the feasibility and reliability of the Erkios framework in a real power grid. Further, it will enrich Erkios by helping to build functionality and libraries to test different RAS.

## Appendix A

---

- Result for PMU performance analyzer

Test results of steady state performance of pmu - angle change: balanced system.

[A.1] Status of time synchronization of the ideal pmu & the test pmu:

<i>Input Voltage Magnitude (in p.u.)</i>	<i>TVE of Phase-A (in percentage)</i>	<i>TVE of Phase-B (in percentage)</i>	<i>TVE of Phase-C (in percentage)</i>
20.000	0.007	0.022	0.016
40.000	0.006	0.030	0.016
60.000	0.015	0.038	0.016
80.000	0.008	0.019	0.015
100.000	0.016	0.017	0.015
120.000	0.022	0.015	0.026
140.000	0.008	0.013	0.023
160.000	0.005	0.015	0.012
180.000	0.006	0.007	0.009
200.000	0.006	0.009	0.023
220.000	0.004	0.019	0.019
240.000	0.015	0.023	0.018
260.000	0.012	0.009	0.016
280.000	0.009	0.012	0.015
300.000	0.016	0.012	0.024
320.000	0.009	0.014	0.020
340.000	0.010	0.020	0.015

[A.2] Analysis of Average TVE in Voltage Phasor Measurement:

Average TVE of Phase-A (in percentage)	Average TVE of Phase-B (in percentage)	Average TVE of Phase-C (in percentage)	Average TVE of + Seq. (in percentage)
0.010	0.017	0.018	0.008

Standard Deviation of TVE of Phase-A (in percentage)	Standard Deviation of TVE of Phase-B (in percentage)	Standard Deviation of TVE of Phase-C (in percentage)	Standard Deviation of TVE of + Seq. (in percentage)
0.005	0.008	0.004	0.002

[A.3] Analysis of Maximum & Minimum TVE in Voltage Phasor Measurement:

Maximum TVE of Phase-A (in percentage)	Minimum TVE of Phase-A (in percentage)	Maximum TVE of Phase-B (in percentage)	Minimum TVE of Phase-B (in percentage)	Maximum TVE of Phase-C (in percentage)	Minimum TVE of Phase-C (in percentage)	Maximum TVE of + Seq. (in percentage)	Maximum TVE of + Seq. (in percentage)
0.022	0.004	0.038	0.007	0.026	0.009	0.012	0.003

[A.4] Verification of PMU Performance - Maximum TVE in Voltage Phasor Measurement:

Maximum TVE (in percentage)	Allowed Maximum TVE (in percentage)	Test Result
0.038	1.000	PASS

[A.5] Magnitude Error in Voltage Phasor Measurement:

Mean M_E of Phase-A (in percentage)	Stand. Dev. of M_E of Phase-A (in percentage)	Minimum M_E of Phase-A (in percentage)	Maximum M_E of Phase- A (in percentage)
0.003	0.001	0.002	0.005
Mean M_E of Phase-B (in percentage)	Stand. Dev. of M_E of Phase-B (in percentage)	Minimum M_E of Phase-B (in percentage)	Maximum M_E of Phase- B (in percentage)
0.004	0.001	0.003	0.005
Mean M_E of Phase-C (in percentage)	Stand. Dev. of M_E of Phase-C (in percentage)	Minimum M_E of Phase- C (in percentage)	Maximum M_E of Phase-C (in percentage)
0.003	0.001	0.002	0.004

Mean P_E of Phase-C (in degrees)	Stand. Dev. of P_E of Phase-C (in degrees)	Minimum P_E of Phase-C (in degrees)	Maximum P_E of Phase-C (in degrees)
0.010	0.003	0.005	0.015

Mean M_E of + Seq. (in percentage)	Stand. Dev. of M_E of + Seq. (in percentage)	Minimum M_E of + Seq. (in percentage)	Maximum M_E of + Seq. (in percentage)
0.003	0.000	0.002	0.003

[A.6] Phasor Error in Voltage Phasor Measurement:

Mean P_E of Phase-A (in degrees)	Stand. Dev. of P_E of Phase-A (in degrees)	Minimum P_E of Phase-A (in degrees)	Maximum P_E of Phase-A (in degrees)
0.006	0.003	0.002	0.012

Mean P_E of Phase-B (in degrees)	Stand. Dev. of P_E of Phase-B (in degrees)	Minimum P_E of Phase-B (in degrees)	Maximum P_E of Phase- B (in degrees)
0.010	0.005	0.004	0.022

Mean P_E of + Seq. (in degrees)	Stand. Dev. of P_E of + Seq. (in degrees)	Minimum P_E of + Seq. (in degrees)	Maximum P_E of + Seq. (in degrees)
0.004	0.002	0.000	0.007

[B.1] Analysis of TVE in Current Phasor Measurement:

Input Voltage magnitude (in p.u.)	TVE of Phase-A (in percentage)	TVE of Phase-B (in percentage)	TVE of Phase-C (in percentage)
20.000	0.111	0.099	0.178
40.000	0.131	0.123	0.199
60.000	0.137	0.145	0.142
80.000	0.148	0.150	0.131
100.000	0.137	0.114	0.165
120.000	0.147	0.126	0.192
140.000	0.139	0.112	0.145
160.000	0.137	0.136	0.117
180.000	0.122	0.141	0.111
200.000	0.134	0.118	0.166
220.000	0.166	0.125	0.139
240.000	0.148	0.115	0.152
260.000	0.149	0.146	0.133
280.000	0.135	0.109	0.167
300.000	0.147	0.135	0.143
320.000	0.177	0.116	0.148
340.000	0.152	0.128	0.153

[B.2] Analysis of Average TVE in Current Phasor Measurement:

Average TVE of Phase-A (in percentage)	Average TVE of Phase-B (in percentage)	Average TVE of Phase-C (in percentage)	Average TVE of + Seq. (in percentage)
0.142	0.126	0.152	0.087

Standard Deviation of TVE of Phase-A (in percentage)	Standard Deviation of TVE of Phase-B (in percentage)	Standard Deviation of TVE of Phase-C (in percentage)	Standard Deviation of TVE of + Seq. (in percentage)
0.015	0.015	0.024	0.008

[B.3] Analysis of Maximum & Minimum TVE in Current Phasor Measurement:

Max. TVE of Phase-A (in %)	Min. TVE of Phase-A (in %)	Max. TVE of Phase-B (in %)	Min. TVE of Phase-B (in %)	Max. TVE of Phase-C (in %)	Min. TVE of Phase-C (in %)	Max. TVE of + Seq. (in %)	Max. TVE of + Seq. (in %)
0.177	0.111	0.150	0.099	0.199	0.111	0.096	0.066

[B.4] Verification of PMU Performance - Maximum TVE in Current Phasor Measurement:

Maximum TVE (in percentage)	Allowed Maximum TVE (in percentage)	Test Result
0.199	1.000	PASS

[B.5] Magnitude Error in Current Phasor Measurement:

Mean M_E of Phase-A (in percentage)	Stand. Dev. of M_E of Phase-A (in percentage)	Minimum M_E of Phase-A (in percentage)	Maximum M_E of Phase-A (in percentage)
0.110	0.021	0.080	0.137

Mean M_E of Phase-B (in percentage)	Stand. Dev. of M_E of Phase-B (in percentage)	Minimum M_E of Phase-B (in percentage)	Maximum M_E of Phase-B (in percentage)
0.104	0.014	0.075	0.131

Mean M_E of Phase-C (in percentage)	Stand. Dev. of M_E of Phase-C (in percentage)	Minimum M_E of Phase-C (in percentage)	Maximum M_E of Phase-C (in percentage)
0.078	0.015	0.063	0.092

Mean M_E of + Seq. (in percentage)	Stand. Dev. of M_E of + Seq. (in percentage)	Minimum M_E of + Seq. (in percentage)	Maximum M_E of + Seq. (in percentage)
0.057	0.006	0.049	0.068

[B.6] Phasor Error in Current Phasor Measurement:

Mean P_E of Phase-A (in degrees)	Stand. Dev. of P_E of Phase-A (in degrees)	Minimum P_E of Phase-A (in degrees)	Maximum P_E of Phase-A (in degrees)
0.071	0.012	0.052	0.097
Mean P_E of Phase-B (in degrees)	Stand. Dev. of P_E of Phase-B (in degrees)	Minimum P_E of Phase-B (in degrees)	Maximum P_E of Phase-B (in degrees)
0.063	0.009	0.047	0.084

Mean P_E of Phase- C (in degrees)	Stand. Dev. of P_E of Phase-C (in degrees)	Minimum P_E of Phase-C (in degrees)	Maximum P_E of Phase-C (in degrees)
0.083	0.014	0.057	0.111

Mean P_E of + Seq. (in degrees)	Stand. Dev. of P_E of + Seq. (in degrees)	Minimum P_E of + Seq. (in degrees)	Maximum P_E of + Seq. (in degrees)
0.045	0.013	-0.001	0.055

[C.1] Analysis of FE in Frequency Measurement:

Input Voltage Magnitude (in p.u.)	FE (in Hz)
20.000	0.000
40.000	0.000
60.000	0.000
80.000	0.000
100.000	0.000
120.000	0.000
140.000	0.000
160.000	0.000
180.000	0.000
200.000	0.000
220.000	0.000
240.000	0.000
260.000	0.000
280.000	0.000
300.000	0.000
320.000	0.000
340.000	0.000

Mean FE (in Hz)	Stand. Dev. of FE (in Hz)	Minimum FE (in Hz)	Maximum FE (in Hz)
0.000	0.000	0.000	0.000

[C.2] Verification of PMU Performance - Maximum FE in Frequency Measurement:

Maximum FE (in Hz)	Allowed Maximum FE (in Hz)	Test Result
0.000	0.010	PASS

[D.1] Analysis of RFE in Frequency Measurement:

Input Voltage Magnitude (in p.u.)	RFE (in Hz/s)
20.000	0.001
40.000	0.002
60.000	0.001
80.000	0.002
100.000	0.001
120.000	0.002
140.000	0.002
160.000	0.001
180.000	0.002
200.000	0.001
220.000	0.001
240.000	0.002
260.000	0.001
280.000	0.001
300.000	0.002
320.000	0.001
340.000	0.001

Mean FE (in Hz/s)	Stand. Dev. of FE (in Hz/s)	Minimum FE (in Hz/s)	Maximum FE (in Hz/s)
0.002	0.000	0.001	0.002

[D.2] Verification of PMU Performance - Maximum RFE in ROCOF Measurement:

Maximum RFE (in Hz/s)	Allowed Maximum RFE (in Hz/s)	Test Result
0.002	1.000	PASS

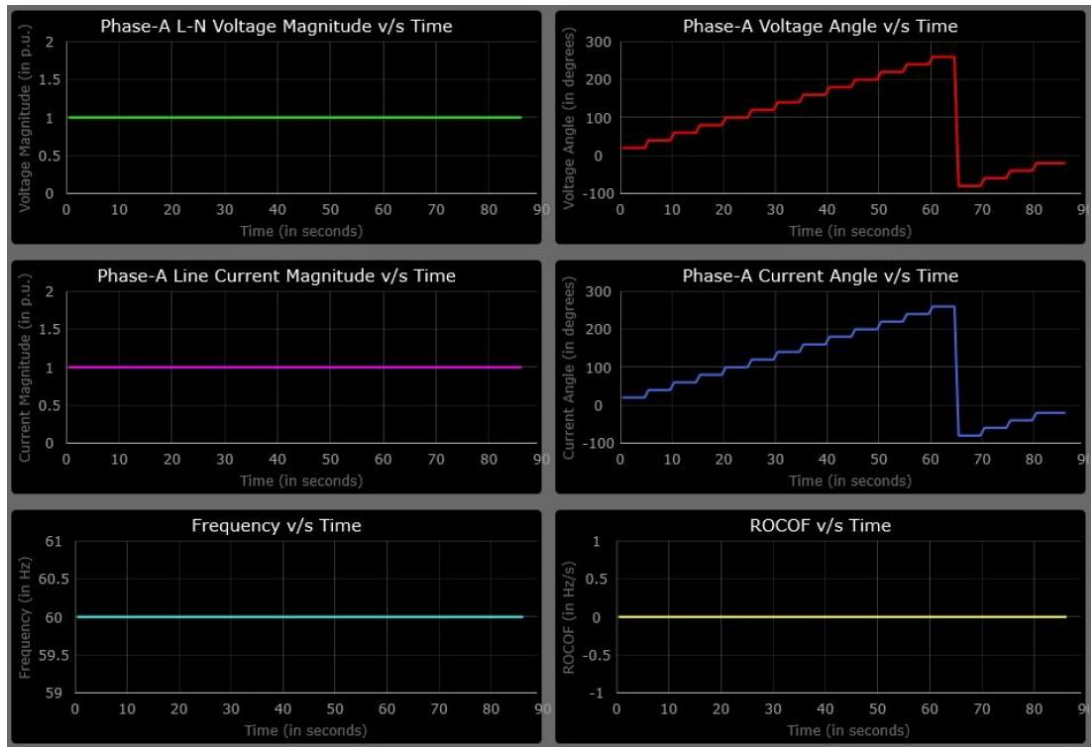


Figure A1.1 PPA test for balanced system with angle change.

## References

---

- [1] Real-time applications of phasor measurement units (PMU) for visualization, reactive power monitoring and voltage stability protection,” The New York State Energy Research and Development Authority, Nov 2010. [Online]. Available: <https://www.nyserda.ny.gov/-/media/Files/Publications/Research/Electic-Power-Delivery/real-time-applications-PMU.pdf>
- [2] “IEEE standard for synchrophasor measurements for power systems,” IEEE Std. C37.118.1-2011 (Revision of IEEE Std. C37.118-2005), Dec. 2011.
- [3] “IEEE standard for synchrophasor measurements for power systems-Amendment 1: modification of selected performance requirements,” IEEE Std. C37.118.1a-2014 (Amendment to IEEE Std. C37.118.1-2011), Apr. 2014.
- [4] “Advancement of synchrophasor technology in projects funded by the american recovery and reinvestment act of 2009,” U.S. Department of Energy, Mar 2016. [Online]. Available: [https://www.smartgrid.gov/files/20160320 Synchrophasor Report.pdf](https://www.smartgrid.gov/files/20160320%20Synchrophasor%20Report.pdf)
- [5] “Phasor measurement units gain credibility through improved test and calibration standards,” Fluke Calibration, 2017. [Online]. Available:[http://download.flukecal.com/pub/literature/3780120C EN w.pdf](http://download.flukecal.com/pub/literature/3780120C%20EN%20w.pdf)
- [6] S. S. Biswas, A. K. Srivastava, J. S. Park, and J. Castaneda, “Tool for testing of phasor measurement units: Pmu performance analyser,” IET Generation, Transmission Distribution, vol. 9, no. 2, pp. 154–163, 2015.
- [7] P. Komarnicki, C. Dzienis, Z. A. Styczynski, J. Blumschein, and V. Centeno, “Practical experience with pmu system testing and calibration requirements,” in 2008 IEEE Power and Energy Society General Meeting - Conversion and Delivery of Electrical Energy in the 21st Century, July 2008, pp. 1–5.
- [8] Y. H. Tang, G. N. Stenbakken, and A. Goldstein, “Calibration of phasor measurement unit at nist,” IEEE Transactions on Instrumentation and Measurement, vol. 62, no. 6, pp. 1417–1422, June 2013.
- [9] D. Georgakopoulos and S. Quigg, “Precision measurement system for the calibration of phasor measurement units,” IEEE Transactions on Instrumentation and Measurement, vol. 66, no. 6, pp. 1441–1445, June 2017.
- [10] OPENPDC, “OPENPDC.” [Online]. Available: <http://www.gridprotectionalliance.org>
- [11] S. S. Biswas, A. K. Srivastava, J. S. Park, and J. Castaneda, “Tool for testing of phasor measurement units: Pmu performance analyser,” IET Generation, Transmission Distribution, vol. 9, no. 2, pp. 154–163, 2015.
- [12] A. Goldstein et al., “Ieee synchrophasor measurement test suite specification,” New York: IEEE 2014
- [13] M. Karimi-Ghartemani, B. T. Ooi, and A. Bakhshai, “Application of enhanced phase-locked loop system to the computation of synchrophasors,” IEEE Transactions on Power Delivery, vol. 26, no. 1, pp. 22–32, Jan 2011.
- [14] J. A. de la O Serna, “Synchrophasor estimation using prony's method,” IEEE Transactions on Instrumentation and Measurement, vol. 62, no. 8, pp. 2119–2128, Aug 2013.
- [15] A. G. Phadke, J. S. Thorp, and M. G. Adamiak, “A new measurement technique for tracking voltage phasors, local system frequency, and rate of change of frequency,” IEEE Transactions on Power Apparatus and Systems, vol. PAS-102, no. 5, pp. 1025–1038, May 1983.

- [16] A. E. Patel M., Aivolaityas S., \Real-Time Application of Synchrophasors for Improving Reliability ,\" NERC, Tech. Rep., October 2010.
- [17] L. Chavez, D. Bakken, A. Bose, and P. Panciatici, “Erkios: End-to-end field-based RAS testing,” in Innovative Smart Grid Technologies (ISGT), 2015 IEEE PES, Feb 2015.
- [18] “WECC policy regarding extreme contingencies and unplanned events,” Western Electric Coordinating Council, May 2002.
- [19] “Special protection system criteria,” North East Power Coordinating Council, p. 11, November 2002.
- [20] D. Karlsson and X. Waymel, “System protection schemes in power networks,” CIGRE Task Force 38.02.19, June 2001.
- [21] M. Vaiman, P. Hines, J. Jiang, S. Norris, M. Papic, A. Pitto, Y. Wang, and G. Zweigle, “Mitigation and prevention of cascading outages: Methodologies and practical applications,” in Power and Energy Society General Meeting (PES), 2013 IEEE, July 2013, pp. 1–5.
- [22] “Minimum operating reliability criteria (more),” Western Electric Coordinating Council, April 2005.
- [23] J. Wen, W. Liu, P. Arons, and S. Pandey, “Evolution pathway towards wide area monitoring and protection - a real-world implementation of centralized RAS system,” Smart Grid, IEEE Transactions on, vol. 5, no. 3, pp. 1506–1513, May 2014.

## **Part III**

### **PMU/MU Characterization and Data Validation via Substation Dynamic State Estimation**

Sakis A. P. Meliopoulos  
George J. Cokkinides  
Boqi Xie, Graduate Student  
Jiahao Xie, Graduate Student  
Yu Liu, Graduate Student  
Liangyi Sun, Graduate Student  
Yuan Kong, Graduate Student  
Chiyang Zhong, Graduate Student  
Orestis Vasios, Graduate Student

Georgia Institute of Technology

**For information about this project, contact:**

Sakis A.P. Meliopoulos  
Georgia Institute of Technology  
School of Electrical and Computer Engineering  
777 Atlantic Dr. E164  
Atlanta, Georgia 30332-0250  
Phone: 404-894-2926  
E-mail: sakis.m@gatech.edu

**Power Systems Engineering Research Center**

The Power Systems Engineering Research Center (PSERC) is a multi-university Center conducting research on challenges facing the electric power industry and educating the next generation of power engineers. More information about PSERC can be found at the Center's website: <http://www.pserc.org>.

**For additional information, contact:**

Power Systems Engineering Research Center  
Arizona State University  
527 Engineering Research Center  
Tempe, Arizona 85287-5706  
Phone: 480-965-1643  
Fax: 480-727-2052

**Notice Concerning Copyright Material**

PSERC members are given permission to copy without fee all or part of this publication for internal use if appropriate attribution is given to this document as the source material. This report is available for downloading from the PSERC website.

**© 2018 Georgia Institute of Technology. All rights reserved**

## Table of Contents

1. Introduction .....	1
1.1 Background .....	1
1.2 Overview of the Problem .....	1
1.3 PMU and Merging Unit Testing Lab Development .....	2
1.4 Dynamic State Estimation Based Data Validation and Correction .....	3
1.5 Field Demonstration .....	6
1.6 Report Organization .....	6
2. PMU and Merging Unit Testing Lab Development .....	7
3. Substation Based Dynamic State Estimation .....	16
4. Substation Based Dynamic State Estimation: Numerical Example .....	23
4.1 System Configuration .....	23
4.2 Measurement Model Creation .....	24
4.3 Evaluation Method .....	26
4.4 State Estimation Results .....	28
5. Distributed System Quasi-Dynamic State Estimation: Use Case - Marcy Substation .....	35
5.1 Overview .....	35
5.2 Use Case System .....	35
5.3 Marcy System Model in WinIGS - SCAQCF Standard .....	37
5.4 Marcy co-Model: Physical System and IEDs .....	44
5.4.1 Instrumentation Channels .....	46
5.4.2 Measurement Channel .....	53
5.5 Use Case: Normal Operation with Load Variation .....	56
5.5.1 Event Description and Sampled Data .....	56
5.5.2 Setup DS-QSE for Marcy Substation .....	63
5.5.3 Execute DS-QSE and Record Performance .....	68
6. Conclusions .....	76
Appendix A. Object Oriented Modeling Standard .....	78
A.1 Quasi-dynamic Domain SCAQCF Device Model Description .....	78
A.2 Quasi-dynamic Domain SCAQCF Measurement Model Description .....	83
A.3 Modeling Example: Single-Phase Transformer Model .....	87
A.3.1 Single-Phase Transformer – Compact Form .....	87

A.3.2 Single-Phase Transformer – Quadratized Form.....	89
References .....	93

## List of Figures

Figure 1.1: Laboratory Infrastructure for Testing the Distributed Dynamic State Estimation .....	3
Figure 1.2: Connectivity and Data Flow of the Distributed Dynamic State Estimator .....	5
Figure 2.1: Functional Laboratory Setup for Testing and Characterizing PMUs (Similar Arrangement for Merging Units) .....	7
Figure 2.2: Photograph of Laboratory Equipment 1 .....	8
Figure 2.3: Photograph of Laboratory Equipment 2 .....	9
Figure 2.4: User Interface of the Merging Unit Data Concentrator .....	11
Figure 2.5: User Interface of the Measurement Selection .....	12
Figure 2.6: Example Test Signal: Total Time of graph: 15 seconds, Frequency Ramp of +0.1 Hz/sec for 5 secs Starting at time t=5 seconds .....	13
Figure 2.7: Performance evaluation of fractional sample correction method .....	14
Figure 2.8: Example Maximum Absolute Error (Magnitude, Phase, and TVE) for Six Test Signals .....	15
Figure 2.9: Verification of A/D Converter Sample Clock Synchronization .....	15
Figure 3.1: Laboratory Infrastructure for Testing the Distributed Dynamic State Estimation .....	17
Figure 3.2: Architecture of the Distributed Quasi-Dynamic State Estimator .....	18
Figure 3.3: Substation Based Quasi-Dynamic State Estimator User Interface .....	20
Figure 3.4: k Value versus Confidence Level for a Sample Run .....	21
Figure 4.1: The Example Substation and Interconnected Circuits .....	24
Figure 4.2: Voltage Actual and Estimated Phasor Measurements in Relay 4, Event 1 .....	29
Figure 4.3: Current Actual and Estimated Phasor Measurements in Relay 4, Event 1 .....	30
Figure 4.4: Estimated Angle Difference in Event 1 .....	30
Figure 4.5: Voltage Actual and Estimated Phasor Measurements of Phase A in Relay 4, Event 2 .....	31
Figure 4.6: Current Actual and Estimated Phasor Measurements of Phase A in Relay 4, Event 2 .....	32
Figure 4.7: Estimated Angles and Confidence Level in Event 2 .....	33
Figure 4.8: Square Root of the Variance of Voltage and Current Estimated Measurements in Relay 4, Event 2 .....	34
Figure 5.2.1: Marcy Substation .....	35
Figure 5.3.1: Three-Phase Autotransformer with Tertiary (M106) .....	40
Figure 5.3.2: Three-Phase Three-Winding Transformer (M105) .....	41
Figure 5.3.3: Three-Phase Two-Winding Transformer Model (M104) .....	41

Figure 5.3.4: Reactor Bank Model (M116) .....	42
Figure 5.3.5: Capacitor Bank Model (M116) .....	42
Figure 5.3.6: Three-Phase Constant Power Load Model (M161).....	43
Figure 5.3.7: Three-Phase Breaker Model (M192).....	43
Figure 5.3.8: Node Connector Model (M191).....	44
Figure 5.4.1: Marcy Substation with IEDs .....	45
Figure 5.4.2: IED and its user interface .....	46
Figure 5.4.3: Instrumentation Channel List Dialog of One IED .....	47
Figure 5.4.4: Example of a Voltage Phasor Instrumentation Channel Dialog.....	47
Figure 5.4.5: Example of a Current Phasor Instrumentation Channel Dialog .....	48
Figure 5.4.6: Measurement List Dialog .....	53
Figure 5.4.7: Voltage Phasor Measurement Parameters Dialog .....	54
Figure 5.4.8: Current Phasor Measurement Parameters Dialog .....	54
Figure 5.5.1: Perform Simulation for the Example System.....	56
Figure 5.5.2: Three-phase Voltage Measurements at MRC-AT1H, MRC-AT1L, and MARCY-T1 .....	57
Figure 5.5.3: Three-phase Current Measurements for the Three Single-Phase Autotransformers at Auto Bank 1 .....	58
Figure 5.5.4: Three-phase Voltage Measurements at MRC-AT2H, MRC-AT2L, and MARCY-T2 .....	59
Figure 5.5.5: Three-phase Current MeasureFments for the Three Single-Phase Autotransformers at Auto Bank 2 .....	60
Figure 5.5.6: Three-phase Voltage and Current Measurements for the Capacitor Bank at Bus M345-CAP1 .....	61
Figure 5.5.7: Three-phase Voltage and Current Measurements for the Transformer from MRC-CCB1 to MRC-CCB2 .....	62
Figure 5.5.8: Add State Estimator Object.....	63
Figure 5.5.9: User Interface of State Estimator .....	64
Figure 5.5.10: Test Data Server Interface .....	65
Figure 5.5.11: PDC Client Interface .....	66
Figure 5.5.12: Measurement Mapping.....	67
Figure 5.5.13: All Measurements Are Matched with PDC Channels.....	67
Figure 5.5.14: User Interface of Estimator Setup .....	68
Figure 5.5.15: Ready to Run the State Estimator.....	69

Figure 5.5.16: State Estimator is Running .....	71
Figure 5.5.17: Estimated State Report .....	72
Figure 5.5.18: State Estimator Measurement Report.....	72
Figure 5.5.19: State Estimator Detailed Measurement Report .....	73
Figure 5.5.20: Performance of the State Estimator.....	74
Figure 5.5.21: 3D Visualization Screenshot .....	75
Figure A.1: Single-Phase Variable Tap Transformer .....	87
Figure A.2: Single-Phase Transformer Equivalent Circuit.....	88

## **List of Tables**

Table 5.2.1: Summary of Devices in Use Case Test System.....	36
Table 5.3.1: Parameters of Autotransformers with Tertiary .....	37
Table 5.3.2: Parameters of Three-Phase Three-Winding Transformers .....	38
Table 5.3.3: Parameters of Three-Phase Two-Winding Transformers .....	38
Table 5.3.4: Parameters of Capacitor/Reactor Bank.....	38
Table 5.3.5: Parameters of Load Models .....	38
Table 5.3.6: Parameters of Three-Phase Breaker.....	39
Table 5.3.7: Parameters of Two-Node Connectors.....	40
Table 5.4.1: Instrumentation Channel Parameters – User Entry Fields.....	48
Table 5.4.2: Instrumentation Channels of IEDs in the Selected Section .....	50
Table 5.4.3: Measurement Parameters – User Entry Fields.....	55
Table A.1: Definitions of Quasi-dynamic Domain SCAQCF Variables in Power Device Class Implementation.....	80

# **1. Introduction**

---

## **1.1 Background**

Prior research by PSerc researchers have addressed a number of issues related to the future mission-critical systems. The authors of this part of the report have performed the following projects: (1) Real Time PMU-Based Stability Monitoring, S-50, (2) Adaptive and Intelligent PMUs for Smarter Applications, S-57, (3) Setting-less Protection: Laboratory Demonstrations, T-52G, (4) Setting-less Protection Methods, T-49G, and (5) Substation of the Future: A Feasibility Study, T-38.

The extensive PSerc body of knowledge acquired from these projects formed the basis for this project. The body of knowledge from these projects relate to the design and use of the mission-critical systems. Specifically, the following conclusions were reached. (1) Mission-critical systems heavily depend on the quality of service supplied by the measurement infrastructure that includes the sensors, as well as communications and software middleware, (2) To preserve quality of service, the systems need to be tested keeping in mind different aspects of its deployment: equipment selection, commissioning, in-service operation, and risk assessment, and (3) The techniques for testing and evaluation may range from substation test equipment to system-wide IT assessment tools, all needed to address different robustness issues and user awareness. It is clear that technology exists today to achieve the goal of monitoring and assessing the performance of these systems in real time. This in turn automates and simplifies the management of these important assets of the power system. The objective of this project is exactly that, to automate and simplify the management of these assets.

## **1.2 Overview of the Problem**

Presently data from relays, PMUs, FDRs, and in general any IED in the substation are treated as separate entities without any tools to test their cross correlation and in general to provide automated checking of the validity of the data. If for some reason gaps and errors are generated in the data, these gaps/errors remain and propagate upstream to higher level devices. Furthermore, if any physical anomalies occur (such as a blown fuse, a damaged wire, etc.) they will affect the quality and validity of the data, yet there is no mechanism to determine the root cause of these anomalies. The idea is to integrate technologies developed under previous projects into an integrated physical-and-protection co-model and analysis software that will perform the following: (a) validate all data coming out of all relays, PMUs, and in general IEDs via the distributed state estimator, (b) detect anomalies and identify the root cause of these anomalies (hidden failures such as blown fuses, cut wires, etc. or human errors such as incorrect entry of system parameters such as CT and VT ratios, incorrect instrument transformer connection (delta/wye), etc.), (c) in case of temporary loss of data, it creates the missing data from the state estimator and inserts the estimated data into the stream, and (d) it provides the validated data and the substation state upstream for further utilization, such as construction of the system wide real time model at the control center. These objectives have been achieved by a two parts process: (a) construction of a laboratory for the purpose of fully characterizing the individual components of the system, i.e. PMUs, merging units, digital fault recorders, etc. and (b) by constructing a laboratory that comprises the protective relaying scheme of a small substation, the substation automation infrastructure and a simulator to

drive the system for the purpose of managing the data, identifying bad data and correcting bad data before the data are sent upstream. These two developments are briefly described next.

### **1.3 PMU and Merging Unit Testing Lab Development**

Phasor Measurement Units are instruments that can provide a precise and comprehensive view of the system. They can capture the state of the system in real time by measuring the voltage phasor, current phasor, frequency and rate of change of frequency at rates of 1 to 60 frames per second for 60 Hz systems. While PMUs are in general highly accurate instruments, they are subject to degradation for many reasons, such as loss of synchronizations, transients, connection to non-ideal instrumentation channels, hidden failures and manufacturer algorithmic inconsistencies. The characteristics of the PMUs are very important to the dynamic state estimator and a number of other applications. The correct model of the accuracy of PMUs can drastically improve the performance of the dynamic state estimator and result in well validated data. For this reason it is important to characterize PMUs by laboratory measurements.

In a present day substation it is possible that some or all of the data are collected with merging units. Merging units are pure data acquisition systems, GPS synchronized that provide the sampled values of voltage/current waveform. Application of the standard PMU on the sample values provides the voltage and current phasors, frequency and rate of frequency change. Therefore merging units coupled with phasor computation software act as Phasor Measurements Units. As such they must be characterized by measurement for the same reason as the legacy PMUs.

For the purpose of characterizing PMUs and Merging Units, an integrated testing platform based on the Standard PMU was developed. Previously developed technology was integrated into a laboratory set up for routine testing and characterization of PMUs and merging units for a variety of events such as steady state under nominal or off nominal frequency, frequency ramps, magnitude changes (smooth or abrupt), combination of frequency and magnitude changes, combination of above plus faults and others. The response of PMUs to these waveforms is tested against the standard PMU, a highly accurate algorithm to compute the phasors in real time when frequency changes occur as well as the waveform may be distorted with harmonics and transients. The standard PMU algorithm is based on (a) accurate tracking the frequency of the waveforms (b) representation of the waveform between two sample points as a quadratic function, and (c) computing the Fourier transform over a time window which is an integer number of cycles long; as the frequency changes the time window is accordingly adjusted. The standard PMU algorithm has been extensively tested and is more accurate than traditional methods. The developed hardware and software testing methods support and exceed the requirements of the standards, i.e. IEEE Std C37.118.1a™-2014 and IEEE Synchrophasor Test Suit Specifications [TSS].

The standard PMU algorithm is also used to convert merging units into phasor measurements units. Specifically, the sampled data from merging units are fed into the “standard PMU” which computes the phasors and creates a C37.118 stream of phasors. In addition, we develop software to communicate with multiple vendor merging units using IEC 61850 2-LE. This software is integrated into the overall testing platform. We have tested merging units from various manufacturers.

## 1.4 Dynamic State Estimation Based Data Validation and Correction

A laboratory has been developed that comprises the protective relaying scheme of a small substation, the substation automation infrastructure and a simulator to drive the system for the purpose of managing the data, identifying bad data and correcting bad data before the data are send upstream. The laboratory set up is shown in the Figure 1-1. The simulator is not shown in the figure. Note that the illustrated substation infrastructure combines the present technology of modern substations (numerical relays connected to a substation bus) and the most recent technology of merging units connected to process bus and protection computers connected between the process bus and substation bus. The laboratory enables research and development for in-service calibration and testing of relays, PMUs, merging units, etc., detection of physical system hidden failures, and data compression via the distributed dynamic state estimation. In addition, software products developed in this environment are readily transferable to actual substations. A brief description of the approach follows.

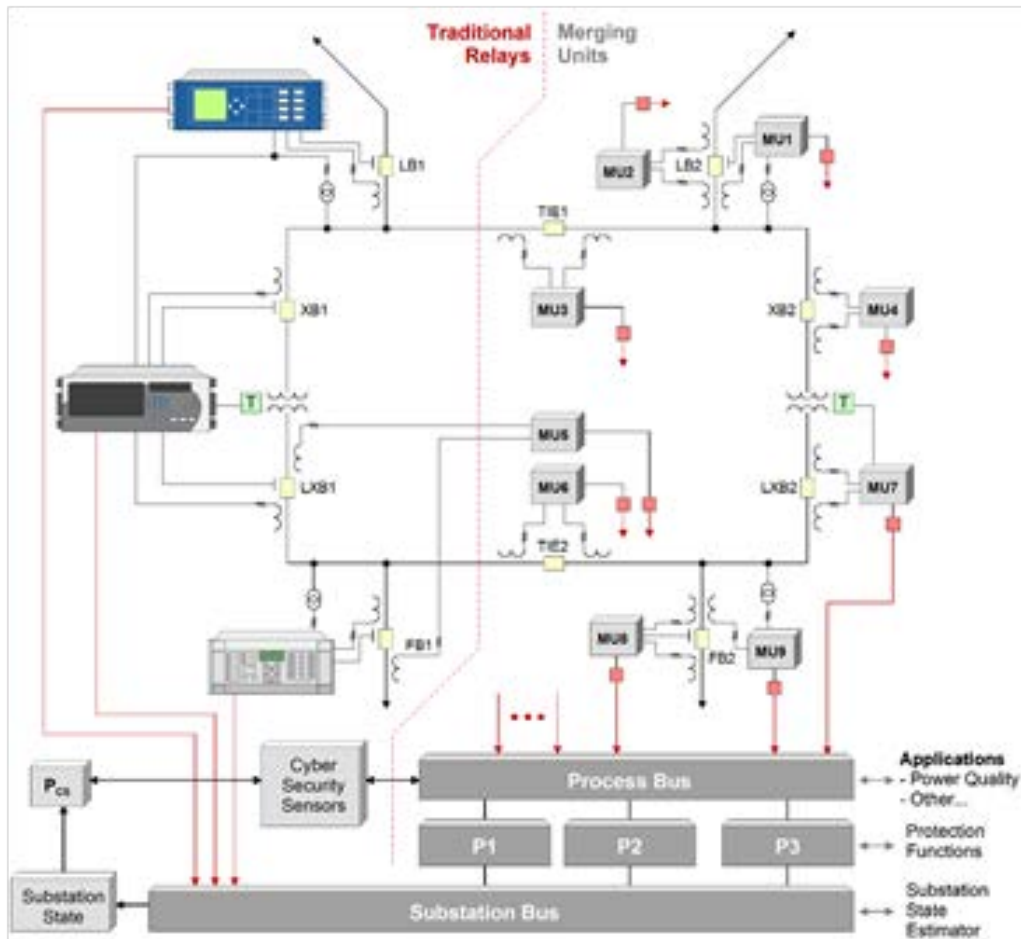


Figure 1.1: Laboratory Infrastructure for Testing the Distributed Dynamic State Estimation

The central component of the approach is the substation based distributed state estimator. This technology has been developed under a number of previous projects and was further improved under this project. This state estimator utilizes all available data from the relays, merging units, PMUs, meters and any IED in the substation and fits the data to a three-phase, breaker oriented

model of the substation including the circuits connected to the substation up to the next substation. Previous projects have demonstrated the ability of this state estimator to execute at rates of 60 times per second (each cycle). Details of the method and implementation issues have been described in a number of previous publications. In this project we utilized the statistical properties of the state estimator to fully characterize the validity of the data and the expected errors. Specifically, the statistical properties of the state estimator were used to detect and identify bad data. Bad data analysis determines the location and root cause of the bad data. Subsequently the bad data are removed and replaced with estimated values using the real time model of the substation. The end result is that all data are validated before are send to upstream devices and the system operator. The analysis identifies calibration issues, physical system failures (hidden failures), human errors (for example, incorrect entry of CT or VT ratios), subsystem failures (such as loss of GPS synchronization in some part of the system) and other. The overall process is illustrated in Figure 1-2.

Some of these sources of errors can be corrected in real time and automatically. For example, calibration errors can be corrected by resetting the appropriate parameters in the relays, human errors (incorrect entries) can be also corrected in real time and automatically. Other sources of error may require human intervention, such as blown fuses, etc.

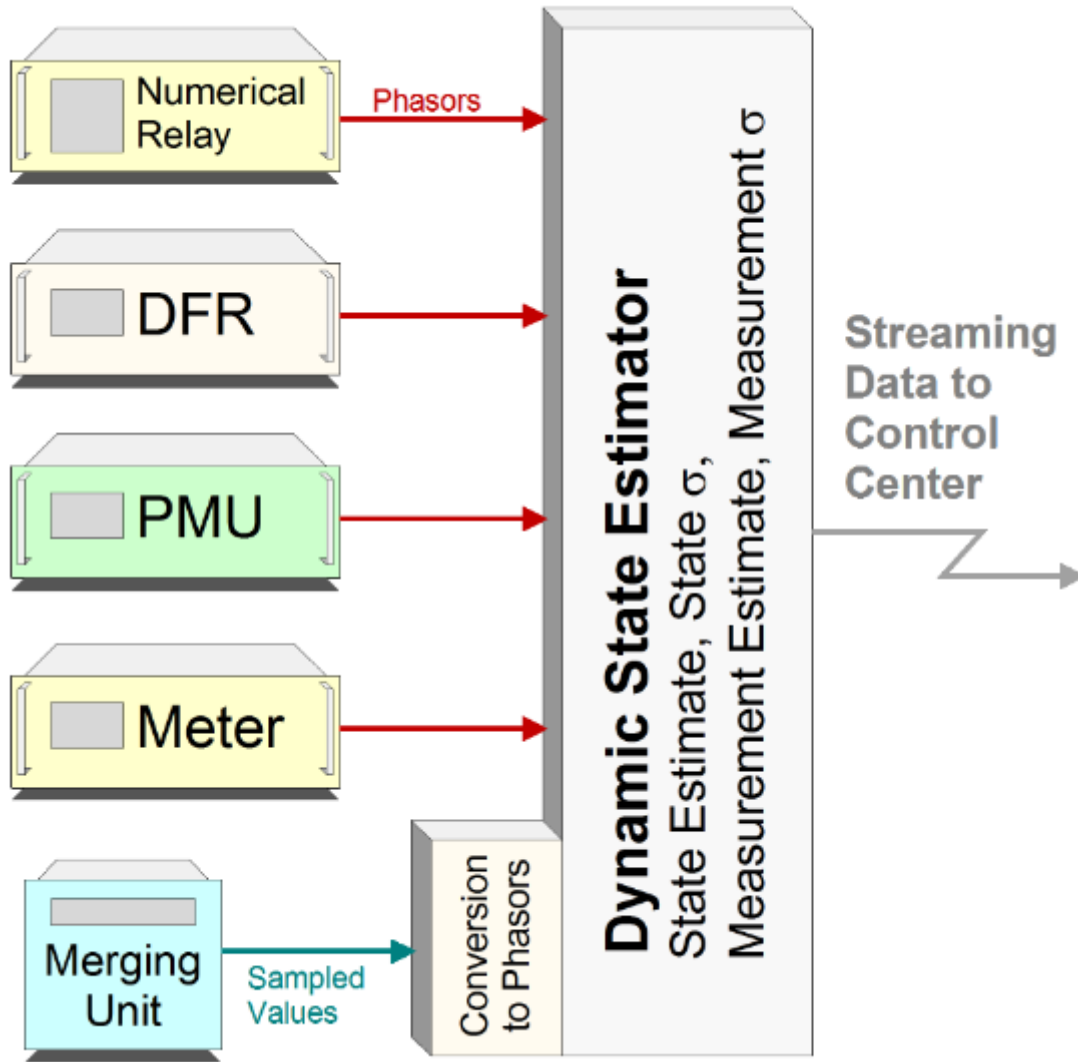


Figure 1.2: Connectivity and Data Flow of the Distributed Dynamic State Estimator

In summary, the substation based dynamic state estimation is used for validating all data collected in the substation and identify and correct any data anomalies. We integrated previously developed technology into an integrated data validation procedure for all PMUs and other relay, fault recorder, meter data in the entire substation. The data validation procedure is based on an integrated physical-and-protection co-model and dynamic state estimation methods. It requires high accuracy models of all components in the substation as well as the interconnecting transmission lines. This work was implemented at the Georgia Tech the laboratory and extensively tested with a model of the MARCY substation. The plan was to install the distributed dynamic state estimator in the field (MARCY substation). Because of delays in equipment installation at MARCY substation, we were unable to install the dynamic state estimator at MARCY. However, it appears that the installation of the equipment at MARCY will be completed in November of 2018. We plan to install the dynamic state estimator in the field at that time.

## **1.5 Field Demonstration**

During this project we worked with the MARCY substation model of NYPA and the plan is to install the Dynamic State Estimation based data validation and correction on the MARCY substation. Preparations of this field demonstration have been completed (see section 5 of the report). However the installation of the required hardware for this demonstration has not been complete at NYPA as of the end of this project. It is expected that the hardware will be installed during the Fall 2018 planned outage at MARCY. We expect to install the Dynamic State Estimator with data validation and correction at that time.

## **1.6 Report Organization**

This report describes the Georgia Tech work on project T-57HI. It is organized as follows: First a brief summary of the work is provided. Next, section 2 provides summary of the work towards the development of a PMU and Merging Unit Testing Laboratory. Section 3 provides summary of the work towards a substation based state estimator with capability to validate data and detect hidden failures. Section 4, a numerical example is used to demonstrate the substation based dynamic state estimator. In section 5, a use case for the application of the quasi-dynamic state estimator on the MARCY substation is described. In Appendix A, the object-oriented modeling approach used in state estimation is described, and an example is provided. Finally, the section “Papers Published” provides a list of publications resulted from this work.

## 2. PMU and Merging Unit Testing Lab Development

An integrated testing platform based on the Standard PMU is described in this section. We integrate previously developed technology into an integrated laboratory set up for routine testing and characterization of PMUs and merging units for a variety of events such as steady state under nominal or off nominal frequency, frequency ramps, magnitude changes (smooth or abrupt), combination of frequency and magnitude changes, combination of above plus faults and others. The approach used to achieve this goal is briefly described below. The method and techniques used support and exceed the requirements of the standards, i.e. IEEE Std C37.118.1a™-2014 and IEEE Synchrophasor Test Suit Specifications [TSS]. The method is also used to convert merging units into phasor measurements units. Specifically, the sampled data from merging units are fed into the “standard PMU” which computes the phasors and creates a C37.118 stream.

A laboratory infrastructure for high precision testing and characterization of PMUs and merging units is constructed. The performance metrics of the PMU accuracy or merging unit accuracy are: (a) Magnitude Accuracy, (b) Time or Phase Angle Accuracy, (c) Frequency Accuracy, (d) Communication Compliance to IEEE Standard C37.118, and (e) communication compliance with IEC 61850-LE-2. The functional laboratory infrastructure for testing PMUs is shown in Figure 2.1.

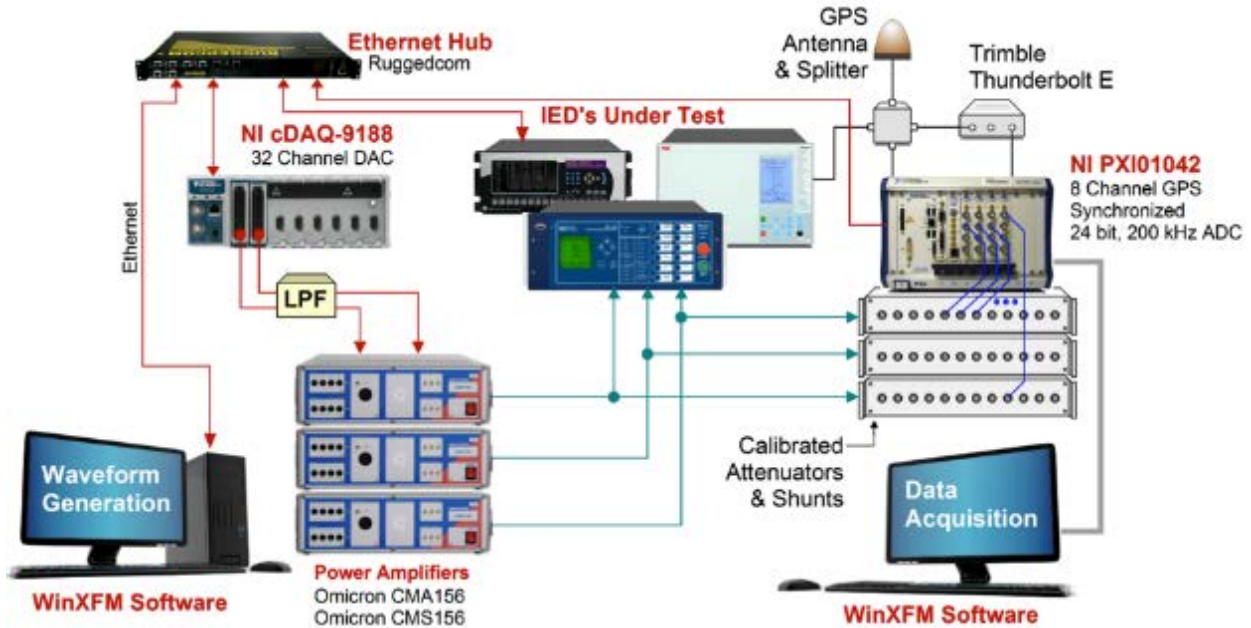


Figure 2.1: Functional Laboratory Setup for Testing and Characterizing PMUs (Similar Arrangement for Merging Units)

A similar setup is used for merging units. Photographs of the laboratory components are shown in Figures 2.2 and 2.3. Presently, the laboratory includes several PMUs (SEL, GE, USI, etc.) and several Merging Units (2 GE Hardfiber, 1 Alstom, 2 Siemens). The method is applicable to any manufacturer relays, PMU, merging units, and fault recorders. A short description of the laboratory work follows.



Figure 2.2: Photograph of Laboratory Equipment 1 – View 1



Figure 2.3: Photograph of Laboratory Equipment 2 – View 2

**Testing and characterization of the PMUs:** The basic approach is based on injecting signals into the PMU (or merging unit) through a simulator, a bank of D/A converters, and a bank of amplifiers, as shown in Figure 2.1; then capture the input to the PMU (or merging unit) via a high accuracy (magnitude and time) data acquisition system (the NI PXI01042, Trimble, GPS antenna) and compute the phasors with a high precision method (see the standard PMU); then capture the output of the PMU (or merging unit), and finally compute the errors of the PMU (or merging unit) versus the standard PMU. Multiple error metrics are used, examples are: (a) timing error (with precision 0.1 microsecond), (b) magnitude error on a sample by sample basis, (c) magnitude error over a user defined time interval, (d) total vector error, and others.

The PMU and MU testing lab consists of a signal generation system and a benchmark data acquisition system. The signal generation system consists of a personal computer running the WinXFM program which transmits streaming sampled value data stored in COMTRADE files to D/A converters. Specifically, the sample values are transmitted to a National Instrument 16 bit, 36 channel D/A converter unit (NI9188) via a local area network (Ethernet). The maximum D/A converter sampling rate is 25 kps per channel. The local area network is based on a Ruggedcom Ethernet hub. The D/A converter analog output is a low power voltage signal with maximum amplitude of 10 Volts peak. These signals are fed into a bank of Omicron voltage and current amplifiers which raise the output voltage and current to standard levels required by relays, PMUs and MUs. The omicron voltage amplifiers peak output voltage is 250 volts, and the current amplifiers can generate peak output currents 5 amperes continuously, and up to 25 amperes for short periods of time (few seconds).

The benchmark data acquisition system is based on a national instrument PXI chassis containing 8 channels of high quality A/D converters which are synchronized to a GPS disciplined clock. The A/D converters sample the analog signals with 24-bit resolution using Sigma-Delta architecture. The clock driving the A/D converters is a 10 MHz signal generated by a Trimble Thunderbolt-E GPS disciplined oven-controlled crystal oscillator. The A/D converter digital filters are also periodically synchronized using the 1-PPS signal provided by the Trimble GPS receiver. This system achieves UTC synchronized sampling with typical accuracy of less than 100 nanoseconds. The PXI chassis also contains a Windows-based Quad-Core PC which processes the A/D converter data and computes phasors. The phasor computations are carried out in the WinXFM software running in this PC using the “Standard PMU” algorithm (The standard PMU algorithm is described in a technical paper). The Standard PMU algorithm generates a high quality synchro-phasor output which is used as a benchmark for evaluating the performance of the various devices under test.

At the same time, the WinXFM program captures the output of the device under test (in IEEE-C38.118 synchro-phasor stream format) and displays the discrepancies between the device under test and the standard PMU output. Various test signals are used, including steady state, frequency ramps, amplitude transients, etc. The results are displayed in plot format as phase, amplitude and frequency error versus time. Note that the WinXFM program includes a waveform calculator feature, which allows the user to define arbitrary functions of all captured waveforms, and thus various error metrics can be easily specified and displayed.

Note that the performance of the described evaluation system is solely determined by the accuracy of the benchmark data acquisition system, and not affected by the accuracy of the signal generation system. This is an important advantage of the described approach, since it is immune to the inevitable amplitude and phase errors inherent in power amplifiers and delays and other errors generated by free-running D/A converters.

A similar approach has been developed for merging unit evaluation. Note that the outputs of merging units are “point-of-time” sample values. Specifically, the evaluation of the merging units is performed in two ways: (a) direct comparison of the point-of-time samples from the merging unit under test to the corresponding point-of-time samples generated by the benchmark data acquisition system, and (b) comparison of the synchro-phasor data derived from the merging unit data using the standard PMU algorithm to synchro-phasors generated by the benchmark data acquisition system.

In order to facilitate merging unit characterization, a “Merging Unit Data Concentrator” (MUDC) software module has been developed and integrated into the WinXFM program. The MUDC collects sampled values from multiple MUs, time aligns the data, and adds time stamps. This process facilitates the proper processing of the sample values. The user interface of the Merging Unit Data Concentrator is shown in Figure 2.4. The sampling rate, the base frequency, maximum latency and buffer size can be user selected set. The merging units can be chosen from the "Merging Units" tab, and the available measurements from the selected merging units can be chosen in the "Measurements" tab. An example of the measurement selection user interface is shown in Figure 2.5. Any errors detected in the incoming merging unit data are reported in the "Error Counts" block.

A unique feature is that the system can test and characterize multiple Merging Units simultaneously. This allows comparisons of merging units by various manufacturers in order to determine interoperability characteristics.

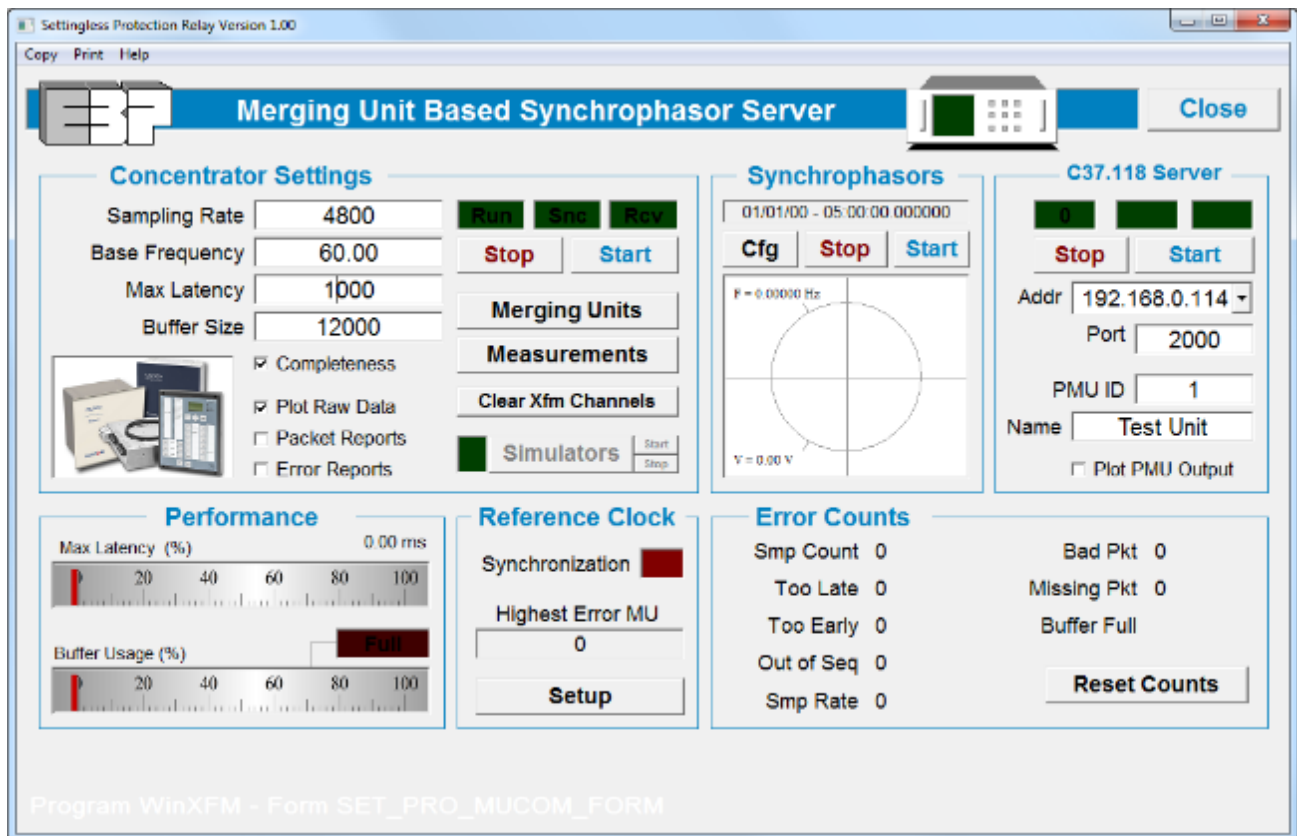


Figure 2.4: User Interface of the Merging Unit Data Concentrator

Figure 2.5: User Interface of the Measurement Selection

**Processing of the sample data using the standard PMU and creating a C37.118 stream:** The output of the merging units is sampled values with GPS time stamps. The standard PMU is used to convert the sampled values into streaming data in C37.118 format. The performance of the Merging Units is performed in two ways. First the timing accuracy of each sampled value is checked by comparing the input value and coincidental GPS time to the output sample and time tag. The GPS time and time tag should be less than 1 microsecond. The second test is to compare the input phasor captured with the method as described in the previous paragraph to the output phasor.

**Organizing and Standardizing the Testing:** A library of signals is generated and stored in COMTRADE format for testing PMUs and merging nits. The library contains various events. A sample of these events is: (a) steady state operation at various frequencies (nominal frequency, nominal frequency plus 0.1 Hz, 0.2 Hz, minus 0.1 Hz, etc.), (b) events with frequency ramps of various rates, (c) events with abrupt and gradual magnitude changes, (d) events with combination of magnitude and frequency changes during a fault, and others. Figure 2.6 shows a test signal from the library. The test signal represents a frequency ramp from 60 Hz to 60.5 Hz. Note that the actual waveforms are not clear in the figure. However, the data are in COMTRADE format and are available to be viewed with any COMTRADE reader.

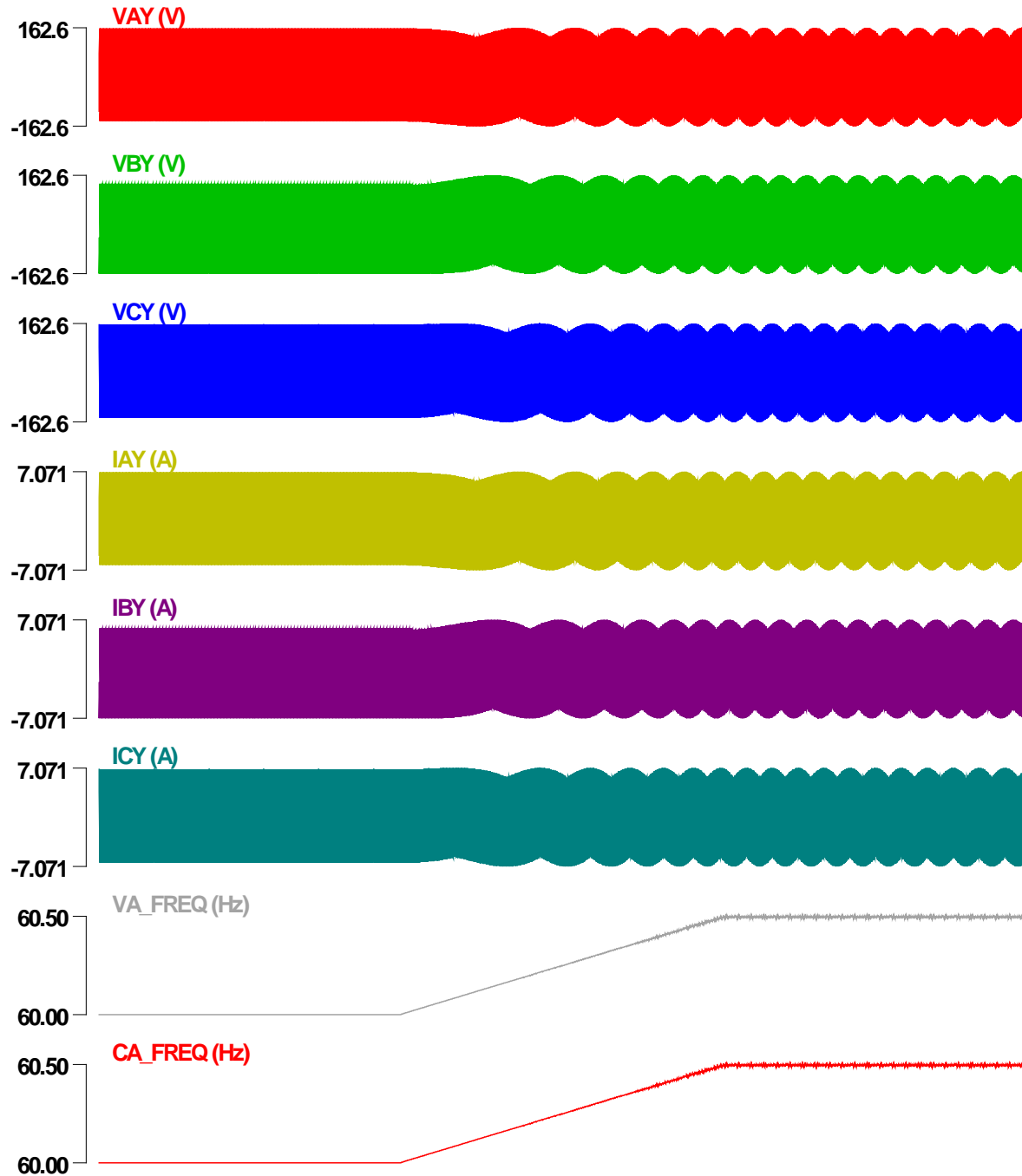


Figure 2.6: Example Test Signal: Total Time of graph: 15 seconds, Frequency Ramp of +0.1 Hz/sec for 5 secs Starting at time t=5 seconds

A basic characteristic of the testing method is its ability to (a) accurately capture the input signal and (b) accurately compute the phasors of the input signal. We have verified that the input signal is captured with accuracy: magnitude 0.01% and timing 0.1 microsecond. The accuracy of the computed input phasors is achieved with the Standard PMU. The Standard PMU algorithm uses an advanced method for estimating the frequency of the input signals and a quadratic fitting of the signal between samples. As the frequency changes, the time window changes as it is defined as an

integer number of cycles and the number of samples in the time window changes (non-integer number of cycles). The analog signal is recreated by a quadratic fitting as discussed earlier. The Fourier transform is applied to the signal over the time window which is an exact integer number of cycles (one cycle for 60 phasors/sec, two cycles for 30 phasors per sec, etc.). This approach eliminates spectral leakage, a well-known source of PMU errors. We also refer to this method as fractional sample correction method. The performance evaluation of this method is shown in Figure 2.7. This figure above shows the performance of the Standard PMU algorithm for a range of sampling rates (1 to 10 ks/s), different time windows (number of cycles) and different approximation methods for a 60 Hz waveform. The phase angle error of the quadratic integration method (the Standard PMU) is plotted (green curve) for sampling rates ranging from 1 to 10 kHz. For comparison purposes, the plot also includes the results of the discrete time phasor computation without any fractional sample correction (red curve), and phasor computation with fractional sample correction based on trapezoidal integration (blue curve). Note that if one standardizes to 128 samples per cycle (or 7.68 ks/s as suggested by IEC), the phase error of the Standard PMU is less than 0.00005 degrees. The Standard PMU is an integral part of the testing laboratory for PMUs and merging units.

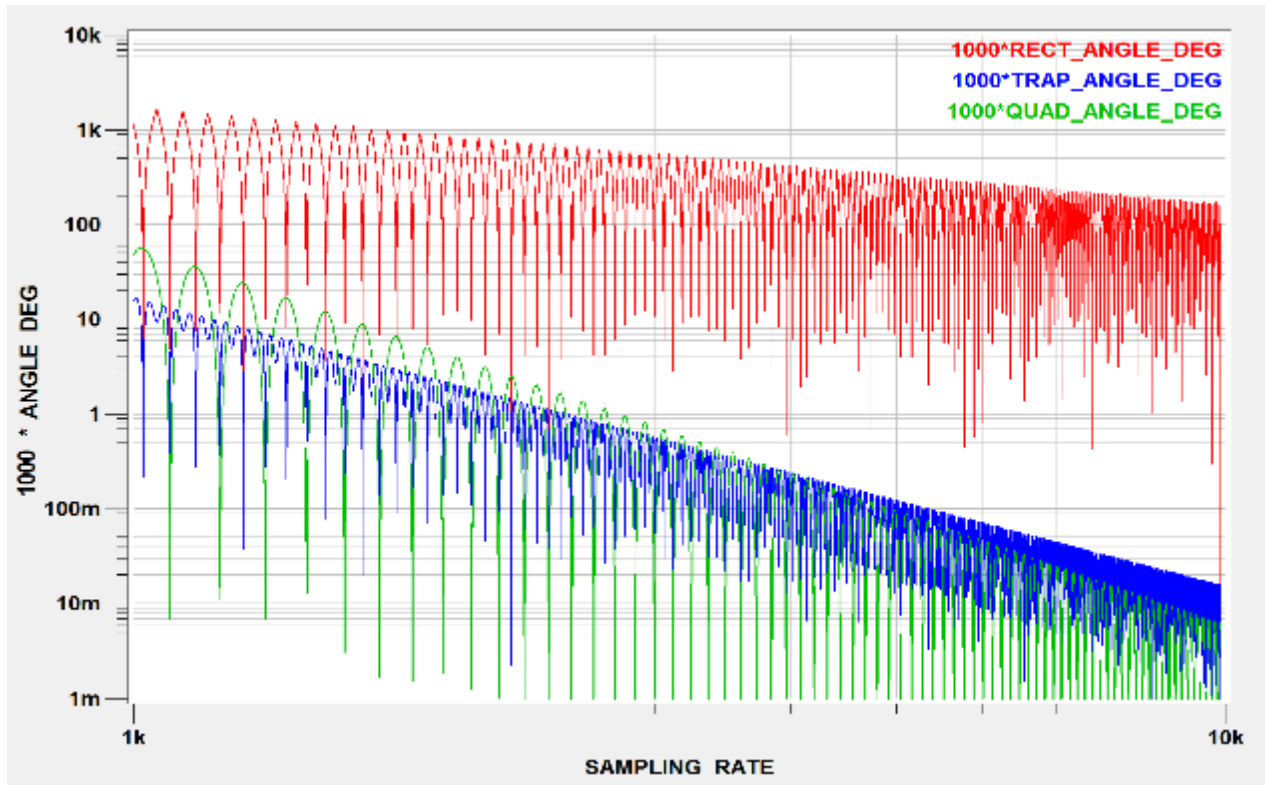


Figure 2.7: Performance evaluation of fractional sample correction method

Results of data capturing accuracy (hardware) and accuracy of phasor computation using the standard PMU (software) are presented in this section. As an example, Figure 2.8 shows the performance of a specific PMU (in this case a fault recorder) during testing with six test signals. Figure 2.9 shows the timing accuracy of the hardware. Note the accuracy exceeds 0.1 microsecond. The accuracy of the software has been evaluated with a number of numerical experiments.

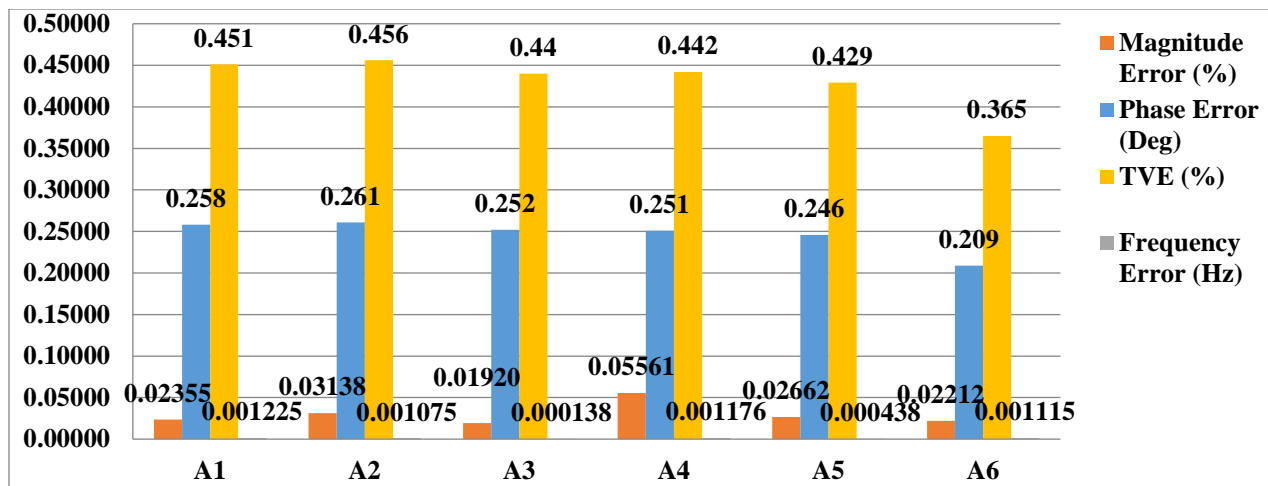


Figure 2.8: Example Maximum Absolute Error (Magnitude, Phase, and TVE) for Six Test Signals

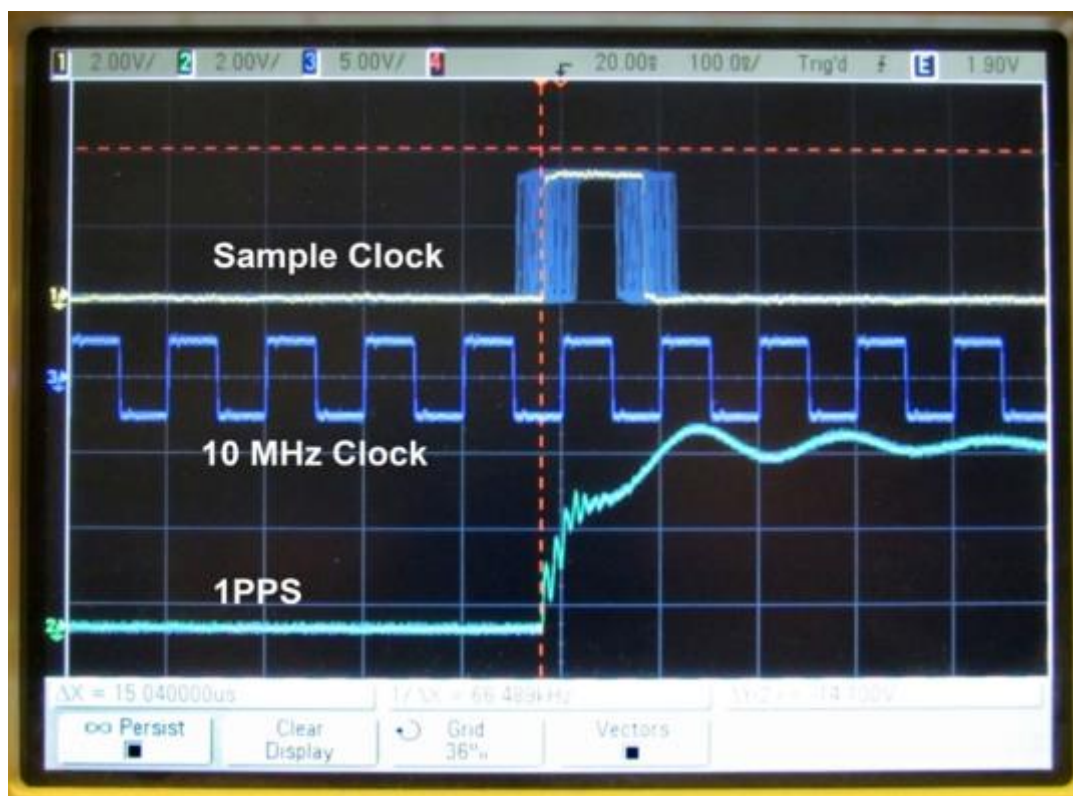


Figure 2.9: Verification of A/D Converter Sample Clock Synchronization

### 3. Substation Based Dynamic State Estimation

---

In this section, an integrated data validation procedure for all PMUs and other data in the entire substation is elaborated. The data validation procedure is model based using the distributed dynamic state estimation. It requires the model of all components in the substation as well as the interconnecting transmission lines. The validation provides quantitative characterization of the data, i.e. percent error, it detects and identifies bad PMU or other data, and it identifies the source of bad data, including hidden failures. The methodology is implemented in the laboratory before deploying it in the field. The laboratory setup will demonstrate the characterization of PMU and other data and the detection and identification of hidden failures.

We propose to integrate technologies developed under previous projects into an integrated physical-and-protection co-model and analysis software that performs the following: (a) validates all data coming out of all relays, PMUs, and in general all IEDs via the distributed state estimator, (b) detects anomalies and identifies the root cause of these anomalies (hidden failures such as blown fuses, cut wires, etc. or human errors such as incorrect entry of system parameters such as CT and VT ratios, incorrect instrument transformer connection (delta/wye), etc.), (c) in case of temporary loss of data, it will create the missing data from the state estimator and will insert the estimated data into the stream, and (d) provides the validated data and the substation state up stream for further utilization, such as construction of the system wide real time model at the control center. These objectives will be achieved by constructing a laboratory that will comprise the protective relaying scheme of a small substation, the substation automation infrastructure and a simulator to drive the system.

Presently data from relays, PMUs, FDRs, and in general any IED in the substation are treated as separate entities without any tools to test their cross correlation and in general to provide automated checking of the validity of the data. If for some reason gaps are generated in the data, these gaps remain and propagate to higher level devices. Furthermore, if any physical anomalies occur (such as a blown fuse, a damaged wire, incorrect settings in electronic meters or PMUs, etc.) they will affect the quality and validity of the data, yet there is no mechanism to determine the root cause of these anomalies. The evaluation method consists of comparing the collected data to the physical model of the system. To limit the size of the problem, this task is performed at each substation independently from other substations. A systematic and mathematically rigorous method is used for setting up the substation model and collecting the PMU data and data from other devices and correlating them to the model. Discrepancies will trigger a procedure to determine the level of discrepancy and the source of the discrepancy by backtracking on the physical model. This procedure will identify any hidden failures.

The central component of the approach is the substation based distributed state estimator. This technology has been developed under a number of previous projects and it is further improved to achieve the goals of this project. The state estimator utilizes all available data from the relays, merging units, PMUs, meters and any IED in the substation and fits the data to a three-phase, breaker-oriented model of the substation including the circuits connected to the substation up to the next substation. Previous projects have demonstrated the ability of this state estimator to execute at rates of 60 times per second (each cycle). The statistical properties of the state estimator is used to detect and identify bad data. The bad data are further analyzed to determine the root

cause of the bad data and to make corrections or send this information to the operator for further action. This analysis identifies any calibration issues, physical system failures (hidden failures), human errors (for example, incorrect entry of CT or VT ratios), subsystem failures (such as loss of GPS synchronization in some part of the system) and other. Some of these sources of errors can be corrected in real time and automatically. For example, calibration errors can be corrected by resetting the appropriate parameters in the relays, human errors (incorrect entries) can be also corrected in real time and automatically. Other sources of error may require human intervention, such as blown fuses, etc. Not that the system operates in real time and therefore any problems that may arise will be detected within a couple of cycles after their occurrence.

The initial laboratory set up is shown in the Figure 3.1. The simulator is not shown in the figure. Note that the proposed substation infrastructure combines present technology of modern substations (numerical relays connected to a substation bus) as well as recent technology of merging units connected to process bus and protection computers connected between the process bus and substation bus. Equipment for completing this laboratory set up has been procured as well as donated by the industry.

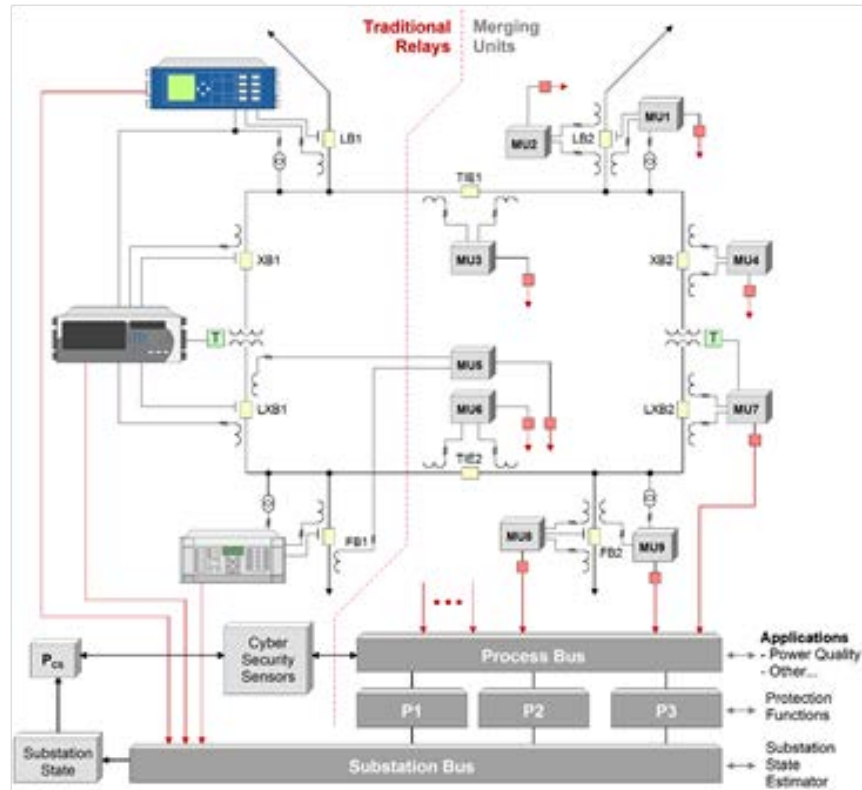


Figure 3.1: Laboratory Infrastructure for Testing the Distributed Dynamic State Estimation

The substation based dynamic state estimator collects the data and performs the dynamic state estimation. Specifically, all the data from all IEDs in the specific substation are first be collected into a data concentrator and converted to C37.118 data stream. Then the data stream run through the state estimator in each substation separately where the quasi-dynamic state estimation (QSE)

is performed. To be more specific, the dynamic state estimator uses the substation model and outputs estimated substation states, estimated measurements, expected errors on states and measurements and the corresponding confidence level. Furthermore, it detects and corrects bad data so that the streaming data outputs (in C37.118 format) to the control center contain only validated data. The overall structure is illustrated in Figure 3.2.

The estimator is defined in terms of models, states, measurement sets and estimation methods. The dynamic state estimation algorithm is object-oriented, i.e. all the models in the system are expressed in a standard format, namely the state and control algebraic companion form (SCAQCF) and the distributed dynamic state estimation operates directly on these object models. SCAQCF device model is derived from quadratic integration on quadratized physical device model, which describes all the physical laws that a specific component should satisfy. The detailed SCAQCF syntax is described in Appendix A.

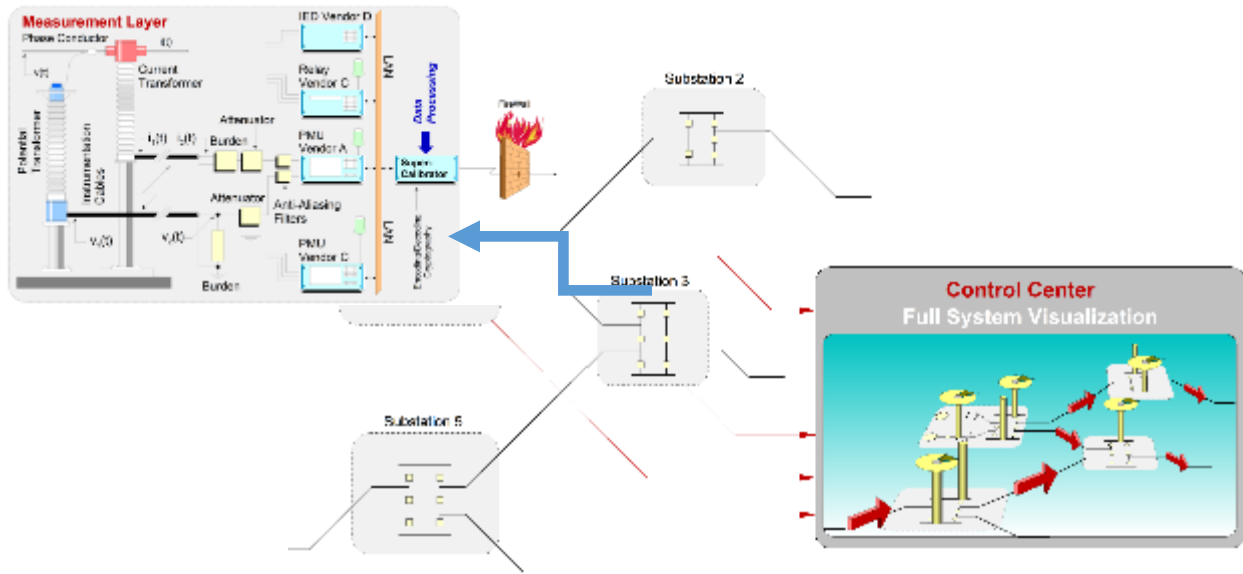


Figure 3.2: Architecture of the Distributed Quasi-Dynamic State Estimator

The QSE models the slow electro-mechanical transients of the power system with differential equations while the fast electrical transients are neglected and electrical quantities are represented with time varying phasors. The architecture illustrated in Figure 3.2 is described as follows: A local state estimator is installed in each substation and utilizes measurements only at the local substation for the purpose of avoiding the requirement of obtaining and transmitting via communication channels measurements from other substations. The quasi-dynamic state estimation is performed in each substation in parallel (i.e. substation level state estimation). The estimated states for each substation are produced and sent to the control center where the system wide estimated states are synthesized by combining all the substation estimated states of the same time instant. Note that for this approach, data from at least one GPS-synchronized device is required in each substation in order to synchronize all the data in the substation.

The measurements in a specific substation can be classified into four types: (a) Actual Measurements: measurements that come from actual measurement channels, i.e. any

measurements from any IEDs (relays, meters, FDR, PMUs, etc.); (b) Derived Measurements: measurements derived from actual measurements based on topology; (c) Pseudo Measurements: not directly measured, represent quantities for which their value is approximately known, such as missing phase measurements, neutral/shield voltage measurements, neutral currents, etc. (d) Virtual Measurements: mathematical quantities defined by physical laws, such as Kirchoff's current law, model equations, etc.

The dynamic state estimator uses three different methods to estimate the states and perform the protection: (a) Unconstrained Least Square Method; (b) Constrained Least Square Method; (c) Extended Kalman Filtering Method.

The unconstrained weighted least square (WLS) method is briefly presented below.

The measurements  $b$  are expressed as functions of the states:

$$\mathbf{b} = h(\mathbf{x}) \quad (3.2)$$

The WLS method minimizes the sum of the weighted squares of the components of the residual vector. Mathematically:

$$\text{Minimize } J = \sum_{i=1}^n \left( \frac{h_i(x) - z_i}{\sigma_i} \right)^2 = \sum_{i=1}^n s_i^2 = \eta^T W \eta \quad (3.3)$$

where  $s_i = \frac{\eta_i}{\sigma_i}$ ,  $W = \text{diag} \left\{ \dots, \frac{1}{\sigma_i^2}, \dots \right\}$  and  $\sigma_i$  is the standard deviation of the meter by which the corresponding measurement  $b$  is measured;

The solution is given with Newton's iterative algorithm:

$$\mathbf{x}^{\nu+1} = \mathbf{x}^{\nu} - (H^T W H)^{-1} H^T W (h(\mathbf{x}^{\nu}) - \mathbf{b}) \quad (3.4)$$

where  $H$  is the Jacobian matrix:

$$H = \frac{\partial h(\mathbf{x})}{\partial \mathbf{x}} \quad (3.5)$$

Once the solution is calculated by equation (3.4), chi-square test is applied. Chi-square test provides the probability that the measurements are consistent with the dynamic model. Chi-square test is applied as follows. First the quantity (errors of estimated data)  $\xi$  is computed:

$$\xi = \sum_i \left( \frac{h_i(x) - z_i}{\sigma_i} \right)^2 \quad (3.6)$$

The probability (confidence level) that the measurements and the model fit together within the accuracy of the meters is computed from:

$$\Pr[\chi^2 \geq \xi] = 1 - \Pr[\chi^2 \leq \xi] = 1 - \Pr(\xi, \nu) \quad (3.7)$$

where  $\nu$  is the degree of freedom and it is the difference between the number of measurements and states.

A confidence level around 100% (small chi-square value) infers the measurements are highly consistent with the dynamic model of the system, while a confidence level around 0% (large chi-square value) means that measurements do not match the dynamic model of the system. In case a low confidence level is obtained, the next task is to identify the bad measurements.

The functionality of the state estimator components can be viewed in Figure 3.3 which illustrates the user interface of the substation based state estimator.

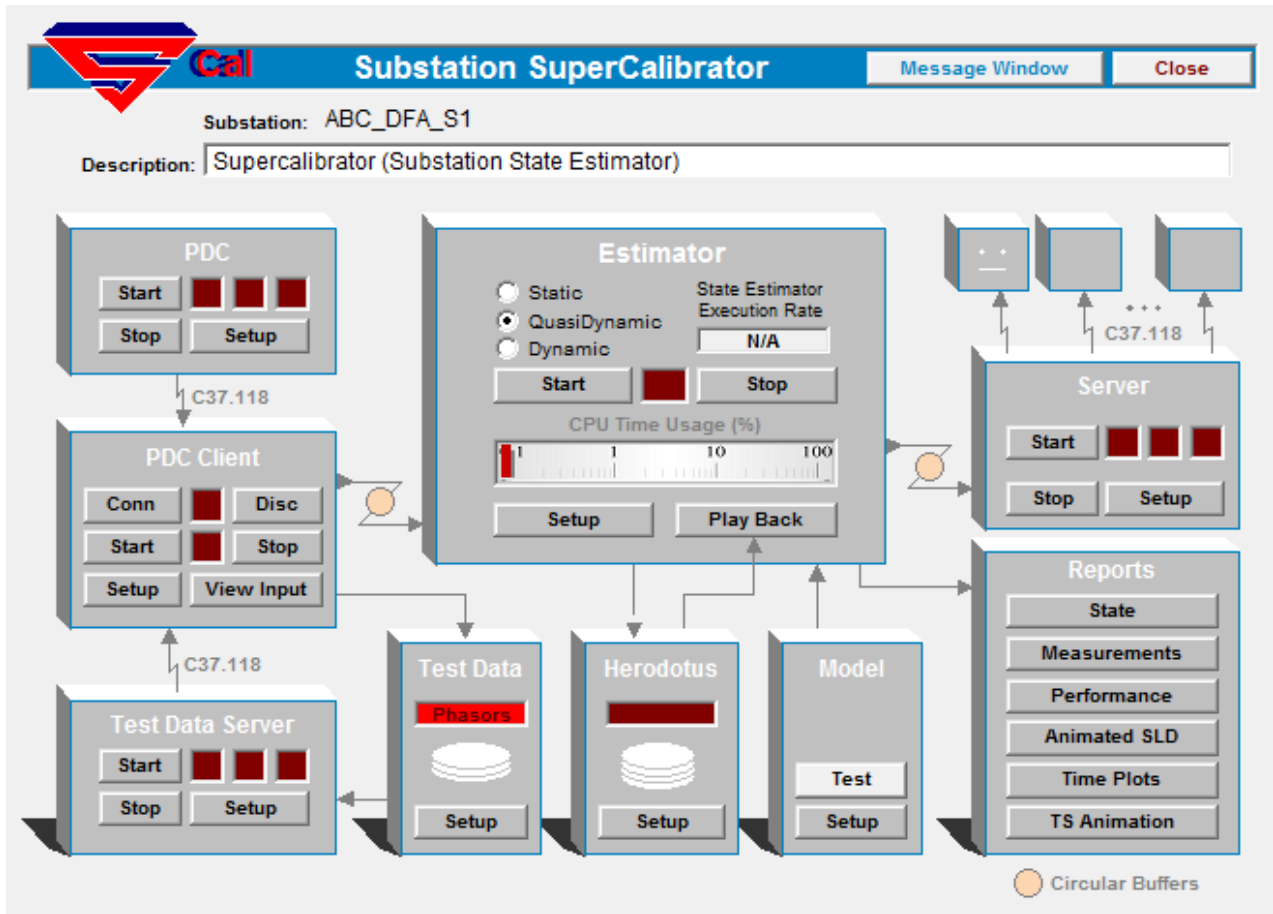


Figure 3.3: Substation Based Quasi-Dynamic State Estimator User Interface

The PDC client connects either to a Phasor Data Concentrator (PDC, for real time data) or to the Test Data Server (for simulation experiments) and receives a C37.118 synchrophasor data stream that may also be mixed with data from standard relays. The data are sent to a circular buffer which is accessed by the state estimator to perform the state estimation.

Before the execution of the state estimator, the user has to (a) enter the network model, and (b) map the measurements to the substation physical system. This is a necessary step because the

measurements must be linked to the model of the system for the purpose of extracting the mathematical model of the measurement.

Several reporting and visualization tools have been implemented for the state estimation results. Performance evaluation of the state estimation results is based on several metrics, and one of them is the parameterized (parameter k) chi-square test shown in Figure 3.4. The parameter k is defined as follows: if it is 1.0 then the standard deviation of each measurement is equal to the accuracy of the measurement error with which this measurement was obtained. If different than 1.0 then the standard deviation of the measurement error equals the accuracy of the measurement error times k.

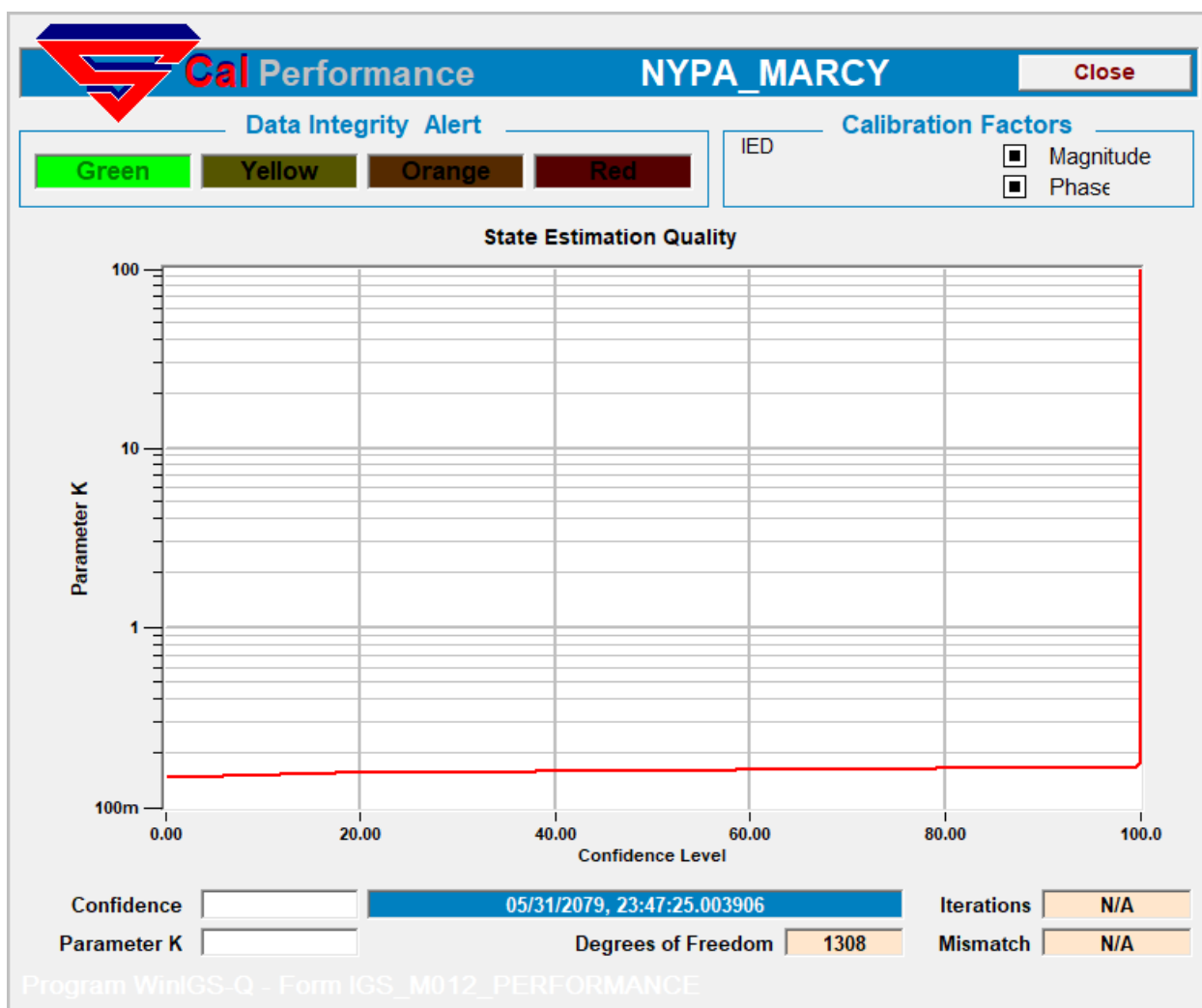


Figure 3.4: k Value versus Confidence Level for a Sample Run

A play back function is also under continuous development and integrated with the state estimator. The purpose of the play back capability is to enable high fidelity disturbance playback (or simply playback of normal operating conditions). For this purpose, it is necessary to store not only real time measurements data as well as state estimation data but also coincidental model of the system. The play back function also provides all the visualization options that are available in real time.

The execution time monitor (CPU Time Usage) in the state estimator monitors the portion of the time used by the state estimation calculations, where 100% corresponds to the time between two successive QSE computations. If the state estimation is set to execute 60 times per second, then 100% corresponds to 16.6 ms. The details of the developed state estimator with a use case can be found in section 5.

## 4. Substation Based Dynamic State Estimation: Numerical Example

---

This section uses a numerical example to demonstrate the substation based dynamic state estimator. The example system shown in Figure 4.1 consists of one substation and interconnected circuits. Note that some of the relays in this substation are GPS-synchronized, and others are not. The substation contains a local state estimator that performs quasi-dynamic state estimation. This numerical example demonstrates that the state estimator is able to accurately estimate the overall states of the substation and the states of interconnecting lines when the collected data contain both GPS-synchronized and non-synchronized measurements. In addition, we simulate measurement errors by injecting errors in the measurements from a Gaussian noise source.

### 4.1 System Configuration

The example substation consists of two buses (Bus 3, 115 kV and Bus 4, 13.8 kV) and a wye-delta transformer that connects them. Additionally, the substation is connected to two transmission systems (sections i1 and i2) and three distribution systems (sections j1, j2, and j3). The substation is protected by seven relays: Relays 1 and 4 are GPS-synchronized while relays 2, 3, 5, 6, and 7 are not. The measurement sampling rate is two phasor samples per cycle. The states of this example system are as follows: (1) 15 voltage phasors of phases A, B, C, N1, and N2 at Buses 1, 2, and 3 (the 115 kV transmission line has two neutral points); (2) 16 voltage phasors of phases A, B, C, and N at Buses 4, 5, 6, and 7; (3) three internal states (voltage phasors) in the transformer; and (4) five synchronous angle differences for non-synchronized relays (relays 2, 3, 5, 6, and 7). Since each phasor consists of a real part and an imaginary part and each synchronous angle difference is represented by cosine and sine functions, the substation consists of 78 states at time  $t$  in total.

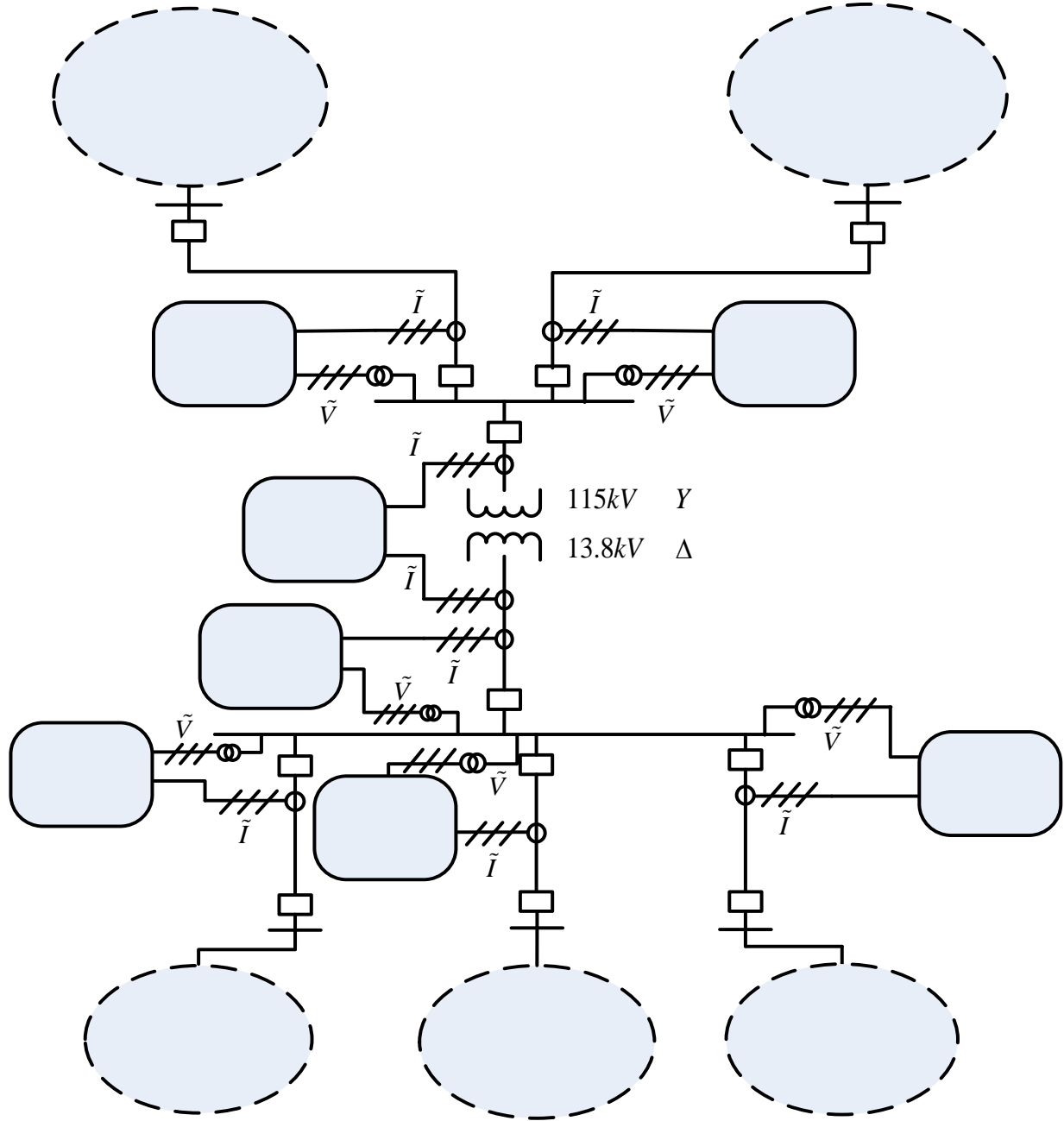


Figure 4.1: The Example Substation and Interconnected Circuits

## 4.2 Measurement Model Creation

The creation of the measurement model is straightforward. If the collected measurements are synchronized, the state estimator directly formulates the measurement equations in the SCAQCF syntax. For instance, synchronized voltage measurement equations are a linear combination of all related state variables:

$$\mathbf{Z}_{V\_Syn} = \mathbf{Y}_{V\_Syn} \mathbf{x}_{abcn} + \boldsymbol{\eta}, \text{ and} \quad (4.1)$$

$$\mathbf{Z}_{V\_Syn} = \mathbf{Y}_{V\_Syn} \mathbf{x}_{abcn} + \boldsymbol{\eta} \quad (4.2)$$

Where  $\mathbf{x}_{abcn} = [\tilde{v}_a \ \tilde{v}_b \ \tilde{v}_c \ \tilde{v}_n]^T$ , and  $\boldsymbol{\eta}$  is the measurement error.

We obtain synchronized current measurement equations from the device model. For instance, the current measurement of the  $j$ th terminal of a device is:

$$\mathbf{Z}_{I\_Syn} = \mathbf{Y}_{x,I\_Syn}^j \mathbf{x} + \mathbf{Y}_{u,I\_Syn}^j \mathbf{u} + \left\{ \mathbf{x}^T \mathbf{F}_{x,I\_Syn}^i \mathbf{x} \right\} + \left\{ \mathbf{u}^T \mathbf{F}_{u,I\_Syn}^i \mathbf{u} \right\} + \left\{ \mathbf{u}^T \mathbf{F}_{ux,I\_Syn}^i \mathbf{x} \right\} - \mathbf{B}_{I\_Syn} + \boldsymbol{\eta} \quad (4.3)$$

where  $\mathbf{x}$  is the corresponding device state vector shown in (1),  $\mathbf{Y}_{x,I\_Syn}^j$  is the linear coefficient matrix consisting of rows corresponding to  $j$ th terminal obtained from  $\mathbf{Y}_{eqx}$ ,  $\mathbf{Y}_{u,I\_Syn}^j$  is the linear coefficient matrix consisting of rows corresponding to  $j$ th terminal obtained from  $\mathbf{Y}_{equ}$ ,  $\mathbf{F}_{x,I\_Syn}^i$  is the nonlinear coefficient matrix corresponding to  $j$ th terminal obtained from  $\mathbf{F}_{eqxx}^i$ ,  $\mathbf{F}_{u,I\_Syn}^i$  is the nonlinear coefficient matrix corresponding to  $j$ th terminal obtained from  $\mathbf{F}_{equu}^i$ ,  $\mathbf{F}_{ux,I\_Syn}^i$  is the nonlinear coefficient matrix corresponding to  $j$ th terminal obtained from  $\mathbf{F}_{equx}^i$ , and  $\mathbf{B}_{I\_Syn}$  is the measurement history-dependent vector.

However, if any measurement is collected from relays without the GPS synchronization functionality, an angle difference between the reference phase angle of this non-synchronized relay and the synchronized reference phase angle may exist. This difference is referred to as the “synchronous angle difference,” which is added to the measurement equation as a new variable,  $\theta$ .

In this case, equation (4.1) and (4.3) are modified as follows:

$$\mathbf{Z}_{V\_UnSyn} = \mathbf{Y}_{V\_Syn} \mathbf{x}_{abcn} (\cos \theta - j \sin \theta) + \boldsymbol{\eta}, \text{ and} \quad (4.4)$$

$$\begin{aligned} \mathbf{Z}_{I\_UnSyn} = & (\mathbf{Y}_{x,I\_Syn}^j \mathbf{x} + \mathbf{Y}_{u,I\_Syn}^j \mathbf{u} + \left\{ \mathbf{x}^T \mathbf{F}_{x,I\_Syn}^i \mathbf{x} \right\} + \left\{ \mathbf{x}^T \mathbf{F}_{x,I\_Syn}^i \mathbf{x} \right\} + \left\{ \mathbf{u}^T \mathbf{F}_{u,I\_Syn}^i \mathbf{u} \right\} \\ & + \left\{ \mathbf{u}^T \mathbf{F}_{ux,I\_Syn}^i \mathbf{x} \right\} - \mathbf{B}_{I\_Syn}) \cdot (\cos \theta - j \sin \theta) + \boldsymbol{\eta} \end{aligned} \quad (4.5)$$

To suit the SCAQCF syntax, the measurement equations above need to be quadratized, so  $x_{\cos \theta} = \cos \theta$  and  $x_{\sin \theta} = \sin \theta$  are two new states and linear coefficient matrices  $\mathbf{Y}_{V\_Syn}$ ,  $\mathbf{Y}_{x,I\_Syn}$ ,  $\mathbf{Y}_{u,I\_Syn}$  become nonlinear coefficient matrices. In addition, as two new states obey mathematical rules, we add one more equation in the measurement model, shown in equation (4.6):

$$0 = x_{\cos \theta}^2 + x_{\sin \theta}^2 - 1 \quad (4.6)$$

The measurements above, collected from IEDs, are actual measurements. With the purpose of increasing redundancy and improving state estimation performance, we create two other measurement types in this example: (1) virtual measurements and (2) pseudo-measurements. Virtual measurements are those that obey physical or mathematical laws of the system, such as

Kirchhoff's current law (KCL). Specifically, internal equations in all device models are virtual measurements. Furthermore, according to KCL, the sum of all currents from various devices connected to one common node is zero, which is also a virtual measurement. Pseudo-measurements are those with known expected values. For instance, the voltage of the neutral phase is close to zero in a normal operation, that is, a pseudo-measurement.

By combining all the measurement types mentioned above and substituting control variables by the values given from the control center, the state estimator is able to generate the measurement model of the entire system, expressed in a similar syntax as the device model syntax:

$$\mathbf{z} = \mathbf{Y}_{\text{eqz}} \mathbf{x} + \begin{Bmatrix} \vdots \\ \mathbf{x}^T \mathbf{F}_{\text{eqz}}^i \mathbf{x} \\ \vdots \end{Bmatrix} - \mathbf{B}_{\text{eqz}} + \boldsymbol{\eta} = h(\mathbf{x}) + \boldsymbol{\eta}, \quad (4.7)$$

where  $\mathbf{z}$  is the measurement vector of the system,  $\mathbf{Y}_{\text{eqz}}$  is the linear coefficient matrix regarding state vector  $\mathbf{x}$ ,  $\mathbf{F}_{\text{eqz}}^i$  is the nonlinear (quadratic) coefficient matrix,  $\mathbf{B}_{\text{eqz}}$  is the history-dependent vector, and  $\boldsymbol{\eta}$  is the measurement error.

In this example system, each relay has two three-phase measurement channels, and each phasor measurement is divided into a real part and an imaginary part. As a result, the entire system has 84 actual measurements. As the voltage of the neutral phase is close to zero during a normal operation, the system measurement model contains 20 pseudo-measurements. In addition, 23 virtual measurements are available: (a) six represent internal equations for the transformer; (b) 12 obey KCL at Buses 3 and 4; and (c) the other five virtual measurements are the mathematical laws shown in (7) for each synchronous angle difference. In summary, the measurement vector contains 127 elements. Meanwhile, the standard deviation is introduced for each measurement to represent the measurement error. For actual measurements, the standard deviations are the meter errors of the corresponding IEDs. Since the virtual measurements are the equations obeying mathematical or physical laws, their errors are much smaller compared to those of actual measurements. Therefore, we set their standard deviations to be relatively low value (e.g., 0.001 p.u.). Similarly, as we only know the expected value of pseudo measurements, they have larger errors than the actual measurements. Thus, we set their standard deviation to be a relatively high value (e.g., 0.1 p.u.).

### 4.3 Evaluation Method

Unconstrained weighted least square (WLS) method is applied in dynamic state estimation. The problem is formulated as follows. The measurements  $\mathbf{z}$  are expressed as functions of the states:

$$\mathbf{z} = h(\mathbf{x}), \quad (4.8)$$

The WLS method minimizes the sum of the weighted squares of the components of the residual vector. Mathematically:

$$\text{Minimize } J = (\mathbf{z}(\mathbf{t}) - h(\mathbf{x}))^T \mathbf{W} (\mathbf{z}(\mathbf{t}) - h(\mathbf{x})) \quad (4.9)$$

where  $\mathbf{W}$  is the weight matrix with the weights defined as the inverse of the squared standard deviation:

$$\mathbf{W} = \text{diag}\{1/\sigma_1^2, 1/\sigma_2^2, \dots, 1/\sigma_n^2\} \quad (4.10)$$

Unknown state vector  $\mathbf{x}$  is obtained by the optimal condition:

$$dJ/d\mathbf{x} = 0 \quad (4.11)$$

To obtain the solution of the nonlinear optimization problem above, we linearize the nonlinear equations (the highest order is the second order in equation (4.8) at the point  $\mathbf{x}^\nu$  by assuming that an initial guess  $\mathbf{x}^\nu$  is very close to the optimal solution:

$$\mathbf{r} = h(\mathbf{x}^\nu) + \partial h(\mathbf{x}) / \partial \mathbf{x} \Big|_{\mathbf{x}=\mathbf{x}^\nu} (\mathbf{x} - \mathbf{x}^\nu) - \mathbf{z} \quad (4.12)$$

After we set  $\mathbf{H} = \partial h(\mathbf{x}) / \partial \mathbf{x} \Big|_{\mathbf{x}=\mathbf{x}^\nu}$ , and  $\mathbf{z}' = -h(\mathbf{x}^\nu) + \mathbf{H}\mathbf{x}^\nu + \mathbf{z}$ , the equation becomes

$$\mathbf{r} = \mathbf{H}\mathbf{x} - \mathbf{z}' \quad (4.13)$$

The optimization problem is now expressed as

$$\text{Minimize } J = (\mathbf{H}\mathbf{x} - \mathbf{z}')^T \mathbf{W} (\mathbf{H}\mathbf{x} - \mathbf{z}') \quad (4.14)$$

Thus, we generalize the solution as an iterative equation:

$$\mathbf{x}^{\nu+1} = (\mathbf{H}^T \mathbf{W} \mathbf{H})^{-1} \mathbf{H}^T \mathbf{W} \mathbf{z}' = \mathbf{x}^\nu - (\mathbf{H}^T \mathbf{W} \mathbf{H})^{-1} \mathbf{H}^T \mathbf{W} (h(\mathbf{x}^\nu) - \mathbf{z}) \quad (4.15)$$

Once the solution is calculated by equation (4.15), chi-square test is applied. Chi-square test qualifies the goodness of fit between the model and measurements by providing the probability that the measurements are consistent with the dynamic model. Chi-square test is applied as follows. First the quantity  $\xi$  is computed:

$$\xi = \sum_i \left( \frac{h_i(x) - z_i}{\sigma_i} \right)^2 \quad (4.16)$$

The probability (confidence level) that the measurements and the model fit together within the accuracy of the meters is computed from:

$$\Pr[\chi^2 \geq \xi] = 1 - \Pr[\chi^2 \leq \xi] = 1 - \Pr(\xi, \nu) \quad (4.17)$$

where  $\nu$  is the degree of freedom, defined as the difference between the number of measurements and states.

A confidence level around 100% (small chi-square value) infers the measurements are highly consistent with the dynamic model of the system, and the estimated states and measurements are trustworthy. A low confidence level (large chi-square value) implies the occurrence of some bad data or hidden failures in the system.

The computed best estimate of the substation state is utilized to compute the best estimate of the bad data, if any, and the best estimate of missing data, if any. The computation of the best estimate of bad data or missing data is calculated from the model of the system and the best estimate of the substation state:

$$\mathbf{z}_{\text{bad}} = \mathbf{Y}_{\text{eqz\_bad}} \mathbf{x} + \left\{ \mathbf{x}^T \mathbf{F}_{\text{eqz\_bad}}^i \mathbf{x} \right\} - \mathbf{B}_{\text{eqz\_bad}} + \boldsymbol{\eta} \quad (4.18)$$

$$\mathbf{z}_{\text{miss}} = \mathbf{Y}_{\text{eqz\_miss}} \mathbf{x} + \left\{ \mathbf{x}^T \mathbf{F}_{\text{eqz\_miss}}^i \mathbf{x} \right\} - \mathbf{B}_{\text{eqz\_miss}} + \boldsymbol{\eta} \quad (4.19)$$

where the model equations for the bad data and missing data are denoted with the subscript “bad” and “miss”. Note the model is quadratic, at most, since the dynamic state estimator operates on the quadratized model of the substation. Finally, the best estimate of the state and data, including the filled-in-data, are sent to the substation UI and the control center as a C37.118 stream.

#### 4.4 State Estimation Results

We create two events and apply quasi-dynamic state estimation to this system. The duration of these two events is 20 seconds each with load changes outside the substation. The results of the events follow.

##### Event 1: Quasi-dynamic state estimation using both GPS- and non-synchronized measurements

During the event, the measurements (phasors) “seen” by the relays in the substation have been stored in a COMTRADE file, and they are used to perform the dynamic state estimation algorithm. The system of the state estimator includes the substation, the two transmission lines, and the three distribution lines. The data generated by the event and by the state estimator are very large, so we present and discuss examples of some specific data. Figures 4.2 and 4.3 show the voltage and the current actual and estimated phasor measurements in relay 4.

Figures 4.2 and 4.3 indicate that the estimated measurements accurately track the actual measurements. In Figure 4.4,  $\theta_1 \sim \theta_5$  are the estimated synchronous angle differences of non-synchronized measurements from relays 2, 3, 5, 6 and 7, respectively. Note that since the voltage channels of relays 5, 6, and 7 measure the voltage at the same node (Bus 4), the estimated synchronous angle differences  $\theta_3$ ,  $\theta_4$ , and  $\theta_5$  are the same. The confidence level remains 100% during the entire event. Therefore, the measurements are consistent with the system model. The state estimator validates the measurements and streams the estimated states to the control center for further application.

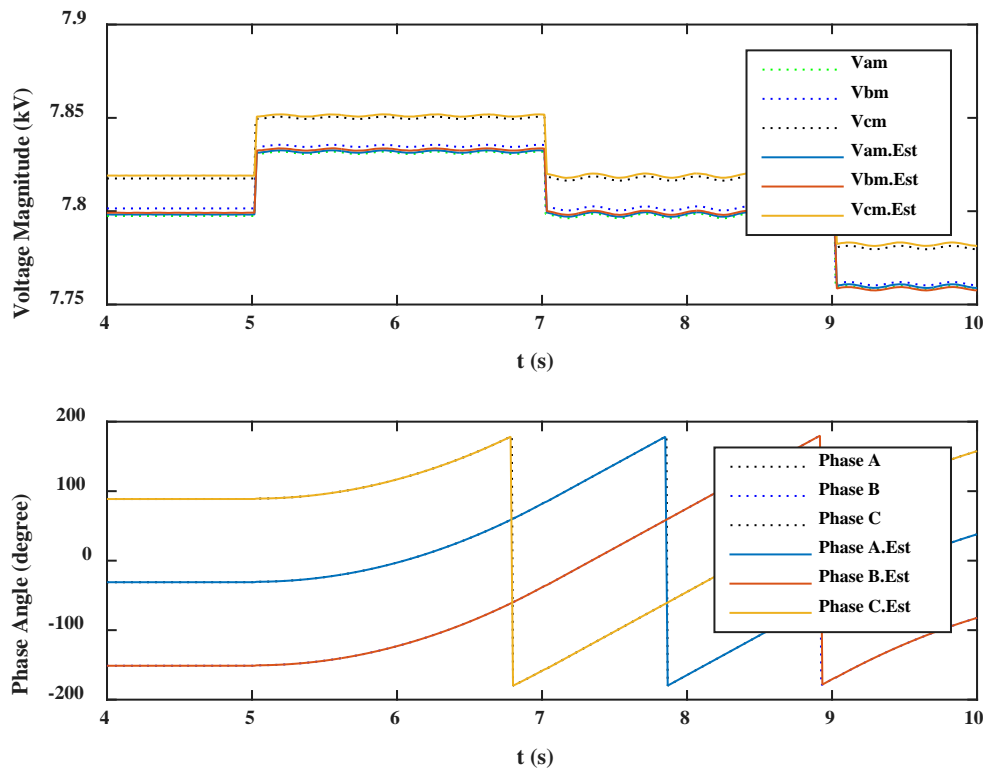


Figure 4.2: Voltage Actual and Estimated Phasor Measurements in Relay 4, Event 1

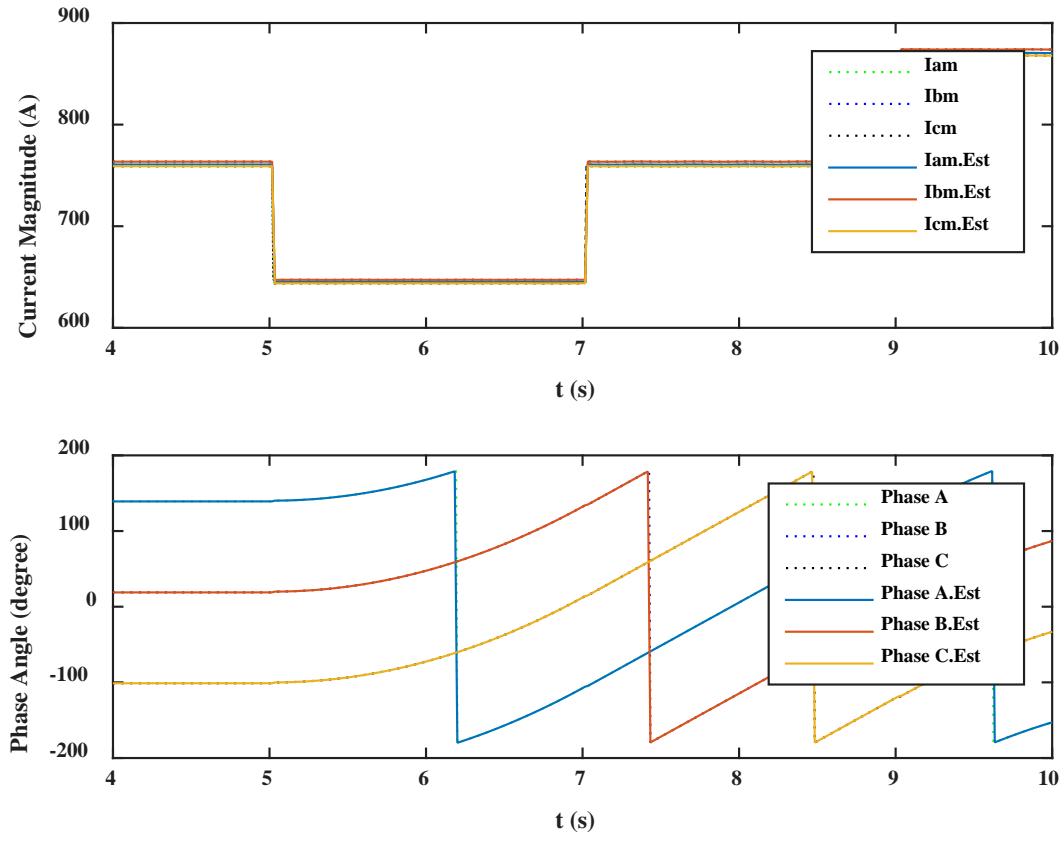


Figure 4.3: Current Actual and Estimated Phasor Measurements in Relay 4, Event 1

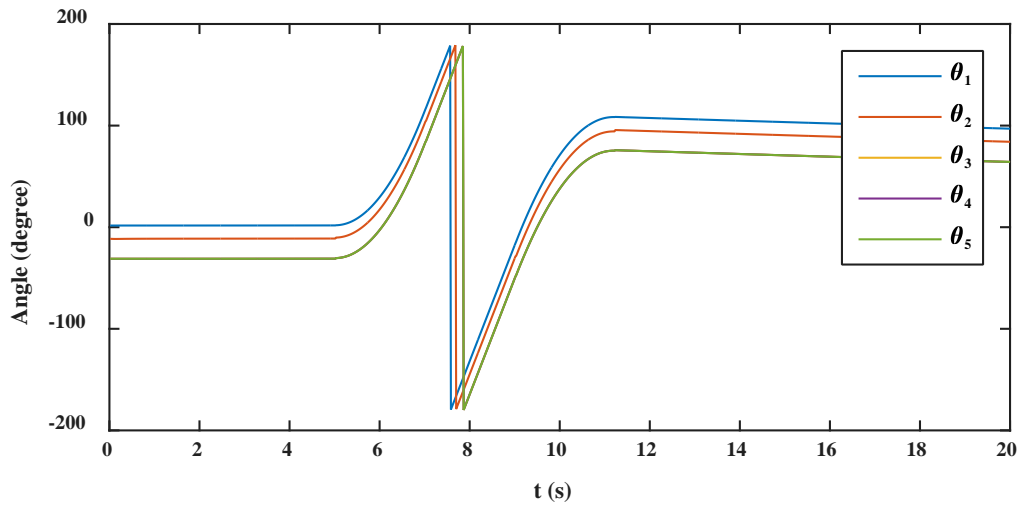


Figure 4.4: Estimated Angle Difference in Event 1

## Event 2: Quasi-dynamic state estimation using both GPS- and non-synchronized measurements with 1% Gaussian noise

Applying the dynamic state estimation algorithm to Event 2, we add a 1% Gaussian noise source to the measurements from relays in the substation and store these measurements in a COMTRADE file. The system of the state estimator is the same as that of Event 1. We present and discuss examples of measurements and generated data from the state estimator. Figures. 4.5 and 4.6 illustrate the voltage and the current actual and estimated measurements of phase A in relay 4. Figures. 4.5 and 4.6 indicate that even with 1% Gaussian noise, estimated measurements can also track actual measurements. Figure 4.7 shows the estimated synchronous angle differences of non-synchronized measurements from relays 2, 3, 5, 6 and 7. The confidence level in Figure 4.7 indicates strong consistency between the measurements and the system model (the probability is always larger than 90%). The DQDSE validates the measurements of this event and streams the estimated states to the control center for further application. Figure 4.8 shows that the square roots of the variance of estimated measurements in relay 4 are close to 0.01 p.u., which reflects the addition of Gaussian noise to the measurements.

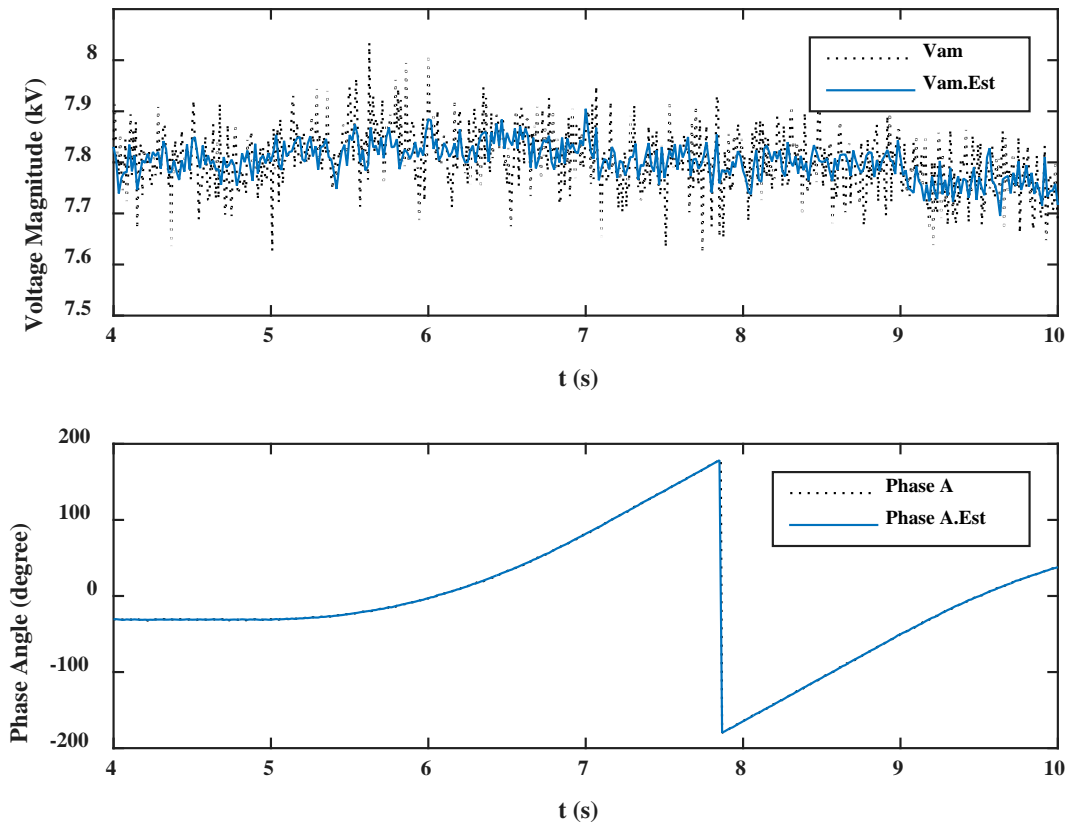


Figure 4.5: Voltage Actual and Estimated Phasor Measurements of Phase A in Relay 4, Event 2

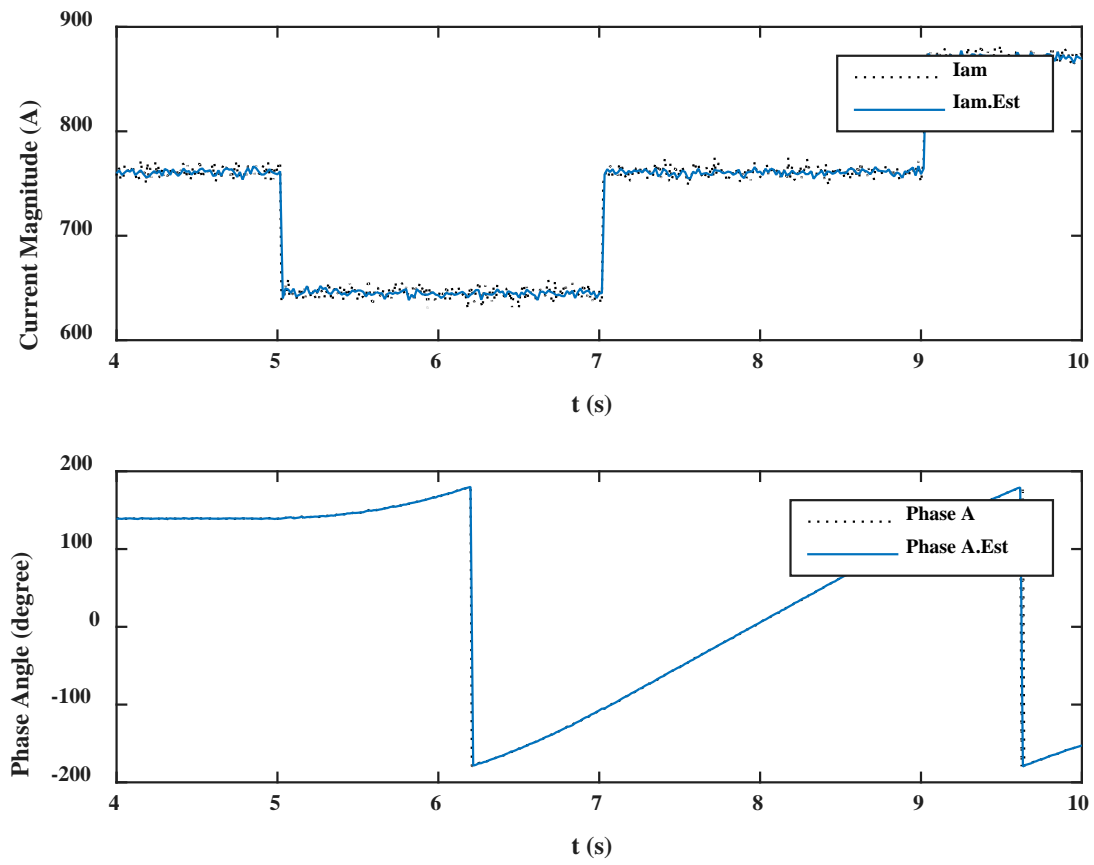


Figure 4.6: Current Actual and Estimated Phasor Measurements of Phase A in Relay 4, Event 2

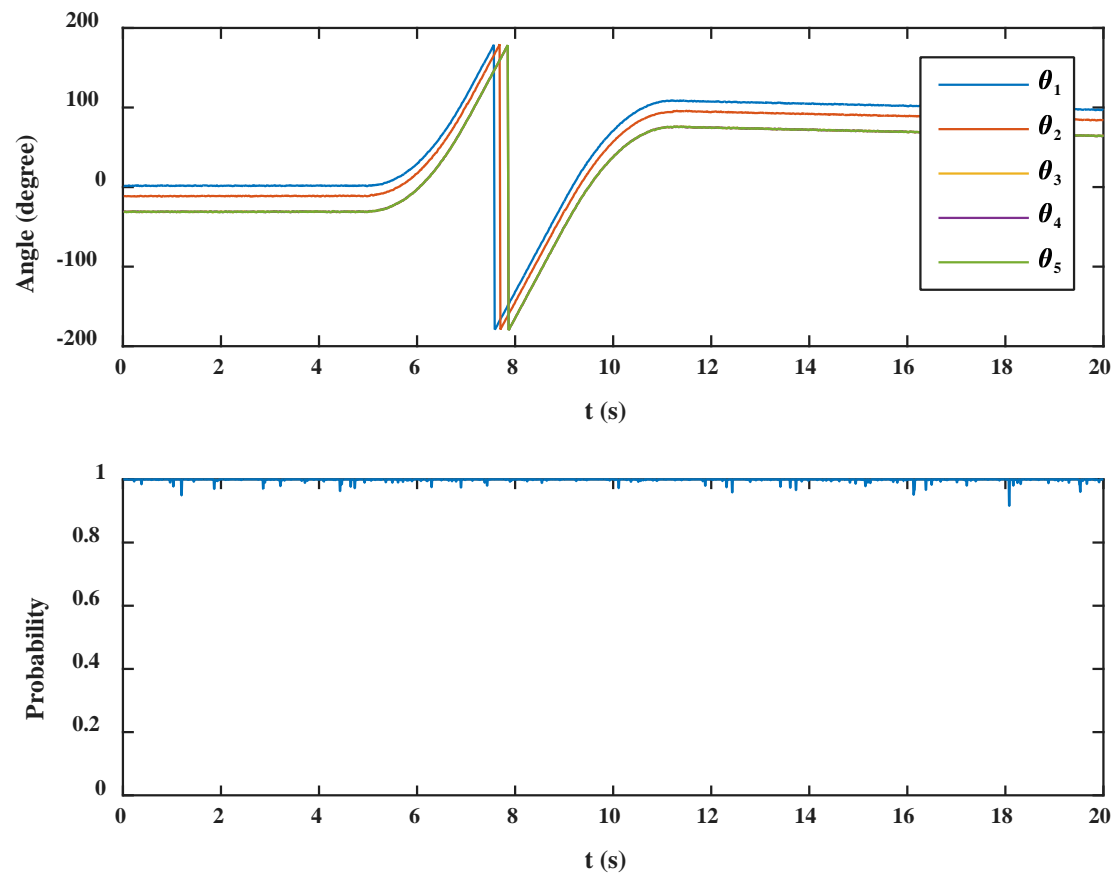


Figure 4.7: Estimated Angles and Confidence Level in Event 2

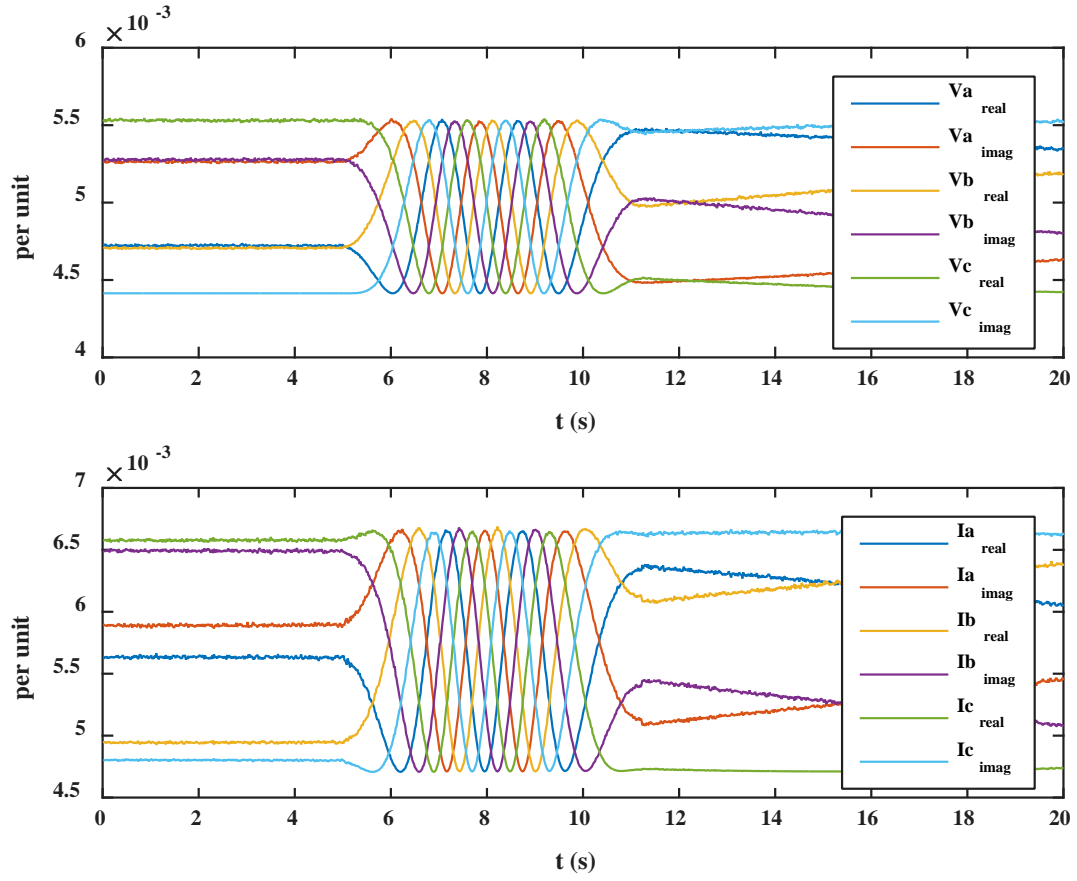


Figure 4.8: Square Root of the Variance of Voltage and Current Estimated Measurements in Relay 4, Event 2

## 5. Distributed System Quasi-Dynamic State Estimation: Use Case - Marcy Substation

### 5.1 Overview

This section describes a use case for the distribution system quasi-dynamic state estimator (DS-QSE). The use case is the Marcy substation of NYPA. The document describes: (a) preparing the example system (i.e., the Marcy substation) in WinIGS-Q, (b) modeling all IEDs providing measurements in this section, (c) simulating example events and store data in COMTRADE format, (d) setting up the state estimator for the system, and (e) executing DS-QSE and record performance.

### 5.2 Use Case System

We select Marcy substation as an example to perform the state estimation. The single-line diagram of the substation is shown in Figure 5.2.1. Marcy substation is connected to Massena substation, Volney substation, Edic substation, Coopers Corner substation, and New Scotland substation. It consists of six single-phase auto transformers with tertiary, two three-phase two-winding transformers, one three-phase three-winding transformer, two capacitor banks, one shunt reactor, four three-phase constant power loads, and nineteen breakers. The parameters of these devices are listed in Table 5.2.1. This substation has 23 buses. All of them are three-phase buses. The total number of states of this section is 74 at time  $t$ , and 74 at time  $t_m$ .

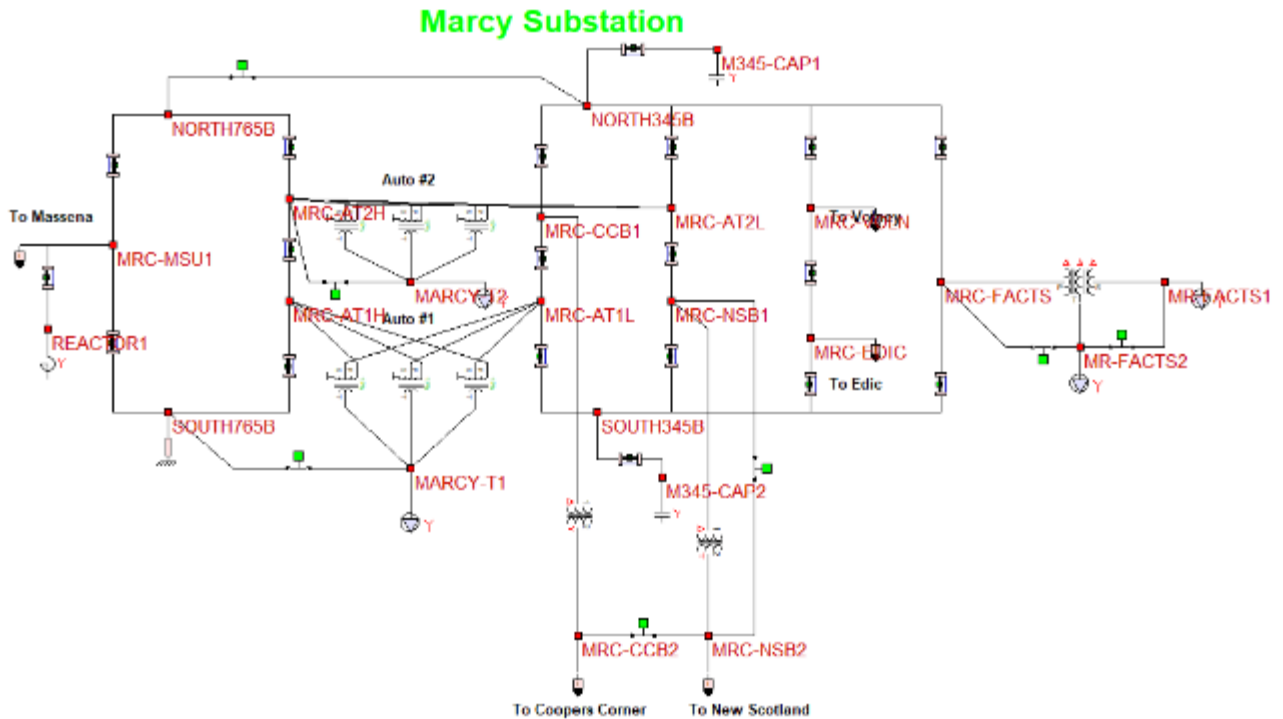


Figure 5.2.1: Marcy Substation

Table 5.2.1: Summary of Devices in Use Case Test System

Devices	Rated Voltage (kV)	Rated Power	# of States
AutoTransformer T-1, Phase A	765/345/13.8 (L-L)	300MVA (primary to secondary), 75MVA (primary to tertiary), 75MVA (secondary to tertiary)	12 at time t 12 at time t <sub>m</sub>
AutoTransformer T-1, Phase B	765/345/13.8 (L-L)	300MVA (primary to secondary), 75MVA (primary to tertiary), 75MVA (secondary to tertiary)	12 at time t 12 at time t <sub>m</sub>
AutoTransformer T-1, Phase C	765/345/13.8 (L-L)	300MVA (primary to secondary), 75MVA (primary to tertiary), 75MVA (secondary to tertiary)	12 at time t 12 at time t <sub>m</sub>
AutoTransformer T-2, Phase A	765/345/13.8 (L-L)	300MVA (primary to secondary), 75MVA (primary to tertiary), 75MVA (secondary to tertiary)	12 at time t 12 at time t <sub>m</sub>
AutoTransformer T-2, Phase B	765/345/13.8 (L-L)	300MVA (primary to secondary), 75MVA (primary to tertiary), 75MVA (secondary to tertiary)	12 at time t 12 at time t <sub>m</sub>
AutoTransformer T-2, Phase C	765/345/13.8 (L-L)	300MVA (primary to secondary), 75MVA (primary to tertiary), 75MVA (secondary to tertiary)	12 at time t 12 at time t <sub>m</sub>
Three-Phase Three-Winding Transformer	345kV/21.4kV/21.4kV	200MVA (primary to secondary), 100MVA (primary to tertiary), 100MVA (secondary to tertiary)	24 at time t 24 at time t <sub>m</sub>
Three-Phase Two-Winding Transformer #1	345kV (delta)/345kV (wye)	1000MVA	20 at time t 20 at time t <sub>m</sub>
Three-Phase Two-Winding Transformer #2	345kV (delta)/345kV (wye)	1000MVA	20 at time t 20 at time t <sub>m</sub>
Capacitor Bank #1	345 kV	100MVA	8 at time t 8 at time t <sub>m</sub>
Capacitor Bank #2	345 kV	100MVA	8 at time t 8 at time t <sub>m</sub>
Shunt Reactor	765 kV	-216MVAR	8 at time t 8 at time t <sub>m</sub>
Load #1 (MARCY-T1)	13.8 kV	1 kW 1 kVar	8 at time t 8 at time t <sub>m</sub>
Load #2 (MARCY-T2)	13.8 kV	1 kW 1 kVar	8 at time t

			8 at time $t_m$
Load #3 (MR-FACTS1)	21.4 kV	10 kW 1 kVar	8 at time $t$ 8 at time $t_m$
Load #4 (MR-FACTS2)	21.4 kV	10 kW 1 kVar	8 at time $t$ 8 at time $t_m$

### 5.3 Marcy System Model in WinIGS - SCAQCF Standard

This section introduces the modeled components in this substation. We use WinIGS-Q to build physically based models. The detailed parameters of autotransformers with tertiary, three-phase three-winding transformers, three-phase two-winding transformers, capacitor/reactor banks, three-phase constant power loads, three-phase breakers, two-node connectors are shown in Table 5.3.1 to 5.3.7. And the model interfaces of these devices are shown in Figure 5.3.1 to 5.3.8.

Table 5.3.1: Parameters of Autotransformers with Tertiary

Single-Phase Autotransformer with Tertiary (M293)					
#	Device Name	Bus Name	Rated Power (MVA)	Rated Voltage (kV)	Tertiary Connection Type
1	AutoTransformer T-1, Phase A	MRC-AT1H MRC-AT1L MARCY-T1	300/75/75	765/345/13.8 (L-L)	DELTA
2	AutoTransformer T-1, Phase B	MRC-AT1H MRC-AT1L MARCY-T1	300/75/75	765/345/13.8 (L-L)	
3	AutoTransformer T-1, Phase C	MRC-AT1H MRC-AT1L MARCY-T1	300/75/75	765/345/13.8 (L-L)	
4	AutoTransformer T-2, Phase A	MRC-AT2H MRC-AT2L MARCY-T2	300/75/75	765/345/13.8 (L-L)	DELTA
5	AutoTransformer T-2, Phase B	MRC-AT2H MRC-AT2L MARCY-T2	300/75/75	765/345/13.8 (L-L)	
6	AutoTransformer T-2, Phase C	MRC-AT2H MRC-AT2L MARCY-T2	300/75/75	765/345/13.8 (L-L)	

Table 5.3.2: Parameters of Three-Phase Three-Winding Transformers

Three-Phase Three-Winding Transformer (M105)					
#	Device Name	Bus Name	Rated Power (MVA)	Rated Voltage (kV)	Connection Type
1	FACTS Shunt Transformer	MRC-FACTS MR-FACTS1 MR-FACTS2	200/100/100	345.0/21.4/21.4	DELTA DELTA DELTA

Table 5.3.3: Parameters of Three-Phase Two-Winding Transformers

Three-Phase Two-Winding Transformer (M104)					
#	Device Name	Bus Name	Rated Power (MVA)	Rated Voltage (kV)	Connection Type
1	FACTS Series Transformer - Coopers Corner Line	MRC-CCB1 MRC-CCB2	1000	345.0/345.0	DELTA WYE
2	FACTS Series Transformer - New Scotland Line	MRC-NSB1 MRC-NSB2	1000	345.0/345.0	DELTA WYE

Table 5.3.4: Parameters of Capacitor/Reactor Bank

Three-Phase Capacitor/Reactor Bank (M116)					
#	Device Name	Bus Name	Rated Power	Rated Voltage	Connection Type
1	Reactor Bank 1, Marcy 765 kV	REACTOR1	-216.0 MVar	765.0 kV	WYE
2	Capacitor Bank 1, Marcy 345 kV	M345-CAP1	100 MVar	345.0 kV	WYE
3	Capacitor Bank 2, Marcy 345 kV	M345-CAP2	100 MVar	345.0 kV	WYE

Table 5.3.5: Parameters of Load Models

Three-Phase Constant Power Load (M161)						
#	Device Name	Bus Name	Real Power (kW)	Reactive Power (kVar)	Rated Voltage	Connection Type
1	Load 1	MARCY-T1	1.0	1.0	13.8	WYE
2	Load 2	MARCY-T2	1.0	1.0	13.8	WYE
3	Load 3	MR-FACTS1	10.0	1.0	21.4	WYE
4	Load 4	MR-FACTS2	10.0	1.0	21.4	WYE

Table 5.3.6: Parameters of Three-Phase Breaker

Three-Phase Breaker (M192)				
#	Device Name	Bus Name	Phases	Open/Closed
1	Breaker 7203	MRC-MSU1 REACTOR1	A, B, C, N	Closed
2	Breaker 7214	NORTH765B MRC-MSU1	A, B, C, N	Closed
3	Breaker 7202	MRC-MSU1 SOUTH765B	A, B, C, N	Closed
4	Breaker 7414	NORTH765B MRC-AT2H	A, B, C, N	Closed
5	Breaker 7402	MRC-AT2H MRC-AT1H	A, B, C, N	Closed
6	Breaker 7302	MRC-AT1H SOUTH765B	A, B, C, N	Closed
7	Breaker 3202	NORTH345B MRC-CCB1	A, B, C, N	Closed
8	Breaker 3208	MRC-CCB1 MRC-AT1L	A, B, C, N	Closed
9	Breaker 3214	MRC-AT1L SOUTH345B	A, B, C, N	Closed
10	Breaker 3402	NORTH345B M345-CAP1	A, B, C, N	Closed
11	Breaker 3414	SOUTH345B M345-CAP2	A, B, C, N	Closed
12	Breaker 3302	NORTH345B MRC-AT2L	A, B, C, N	Closed
13	Breaker 7402	MRC-AT2L MRC-NSB1	A, B, C, N	Closed
14	Breaker 7302	MRC-NSB1 SOUTH345B	A, B, C, N	Closed
15	Breaker 3102	NORTH345B MRC-VOLN	A, B, C, N	Closed
16	Breaker 3108	MRC-VOLN MRC-EDIC	A, B, C, N	Closed
17	Breaker 3114	MRC-EDIC SOUTH345B	A, B, C, N	Closed
18	Breaker 3002	NORTH345B MRC-FACTS	A, B, C, N	Closed
19	Breaker 3014	MRC-FACTS SOUTH345B	A, B, C, N	Closed

Table 5.3.7: Parameters of Two-Node Connectors

Two-Node Connector (M191)				
#	Device Name	Bus Name	Phases	Open/Closed
1	Node Connector 1	NORTH765B NORTH345B	N	Closed
2	Node Connector 2	MRC-AT2H MARCY-T2	N	Closed
3	Node Connector 3	SOUTH765B MARCY-T1	N	Closed
4	Node Connector 4	MRC-CCB2 MRC-NSB2	N	Closed
5	Node Connector 5	MRC-NSB1 MRC-NSB2	N	Closed
6	Node Connector 6	MRC-FACTS MR-FACTS2	N	Closed
7	Node Connector 7	MR-FACTS2 MR-FACTS1	N	Closed

**1-Phase Autotransformer with Tertiary** Cancel Accept

AutoTransformer T-1, Phase A, Marcy Sub

**Short Circuit Test Data (PU)**

	R	X	Base (MVA)
P-S	0.03	0.08	300.0
P-T	0.0519	0.2073	75.0
S-T	0.0866	0.2031	75.0

**Winding Impedances (Ohms)**

	Resistance	Reactance
P	9.7682	36.690
S	6.5510	24.606
T	0.18839	0.68165

☐ Ohms  
☒ Per Unit  
☐ Per Cen

Display Circuit

**Node Names & Voltage Ratings**

Circuit Name: 1

Vprim: 442.0 kV  
 P: MRC-AT1H A  
 Vsec: 199.0 kV  
 S: MRC-AT1L A  
 N: MRC-AT1L N  
 Vter: 13.8 kV  
 T1: MARCY-T1 A  
 T2: MARCY-T1 B

**Core Parameters, pu at 300 MVA**

Nominal Core Loss: 0.005 pu  
 Nominal Magnetizing Current: 0.005 pu  
 Exponent: 1.0  
 Core Time Constant: 5.0 s

Primary Voltage (Vrms) vs Magnetizing Current (Arms) graph showing a linear relationship on a log-log scale.

Im: A Vprim: V

Program WinIGS-Q - Form IGS\_M293

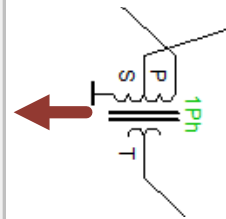



Figure 5.3.1: Three-Phase Autotransformer with Tertiary (M106)

**3-Phase 3-Winding Transformer**  **Cancel** **Accept**

**FACTS Shunt Transformer, 200/100/100 MVA**

**Short Circuit Test Data (PU)**

	R	X	Base (MVA)
<b>P-S</b>	0.003151	0.07992	200.0
<b>P-T</b>	0.004201	0.08465	100.0
<b>S-T</b>	0.004201	0.08454	100.0

☐ Ohms  
☒ Per Unit  
☐ Per Cent

**Winding Impedances (Ohms)**

	Winding Resistance	Leakage Reactance
<b>P</b>	2.8129	96.985
<b>S</b>	2.8129	96.985
<b>T</b>	0.046894	1.2078

**Display Equivalent Circuit**

**Sequence Parameters (PU)**

	R	X
Pos/Neg	0.152	3.87
Primary Zero	OPEN	-0.0000003
Second. Zero	OPEN	0.00253
Ground Zero	0.0000001	0

**Core Parameters (PU)**

Nominal Core Loss : 0.001

Nominal Magnetizing Current : 0.001

Base (MVA) : 600.00

**Primary**

MRC-FACTS

345.0 kV (L-L)

C A B

☒ Delta ☐ Wye

**Secondary**

MR-FACTS1

21.4 kV (L-L)

C A B

☒ Delta ☐ Wye

**Tertiary**

MR-FACTS2

21.4 kV (L-L)

C A B

☒ Delta ☐ Wye

**Circuit Number** 1

**Phase Connection**

☒ Standard ☐ Alternate

Program WinIGS-Q - Form IGS\_M105\_F

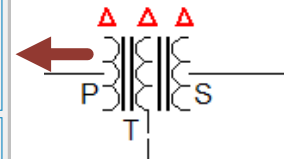



Figure 5.3.2: Three-Phase Three-Winding Transformer (M105)

**3-Phase Transformer**  **Cancel** **Accept**

**FACTS Series Transformer - Coopers Corner Line**

**Side 1 Bus**

MRC-CCB1

345.0 kV

☒ Delta ☐ Wye

**Side 2 Bus**

MRC-CCB2

345.0 kV

☐ Delta ☒ Wye

**Phase Connection**

☒ Standard ☐ Alternate

30°

Transformer Rating (MVA) 1000.0

Winding Resistance (pu) 0.01

Leakage Reactance (pu) 0.1

Nominal Core Loss (pu) 0.005

Nominal Magnetizing Current (pu) 0.005

Tap Setting (pu) 1.0

Minimum (pu) 1.0

Maximum (pu) 1.0

Number of Taps 1

Circuit Number 1

WinIGS-Q - Form IGS\_M104\_F - Copyright © A. P. Meliopoulos 1998-2017

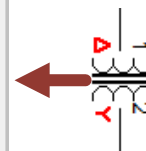


Figure 5.3.3: Three-Phase Two-Winding Transformer Model (M104)

Three Phase Shunt

Cancel
Accept

Reactor Bank 1, Marcy 765 kV

Bus REACTOR1

A

B

C

N

7.187 H

Circuit 2

Connection

☐ Delta

☒ Wye

L-L Rated Voltage (RMS) 765.0 kV

Total Rated Reactive Power -216000.0 kVar  
(Positive for Capacitors, Negative for Reactors)

Series Resistance 0.001 pu

Discharge Conductance 0.001 pu  
(Capacitor Bank Only)

WinIGS-Q - Form: IGS\_M116 - Copyright © A. P. Meliopoulos 1998-2017

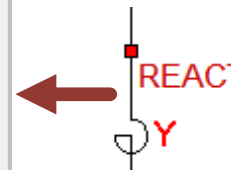


Figure 5.3.4: Reactor Bank Model (M116)

Three Phase Shunt

Cancel
Accept

Capacitor Bank 1, Marcy 345 kV

Bus M345-CAP1

A

B

C

N

2.229 uF

Circuit 1

Connection

☐ Delta

☒ Wye

L-L Rated Voltage (RMS) 345.0 kV

Total Rated Reactive Power 100000.0 kVar  
(Positive for Capacitors, Negative for Reactors)

Series Resistance 0.001 pu

Discharge Conductance 0.001 pu  
(Capacitor Bank Only)

WinIGS-Q - Form: IGS\_M116 - Copyright © A. P. Meliopoulos 1998-2017



Figure 5.3.5: Capacitor Bank Model (M116)

### Constant Power Three-Phase Electric Load

Load1

Accept

Cancel

Rated Voltage

13.8

L-L, kV, RMS

Real Power

1.0

kW (Total)

Reactive Power

1.0

kVar (Total)

Connection

☐ Delta
 ☒ Wye

Real Power Control Coefficients

a0 = 100.0 kW

a1 = 30.0 kW

a2 = -30.0 kW

$(P = a0 + a1 v1 + a2 v2)$

Bus Name

MARCY-T1

Circuit Name

4

Program WinIGS-Q - Form IGS\_M161

Figure 5.3.6: Three-Phase Constant Power Load Model (M161)

### Primary Bus Connector

Breaker 7214

Accept

Cancel

Bus Name

NORTH765B

Circuit Number

1

Bus Name

MRC-MSU1

A

B

C

☒ Closed
 ☒ Neutral Switch
 ☐ Ground Switch

Closed

A

B

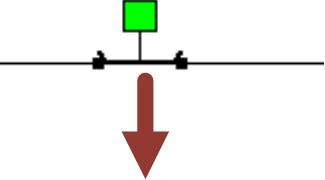
C


N

☐ Show Title

Figure 5.3.7: Three-Phase Breaker Model (M192)

43



Connector / Switch

Cancel
Accept

Node Connector 2

Side 1 Node Name


MRC-AT2H\_N

Side 2 Node Name

MRC-AT2L\_N

Circuit Number

1



☐ Open
☒ Closed
☐ Show Title

Program WinIGS-Q - Form IGS\_M191

Figure 5.3.8: Node Connector Model (M191)

#### 5.4 Marcy co-Model: Physical System and IEDs

This section introduces the procedure that we set up the IEDs in this substation. We use one IED setup as an example, and the other IEDs are set up in the same way. 46 IEDs are placed in this substation. The total number of phasor measurements is 360 (i.e., 720 measurements in real values) at time  $t$ . Since the substation consists of 74 states, the redundancy is 905%. The substation with setup IEDs is shown in Figure 5.4.1.

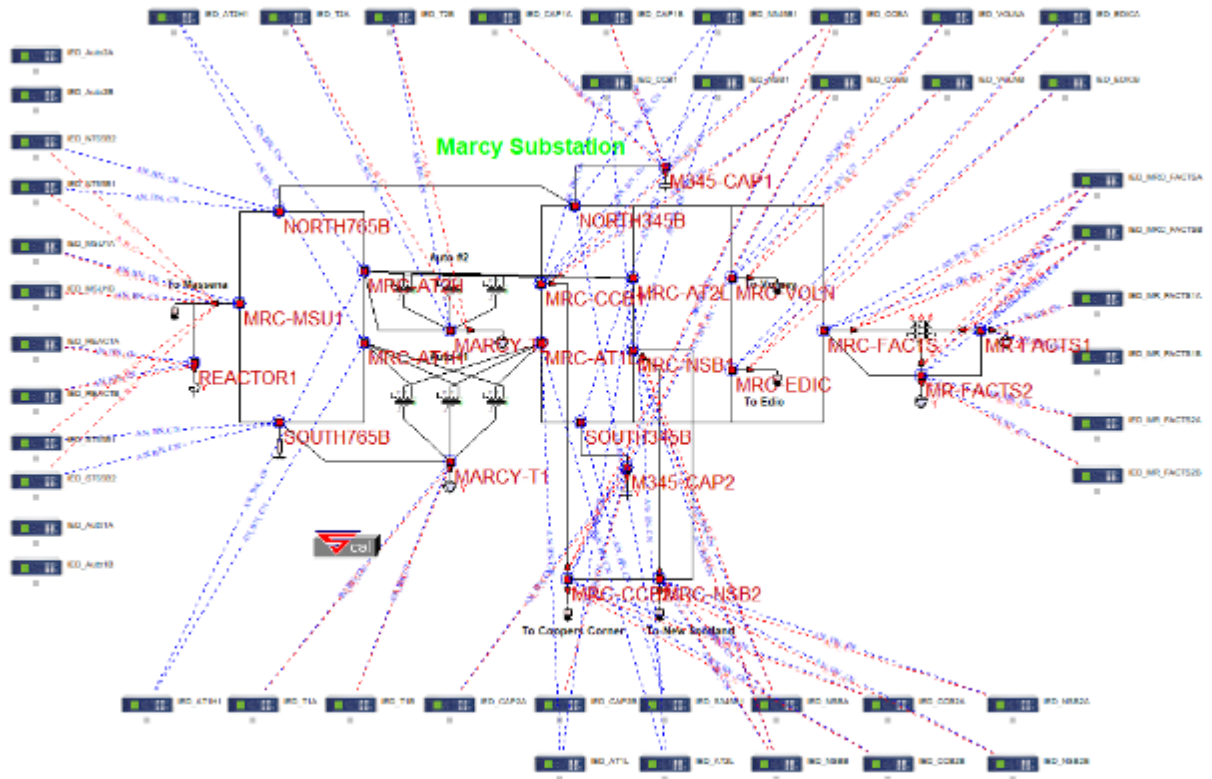


Figure 5.4.1: Marcy Substation with IEDs

### 5.4.1 Instrumentation Channels

The instrumentation channel and measurement parameters to be used by the state estimator are modelled in the IED model (M007, see icon in Figure 5.4.2).

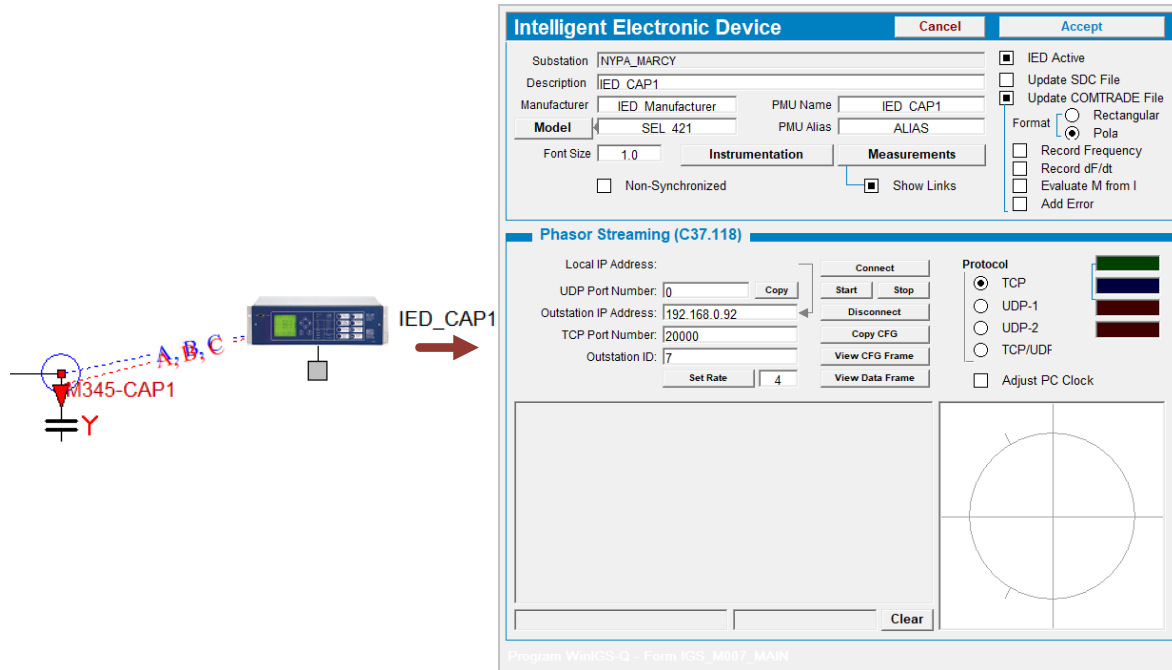


Figure 5.4.2: IED and its user interface

The IED model parameters and instrumentation channel list can be edited by clicking on the IED icon. This action will bring the user interface illustrated in Figure 5.4.2. The user is able to edit the IED name, manufacturer, etc. in this user interface. Click on the instrumentation button to open the instrumentation channel list dialog as shown in Figure 5.4.3.

Double click on each list table entry to inspect the instrumentation channel parameters. Figure 5.4.4 and 5.4.5 illustrate examples of a voltage phasor and a current phasor channel, respectively. Note that one instrumentation channel model includes models of the instrument transformer, instrumentation cable, burdens, and data acquisition device (i.e., a PMU in this example). The instrumentation channel parameters are listed in Table 5.4.1 with detailed descriptions.



Figure 5.4.5: Example of a Current Phasor Instrumentation Channel Dialog

Table 5.4.1: Instrumentation Channel Parameters – User Entry Fields

Parameter	Description
Data Type	Specifies the type of the measured quantity.
Bus Name	The bus name where the measurement is taken
Power Device	Identifies the power device into which the current is measured (not used for voltage measurements)
Phase	The phase of the measured quantity (A, B, C, N, etc.)
Current Direction	The direction of current flow which is considered positive. For example, “into device” indicates that the positive current flow is into the power device terminal (See also Power Device parameter above)
Standard Deviation	Quantifies the expected error of the instrumentation channel in per unit of the maximum value that the channel can measure.
Meter Scale	The maximum peak value that the channel can measure defined at the instrument transformer primary side. Note that this value can be directly entered by the user, or automatically computed from the instrument transformer and data acquisition device characteristics. To automatically compute the, click on the <b>Update</b> button located below the Meter Scale field.
Instrument Transformer Code Name	An identifier of the instrument transformer associated with this channel. Note that WinIGS uses this identifier to generate the channel name. For example, the phase A voltage channel is

	automatically named V_VT_AN, if the instrument transformer name is set to VT.
Instrument Transformer <b>Type</b> and <b>Tap</b>	Selects instrument transformer parameters from a data library. The library includes parameters needed to create instrument channel models such as turns ratio, frequency response, etc. To select an instrument transformer model, click on the <b>type</b> or <b>tap</b> field to open the instrument transformer data library dialog (See also Figure 4.3 and 4.4)
L-L Nominal Primary Voltage	The line to line voltage at the instrument transformer primary side.
Instrumentation Cable Length	The length of the instrumentation cable connecting the instrument transformer secondary with the data acquisition device.
Cable Type	The instrumentation cable type and size. Clicking on this field opens the cable library selection window. Note that if the desired cable is not found in the library, a cable library editor is available allowing adding and modifying cable parameters. (See WinIGS-Q user's manual for details).
Attenuator	Attenuation value of any additional voltage or current reduction divider. Set to 1.0 if none.
Burden	The equivalent resistance of the burdens attached to the instrument transformer secondary.
IED	Selects data acquisition device from a IED library. This setting retrieved the data acquisition device frequency response for applying error correction. Set to UNITY if this information is not available.
Maximum Peak Value	Set to the maximum instantaneous (peak) voltage or current value that will not saturate the data acquisition device input. This value can be found in data acquisition device specifications
Calibration Factor	The channel output is multiplied by this value. Set to 1.0 if none required.
Calibration Offset	This value is added to the channel output. Set to 0.0 if none required.
Time Skew	Time delay in seconds of this channel with respect to time reference. Set to zero for no delay.

Note that the order of the instrumentation channels can be modified using the **Move Up** and **Move Down** buttons of the instrumentation channel list dialog (shown in Figure 4.2). Once the instrumentation channel parameter entry is completed, click on the Accept button of the instrumentation channel list dialog, to save the channel parameters. Note that the instrumentation channel parameters are saved in an ASCII file named:

CASENAME\_Fnnnnn.ich

where case name is the WinIGS-Q network model file name root, and nnnnn is a 5-digit integer. Each IED has its own ‘ich’ file, and these files are stored in the same directory as the WinIGS-Q network model file.

In this example, 46 IEDs are placed in this substation for state estimation. The instrumentation channels of these IEDs are listed in Table 5.4.2. The total number of these channels is 360.

Table 5.4.2: Instrumentation Channels of IEDs in the Selected Section

IED Name	Voltage Channels	Current Channels	# of channels of this IED
IED_MRC_FACTSA	AN, BN, CN at MRC-FACTS	A, B, C at MRC-FACTS (into the transformer)	18
	AN, BN, CN at MR-FACTS1	A, B, C at MR-FACTS1 (into the transformer)	
	AN, BN, CN at MR-FACTS2	A, B, C at MR-FACTS2 (into the transformer)	
IED_MRC_FACTSB	AN, BN, CN at MRC-FACTS	A, B, C at MRC-FACTS (into the transformer)	18
	AN, BN, CN at MR-FACTS1	A, B, C at MR-FACTS1 (into the transformer)	
	AN, BN, CN at MR-FACTS2	A, B, C at MR-FACTS2 (into the transformer)	
IED_MR_FACTS1A	AN, BN, CN at MR-FACTS1	A, B, C at MR-FACTS1 (into the load)	6
IED_MR_FACTS1B	AN, BN, CN at MR-FACTS1	A, B, C at MR-FACTS1 (into the load)	6
IED_MR_FACTS2A	AN, BN, CN at MR-FACTS2	A, B, C at MR-FACTS2 (into the load)	6
IED_MR_FACTS2B	AN, BN, CN at MR-FACTS2	A, B, C at MR-FACTS2 (into the load)	6
IED_Auto1A	AN, BN, CN at MRC-AT1H	A, B, C at MRC-AT1H (into the transformer)	18
	AN, BN, CN at MRC-AT1L	A, B, C at MRC-AT1L (into the transformer)	
	AN, BN, CN at MARCY-T1	A, B, C at MARCY-T1 (into the transformer)	
IED_Auto1B	AN, BN, CN at MRC-AT1H	A, B, C at MRC-AT1H (into the transformer)	18
	AN, BN, CN at MRC-AT1L	A, B, C at MRC-AT1L (into the transformer)	
	AN, BN, CN at MARCY-T1	A, B, C at MARCY-T1 (into the transformer)	
IED_Auto2A	AN, BN, CN at MRC-AT2H	A, B, C at MRC-AT2H (into the transformer)	18

	AN, BN, CN at MRC-AT2L	A, B, C at MRC-AT2L (into the transformer)	
	AN, BN, CN at MARCY-T2	A, B, C at MARCY-T2 (into the transformer)	
IED_Auto2B	AN, BN, CN at MRC-AT2H	A, B, C at MRC-AT2H (into the transformer)	18
	AN, BN, CN at MRC-AT2L	A, B, C at MRC-AT2L (into the transformer)	
	AN, BN, CN at MARCY-T2	A, B, C at MARCY-T2 (into the transformer)	
IED_S765B1	AN, BN, CN at SOUTH765B	A, B, C at MRC-MSU1 (out of the substation)	6
IED_S765B2	AN, BN, CN at SOUTH765B	A, B, C at MRC-MSU1 (out of the substation)	6
IED_N765B1	AN, BN, CN at NORTH765B	A, B, C at MRC-MSU1 (out of the substation)	6
IED_N765B2	AN, BN, CN at NORTH765B	A, B, C at MRC-MSU1 (out of the substation)	6
IED_MSU1A	AN, BN, CN at MRC-MSU1	A, B, C at MRC-MSU1 (out of the substation)	6
IED_MSU1B	AN, BN, CN at MRC-MSU1	A, B, C at MRC-MSU1 (out of the substation)	6
IED_REACTA	AN, BN, CN at REACTOR1	A, B, C at REACTOR1 (into the reactor)	6
IED_REACTB	AN, BN, CN at REACTOR1	A, B, C at REACTOR1 (into the reactor)	6
IED_AT1H1	AN, BN, CN at MRC-AT1H	none	6
	AN, BN, CN at MRC-AT2H		
IED_AT2H1	AN, BN, CN at MRC-AT1H	none	6
	AN, BN, CN at MRC-AT2H		
IED_T1A	AN, BN, CN at MARCY-T1	A, B, C at MARCY-T1 (into the load)	6
IED_T1B	AN, BN, CN at MARCY-T1	A, B, C at MARCY-T1 (into the load)	6
IED_T2A	AN, BN, CN at MARCY-T2	A, B, C at MARCY-T2 (into the load)	6
IED_T2B	AN, BN, CN at MARCY-T2	A, B, C at MARCY-T2 (into the load)	6
IED_CAP1A	AN, BN, CN at M345-CAP1	A, B, C at M345-CAP1 (into the cap bank)	6
IED_CAP1B	AN, BN, CN at M345-CAP1	A, B, C at M345-CAP1 (into the cap bank)	6
IED_CAP2A	AN, BN, CN at M345-CAP2	A, B, C at M345-CAP2 (into the cap bank)	6
IED_CAP2B	AN, BN, CN at M345-CAP2	A, B, C at M345-CAP2 (into the cap bank)	6

IED_N345B1	AN, BN, CN at NORTH345B	none	6
	AN, BN, CN at SOUTH345B		
IED_S345B1	AN, BN, CN at NORTH345B	none	6
	AN, BN, CN at SOUTH345B		
IED_CCB1	AN, BN, CN at MRC-CCB1	none	6
	AN, BN, CN at MRC-NSB1		
IED_NSB1	AN, BN, CN at MRC-CCB1	none	6
	AN, BN, CN at MRC-NSB1		
IED_AT1L	AN, BN, CN at MRC-AT1L	none	6
	AN, BN, CN at MRC-AT2L		
IED_AT2L	AN, BN, CN at MRC-AT1L	none	6
	AN, BN, CN at MRC-AT2L		
IED_CCBA	AN, BN, CN at MRC-CCB1	A, B, C from MRC-CCB1 to MRC-CCB2	12
	AN, BN, CN at MRC-CCB2	A, B, C from MRC-CCB2 to MRC-CCB1	
IED_CCBB	AN, BN, CN at MRC-CCB1	A, B, C from MRC-CCB1 to MRC-CCB2	12
	AN, BN, CN at MRC-CCB2	A, B, C from MRC-CCB2 to MRC-CCB1	
IED_NSBA	AN, BN, CN at MRC-NSB1	A, B, C from MRC-NSB1 to MRC-NSB2	12
	AN, BN, CN at MRC-NSB2	A, B, C from MRC-NSB2 to MRC-NSB1	
IED_NSBB	AN, BN, CN at MRC-NSB1	A, B, C from MRC-NSB1 to MRC-NSB2	12
	AN, BN, CN at MRC-NSB2	A, B, C from MRC-NSB2 to MRC-NSB1	
IED_VOLNA	AN, BN, CN at MRC-VOLN	A, B, C at MRC-VOLN (out of the substation)	6
IED_VOLNB	AN, BN, CN at MRC-VOLN	A, B, C at MRC-VOLN (out of the substation)	6
IED_EDICA	AN, BN, CN at MRC-EDIC	A, B, C at MRC-EDIC (out of the substation)	6
IED_EDICB	AN, BN, CN at MRC-EDIC	A, B, C at MRC-EDIC (out of the substation)	6
IED_CCB2A	AN, BN, CN at MRC-CCB2	A, B, C at MRC-CCB2 (out of the substation)	6

IED_CCB2B	AN, BN, CN at MRC-CCB2	A, B, C at MRC-CCB2 (out of the substation)	6
IED_NSB2A	AN, BN, CN at MRC-NSB2	A, B, C at MRC-NSB2 (out of the substation)	6
IED_NSB2B	AN, BN, CN at MRC-NSB2	A, B, C at MRC-NSB2 (out of the substation)	6

### 5.4.2 Measurement Channel

The next step is to define the measurements to be used for the state estimator, in terms of the defined instrumentation channels. This is accomplished by clicking on the **Measurement** button of the IED user interface (shown in Figure 5.4.2). This action opens the measurement list dialog illustrated in Figure 5.4.6.

For most cases (including the example described in this document), the measurement parameters can be created automatically using the **Auto Create** button from the measurement list dialog.

Measurement Channels

Manual Edit Mode

Name	IED Alias	Type	Value	Nominal	Scale	St.Dev	Correction
V_M345-CAP1_AN		V-Phasor		345.0 kV	600.0 kV	0.01000 pu	1.675 / 0.057
V_M345-CAP1_BN		V-Phasor		345.0 kV	600.0 kV	0.01000 pu	1.675 / 0.057
V_M345-CAP1_CN		V-Phasor		345.0 kV	600.0 kV	0.01000 pu	1.675 / 0.057
C_M345~CAP1_2_M345~CAP1_A		C-Phasor		40.00 A	2.000 kA	0.01000 pu	0.968 / 1.647
C_M345~CAP1_2_M345~CAP1_B		C-Phasor		40.00 A	2.000 kA	0.01000 pu	0.968 / 1.647
C_M345~CAP1_2_M345~CAP1_C		C-Phasor		40.00 A	2.000 kA	0.01000 pu	0.968 / 1.647

▲ Move Up

▼ Move Down

New

Edit

Delete

Auto Create

Auto Update

Auto Mapping

Cancel

Accept

Program WinIGS-Q - Form IGS\_MCHAN\_LIST

Figure 5.4.6: Measurement List Dialog

Measurement parameters can be manually created and edited using the New and Edit buttons of the measurement list dialog (shown in Figure 5.4.6), which open the measurement parameter dialog illustrated in Figure 5.4.7 and Figure 5.4.8. The fields in this dialog are briefly described in Table 5.4.2.

Measurement Definition		Cancel	Accept																																								
<b>Instrumentation Channels</b>	<b>Measurement Formula</b>																																										
<table border="1"> <tr><td>1</td><td>V_VT1_AN</td></tr> <tr><td>2</td><td>V_VT1_BN</td></tr> <tr><td>3</td><td>V_VT1_CN</td></tr> <tr><td>4</td><td>C_CT1_A</td></tr> <tr><td>5</td><td>C_CT1_B</td></tr> <tr><td>6</td><td>C_CT1_C</td></tr> </table>	1	V_VT1_AN	2	V_VT1_BN	3	V_VT1_CN	4	C_CT1_A	5	C_CT1_B	6	C_CT1_C	V_VT1_AN																														
1	V_VT1_AN																																										
2	V_VT1_BN																																										
3	V_VT1_CN																																										
4	C_CT1_A																																										
5	C_CT1_B																																										
6	C_CT1_C																																										
<div> <div>Validate</div> <div>Auto Update</div> </div>																																											
<table border="1"> <tr> <td>Measurement Name</td> <td colspan="3">V M345-CAP1 AN</td> </tr> <tr> <td>Name at IED</td> <td></td> <td>IED Channel Order</td> <td>0</td> </tr> <tr> <td>IED</td> <td colspan="3">NYPA_MARCY_IED_CAP1</td> </tr> <tr> <td>Power Device</td> <td></td> <td>Referred to</td> <td>Primary</td> </tr> <tr> <td colspan="4">Capacitor Bank 1, Marcy 345 kV (Device at M345-CAP1, Circuit: 2)</td> </tr> <tr> <td>Bus &amp; Phase</td> <td>M345-CAP1_AN</td> <td>Meter Scale (Primary)</td> <td>600.0 kV</td> </tr> <tr> <td>Measurement Type</td> <td>V-Phasor</td> <td>Nominal Value</td> <td>345.0 kV</td> </tr> <tr> <td>Channel Correction</td> <td>1.6750, 0.057 Deg</td> <td>Std. Deviation (pu)</td> <td>0.01000 pu</td> </tr> <tr> <td>MU Scale Factor</td> <td>1.000000</td> <td>MU Offset</td> <td>0.000000</td> </tr> <tr> <td>Magnitude Calibration</td> <td>1.00000</td> <td>Phase Calibration (deg)</td> <td>0.00000</td> </tr> </table>				Measurement Name	V M345-CAP1 AN			Name at IED		IED Channel Order	0	IED	NYPA_MARCY_IED_CAP1			Power Device		Referred to	Primary	Capacitor Bank 1, Marcy 345 kV (Device at M345-CAP1, Circuit: 2)				Bus & Phase	M345-CAP1_AN	Meter Scale (Primary)	600.0 kV	Measurement Type	V-Phasor	Nominal Value	345.0 kV	Channel Correction	1.6750, 0.057 Deg	Std. Deviation (pu)	0.01000 pu	MU Scale Factor	1.000000	MU Offset	0.000000	Magnitude Calibration	1.00000	Phase Calibration (deg)	0.00000
Measurement Name	V M345-CAP1 AN																																										
Name at IED		IED Channel Order	0																																								
IED	NYPA_MARCY_IED_CAP1																																										
Power Device		Referred to	Primary																																								
Capacitor Bank 1, Marcy 345 kV (Device at M345-CAP1, Circuit: 2)																																											
Bus & Phase	M345-CAP1_AN	Meter Scale (Primary)	600.0 kV																																								
Measurement Type	V-Phasor	Nominal Value	345.0 kV																																								
Channel Correction	1.6750, 0.057 Deg	Std. Deviation (pu)	0.01000 pu																																								
MU Scale Factor	1.000000	MU Offset	0.000000																																								
Magnitude Calibration	1.00000	Phase Calibration (deg)	0.00000																																								

Program WinIGS-Q - Form IGS\_MCHAN\_EDIT\_2

Figure 5.4.7: Voltage Phasor Measurement Parameters Dialog

Measurement Definition		Cancel	Accept																																								
<b>Instrumentation Channels</b>	<b>Measurement Formula</b>																																										
<table border="1"> <tr><td>1</td><td>V_VT1_A</td></tr> <tr><td>2</td><td>V_VT1_B</td></tr> <tr><td>3</td><td>V_VT1_C</td></tr> <tr><td>4</td><td>C_CT1_A</td></tr> <tr><td>5</td><td>C_CT1_B</td></tr> <tr><td>6</td><td>C_CT1_C</td></tr> </table>	1	V_VT1_A	2	V_VT1_B	3	V_VT1_C	4	C_CT1_A	5	C_CT1_B	6	C_CT1_C	C_CT1_A																														
1	V_VT1_A																																										
2	V_VT1_B																																										
3	V_VT1_C																																										
4	C_CT1_A																																										
5	C_CT1_B																																										
6	C_CT1_C																																										
<div> <div>Validate</div> <div>Auto Update</div> </div>																																											
<table border="1"> <tr> <td>Measurement Name</td> <td colspan="3">C M345~CAP1 2 M345~CAP1 A</td> </tr> <tr> <td>Name at IED</td> <td></td> <td>IED Channel Order</td> <td>0</td> </tr> <tr> <td>IED</td> <td colspan="3">NYPA_MARCY_IED_CAP1</td> </tr> <tr> <td>Power Device</td> <td></td> <td>Referred to</td> <td>Primary</td> </tr> <tr> <td colspan="4">Capacitor Bank 1, Marcy 345 kV (Device at M345-CAP1, Circuit: 2)</td> </tr> <tr> <td>Bus &amp; Phase</td> <td>M345-CAP1_A</td> <td>Meter Scale (Primary)</td> <td>2.000 kA</td> </tr> <tr> <td>Measurement Type</td> <td>C-Phasor</td> <td>Nominal Value</td> <td>40.00 A</td> </tr> <tr> <td>Channel Correction</td> <td>0.9680, 1.647 Deg</td> <td>Std. Deviation (pu)</td> <td>0.01000 pu</td> </tr> <tr> <td>MU Scale Factor</td> <td>1.000000</td> <td>MU Offset</td> <td>0.000000</td> </tr> <tr> <td>Magnitude Calibration</td> <td>1.00000</td> <td>Phase Calibration (deg)</td> <td>0.00000</td> </tr> </table>				Measurement Name	C M345~CAP1 2 M345~CAP1 A			Name at IED		IED Channel Order	0	IED	NYPA_MARCY_IED_CAP1			Power Device		Referred to	Primary	Capacitor Bank 1, Marcy 345 kV (Device at M345-CAP1, Circuit: 2)				Bus & Phase	M345-CAP1_A	Meter Scale (Primary)	2.000 kA	Measurement Type	C-Phasor	Nominal Value	40.00 A	Channel Correction	0.9680, 1.647 Deg	Std. Deviation (pu)	0.01000 pu	MU Scale Factor	1.000000	MU Offset	0.000000	Magnitude Calibration	1.00000	Phase Calibration (deg)	0.00000
Measurement Name	C M345~CAP1 2 M345~CAP1 A																																										
Name at IED		IED Channel Order	0																																								
IED	NYPA_MARCY_IED_CAP1																																										
Power Device		Referred to	Primary																																								
Capacitor Bank 1, Marcy 345 kV (Device at M345-CAP1, Circuit: 2)																																											
Bus & Phase	M345-CAP1_A	Meter Scale (Primary)	2.000 kA																																								
Measurement Type	C-Phasor	Nominal Value	40.00 A																																								
Channel Correction	0.9680, 1.647 Deg	Std. Deviation (pu)	0.01000 pu																																								
MU Scale Factor	1.000000	MU Offset	0.000000																																								
Magnitude Calibration	1.00000	Phase Calibration (deg)	0.00000																																								

Program WinIGS-Q - Form IGS\_MCHAN\_EDIT\_2

Figure 5.4.8: Current Phasor Measurement Parameters Dialog

Table 5.4.3: Measurement Parameters – User Entry Fields

Parameter	Description
Measurement Formula	Mathematical expression giving measurement value in terms of instrumentation channel values. Note that the measurement formula for automatically created measurements from instrumentation channels is simply the instrumentation channel name. However, a measurement can be manually defined as any expression involving all available instrumentation channels.
Measurement Name	<p><b>Voltage phasor measurements</b> names are automatically formed based on the bus name, phase and measurement type. For example, a phase A to N voltage measurement on Bus M345-CAP1 is automatically named as V_M345-CAP1_AN.</p> <p>Similarly, <b>current phasor measurements</b> are automatically formed by identifying a power device and a specific terminal into which the measured current is flowing. For example, the phase A current into the capacitor bank connected at bus M345-CAP1 is named as C_M345~CAP1_2_M345~CAP1_A, where the part M345~CAP1_2 identifies the power device as circuit 2 connected at bus M345-CAP1, and the last part _M345~CAP1_A identifies the terminal into which the measured current is flowing. Note that the name part 1 is the user specified Circuit Name of the capacitor bank connected at bus M345-CAP1.</p>
Name at IED	The measurement name as defined by the IED.
Meter Scale (Primary)	The maximum peak value that the channel can measure defined at the instrument transformer primary side. Note that this value is obtained from the corresponding instrumentation channel.
Standard Deviation (pu)	Quantifies the expected error of the measurement channel in per unit of the maximum value that the channel can measure.
Magnitude Calibration and Phase Calibration	Measurement magnitude and a phase angle correction values. Default values are 1.0 and 0.0 respectively.

## 5.5 Use Case: Normal Operation with Load VariationEvent Description and Sampled Data

We use WinIGS-Q to define events, simulate events and store the results in COMTRADE format. The WinIGS-Q case file is named as “NYPA\_Q\_Event1.NMT” and is provided with this report. Figure 5.5.1 shows the simulation user interface. The simulation is executed for a period of 1 minute. The measurements generated during the simulation are stored in a COMTRADE file. Figure 5.5.1 shows the quasi-dynamic domain simulation parameters dialog (click the “clock” button on the task bar) where the simulation time step, duration, as well as the COMTRADE output is specified. Note that the time step is selected to be 1 sample per cycle in this example, i.e., 60 samples per second. The simulation results are stored in COMTRADE files. The generated COMTRADE configuration and data files are named “NYPA\_Q\_Event1\_MARCY.cfg” and “NYPA\_Q\_Event1\_MARCY.dat”, respectively.

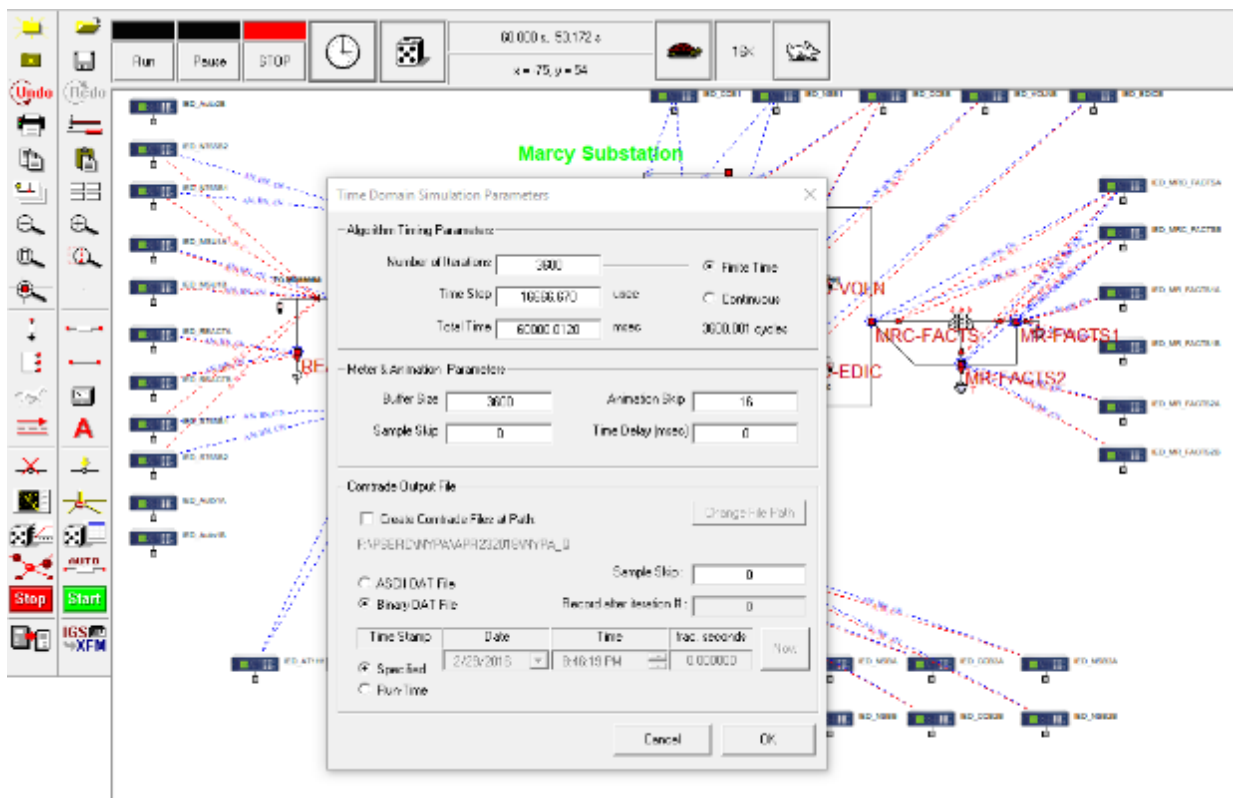


Figure 5.5.1: Perform Simulation for the Example System

In this event, the system is in normal operation with load variations outside the Marcy substation. The load variations are described as follows. At  $t=10.0s$ , a load with 80 MW, 30 MVar is disconnected to the system at Clay substation, and it is reconnected to the system at  $t=13.1s$ . Another load with 70 MW and 20 MVar at Clay substation is connected to the grid at 20.0s and disconnected at 23.1s. A load with 70 MW and 15 MVar is on and off at 28.0s and 30.1s in Edic Substation. Similarly, another load with 70 MW and 20MVar is disconnected at 35.05s and reconnected at 38.1s in Edic Substation. At  $t=45.05s$ , a load with 70 MW and 25 MVar is connected to the grid at Volney substation, and then it is disconnected at 47.1s. Another load with

80 MW and 30 MVar is then switched off at 53.05s, and switched on at 56.1s. Since the generated data is very large, we present the data obtained from some specific relays as shown from Figure 5.5.2 to 5.5.7.

Figure 5.5.2 shows the three-phase voltage phasor measurements at MRC-AT1H, MRC-AT1L, and MARCY-T1 obtained from IED\_Auto1A. Figure 5.5.3 presents the three-phase current phasor measurements for the three single-phase autotransformers obtained from IED\_Auto1A. Figure 5.5.4 shows the three-phase voltage phasor measurements at MRC-AT2H, MRC-AT2L, and MARCY-T2 obtained from IED\_Auto2A. Figure 5.5.5 shows the three-phase current phasor measurements for the three single-phase autotransformers obtained from IED\_Auto2A. Figure 5.5.6 depicts the three-phase voltage and current measurements for the capacitor bank at Bus M345-CAP1 obtained from IED\_CAP1A. Figure 5.5.7 presents the three-phase voltage and current measurements for the three-phase two-winding transformer from MRC-CCB1 to MRC-CCB2 obtained from IED\_CCBA.

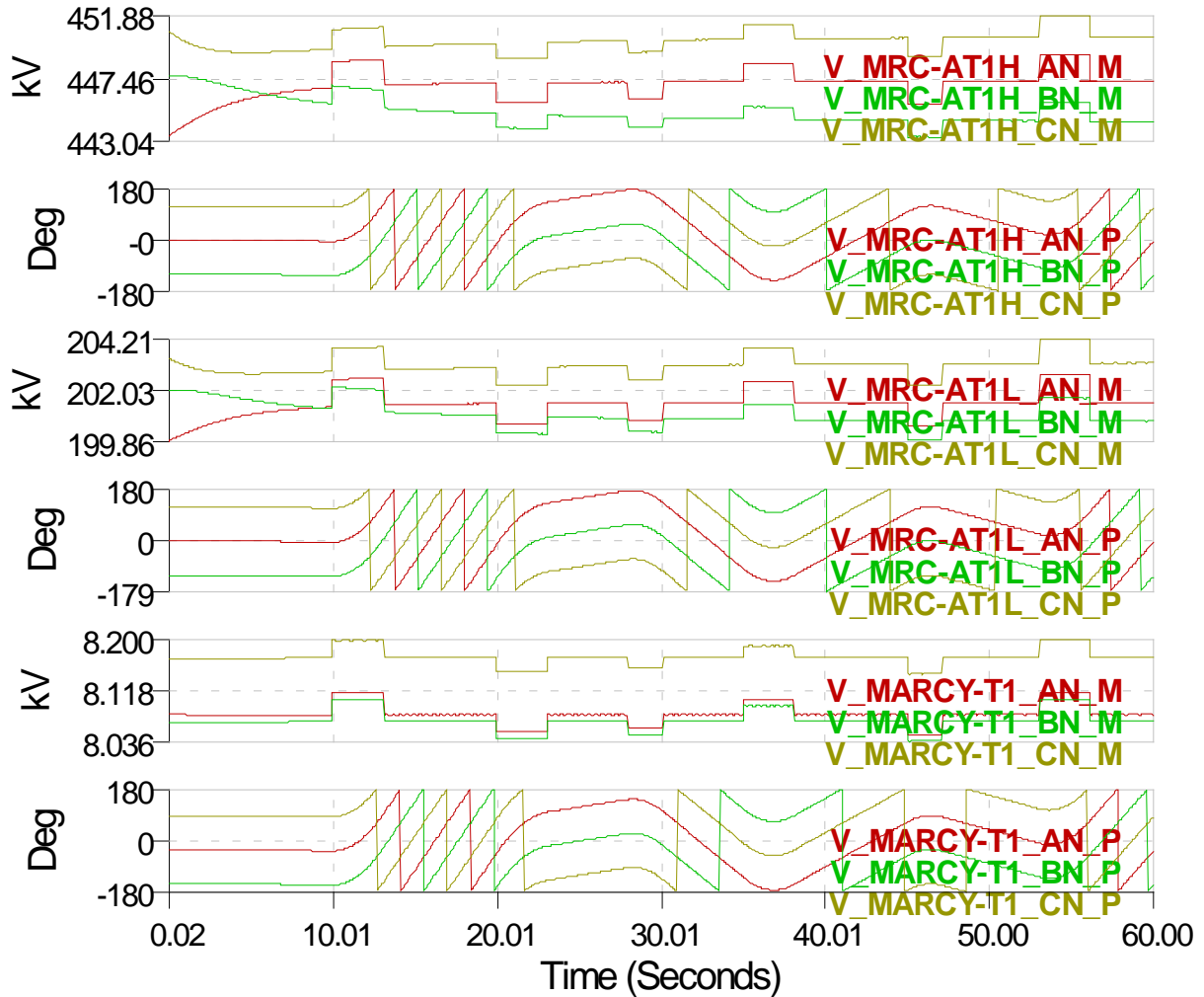


Figure 5.5.2: Three-phase Voltage Measurements at MRC-AT1H, MRC-AT1L, and MARCY-T1

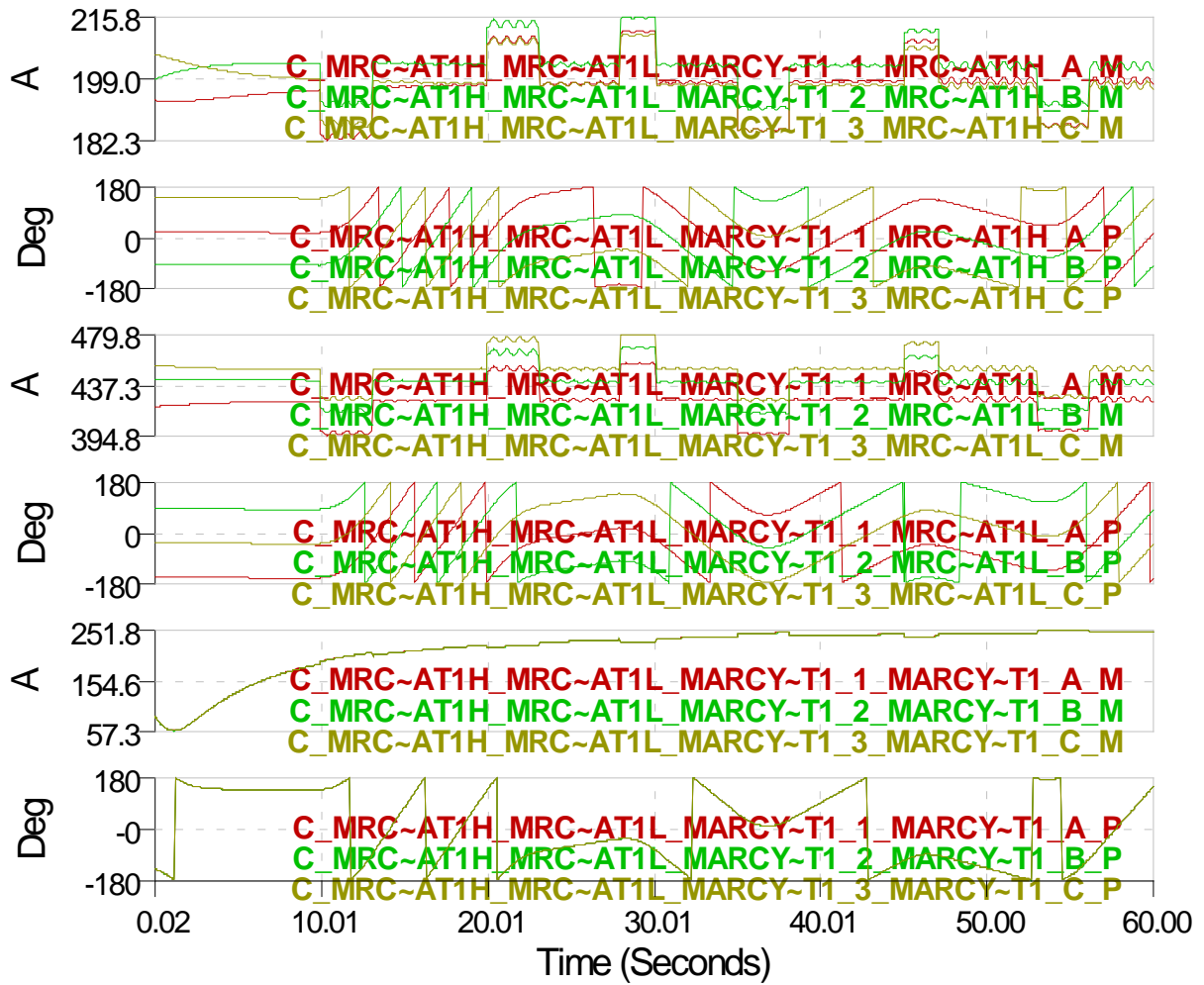


Figure 5.5.3: Three-phase Current Measurements for the Three Single-Phase Autotransformers at Auto Bank 1

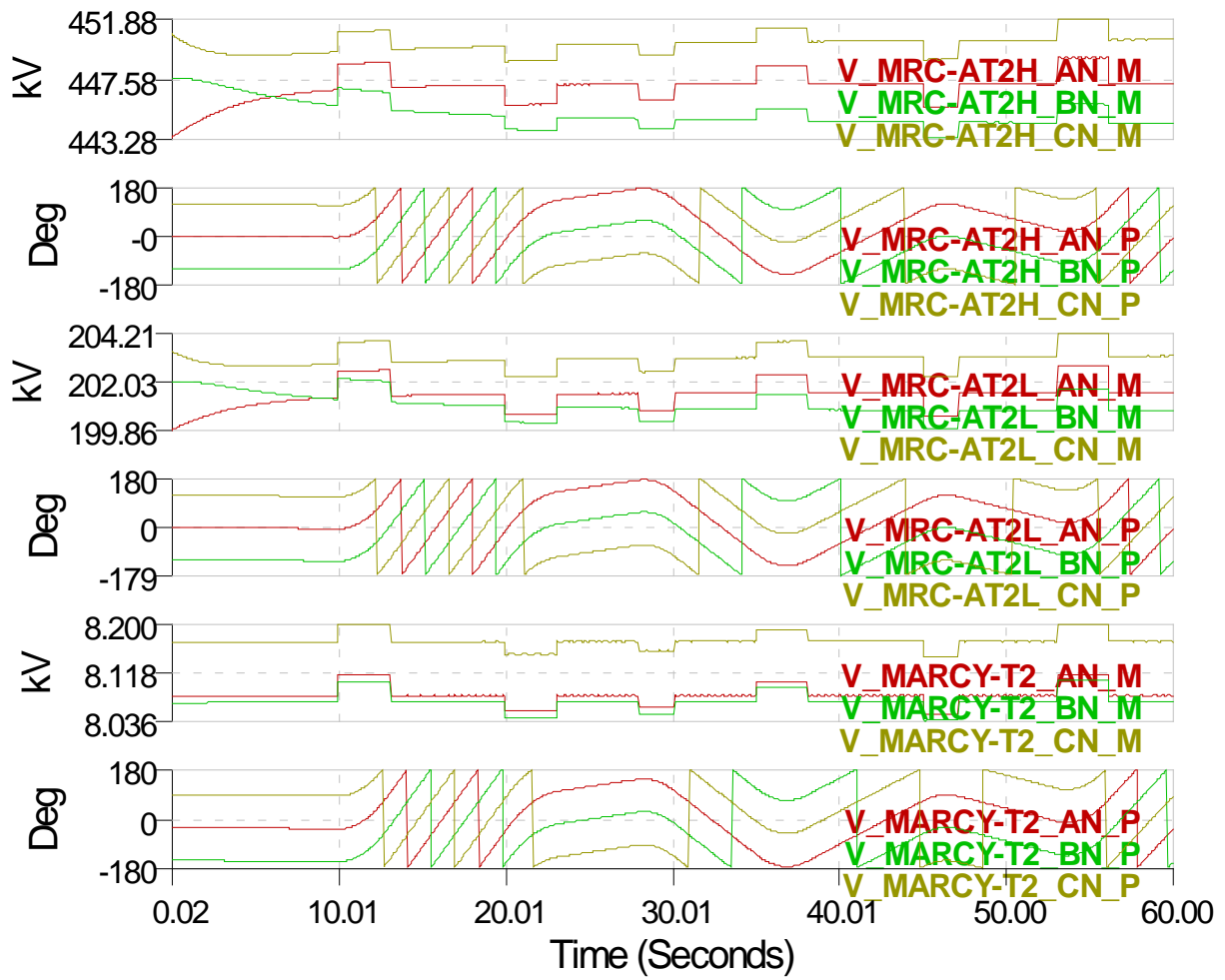


Figure 5.5.4: Three-phase Voltage Measurements at MRC-AT2H, MRC-AT2L, and MARCY-T2

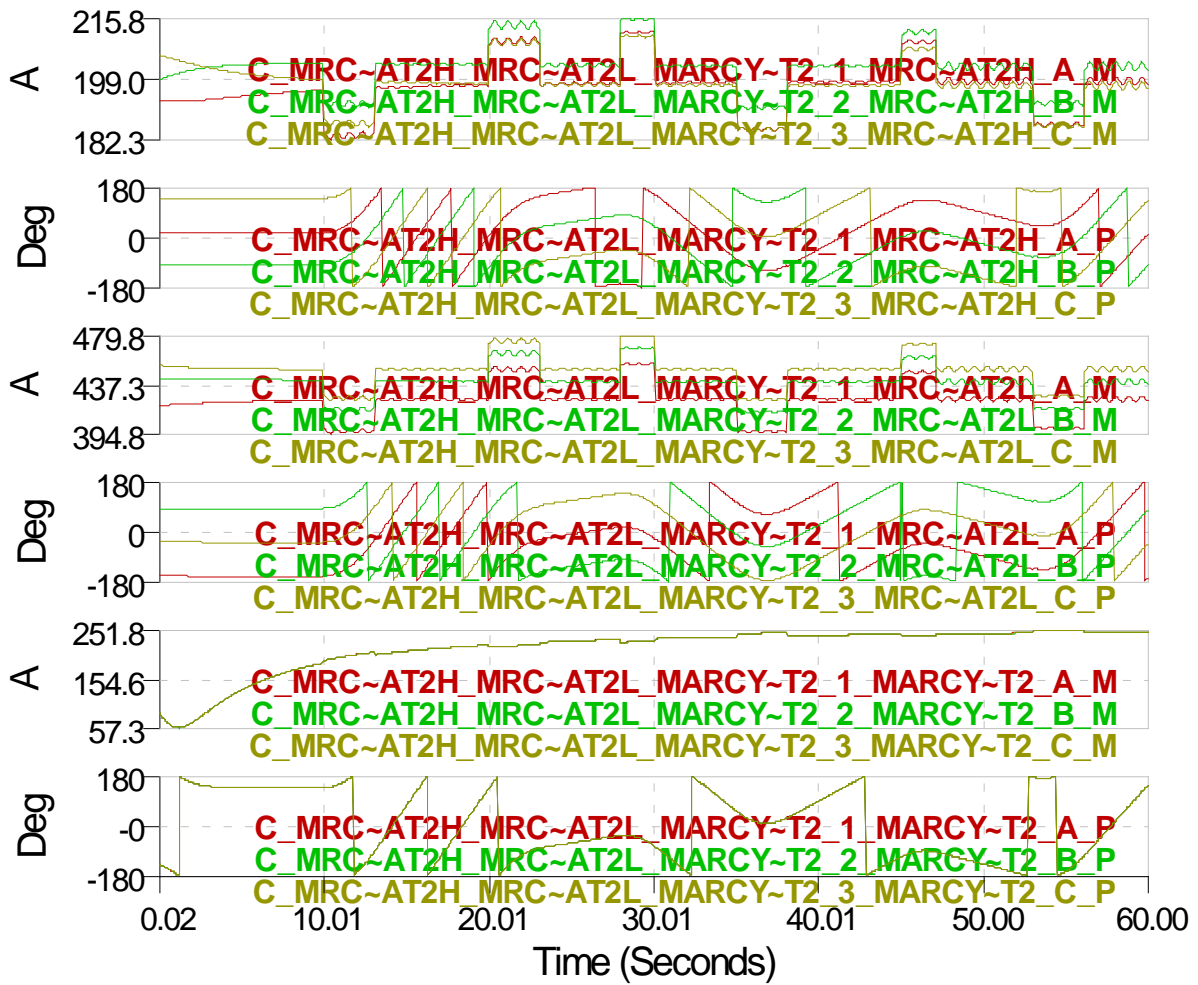


Figure 5.5.5: Three-phase Current Measurements for the Three Single-Phase Autotransformers at Auto Bank 2

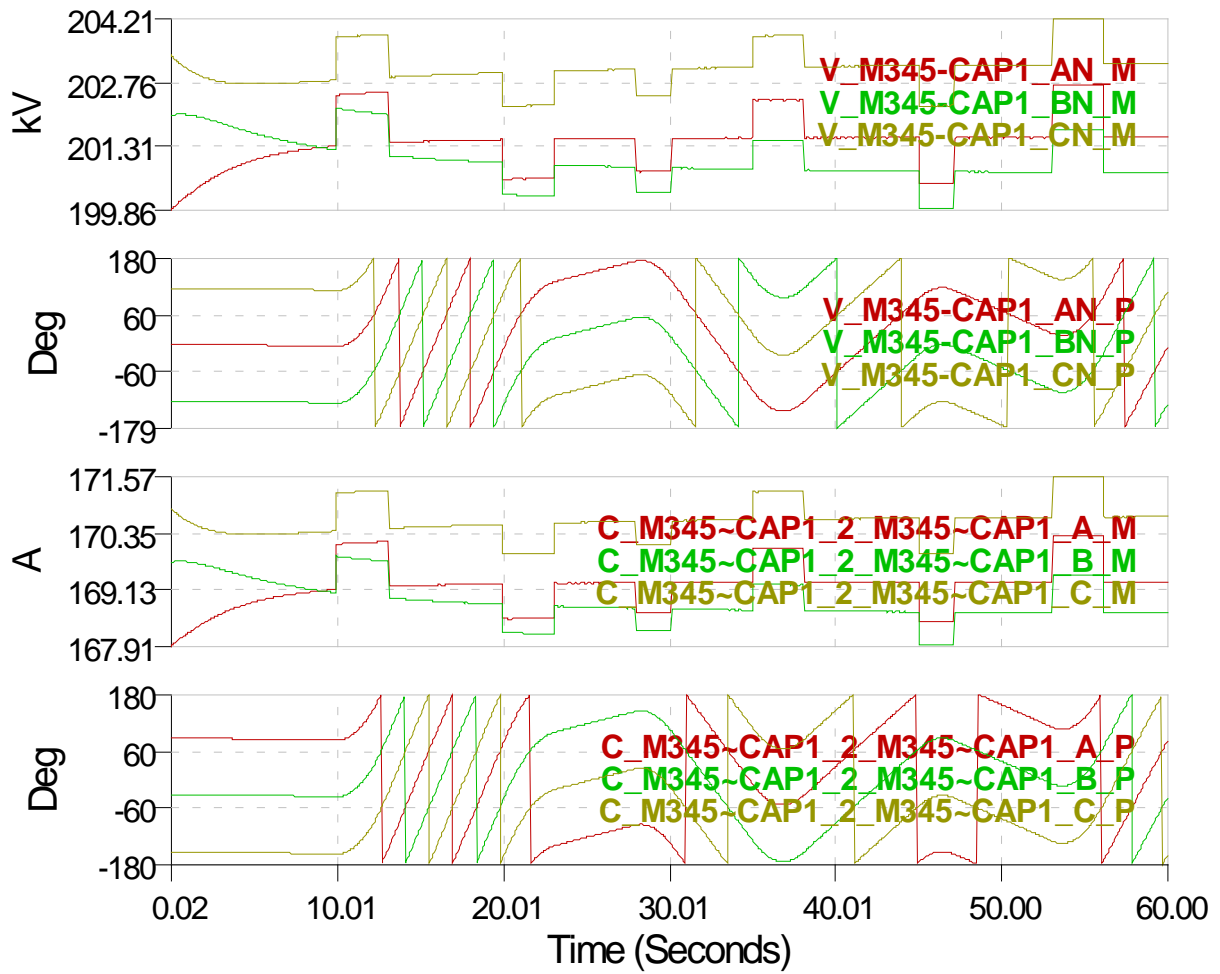


Figure 5.5.6: Three-phase Voltage and Current Measurements for the Capacitor Bank at Bus M345-CAP1

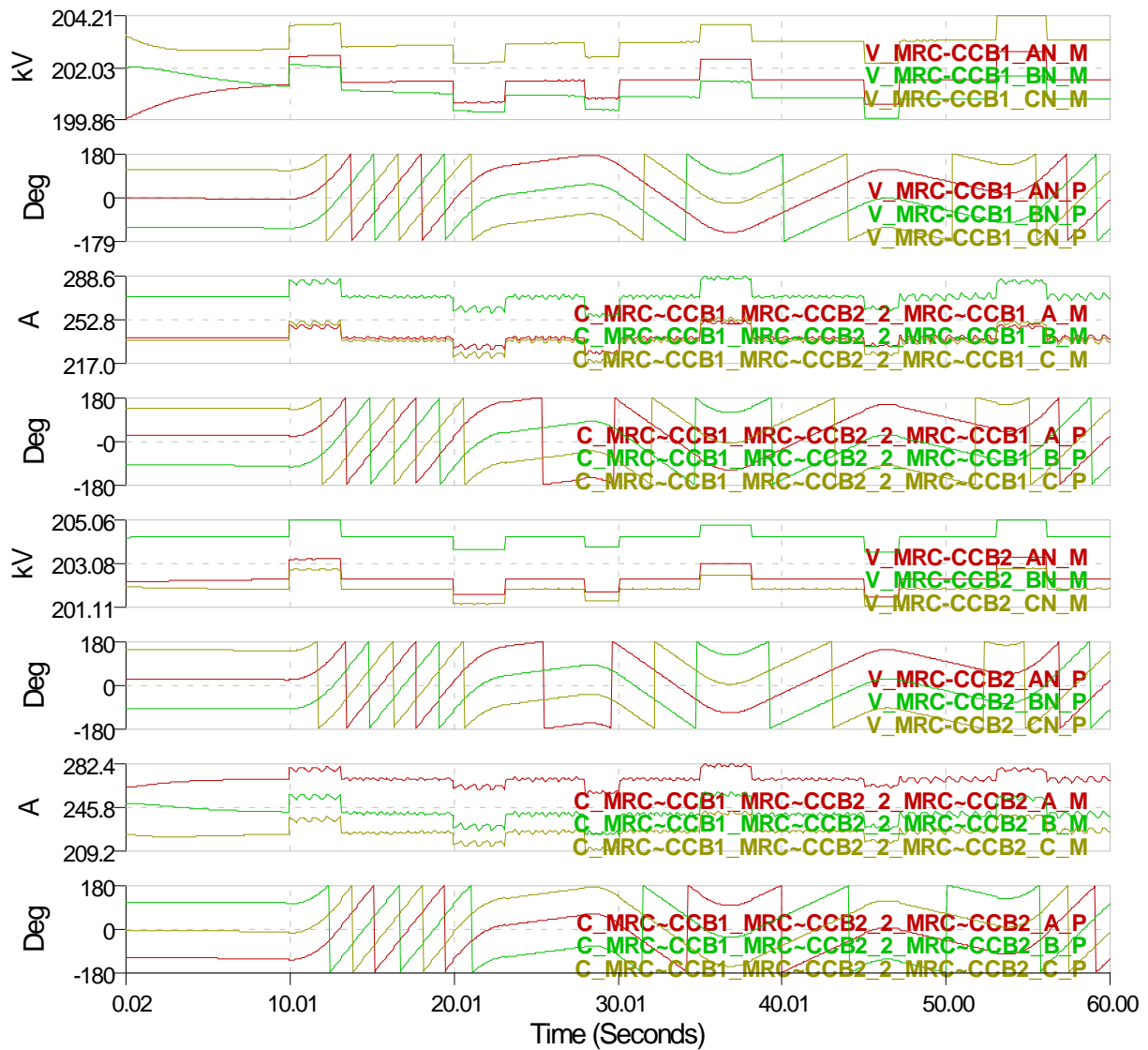



Figure 5.5.7: Three-phase Voltage and Current Measurements for the Transformer from MRC-CCB1 to MRC-CCB2

## 5.5.2 Setup DS-QSE for Marcy Substation

This subsection presents the procedure regarding to setting up the distributed state estimator for the use case. The state estimator has been implemented within the WinIGS-Q program. In order to setup the state estimator, we have to execute the WinIGS-Q program, open the use case, click the meter button , and add the state estimator (M012) into the system. Figure 5.5.8 shows the procedure to add the state estimator icon into the system.

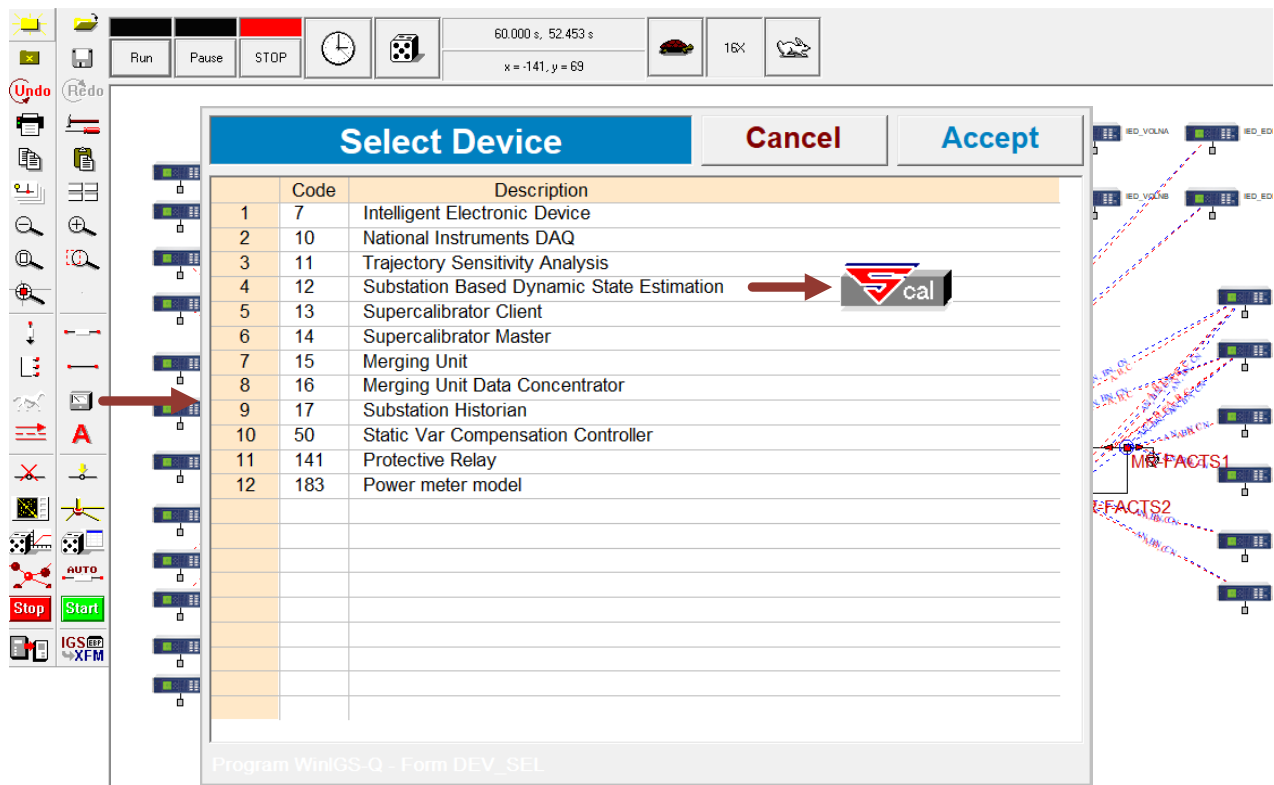


Figure 5.5.8: Add State Estimator Object

The next step is to set up the state estimator. The user interface of the state estimator is shown in Figure 5.5.9. The design of the state estimator supports the connection of the state estimator to a virtual PDC (for field demonstration) or to a phasor data concentrator client (PDC client, for simulation experiments). The PDC client connects to the test data server and receives a C37.118 synchro-phasor data stream. The test data server serves the purpose of numerical experimentation with the quasi-dynamic state estimation where a C37.118 data stream is created that is served to the PDC client. The user can define the data source to be synchro-phasor format or COMTRADE format that has been saved upon the simulation of the system. Notice that in this example, we use the COMTRADE file that is created in Section 5.5.1. The measurement data is streamed to the test data server and then PDC client before the state estimation, and the interface of the test data server and PDC client are shown in Figure 5.5.10 and 5.5.11, respectively.

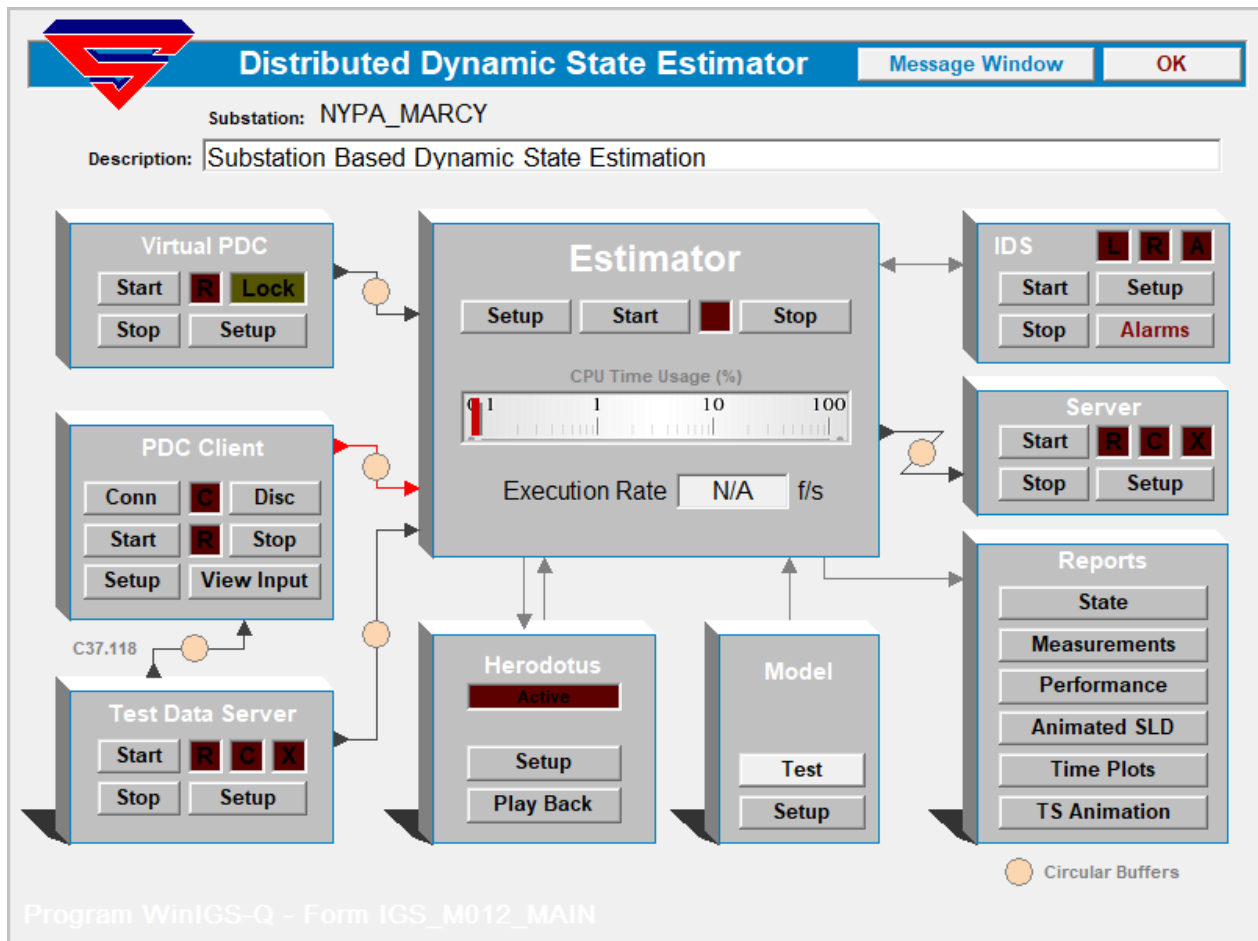


Figure 5.5.9: User Interface of State Estimator

The setup for test data server is as follows. First, we click the “**Setup**” button in the **Test Data Server** section on the lower left corner as shown in Figure 5.5.9. The user interface of the test data server is shown in Figure 5.5.10. Next, the user has to select the data file using the file path button in the middle of the user interface, and also define the data source and data format according to the data file. In this example, since we stream COMTRADE file to the test data server, we select the data source to be **COMTRADE** and data format to be **Phasors (Polar)**. Then we select **Stream (TCP)** in the streaming parameters and click **Play** button. Once all these steps are executed, we can see the streaming phasors on the right lower corner.

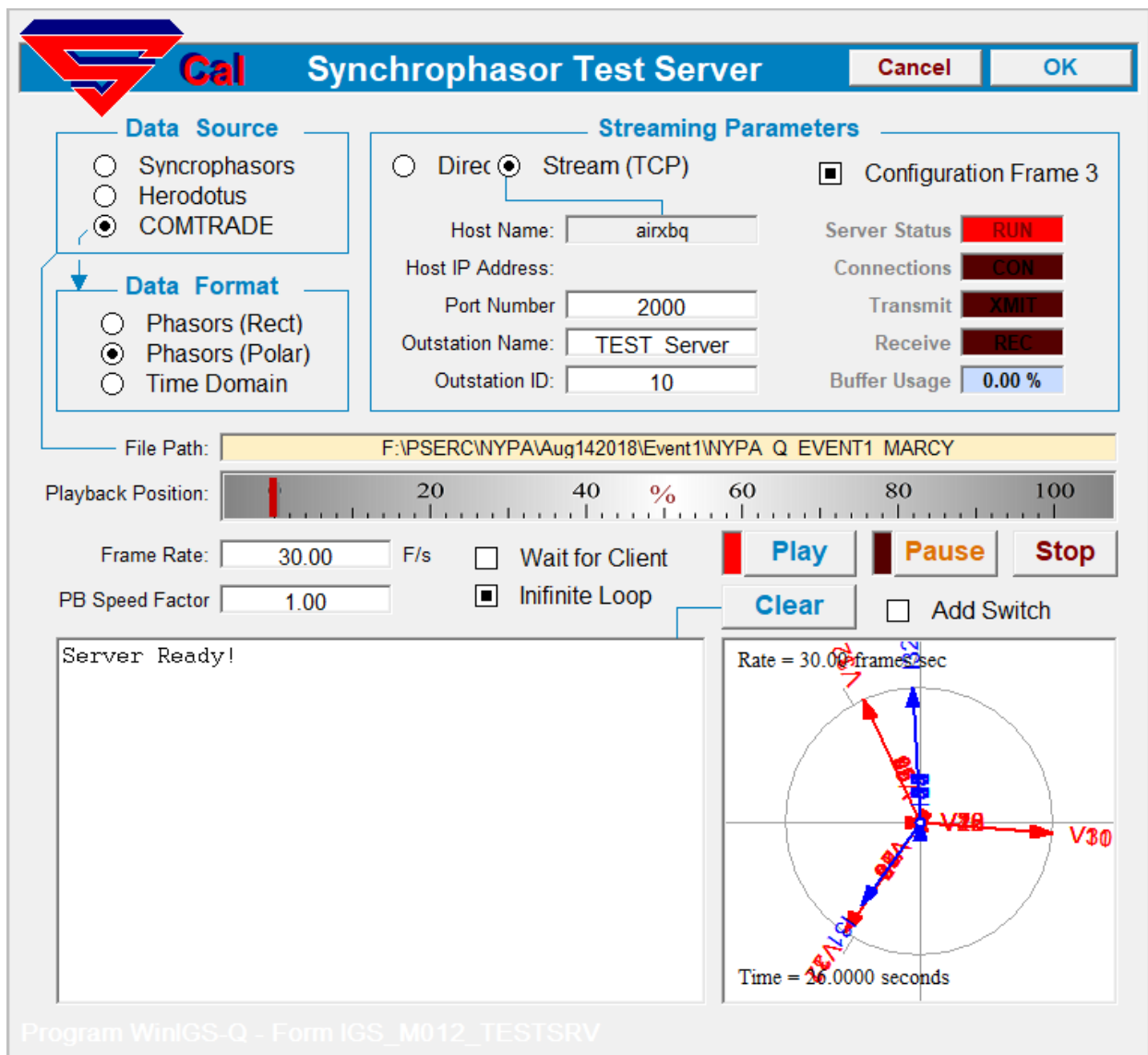


Figure 5.5.10: Test Data Server Interface

The next step is to setup the PDC client as shown in Figure 5.5.11. Notice that for the simulation experiment case as described in this example, the user has to set the **Outstation IP Address** as same as **Local IP Address**. Click **TCP** in protocol section, and then click “**connect**” and “**start**”. And the streaming phasor diagram is shown in the upper right corner. The next step is to map the measurements to the corresponding state estimator measurement channels as shown in Figure 5.5.12. In the measurement mapping dialog, the user has to select the PDC measurement channel to the corresponding state estimator measurement channel one by one. Once all the measurement channels are set up, click “**Verify PDC Mapping**” to verify if all the measurement channels are mapped correctly. If all the measurements are mapped correctly, we will see the dialog as shown in Figure 5.5.13.

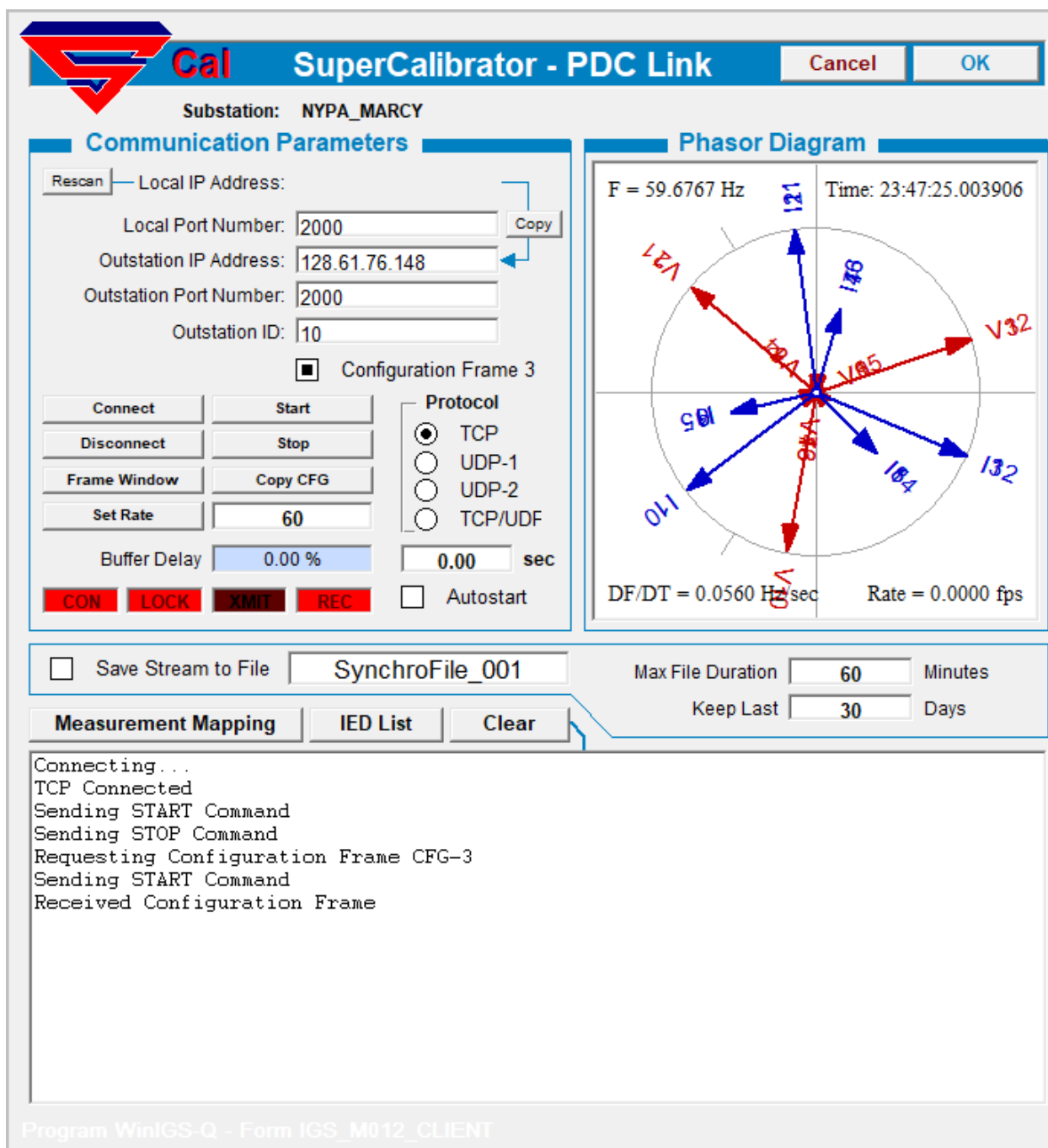



Figure 5.5.11: PDC Client Interface


**SuperCalibrator - PDC Measurement Mapping**
Cancel OK

Substation: Marcy Substation


	IED Name (PDC)	Channel (PDC)	Channel (PDC)	Channel (IED)	Station Name (IED)	IED Index	PDC Index	Channel Match
1	IED_MRC_FACTSA	V_MRC-FACTS_AN	V000		PMU_0	1--1	-1-0	Misr
2		V_MRC-FACTS_BN	V001		PMU_0	1--1	-1-1	Misr
3		V_MRC-FACTS_CN	V002		PMU_0	1--1	-1-2	Misr
4		C_MRC-FACTS_MR-FACTS1_MR-FACTS2_1_MRC-FACTS_A	I003		PMU_0	1--1	-1-3	Misr
5		C_MRC-FACTS_MR-FACTS1_MR-FACTS2_1_MRC-FACTS_B	I004		PMU_0	1--1	-1-4	Misr
6		C_MRC-FACTS_MR-FACTS1_MR-FACTS2_1_MRC-FACTS_C	I005		PMU_0	1--1	-1-5	Misr
7		V_MR-FACTS1_AN	V006		PMU_0	1--1	-1-6	Misr
8		V_MR-FACTS1_BN	V007		PMU_0	1--1	-1-7	Misr
9		V_MR-FACTS1_CN	V008		PMU_0	1--1	-1-8	Misr
10		C_MRC-FACTS_MR-FACTS1_MR-FACTS2_1_MR-FACTS1_A	I009		PMU_0	1--1	-1-9	Misr
11		C_MRC-FACTS_MR-FACTS1_MR-FACTS2_1_MR-FACTS1_B	I010		PMU_0	1--1	-1-10	Misr
12		C_MRC-FACTS_MR-FACTS1_MR-FACTS2_1_MR-FACTS1_C	I011		PMU_0	1--1	-1-11	Misr
13		V_MR-FACTS2_AN	V012		PMU_0	1--1	-1-12	Misr
14		V_MR-FACTS2_BN	V013		PMU_0	1--1	-1-13	Misr
15		V_MR-FACTS2_CN	V014		PMU_0	1--1	-1-14	Misr
16		C_MRC-FACTS_MR-FACTS1_MR-FACTS2_1_MR-FACTS2_A	I015		PMU_0	1--1	-1-15	Misr
17		C_MRC-FACTS_MR-FACTS1_MR-FACTS2_1_MR-FACTS2_B	I016		PMU_0	1--1	-1-16	Misr

Clear
Verify PDC Mapping
Auto-Map
☐ Match IED Names

Double-Click on Table Row to Edit Mapping...

Program WinIGS-Q - Form IGS\_M012\_MEASMAP

Figure 5.5.12: Measurement Mapping


**SuperCalibrator - PDC Measurement Mapping**
Cancel OK

Substation: Marcy Substation

	IED Name (PDC)	Channel (PDC)	Channel (PDC)	Channel (IED)	Station Name (IED)	IED Index	PDC Index	Channel Match
1	IED_MRC_FACTSA	V_MRC-FACTS_AN	V000	V000	PMU_0	1--1	0-0	Yes
2		V_MRC-FACTS_BN	V001	V001	PMU_0	1--1	0-1	Yes
3		V_MRC-FACTS_CN	V002	V002	PMU_0	1--1	0-2	Yes
4		C_MRC-FACTS_MR-FACTS1_MR-FACTS2_1_MRC-FACTS_A	I003	I003	PMU_0	1--1	0-3	Yes
5		C_MRC-FACTS_MR-FACTS1_MR-FACTS2_1_MRC-FACTS_B	I004	I004	PMU_0	1--1	0-4	Yes
6		C_MRC-FACTS_MR-FACTS1_MR-FACTS2_1_MRC-FACTS_C	I005	I005	PMU_0	1--1	0-5	Yes
7		V_MR-FACTS1_AN	V006	V006	PMU_0	1--1	0-6	Yes
8		V_MR-FACTS1_BN	V007	V007	PMU_0	1--1	0-7	Yes
9		V_MR-FACTS1_CN	V008	V008	PMU_0	1--1	0-8	Yes
10		C_MRC-FACTS_MR-FACTS1_MR-FACTS2_1_MR-FACTS1_A	I009	I009	PMU_0	1--1	0-9	Yes
11		C_MRC-FACTS_MR-FACTS1_MR-FACTS2_1_MR-FACTS1_B	I010	I010	PMU_0	1--1	0-10	Yes
12		C_MRC-FACTS_MR-FACTS1_MR-FACTS2_1_MR-FACTS1_C	I011	I011	PMU_0	1--1	0-11	Yes
13		V_MR-FACTS2_AN	V012	V012	PMU_0	1--1	0-12	Yes
14		V_MR-FACTS2_BN	V013	V013	PMU_0	1--1	0-13	Yes
15		V_MR-FACTS2_CN	V014	V014	PMU_0	1--1	0-14	Yes
16		C_MRC-FACTS_MR-FACTS1_MR-FACTS2_1_MR-FACTS2_A	I015	I015	PMU_0	1--1	0-15	Yes
17		C_MRC-FACTS_MR-FACTS1_MR-FACTS2_1_MR-FACTS2_B	I016	I016	PMU_0	1--1	0-16	Yes

Clear
Verify PDC Mapping
Auto-Map
☒ Match IED Names

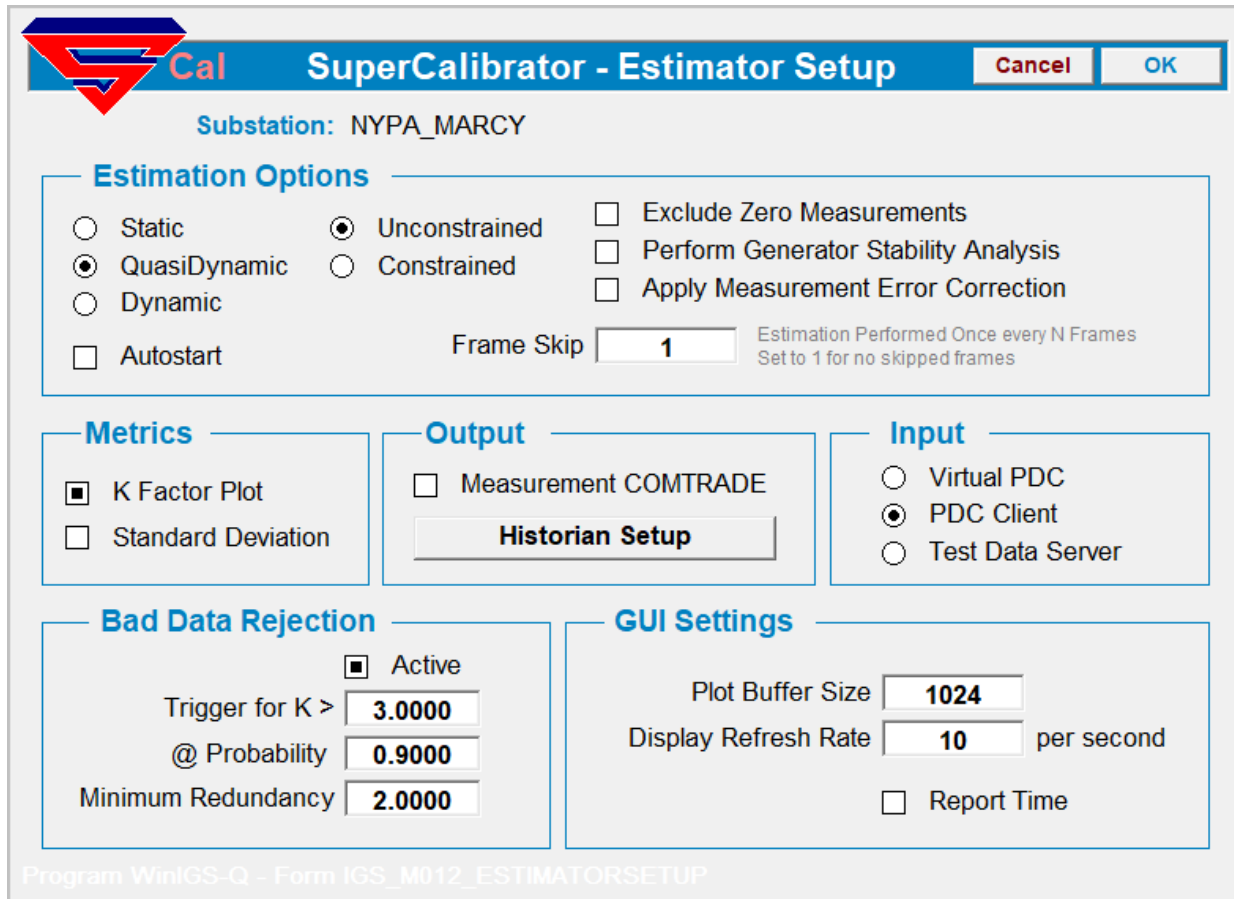
All Measurements matched with PDC Channels

Program WinIGS-Q - Form IGS\_M012\_MEASMAP

Figure 5.5.13: All Measurements Are Matched with PDC Channels

### 5.5.3 Execute DS-QSE and Record Performance

Once the test data server and PDC client are set up, we are ready to run the state estimator. First, click “**Setup**” in the “**Estimator**” section, and we will see a dialog as shown in Figure 5.5.14. Notice that we should select “**QuasiDynamic**” and “**Unconstrained**” in the Estimation Options section and select “**PDC Client**” in the input section. The state estimator after this step is shown in Figure 5.5.15.



The image shows the 'SuperCalibrator - Estimator Setup' dialog box. The title bar includes the 'Cal' logo and buttons for 'Cancel' and 'OK'. The 'Substation' is set to 'NYPA\_MARCY'. The 'Estimation Options' section has radio buttons for 'Static', 'QuasiDynamic' (selected), and 'Dynamic', and checkboxes for 'Unconstrained' (selected), 'Constrained', 'Exclude Zero Measurements', 'Perform Generator Stability Analysis', 'Apply Measurement Error Correction', and 'Autostart'. A 'Frame Skip' field is set to '1' with a note: 'Estimation Performed Once every N Frames Set to 1 for no skipped frames'. The 'Metrics' section has checkboxes for 'K Factor Plot' (checked) and 'Standard Deviation'. The 'Output' section has a checkbox for 'Measurement COMTRADE' and a 'Historian Setup' button. The 'Input' section has radio buttons for 'Virtual PDC', 'PDC Client' (selected), and 'Test Data Server'. The 'Bad Data Rejection' section has a checked 'Active' checkbox and input fields for 'Trigger for K >' (3.0000), '@ Probability' (0.9000), and 'Minimum Redundancy' (2.0000). The 'GUI Settings' section has input fields for 'Plot Buffer Size' (1024) and 'Display Refresh Rate' (10 per second), and a checkbox for 'Report Time'. The footer text is 'Program WinIGS-Q - Form IGS\_M012\_ESTIMATORSETUP'.

**SuperCalibrator - Estimator Setup** [Cancel] [OK]

Substation: NYPA\_MARCY

**Estimation Options**

- ☐ Static
- ☒ QuasiDynamic
- ☐ Dynamic
- ☐ Autostart
- ☒ Unconstrained
- ☐ Constrained
- ☐ Exclude Zero Measurements
- ☐ Perform Generator Stability Analysis
- ☐ Apply Measurement Error Correction

Frame Skip:  Estimation Performed Once every N Frames Set to 1 for no skipped frames

**Metrics**

- ☒ K Factor Plot
- ☐ Standard Deviation

**Output**

- ☐ Measurement COMTRADE
- [Historian Setup]

**Input**

- ☐ Virtual PDC
- ☒ PDC Client
- ☐ Test Data Server

**Bad Data Rejection**

- ☒ Active
- Trigger for K >
- @ Probability
- Minimum Redundancy

**GUI Settings**

- Plot Buffer Size
- Display Refresh Rate  per second
- ☐ Report Time

Program WinIGS-Q - Form IGS\_M012\_ESTIMATORSETUP

Figure 5.5.14: User Interface of Estimator Setup

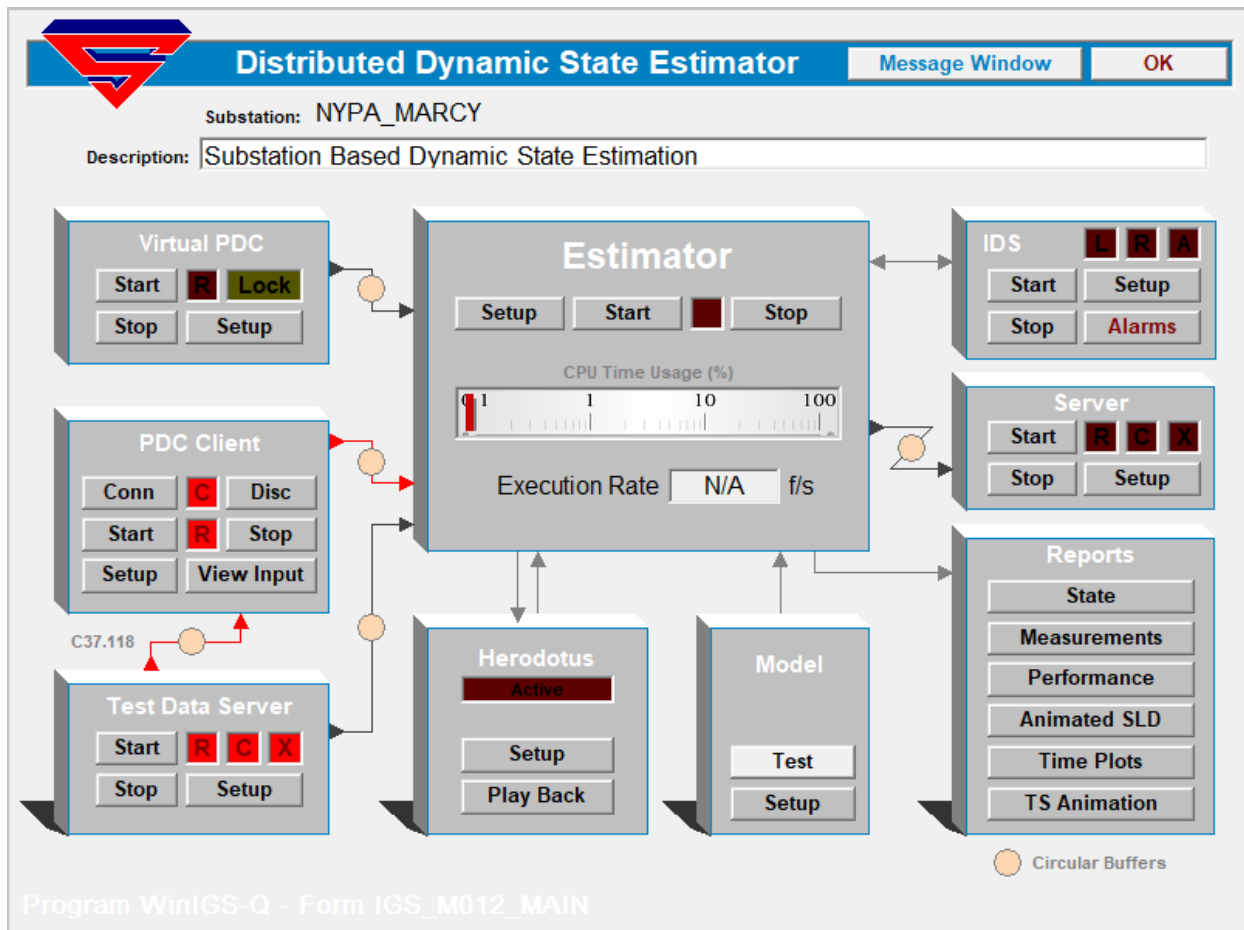


Figure 5.5.15: Ready to Run the State Estimator

Next, click “**Start**” in the “**Estimator**” section, and the estimator starts to perform the state estimation as shown in Figure 5.5.16. The user can view the performance metrics in the **Report** section, where estimated states, measurements, estimated measurements, performance evaluation, and animation are shown. The estimated states of the whole substation can be viewed by clicking the **States** button in the **Report** section as shown in Figure 5.5.17, where all the states of buses as well as the internal states of devices are shown. Notice that the name of an internal state starts from the device code and ends with the number of this internal state in the device.

The measurements and estimated measurements of Marcy Substation can be viewed by clicking the **Measurements** button in the **Report** as shown in Figure 5.5.18, where the user can select the table and diagram to show different measurement types (e.g., field measurement from IEDs, derived measurement, etc.). The user can also let the table and diagram show only the voltage/current measurements by clicking voltage/current option in Figure 5.5.18. Notice that if the user clicks “**S.E.**” option in Figure 5.5.18, a state estimator CSE measurement report is generated as shown in Figure 5.5.19, where all the measurement models (actual, derived, virtual, and pseudo measurements) processed in the state estimator are shown in the table. In this example, we have 774 measurements at time  $t$  and 774 measurements at time  $t_m$ . Since the substation consists of 120 states at time  $t$ , the redundancy is  $(774-120)/120 = 545\%$ . Also notice that all the errors between the measurements and estimated measurements are in very small values, which

substantiates the state estimator running successfully. In addition, the confidence level of this example can be viewed by clicking “**Performance**” button in the Report section shown in Figure 5.5.20. Notice that we use the performance evaluation, which is also called the parameterized (parameter k) chi-square test to validate the model, and it is generated as follows.

All the phasors are divided into real and imaginary parts so that the state estimator is able to manipulate the data in real number. The chi-square test is calculated as:

$$\zeta = \sum_{i=1}^n \left( \frac{r_i}{k\sigma_i} \right)^2,$$

where  $r_i$  is the residual between measurement and estimated measurement i, and  $\sigma_i$  is the standard deviation of the corresponding measurement. Note that the variable k enables to express the results of the chi-square test with only one variable.

And then we compute the confidence level as:

$$\Pr[\chi^2 \geq \zeta] = 1.0 - \Pr(\chi^2, \nu).$$

A confidence level around 100% (small chi-square value) when k=1 infers that the measurements are highly consistent with the dynamic model of the system, i.e., the model is validated, while a confidence level around 0% (large chi-square value) when k=1 means that the measurements do not match the dynamic model of the system. As shown in Figure 5.5.20, the green light is on, and the confidence level is 100% when k=1, which implies the estimation results are trustworthy, i.e., the measurements are consistent with the system model.

In addition, 3D visualizations have been developed. A screenshot of the 3D visualization is shown in Figure 5.5.21. The estimated voltage magnitude for each node is visualized as a tube. The height of the tube is proportional to the voltage magnitude. The estimated voltage phase of a node is visualized as an arc. The angle of the arc is proportional to the voltage phase angle. Surface plots are also available as illustrated in Figure 5.5.21. The voltage estimated measurements are plotted as a contour map to reflect the magnitude of each measurement. The green surface denotes the bus voltages of this substation are around the rated voltage, and the maximum difference between the bus voltage and its rated value is within 0.025 p.u. error.

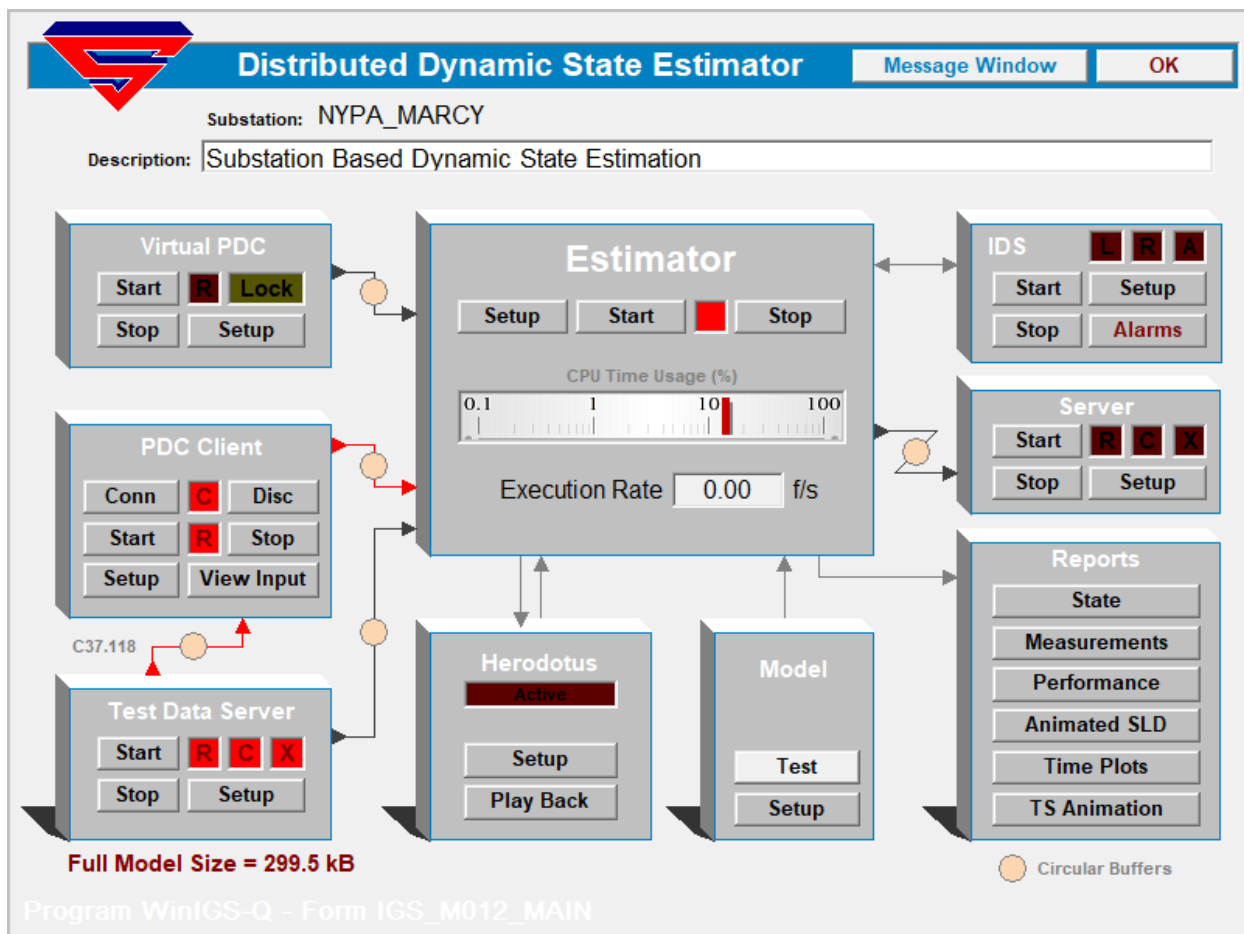


Figure 5.5.16: State Estimator is Running

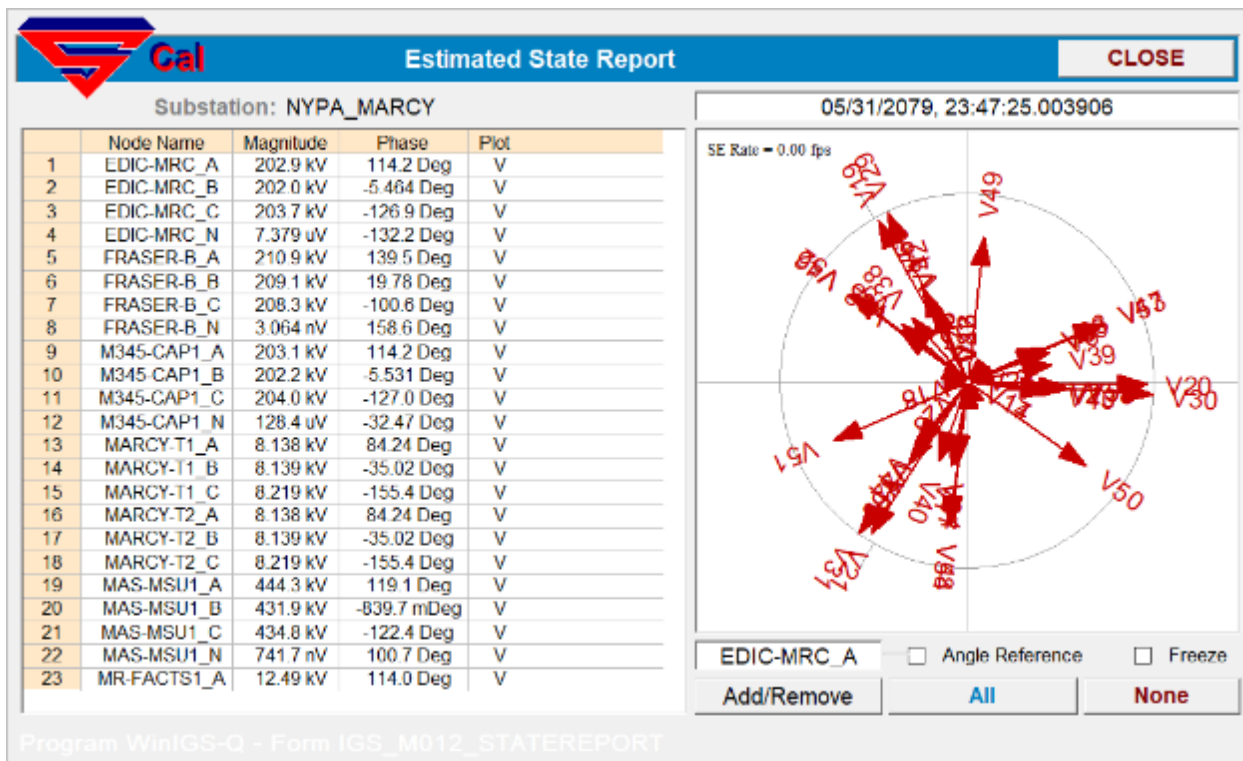


Figure 5.5.17: Estimated State Report

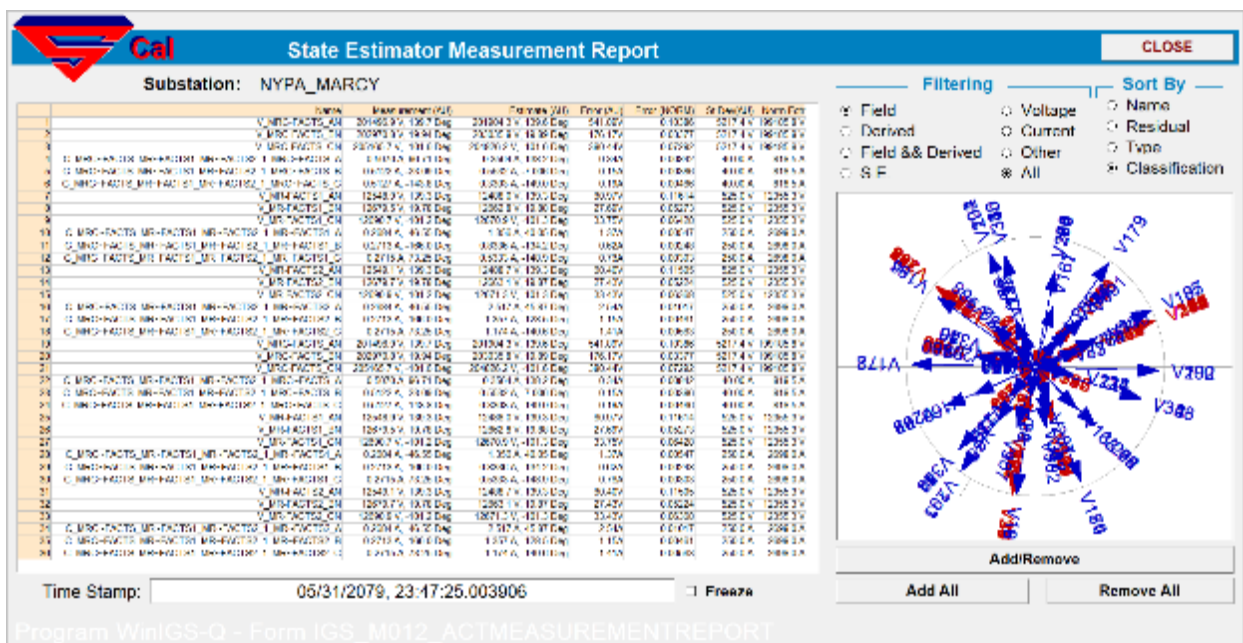


Figure 5.5.18: State Estimator Measurement Report

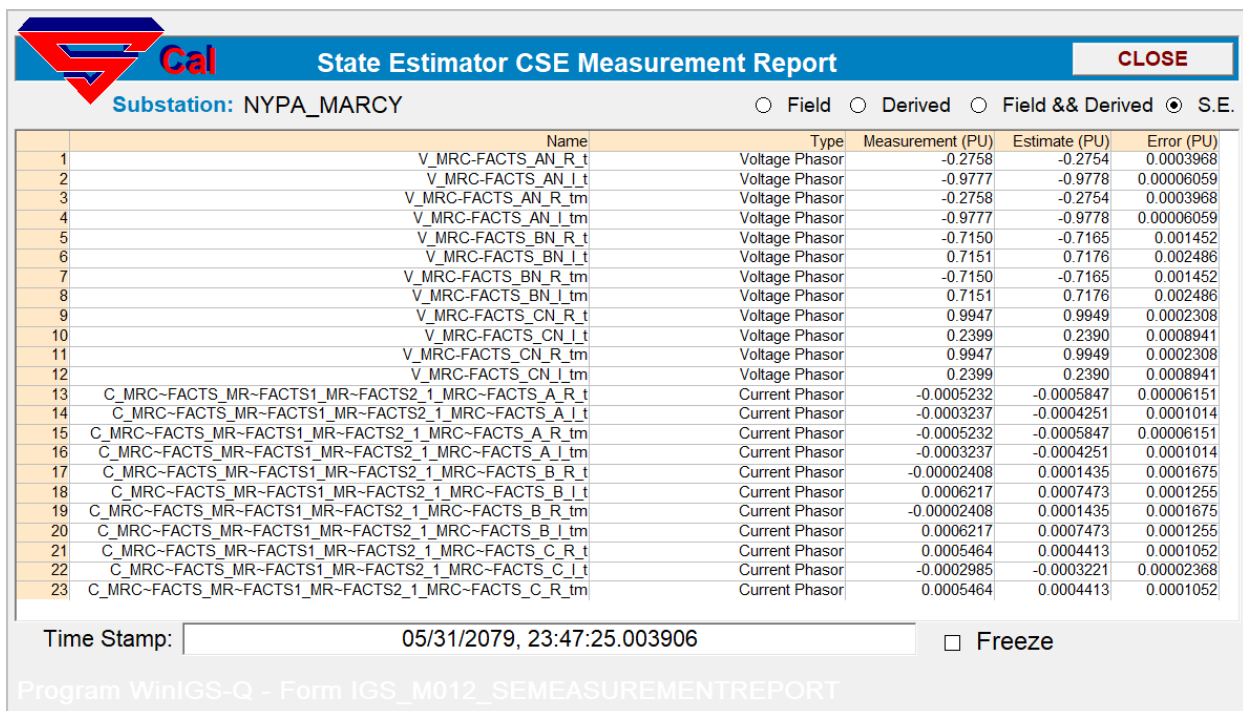


Figure 5.5.19: State Estimator Detailed Measurement Report

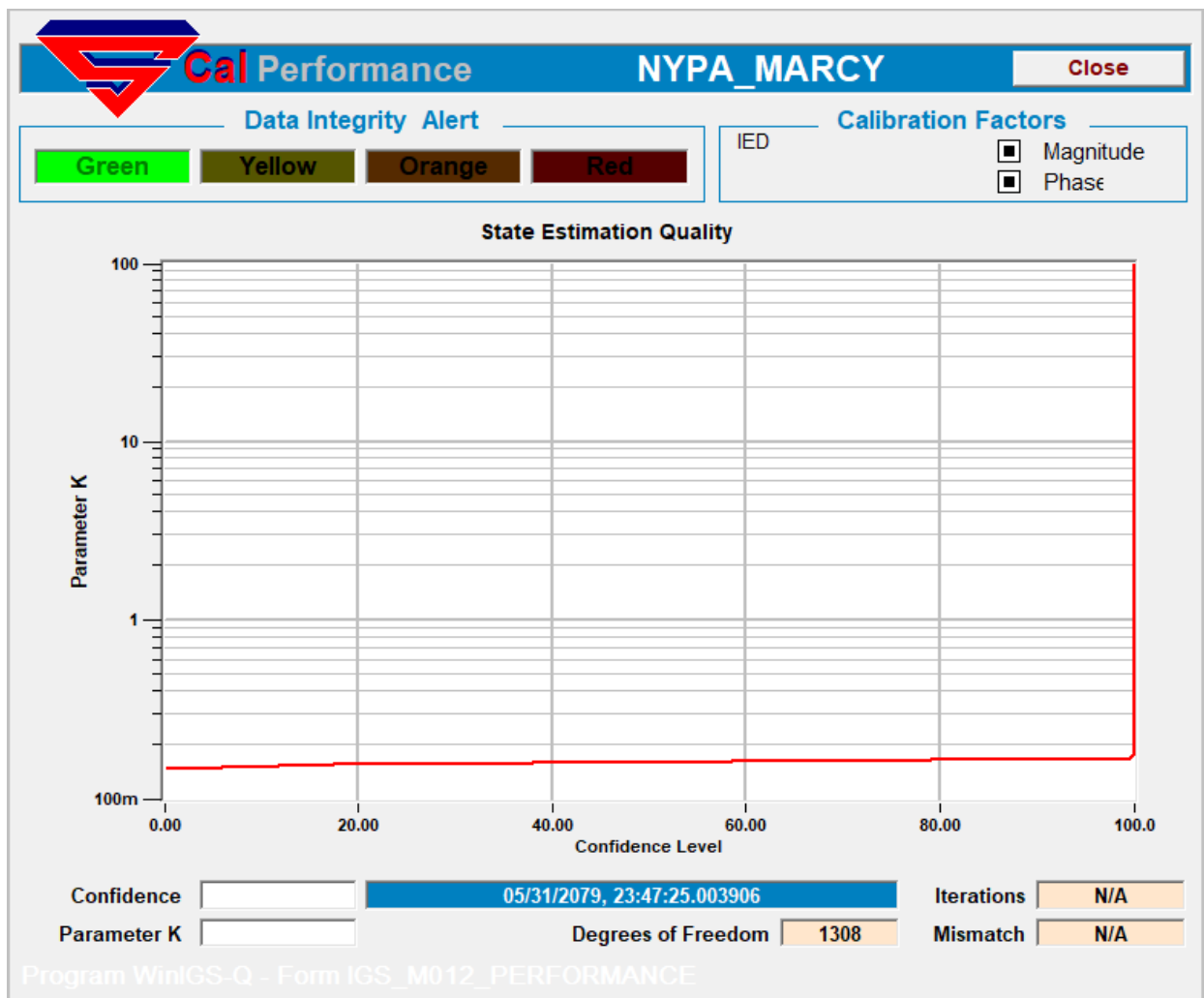


Figure 5.5.20: Performance of the State Estimator

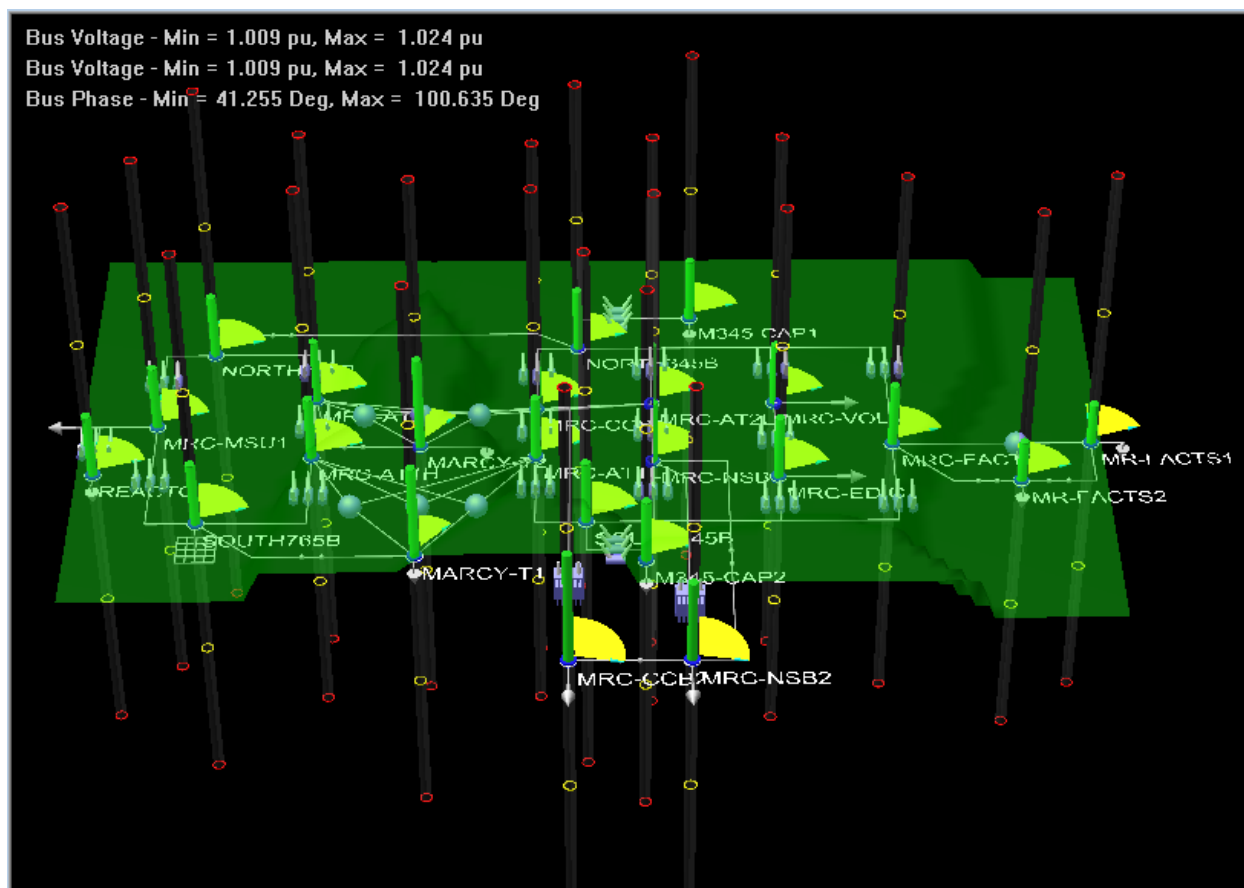


Figure 5.5.21: 3D Visualization Screenshot

## 6. Conclusions

---

Present day PMU and Merging Unit (MU) technologies offer the capability for better, accurate and faster monitoring of the power system. The data generated from these systems are utilized by many applications.

These technologies are complex and many causes can lead to deterioration of the performance of these systems. This project developed methods for the data validation from these systems in real time and in case of data errors and/or missing data it corrects the data and fills in missing data if any. The end result is that the developed technology monitors the entire data acquisition system in a substation and sends validated and corrected data upstream. This has been achieved by methods that characterize PMUs and MUs in the laboratory and (b) constructing a co-model of the physical system of the substation and the PMUs, MUs, relays, etc. in the substation on which the dynamic state estimation is run. The results of the dynamic state estimation are used to determine the accuracy of the data, detect and identify bad data, remove the bad data and replace them with estimated values using the validated substation model.

A field demonstration of the developed methods is planned. Specifically the methods will be demonstrated on the MARCY substation. The required hardware at the substation for this demonstration will be install in Fall 2018 during a planned outage for the substation.

The developed substation based dynamic state estimator operates on dynamic models of the power system and executes once per cycle. The dynamic models of the system are what we refer to as quasi-dynamic models. These models capture the slow dynamics, such as electromechanical oscillations, control response of power electronic converters. They do not capture the fast electrical transients; as a result, electrical quantities are represented with their phasors. This formulation enables the dynamic state estimator to track the slow dynamics of the system with frequency 60 times per second. This is a brand new capability not available before. Tracking the slow dynamics of the power system provides higher accuracy of the operating conditions of the system and opens up new applications. In the next two paragraphs we discuss two important directions for utilization of this technology.

The developed methods and software will be critical components for many applications in the substation and control center. For example, we presently are extending these methods to be part of the protection and control system in the substation by making sure that all relays receive validated data. This application will solve a perennial problem in protection. Specifically, occasionally hidden failures occur in the instrumentation and data acquisition systems resulting in sending erroneous data to the relays and causing relay mis-operations. The data validation methods of this project can identify the hidden failures and correct data thus avoiding relay mis-operations.

Another direction is to use the methods developed in this project to form the basic infrastructure of the next generation management systems. Note that a basic problem at control center operations is the accurate knowledge of the system in real time. The developed methods and software provide the validated data and model of each substation at speeds not possible before, specifically once per cycle. The validated data and validated real time model of each substation can be sent to the control center where the validated real time model of the entire system can be constructed by assembling

the validated substation models of the same instant of time. This task can be achieved once per cycle. Thus the control center can have the validated real time model of the entire system once per cycle and with a delay as short as much time is required to stream the data from each substation to the control center, typically milliseconds. All the applications can now run on a validated real time model. In addition the speed and accuracy opens up a number of new applications such as full state feedback control of many fast responding resources in the power system such as universal power flow controller and other FACTS devices.

## Appendix A. Object Oriented Modeling Standard

---

### A.1 Quasi-dynamic Domain SCAQCF Device Model Description

Each device mathematical model should be also expressed in the generalized State and Control Algebraic Quadratic Companion Form (SCAQCF). The advantage of this SCAQCF device model is that it does not contain differential terms and the highest order is second order so that it is easy for computer to do simulation and computation. This SCAQCF model is derived by applying the quadratic integration method to the differential equation in the previous SCQDM.

The final expression for the Q model SCAQCF device model is:

Model Description: *Type, Code, ID, Title*

$$\begin{Bmatrix} i(t) \\ 0 \\ 0 \\ i(t_m) \\ 0 \\ 0 \end{Bmatrix} = elhs(t) = Y_{eqx} \mathbf{x} + \begin{Bmatrix} \vdots \\ \mathbf{x}^T \langle F_{eqxx}^i \rangle \mathbf{x} \\ \vdots \end{Bmatrix} + Y_{equ} \mathbf{u} + \begin{Bmatrix} \vdots \\ \mathbf{u}^T \langle F_{equu}^i \rangle \mathbf{u} \\ \vdots \end{Bmatrix} + \begin{Bmatrix} \vdots \\ \mathbf{u}^T \langle F_{equx}^i \rangle \mathbf{x} \\ \vdots \end{Bmatrix} - B_{eq}$$

$$B_{eq} = -N_{eqx} \mathbf{x}(t-h) - N_{equ} \mathbf{u}(t-h) - M_{eq} I(t-h) - K_{eq}$$

$$\mathbf{h}(\mathbf{x}, \mathbf{u}) = Y_{feqx} \mathbf{x} + Y_{fequ} \mathbf{u} + \begin{Bmatrix} \vdots \\ \mathbf{x}^T \langle F_{feqx}^i \rangle \mathbf{x} \\ \vdots \end{Bmatrix} + \begin{Bmatrix} \vdots \\ \mathbf{u}^T \langle F_{fequ}^i \rangle \mathbf{u} \\ \vdots \end{Bmatrix} + \begin{Bmatrix} \vdots \\ \mathbf{u}^T \langle F_{fequx}^i \rangle \mathbf{x} \\ \vdots \end{Bmatrix} + C_{feqc}$$

Constraints:  $\mathbf{h}(\mathbf{x}, \mathbf{u}) \leq \mathbf{0}$

$$\mathbf{u}_{min} \leq \mathbf{u} \leq \mathbf{u}_{max}$$

$$|\mathbf{du}| \leq \mathbf{u}_{limit}$$

Model Dimensions:  $n_{equ}, n_{state}, n_{control}, n_{Feqxx}, n_{Fequu}, n_{Fequx}, n_{fconst}, n_{Ffeqxx}, n_{Ffequu}, n_{Ffequx}$

Connectivity:  $nn_i, ivn, inn, onn, S_{st}$

Normalization Factors:  $x_{NF}, e_{NF}, u_{NF}, h_{NF}$

Units:  $xUnit, eUnit, uUnit, hUnit$

The normalization factors, functional constraints and variable limits are the same as the time domain SCQDM.

The SCAQCF coefficients are derived from the SCQDM coefficients as follows:

$$\begin{aligned}
Y_{eqx} &= \begin{bmatrix} \frac{4}{h}D_{eqxd1} + Y_{eqx1} & -\frac{8}{h}D_{eqxd1} \\ \frac{4}{h}D_{eqxd2} + Y_{eqx2} & -\frac{8}{h}D_{eqxd2} \\ Y_{eqx3} & 0 \\ \frac{1}{2h}D_{eqxd1} & \frac{2}{h}D_{eqxd1} + Y_{eqx1} \\ \frac{1}{2h}D_{eqxd2} & \frac{2}{h}D_{eqxd1} + Y_{eqx2} \\ 0 & Y_{eqx3} \end{bmatrix} \\
Y_{equ} &= \begin{bmatrix} Y_{equ1} & 0 \\ Y_{equ2} & 0 \\ Y_{equ3} & 0 \\ 0 & Y_{equ1} \\ 0 & Y_{equ2} \\ 0 & Y_{equ3} \end{bmatrix} \quad F_{eqx} = \begin{bmatrix} 0 & 0 \\ 0 & 0 \\ F_{eqxx3} & 0 \\ 0 & 0 \\ 0 & 0 \\ 0 & F_{eqxx3} \end{bmatrix} \quad F_{equ} = \begin{bmatrix} 0 & 0 \\ 0 & 0 \\ F_{equu3} & 0 \\ 0 & 0 \\ 0 & 0 \\ 0 & F_{equu3} \end{bmatrix} \quad F_{equx} = \begin{bmatrix} 0 & 0 \\ 0 & 0 \\ F_{equx3} & 0 \\ 0 & 0 \\ 0 & 0 \\ 0 & F_{equx3} \end{bmatrix} \\
N_{eqx} &= \begin{bmatrix} -Y_{eqx1} + \frac{4}{h}D_{eqxd1} \\ -Y_{eqx2} + \frac{4}{h}D_{eqxd2} \\ 0 \\ \frac{1}{2}Y_{eqx1} - \frac{5}{2h}D_{eqxd1} \\ \frac{1}{2}Y_{eqx2} - \frac{5}{2h}D_{eqxd2} \\ 0 \end{bmatrix} \quad N_{equ} = \begin{bmatrix} -Y_{equ1} \\ -Y_{equ2} \\ 0 \\ \frac{1}{2}Y_{equ1} \\ \frac{1}{2}Y_{equ2} \\ 0 \end{bmatrix} \quad M_{eq} = \begin{bmatrix} I_{size(i(t))} \\ 0 \\ 0 \\ -\frac{1}{2}I_{size(i(t))} \\ 0 \\ 0 \end{bmatrix} \quad K_{eq} = \begin{bmatrix} 0 \\ 0 \\ C_{eqc3} \\ \frac{3}{2}C_{eqc1} \\ \frac{3}{2}C_{eqc2} \\ C_{eqc3} \end{bmatrix} \\
Y_{feqx} &= \begin{bmatrix} Y_{hfeqx} & 0 \\ 0 & Y_{hfeqx} \end{bmatrix} \quad Y_{fequ} = \begin{bmatrix} Y_{hfequ} & 0 \\ 0 & Y_{hfequ} \end{bmatrix} \quad C_{feqc} = \begin{bmatrix} C_{hfeqc} \\ C_{hfeqc} \end{bmatrix} \\
F_{feqxx} &= \begin{bmatrix} F_{hfeqxx} & 0 \\ 0 & F_{hfeqxx} \end{bmatrix} \quad F_{fequu} = \begin{bmatrix} F_{hfequu} & 0 \\ 0 & F_{hfequu} \end{bmatrix} \quad F_{fequx} = \begin{bmatrix} F_{hfequx} & 0 \\ 0 & F_{hfequx} \end{bmatrix} \\
\mathbf{u}_{min} &= \begin{bmatrix} \mathbf{u}_{hmin} \\ \mathbf{u}_{hmin} \end{bmatrix} \quad \mathbf{u}_{max} = \begin{bmatrix} \mathbf{u}_{hmax} \\ \mathbf{u}_{hmax} \end{bmatrix} \quad \mathbf{u}_{limit} = \begin{bmatrix} \mathbf{u}_{hlimit} \\ \mathbf{u}_{hlimit} \end{bmatrix}
\end{aligned}$$

This quasi-dynamic domain SCAQCF device structure has the following items:

Table A.1: Definitions of Quasi-dynamic Domain SCAQCF Variables in Power Device Class Implementation

Term	Variable Name	Variable Type	Container Type	Description
$Type$	iQDSCAQCFModel_DeviceType	int		Device type (TA, TD, QA, QD, CONNECTOR)
$Code$	iQDSCAQCFModel_ModelCode	int		Model code
$ID$	iQDSCAQCFModel_ModelID	int		Model ID
$Title$	sQDSCAQCFModel_ModelTitle	CString		Model title
$i(t, t_m)$	vQDSCAQCFModel_i	double	vector	Through variable vector
$elhs(t)$	vQDSCAQCFModel_elhs	double	vector	Equation left hand side values
$x(t, t_m)$	vQDSCAQCFModel_x	double	vector	State variable vector
$u(t, t_m)$	vQDSCAQCFModel_u	double	vector	Control variable vector
$Y_{eqx}$	vQDSCAQCFModel_Yeqx	CTriplet	vector	Coefficients of the linear terms associated with state variables
$Y_{equ}$	vQDSCAQCFModel_Yequ	CTriplet	vector	Coefficients of the linear terms associated with control variables
$F_{eqxx}$	vQDSCAQCFModel_Feqxx	CCubelet	vector	Coefficients of the quadratic terms associated with state variables
$F_{equu}$	vQDSCAQCFModel_Fequu	CCubelet	vector	Coefficients of the quadratic terms associated with control variables
$F_{equx}$	vQDSCAQCFModel_Fequx	CCubelet	vector	Coefficients of the quadratic terms associated with the products of state and control variables
$B_{eq}$	vQDSCAQCFModel_Beq	double	vector	Past history vector
$N_{eqx}$	vQDSCAQCFModel_Neqx	CTriplet	vector	Coefficients associated with state variables in past history
$N_{equ}$	vQDSCAQCFModel_Nequ	CTriplet	vector	Coefficients associated with control variables in past history
$M_{eq}$	vQDSCAQCFModel_Meq	CTriplet	vector	Coefficients associated with through variables in past history
$K_{eq}$	vQDSCAQCFModel_Keq	CDoublet	vector	Constant terms
$h(x, u)$	vQDSCAQCFModel_h	double	vector	Functional constraints
$Y_{feqx}$	vQDSCAQCFModel_Yfeqx	CTriplet	vector	Coefficients of the linear terms associated with state variables in functional constraints

$Y_{fequ}$	vQDSCAQCFModel_Y fequ	CTriplet	vector	Coefficients of the linear terms associated with control variables in functional constraints
$F_{feqxx}$	vQDSCAQCFModel_F feqxx	CCubelet	vector	Coefficients of the quadratic terms associated with state variables in functional constraints
$F_{fequu}$	vQDSCAQCFModel_F fequu	CCubelet	vector	Coefficients of the quadratic terms associated with control variables in functional constraints
$F_{fequx}$	vQDSCAQCFModel_F fequx	CCubelet	vector	Coefficients of the quadratic terms associated with the products of state and control variables in functional constraints
$C_{feqc}$	vQDSCAQCFModel_C feqc	CDoublet	vector	Constant terms in functional constraints
$u_{min}$	vQDSCAQCFModel_u min	double	vector	Lower bounds of control variables
$u_{max}$	vQDSCAQCFModel_u max	double	vector	Upper bounds of control variables
$u_{limit}$	vQDSCAQCFModel_u LnzLimit	double	vector	Maximum permissible control variable excursions to maintain linearization error below a threshold
$n_{equ}$	nQDSCAQCFModel_E qu	int		Number of equations
$n_{state}$	nQDSCAQCFModel_S tate	int		Number of state variables
$n_{control}$	nQDSCAQCFModel_ Control	int		Number of control variables
$n_{Feqxx}$	nQDSCAQCFModel_F eqxx	int		Number of Feqxx terms
$n_{Fequu}$	nQDSCAQCFModel_F equu	int		Number of Fequu terms
$n_{Fequx}$	nQDSCAQCFModel_F equx	int		Number of Fequx terms
$n_{fconst}$	nQDSCAQCFModel_F constraint	int		Number of functional constraints
$n_{Ffeqxx}$	nQDSCAQCFModel_F feqxx	int		Number of Ffeqxx terms in functional constraints
$n_{Ffequu}$	nQDSCAQCFModel_F fequu	int		Number of Ffequu terms in functional constraints
$n_{Ffequx}$	nQDSCAQCFModel_F fequx	int		Number of Ffequx terms in functional constraints
$nn_t$	vQDSCAQCFModel_N odeName	CString	vector	Terminal node names
$ivn$	vQDSCAQCFModel_I nternalVarNam	CString	vector	Internal state variable names

$inn$	vQDSCAQCFModel_I nternalNodeNumber	int	vector	Internal node numbers
$onn$	vQDSCAQCFModel_ OptimalNodeNumber	int	vector	Optimal numbers of all device states with external states placed first
$S_{st}$	vQDSCAQCFModel_S witchStatus	int	vector	Switch status for each terminal pair (used in connector devices)
$x_{NF}$	vQDSCAQCFModel_S tateNormFactor	double	vector	Normalization factors for state variables
$e_{NF}$	vQDSCAQCFModel_E quationNormFactor	double	vector	Normalization factors for equations
$u_{NF}$	vQDSCAQCFModel_C ontrolNormFactor	double	vector	Normalization factors for control variables
$h_{NF}$	vQDSCAQCFModel_C onstraintNormFactor	double	vector	Normalization factors for functional constraints
$xUnit$	vQDSCAQCFModel_x Unit	CString	vector	Units (metric) of state variables
$eUnit$	vQDSCAQCFModel_e Unit	CString	vector	Units (metric) of equations
$uUnit$	vQDSCAQCFModel_u Unit	CString	vector	Units (metric) of control variables
$hUnit$	vQDSCAQCFModel_h Unit	CString	vector	Units (metric) of functional constraints

## A.2 Quasi-dynamic Domain SCAQCF Measurement Model Description

The quasi-dynamic domain SCAQCF measurement model is the matrix expression for each measurement in SCAQCF. The primary data that define a measurement are pointers and the measurement error. This model is also created by the program automatically.

The quasi-dynamic domain SCAQCF measurement model comes from two parts: 1) quasi-dynamic domain SCAQCF device model; 2) quadratic integration of quasi-dynamic domain SCQDM.

If the measurement equation is derived from quasi-dynamic domain SCAQCF device model, it just pulls equation from the quasi-dynamic domain SCAQCF device model.

If the measurement equation comes from the quasi-dynamic domain SCQDM, the quadratic integration algorithm should be applied to this equation. The procedure is the same as deriving the quasi-dynamic domain SCAQCF device model from quasi-dynamic domain SCQDM.

The above two steps are processed for each measurement. Then all the equations are stacked into the following standard quasi-dynamic domain SCAQCF measurement model:

$$\tilde{\mathbf{z}} = Y_{qm,x} \tilde{\mathbf{x}} + \left\{ \begin{matrix} \vdots \\ \tilde{\mathbf{x}}^T F_{qm,x}^i \tilde{\mathbf{x}} \\ \vdots \end{matrix} \right\} + Y_{qm,u} \tilde{\mathbf{u}} + \left\{ \begin{matrix} \vdots \\ \tilde{\mathbf{u}}^T F_{qm,u}^i \tilde{\mathbf{u}} \\ \vdots \end{matrix} \right\} + \left\{ \begin{matrix} \vdots \\ \tilde{\mathbf{u}}^T F_{qm,ux}^i \tilde{\mathbf{x}} \\ \vdots \end{matrix} \right\} + C_{qm}$$

$$C_{qm} = N_{qm,x} \tilde{\mathbf{x}}(t-h) + N_{qm,u} \tilde{\mathbf{u}}(t-h) + M_{qm} \tilde{\mathbf{I}}(t-h) + K_{qm}$$

Measurement noise error: dMeterScale, dMeterSigmaPU

Note: All the above variables are in metric system.

where:

$\tilde{\mathbf{z}}$  : measurement variables at both time  $t$  and time  $t_m$ ,  $\tilde{\mathbf{z}} = [\tilde{\mathbf{z}}(t), \tilde{\mathbf{z}}(t_m)]$

$\tilde{\mathbf{x}}$  : external and internal state variables of the measurement model,  $\tilde{\mathbf{x}} = [\tilde{\mathbf{x}}(t), \tilde{\mathbf{x}}(t_m)]$

$\tilde{\mathbf{u}}$  : control variables of the measurement model, i.e. transformer tap, etc.  $\tilde{\mathbf{u}} = [\tilde{\mathbf{u}}(t), \tilde{\mathbf{u}}(t_m)]$

$Y_{qm,x}$  : matrix defining the linear part for state variables,

$F_{qm,x}$  : matrices defining the quadratic part for state variables,

$Y_{qm,u}$  : matrix defining the linear part for control variables,

$F_{qm,u}$  : matrices defining the quadratic part for control variables,

$F_{qm,ux}$  : matrices defining the quadratic part for the product of state and control variables,

$C_{qm}$  : history dependent vector of the measurement model,

$N_{qm,x}$  : matrix defining the last integration step state variables part,

$N_{qm,u}$  : matrix defining the last integration step control variables part,

$M_{qm}$  : matrix defining the last integration step through variables part,  
 $K_{qm}$  : constant vector of the measurement model,  
 $dMeterScale$  : the scale that meters use (in metric units),  
 $dMeterSigmaPU$  : the standard deviation for the measurements (in per. unit),

### **Quasi-dynamic Domain SCAQCF Measurement Model Structure**

This quasi-dynamic domain SCAQCF measurement model structure has the following items:

**int**            **m\_iMeasDeviceID;**  
 Device ID from which the measurement is measured

**BOOL**        **m\_bMeasLinearity;**  
 Linearity of each measurement: 0(False) Nonlinear, 1(True) Linear

**int**            **m\_iMeasType;**  
 Measurement type: 0 Actual, 1 Derived, 2 Pseudo, 3 Virtual

**int**            **m\_iMeasQuantity;**  
 Measurement quantity: 14 Torque, 15 Speed, 16 Voltage, 17 Current

**double**       **m\_dMeasMeterSigmaPU;**  
 Standard deviation for the measurements (in per. unit system)

**double**       **m\_dMeasMeterScale;**  
 Meter scales (in metric unit system)

**CString**      **m\_sMeasName;**  
 Name for the measurement

**CString**      **m\_sMeasUnit;**  
 Unit for the measurement

**double**       **m\_dMeasRatio;**  
 Ratio for the derived measurement

**vector<int>**   **m\_viMeasTerminals;**  
 Terminal numbers where the measurement is measured

**vector<CSting>**   **m\_vsMeasTerminals;**  
 Terminal names where the measurement is measured

**double**       **m\_dQDSCAQCFMeasValue;**  
 Measurement value in metric system

**double**       **m\_dQDSCAQCFMeasValuePU;**  
 Measurement value in PU system

**double**            **m\_dQDSCAQCFMeasScale;**  
                      system consistent scaling factor for measurement in metric system

**double**            **m\_dQDSCAQCFMeasSigmaPU;**  
                      Standard deviation for the measurements (in per. unit system) in the measurement model

**int**                **m\_iQDSCAQCFMeasDefinitionIndex;**  
                      Measurement definition index

**int**                **m\_iQDSCAQCFMeasTime;**  
                      Measurement time: 0: time t, 1: time tm

**BOOL**            **m\_iQDSCAQCFMeasVirtual;**  
                      Virtual measurement false/true

**vector<SP\_LINEAR>**            **m\_vlQDSCAQCFMeasLinTermX;**  
                      Coefficients of the linear state for the q domain SCAQCF measurement model  
                      It stores the entry's corresponding state number and entry value.

**vector< SP\_LINEAR >**            **m\_vlQDSCAQCFMeasLinTermU;**  
                      Coefficients of the linear control for the q domain SCAQCF measurement model  
                      It stores the entry's corresponding control number and entry value.

**double**            **m\_dQDSCAQCFMeasConstantK;**  
                      Constant for the q domain SCAQCF measurement model

**vector<SP\_QUAD>**            **m\_vqQDSCAQCFMeasNonlinTermX;**  
                      Coefficients of the quadratic state variables for the q domain SCAQCF measurement model  
                      It stores the entry's row number, column number and entry value.

**vector<SP\_QUAD>**            **m\_vqQDSCAQCFMeasNonlinTermU;**  
                      Coefficients of the quadratic control variables for the q domain SCAQCF measurement model  
                      It stores the entry's row number, column number and entry.

**vector<SP\_QUAD>**            **m\_vqQDSCAQCFMeasNonlinTermUX;**  
                      Coefficients of the production of state and control variables for the q domain SCAQCF measurement model  
                      It stores the entry's row number, column number and entry value.

**double**            **m\_dQDSCAQCFMeasConstantC;**  
                      Constant containing past history for the q domain SCAQCF measurement model

**vector< SP\_LINEAR >**            **m\_vlQDSCAQCFMeasPastTermX;**  
                      Coefficients of the linear state past history for the q domain SCAQCF measurement model  
                      It stores the entry's corresponding state number and entry value.

**vector< SP\_LINEAR >        m\_vIQDSCAQCFMeasPastTermU;**

Coefficients of the linear control past history at time t for the q domain SCAQCF measurement model

It stores the entry's corresponding control number and entry value.

**vector< SP\_LINEAR >        m\_vIQDSCAQCFMeasPastTermI;**

Coefficients of the through variable past history at time t for the q domain SCAQCF measurement model

It stores the entry's corresponding control number and entry value.

**vector<SP\_LINEAR>                    m\_vIQDSCAQCFMeasLinTermX\_PU;**

Coefficients of the linear state for the q domain SCAQCF measurement model in per unit system

It stores the entry's corresponding state number and entry value.

**vector< SP\_LINEAR >        m\_vIQDSCAQCFMeasLinTermU\_PU;**

Coefficients of the linear control for the q domain SCAQCF measurement model in per unit system

It stores the entry's corresponding control number and entry value.

**double                                m\_dQDSCAQCFMeasConstantK\_PU;**

Constant for the q domain SCAQCF measurement model in per unit system

**vector<SP\_QUAD>                    m\_vqQDSCAQCFMeasNonlinTermX\_PU;**

Coefficients of the quadratic state variables for the q domain SCAQCF measurement model in per unit system

It stores the entry's row number, column number and entry value.

**vector<SP\_QUAD>                    m\_vqQDSCAQCFMeasNonlinTermU\_PU;**

Coefficients of the quadratic control variables for the q domain SCAQCF measurement model in per unit system

It stores the entry's row number, column number and entry.

**vector<SP\_QUAD>                    m\_vqQDSCAQCFMeasNonlinTermUX\_PU;**

Coefficients of the production of state and control variables for the q domain SCAQCF measurement model in per unit system

It stores the entry's row number, column number and entry value.

**double                                m\_dQDSCAQCFMeasConstantC\_PU;**

Constant for the q domain SCAQCF measurement model in per unit system

**vector< SP\_LINEAR >        m\_vIQDSCAQCFMeasPastTermX\_PU;**

Coefficients of the linear state past history for the q domain SCAQCF measurement model in per unit system

It stores the entry's corresponding state number and entry value.

**vector< SP\_LINEAR >      m\_vIQDSCAQCFMeasPastTermU\_PU;**

Coefficients of the linear control past history for the q domain SCAQCF measurement model in per unit system

It stores the entry's corresponding control number and entry value.

**vector< SP\_LINEAR >      m\_vIQDSCAQCFMeasPastTermI\_PU;**

Coefficients of the through variable past history for the q domain SCAQCF measurement model in per unit system

It stores the entry's corresponding control number and entry value.

### A.3 Modeling Example: Single-Phase Transformer Model

This section describes an example for the modeling approach via a single-phase transformer. First the model is provided in compact form. Subsequently its quadratic form is derived.

#### A.3.1 Single-Phase Transformer – Compact Form

Figure A-1 illustrates the physical model of a single-phase variable tap transformer. Three of these models can be used to construct four types of three-phase transformers, with connections of Y-Y, Y-Δ, Δ-Y, and Δ-Δ.

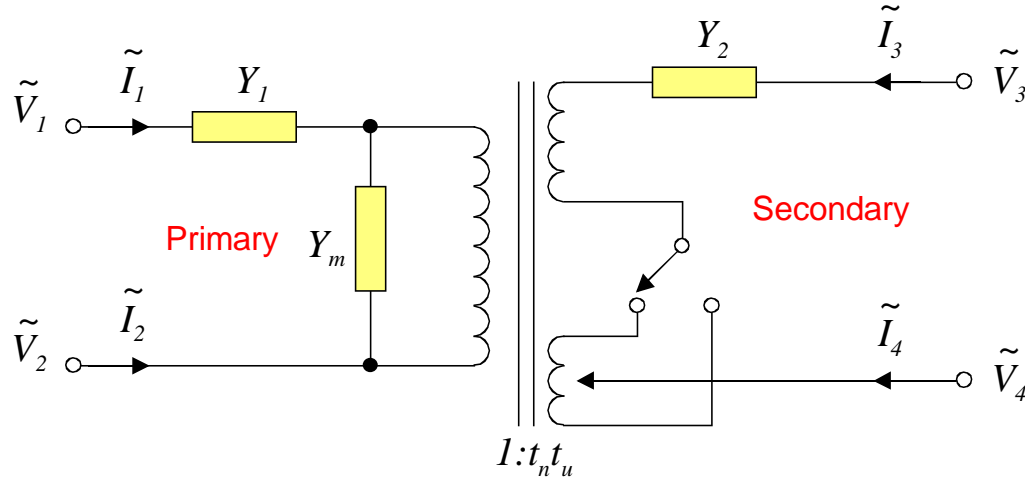


Figure A.1: Single-Phase Variable Tap Transformer

In Figure A-1, the turn ratio  $t$  consists of two parts. One is the nominal transformation ratio  $t_n$  and the other is the per-unit tap selection  $t_u$ . The overall turn ratio is  $t = t_u t_n$ . The primary, secondary, and shunt admittances  $Y_1$ ,  $Y_2$ , and  $Y_m$  of the transformer when  $t_u = 1$  are expressed as

$$Y_1 = 2Y_{pu} Y_{base1}$$

$$Y_2 = 2Y_{pu} Y_{base2}$$

$$Y_m = Y_{pu}^m Y_{base1}$$

where  $Y_{pu}$  is the per-unit series admittance and  $Y_{pu}^m$  is the shunt admittance of the transformer. Note that  $Y_{base1} = t_n^2 Y_{base2}$ . Considering  $t_u$  as a control variable in a more general sense, the single-phase transformer equivalent circuit is illustrated in Figure A-2.

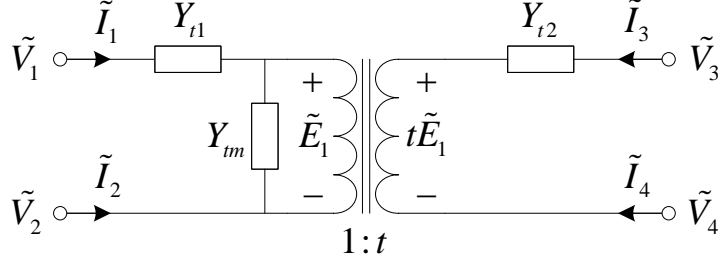


Figure A.2: Single-Phase Transformer Equivalent Circuit

With a variable  $t_u$ , the actual primary, secondary, and shunt admittances  $Y_{t1}$ ,  $Y_{t2}$ , and  $Y_{tm}$  becomes:

$$\begin{aligned} Y_{t1} &= Y_1 \\ Y_{t2} &= \frac{Y_2}{1 + |1 - t_u|} \\ Y_{tm} &= Y_m \end{aligned}$$

Applying Kirchhoff's laws in the circuit of Figure A-2 and substituting  $Y_{t1}$ ,  $Y_{t2}$ ,  $Y_{tm}$  respectively with  $Y_1$ ,  $Y_2$ ,  $Y_m$  according to the above equations, the single-phase transformer equations are:

$$\begin{aligned} \tilde{I}_1 &= Y_1 (\tilde{V}_1 - \tilde{V}_2 - \tilde{E}_1) \\ \tilde{I}_2 &= -\tilde{I}_1 \\ \tilde{I}_3 &= \frac{Y_2}{1 + |1 - t_u|} (\tilde{V}_3 - \tilde{V}_4 - t_n t_u \tilde{E}_1) \\ \tilde{I}_4 &= -\tilde{I}_3 \\ 0 &= -Y_1 (\tilde{V}_1 - \tilde{V}_2 - \tilde{E}_1) - t_n t_u \frac{Y_2}{1 + |1 - t_u|} (\tilde{V}_3 - \tilde{V}_4 - t_n t_u \tilde{E}_1) + Y_m \tilde{E}_1 \end{aligned}$$

### A.3.2 Single-Phase Transformer – Quadratized Form

The single-phase transformer quadratized device model (QDM) separates the real and imaginary parts. During this process, additional states  $w_1$  and  $w_2$  are introduced to eliminate  $1 + |1 - t_u|$  from the denominator. They are defined as

$$y_1 = \frac{1}{1 + |1 - t_u|}$$

$$y_2 = t_u y_1$$

As a result, the following equation holds.

$$y_2^2 - 2 y_1 y_2 = 1 - 2 y_1$$

In order to transform the single-phase transformer model into the standard QDM syntax, the following variables are required to move the quadratic terms out of the through equations.

$$w_1 = y_1 V_{3r} - y_1 V_{4r} - t_n y_2 E_{1r}$$

$$w_2 = y_1 V_{3i} - y_1 V_{4i} - t_n y_2 E_{1i}$$

The transformer quadratized model is given by

$$\begin{aligned} I_{1r} &= Y_{1r} (V_{1r} - V_{2r} - E_{1r}) - Y_{1i} (V_{1i} - V_{2i} - E_{1i}) \\ I_{1i} &= Y_{1r} (V_{1i} - V_{2i} - E_{1i}) + Y_{1i} (V_{1r} - V_{2r} - E_{1r}) \\ I_{2r} &= -Y_{1r} (V_{1r} - V_{2r} - E_{1r}) + Y_{1i} (V_{1i} - V_{2i} - E_{1i}) \\ I_{2i} &= -Y_{1r} (V_{1i} - V_{2i} - E_{1i}) - Y_{1i} (V_{1r} - V_{2r} - E_{1r}) \\ I_{3r} &= Y_{2r} w_1 - Y_{2i} w_2 \\ I_{3i} &= Y_{2r} w_2 + Y_{2i} w_1 \\ I_{4r} &= -Y_{2r} w_1 + Y_{2i} w_2 \\ I_{4i} &= -Y_{2r} w_2 - Y_{2i} w_1 \\ 0 &= -Y_{1r} (V_{1r} - V_{2r} - E_{1r}) + Y_{1i} (V_{1i} - V_{2i} - E_{1i}) + Y_{mr} E_{1r} - Y_{mi} E_{1i} - t_n Y_{2r} t_u w_1 + t_n Y_{2i} t_u w_2 \\ 0 &= -Y_{1r} (V_{1i} - V_{2i} - E_{1i}) - Y_{1i} (V_{1r} - V_{2r} - E_{1r}) + Y_{mr} E_{1i} + Y_{mi} E_{1r} - t_n Y_{2r} t_u w_2 - t_n Y_{2i} t_u w_1 \\ 0 &= y_1 V_{3r} - y_1 V_{4r} - t_n y_2 E_{1r} - w_1 \\ 0 &= y_1 V_{3i} - y_1 V_{4i} - t_n y_2 E_{1i} - w_2 \\ 0 &= 2 y_1 - 2 y_1 y_2 + y_2^2 - 1 \\ 0 &= t_u y_1 - y_2 \end{aligned}$$

where the state vector is:

$$\mathbf{x} = [V_{1r}, V_{1i}, V_{2r}, V_{2i}, V_{3r}, V_{3i}, V_{4r}, V_{4i}, E_{1r}, E_{1i}, w_1, w_2, y_1, y_2]$$

and the control vector is:

$$\mathbf{u} = [t_u]$$

Above equations are cast in the standard SCQDM syntax. The syntax of the SCDQM is:

$$\begin{aligned} \tilde{I}(t) &= Y_{eqx1} \tilde{\mathbf{x}}(t) + Y_{equ1} \tilde{\mathbf{u}}(t) + D_{eqxd1} \frac{d\tilde{\mathbf{x}}(t)}{dt} + C_{eqc1} \\ 0 &= Y_{eqx2} \tilde{\mathbf{x}}(t) + Y_{equ2} \tilde{\mathbf{u}}(t) + D_{eqxd2} \frac{d\tilde{\mathbf{x}}(t)}{dt} + C_{eqc2} \\ 0 &= Y_{eqx3} \tilde{\mathbf{x}}(t) + Y_{equ3} \tilde{\mathbf{u}}(t) + \left\{ \tilde{\mathbf{x}}(t)^T \begin{Bmatrix} \vdots \\ F_{eqxx3}^i \\ \vdots \end{Bmatrix} \tilde{\mathbf{x}}(t) \right\} + \left\{ \tilde{\mathbf{u}}(t)^T \begin{Bmatrix} \vdots \\ F_{equu3}^i \\ \vdots \end{Bmatrix} \tilde{\mathbf{u}}(t) \right\} + \left\{ \tilde{\mathbf{u}}(t)^T \begin{Bmatrix} \vdots \\ F_{equx3}^i \\ \vdots \end{Bmatrix} \tilde{\mathbf{x}}(t) \right\} + C_{eqc3} \\ \mathbf{h}(\tilde{\mathbf{x}}(t), \tilde{\mathbf{u}}(t)) &= Y_{fx} \tilde{\mathbf{x}}(t) + Y_{fu} \tilde{\mathbf{u}}(t) + \left\{ \tilde{\mathbf{x}}(t)^T \begin{Bmatrix} \vdots \\ F_{fx}^i \\ \vdots \end{Bmatrix} \tilde{\mathbf{x}}(t) \right\} + \left\{ \tilde{\mathbf{u}}(t)^T \begin{Bmatrix} \vdots \\ F_{fu}^i \\ \vdots \end{Bmatrix} \tilde{\mathbf{u}}(t) \right\} + \left\{ \tilde{\mathbf{u}}(t)^T \begin{Bmatrix} \vdots \\ F_{fux}^i \\ \vdots \end{Bmatrix} \tilde{\mathbf{x}}(t) \right\} + C_{fc} \end{aligned}$$

Connectivity: *TerminalNodeName*

Normalization Factors: StateNormFactor, ThroughNormFactor, ControlNormFactor

subject to:  $\mathbf{h}_{\min} \leq \mathbf{h}(\mathbf{x}, \mathbf{u}) \leq \mathbf{h}_{\max}$

$$\mathbf{u}_{\min} \leq \mathbf{u} \leq \mathbf{u}_{\max}, \quad \mathbf{x}_{\min} \leq \mathbf{x} \leq \mathbf{x}_{\max}$$

Note: All the above variables are in metric system.

Thus, the single-phase transformer model in the standard SCQDM is:

$$Y_{eqx1} = \begin{bmatrix} Y_{1r} & -Y_{1i} & -Y_{1r} & Y_{1i} & 0 & 0 & 0 & 0 & -Y_{1r} & Y_{1i} & 0 & 0 & 0 & 0 \\ Y_{1i} & Y_{1r} & -Y_{1i} & -Y_{1r} & 0 & 0 & 0 & 0 & -Y_{1i} & -Y_{1r} & 0 & 0 & 0 & 0 \\ -Y_{1r} & Y_{1i} & Y_{1r} & -Y_{1i} & 0 & 0 & 0 & 0 & Y_{1r} & -Y_{1i} & 0 & 0 & 0 & 0 \\ -Y_{1i} & -Y_{1r} & Y_{1i} & Y_{1r} & 0 & 0 & 0 & 0 & Y_{1i} & Y_{1r} & 0 & 0 & 0 & 0 \\ 0 & 0 & 0 & 0 & 0 & 0 & 0 & 0 & 0 & 0 & Y_{2r} & -Y_{2i} & 0 & 0 \\ 0 & 0 & 0 & 0 & 0 & 0 & 0 & 0 & 0 & 0 & Y_{2i} & Y_{2r} & 0 & 0 \\ 0 & 0 & 0 & 0 & 0 & 0 & 0 & 0 & 0 & 0 & -Y_{2r} & Y_{2i} & 0 & 0 \\ 0 & 0 & 0 & 0 & 0 & 0 & 0 & 0 & 0 & 0 & -Y_{2i} & -Y_{2r} & 0 & 0 \end{bmatrix}$$

$$Y_{equ1} = 0$$

$$D_{eqxd1} = 0$$

$$C_{eqc1} = 0$$

$$Y_{eqx2} = 0$$

$$Y_{equ2} = 0$$

$$D_{eqxd2} = 0$$

$$C_{eqc2} = 0$$

$$Y_{eqx3} = \begin{bmatrix} -Y_{lr} & Y_{li} & Y_{lr} & -Y_{li} & 0 & 0 & 0 & 0 & Y_{lr} + Y_{mr} & -Y_{li} - Y_{mi} & 0 & 0 & 0 & 0 \\ -Y_{li} & -Y_{lr} & Y_{li} & Y_{lr} & 0 & 0 & 0 & 0 & Y_{li} + Y_{mi} & Y_{lr} + Y_{mr} & 0 & 0 & 0 & 0 \\ 0 & 0 & 0 & 0 & 0 & 0 & 0 & 0 & 0 & 0 & -1 & 0 & 0 & 0 \\ 0 & 0 & 0 & 0 & 0 & 0 & 0 & 0 & 0 & 0 & 0 & -1 & 0 & 0 \\ 0 & 0 & 0 & 0 & 0 & 0 & 0 & 0 & 0 & 0 & 0 & 0 & 2 & 0 \\ 0 & 0 & 0 & 0 & 0 & 0 & 0 & 0 & 0 & 0 & 0 & 0 & 0 & -1 \end{bmatrix}$$

$$Y_{equ3} = 0$$

$$F_{eqxx3}^0 = \{2, 4, 12, 1\}$$

$$F_{eqxx3}^1 = \{2, 6, 12, -1\}$$

$$F_{eqxx3}^2 = \{2, 8, 13, -t_n\}$$

$$F_{eqxx3}^3 = \{3, 5, 12, 1\}$$

$$F_{eqxx3}^4 = \{3, 7, 12, -1\}$$

$$F_{eqxx3}^5 = \{3, 9, 13, -t_n\}$$

$$F_{eqxx3}^6 = \{4, 12, 13, -2\}$$

$$F_{eqxx3}^7 = \{4, 13, 13, 1\}$$

$$F_{equu3}^i = 0$$

$$F_{equx3}^0 = \{0, 0, 10, -t_n Y_{2r}\}$$

$$F_{equx3}^1 = \{0, 0, 11, t_n Y_{2i}\}$$

$$F_{equx3}^2 = \{1, 0, 10, -t_n Y_{2i}\}$$

$$F_{equx3}^3 = \{1, 0, 11, -t_n Y_{2r}\}$$

$$F_{equx3}^4 = \{5, 0, 12, 1\}$$

$$C_{eqc3} = \begin{bmatrix} 0 \\ 0 \\ 0 \\ 0 \\ -1 \\ 0 \end{bmatrix}$$

$$u_{\min} = [0.9]$$

$$u_{\max} = [1.1]$$

## References

---

- [1] IEEE Standard for Synchrophasor Measurements for Power Systems," IEEE Std C37.118.1-2011 (Revision of IEEE Std C37.118-2005)
- [2] IEEE Guide for Synchronization, Calibration, Testing, and Installation of Phasor Measurement Units (PMUs) for Power System Protection and Control," IEEE C37.242-2013.
- [3] S. Biswas, F. Shariatzadeh, R. Beckstrom, A. Srivastava, AK., "Real time testing and validation of Smart Grid devices and algorithms," IEEE Power and Energy Society General Meeting (PES), pp.1-5, 21-25 July 2013
- [4] S. Biswas, A. Srivastava, J. Park, J. Castaneda, "Tool for testing of phasor measurement units: PMU performance analyzer", IET Generation, Transmission & Distribution, 2014, DOI: 10.1049/iet-gtd.2014.0104
- [5] S. Dutta and T. J. Overbye, "Information Processing and Visualization of Power System Time Varying Data," Proc. 2013 IEEE Symposium Series on Computational Intelligence (SSCI), Singapore, Apr. 16–19, 2013.
- [6] S. Dutta and T.J. Overbye, "Feature Extraction and Visualization of Power System Transient Stability Results," Proc. IEEE Transactions on Power Systems, vol. 29, March 2014, pp. 966-973.

## **Part IV**

### **Prototype Algorithms and Visualization for PMU Data Error Identification and Oscillation Analysis**

Tom Overbye  
Ikponmwosa Idehen (Iyke), Graduate Student

Texas A&M University

**For information about this project, contact:**

Tom Overbye  
Texas A&M University  
Department of Electrical and Computer Engineering  
301 Wisenbaker Engineering Building  
College Station, TX  
77843-3128  
Phone: 979-458-5001  
Email: overbye@tamu.edu

**Power Systems Engineering Research Center**

The Power Systems Engineering Research Center (PSERC) is a multi-university Center conducting research on challenges facing the electric power industry and educating the next generation of power engineers. More information about PSERC can be found at the Center's website: <http://www.pserc.org>.

**For additional information, contact:**

Power Systems Engineering Research Center  
Arizona State University  
527 Engineering Research Center  
Tempe, Arizona 85287-5706  
Phone: 480-965-1643  
Fax: 480-727-2052

**Notice Concerning Copyright Material**

PSERC members are given permission to copy without fee all or part of this publication for internal use if appropriate attribution is given to this document as the source material. This report is available for downloading from the PSERC website.

**© 2018 Texas A&M University. All rights reserve**

## Table of Contents

1. Introduction.....	1
1.1 Background.....	1
1.2 Summary of Chapters .....	2
2. Categorization of Data Error Sources and Mechanisms of Time-Related Issues in Phasor Measurement Units .....	4
2.1 Categorization of PMU Error Sources .....	4
2.2 PMU Error Mechanisms.....	4
2.2.1 Time Errors and Error Propagation Models.....	4
2.2.2 Non-Time Errors .....	6
2.2.3 Updating Derived Measurements (Frequency and ROCOF).....	6
2.3 Synthetic Networks .....	7
2.4 PMU Data Prototypes for Time Errors.....	8
3. Large-Scale System Data Error Analysis for PMU Synchrophasor Data .....	10
3.1 Distributed Application of a Local Outlier Factor Analysis Method .....	10
3.2 Procedures in a Distributed Error Analysis .....	12
3.2.1 Bus Aggregation .....	12
3.2.2 Error Assessment of Bus Measurements .....	14
3.3 Simulation and Results .....	14
4. Presenting Computed Data Error Results of Large-Scale System Through Multidimensional Scaling Visualization .....	20
4.1 Data Error Visualization Using Multidimensional Scaling.....	20
4.2 Generating Data Error, Hybrid Correlation Charts .....	21
4.3 Simulation and Results .....	22
5. Wide-Area Visualization of Large-Scale, Grid Oscillation Results Obtained from the Analysis of Synchrophasor Data.....	26
5.1 Oscillation Monitoring .....	26
5.2 Wide-Area Visualization of Modal Information .....	27
5.2.1 Quality Estimation of Modal Analysis Technique.....	27
5.2.2 Oscillation Modes .....	29
5.3 Visualization of Oscillation Sources .....	31
6. Conclusions .....	34
Appendix A .....	35

Appendix B .....	36
References .....	37

## List of Figures

Fig.1.1. Framework for studying PMU data errors.....	2
Fig. 2.1. A 2,000-bus synthetic network.....	7
Fig.2.2. Prototype voltage angles for GSL and signal spoof .....	8
Fig.2.3. Prototype voltage angles for clock drift and intermittent GPS.....	8
Fig.2.4. Derived ROCOF data for prototyped PMU voltage angles in Fig. (2.2).....	9
Fig.2.5. Derived ROCOF data for prototyped PMU voltage angles in Fig. (2.3).....	9
Fig. 3.1. 3-second voltage measurement.....	11
Fig. 3.2. Wide-area search for data errors.....	12
Fig. 3.3. First eight principal component vectors .....	13
Fig. 3.4. Window technique for assessing error level in data segments .....	14
Fig. 3.5. Voltage magnitude measurements at event bus locations .....	15
Fig. 3.6. Event buses re-distributed to three clusters .....	16
Fig. 3.7. Voltage angle measurements at time-error bus locations .....	17
Fig. 3.8. Data segment errors in all 2,000 voltage magnitude measurements for error case #1 ...	19
Fig. 3.9. Data segment errors in all 2,000 voltage angle measurements for error case #2 .....	19
Fig. 4.1. Bit flag updates for clock drift error .....	23
Fig. 4.2. Bit flag updates for intermittent GPS error .....	23
Fig. 5.1. The cost functions, actual and reproduced frequency signals at 9 locations .....	28
Fig. 5.2. Wide-area system cost function.....	28
Fig. 5.3. (a)Wide-area cost function using voltage measurements; (b) with noise signal at bus 1017.....	29
Fig. 5.4 Phasor vector plot of mode shapes at 20 bus locations .....	30
Fig. 5.5. Frequency mode shape for (a) local, and (b) inter-area modes .....	31
Fig. 5.6. Local oscillation - All branch oscillation energies and dissipating energy ( $DE$ ) coefficients .....	32
Fig. 5.7. Local oscillation - Oscillation source and branch $DE$ flow.....	32
Fig. 5.8. Inter-area oscillation - Oscillation source and branch $DE$ flow .....	33
Fig. 5.9. Inter-area oscillation - All branch oscillation energies and dissipating energy ( $DE$ ) coefficients .....	33
Fig. A-1. (a) 2,000-bus network (b) 10,000-bus network.....	35

## List of Tables

Table 2.1. Categorization of PMU error sources .....	4
Table 3.1. LOF results for all 11 signals.....	11
Table 3.2. LOF results for all 11 signals using two sets of clustering.....	11
Table 3.3. Variance percentage of principal components - $(PC_i PC_i) \times 100\%$ .....	13
Table 3.4. Summary of computed phasor magnitude LOFs (event only).....	15
Table 3.5. Summary of computed phasor magnitude LOFs (event and noise error).....	16
Table 3.6. Cluster formation .....	17
Table 3.7. Simulated time errors .....	17
Table 3.8. Summary of computed phasor angle LOFs (event, noise and time errors) .....	18
Table 3.9. LOF execution time for different system configurations.....	18
Table 4.1. Expression of binary instances .....	21
Table. 4.2. MDS coordinates for PMU bit-13 status flag and phasor angle error .....	24
Table A-1. Network Information .....	35

# 1. Introduction

---

## 1.1 Background

Synchrophasor data are now increasingly used for monitoring the health of power grids. After the 2003 U.S. Northeastern blackout, recommendations for an improved wide-area situational awareness of the grid led to the development and deployment of phasor measurement units (PMUs) and other similar synchrophasor devices equipped to measure power system quantities – synchrophasor data – at rates as high as 120 samples per second in 60 Hz operating systems. Through the aid of a time reference provided by a global positioning system (GPS) signal, high resolution, synchrophasor data are time-synchronized phasor measurements which enable wide-area monitoring and control of the grid by making use of measurements obtained from remote locations. As of September 2017, it was reported that over 2,500 networked PMU devices had been installed on the North American grid [1]. Consequently, large amounts of data can now be generated, thus presenting several opportunities for monitoring personnel to have a higher level of visibility of the system.

Like most measurement devices, a failure in the operational mode of a PMU device introduces potential sources of errors in reported measurements. As a result, the level of data quality - which encompasses the aspects of data accuracy, timeliness and availability - is compromised. The synchrophasor network, comprising of PMU devices, data concentrators, communication links and the phasor applications, is exposed to a variety of errors which ultimately affect any of the reported PMU measurement quantities- voltage (or current) phasor magnitude and angle, frequency and rate of change of frequency (ROCOF). Electrical noise, due to harmonic distortions, wiring of input signals, leakage effect caused by phasor estimation windowing function, was discussed in [2-5]. Time mis-synchronization issues [6-10], caused by clock delays, intermittent reception of global positioning system (GPS) signals, loose cable wiring, spoof attacks, and which lead to phasor angle errors have also been mentioned in the literature. These error types are often attributed to the internal working mechanism of the device; are manifested in the data, and thus result in low quality data reported by the device. References [11, 12] also show that data quality issues result from low latency, low bandwidth, data drop-offs, wrong data alignment and limited capacities of the communication network. These errors are external, and reflect the limitations of the existing PMU network infrastructure. Finally, as observed from an application level, [13] reported on how an increased deployment of endpoint phasor applications can also reduce PMU data quality.

The distinct mode of PMU device operation (such as time synchronization and time stamping [2]), unfortunately, exposes reported data measurements to a new paradigm of time-based errors. For example, the ability to report phasor angle measurements makes the PMU a critical device in monitoring the stress level of the grid (by checking the phase angle differences between system nodes), which could not be done through the use of conventional devices like the remote terminal units (RTUs) and supervisory control and data acquisition (SCADA) devices [14]. However, it is important that PMU devices be accurately synchronized to an external reference, otherwise device time errors, which causes mis-synchronization and angle measurement errors, could cause Engineers to lose sight of the true stress levels on the grid.

These unique measurement errors pose newer data quality issues which must be handled by control center applications, and thus motivates the need to study data anomalies associated with PMU synchrophasor measurements. The report develops a framework used to study PMU data errors – the generation of synthetic errors based on known error mechanisms, utilization of intelligent analytic techniques to analyze data errors, and data visualization via the presentation of data error information in a large-scale system. Fig. 1.1. shows different implementation blocks in the developed framework used to achieving these goals.

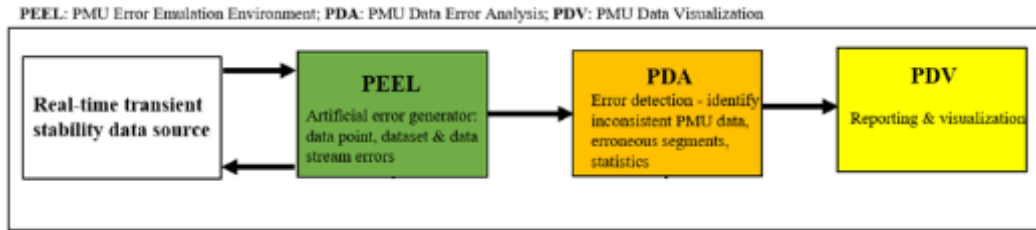


Fig.1.1. Framework for studying PMU data errors

The process of studying mechanisms of PMU data errors involved the study of actual, field synchrophasor data obtained from different utilities, and comparisons drawn with the physical processes associated with these errors as described in the literature. For further research purposes, developed error propagation models were then used to synthesize prototype data errors used in subsequent research activities.

Large amounts of PMU data have enabled online oscillation monitoring and control [15, 16] - a critical task in preserving the safe and secure operation of the power grid. Through visualization, current methods often used to present oscillation information to engineers display oscillation information on a bus node or limited area basis, and do not capture the overall state of the grid. Reference [17] emphasizes the need for engineers to have a comprehensive picture of system states when monitoring grid trends and dynamics. Moreover, as the grid becomes more interconnected and larger in scale, it becomes more imperative for data presentation methods to provide holistic perspectives of the grid to system operators.

## 1.2 Summary of Chapters

This report is structured as follows. In chapter 2, data quality issues due to associated PMU data errors are presented. In particular, the mechanisms of time-related, PMU errors are used to develop error propagation models for the prototyping of synthetic errors.

In chapter 3, an analytic method for the study of data errors in a large-scale system, using a 2,000-bus synthetic network, is developed. Thereafter, effectiveness of the proposed technique is assessed by carrying out different simulation studies on the test, large-scale system.

In chapter 4, error metrics obtained for the large-scale system is presented through the use of MDS visualization – it provides a comparative assessment of error levels in measurements obtained from different buses in the system.

In chapter 5, wide-area visualization methods are used to present system-based, large-scale oscillation mode information which are obtained from the modal analysis and processing of synchrophasor data. Currently, these methods are being implemented in the PowerWorld simulator software [18], and the case studies presented in this chapter demonstrate the application of these wide-area visualization techniques.

Finally, the conclusions are presented in chapter 6.

## 2. Categorization of Data Error Sources and Mechanisms of Time-Related Issues in Phasor Measurement Units

---

In this chapter, different data errors and quality issues associated with PMU and other synchrophasor devices are presented. Error mechanisms and time error propagation models of PMUs, which are used to generate the synthetic data errors used in this work, are then discussed. Finally, the use of synthetic networks for artificially generating data in research studies, followed by the presentation of prototype and actual time errors in data measurements are discussed. These constitute the PMU data error emulation (PEEL) block in the proposed framework of Fig. 1.1.

### 2.1 Categorization of PMU Error Sources

Reference [19] identified groups of PMU data using three levels of attributes: attributes of single data points, dataset and data stream availability. Attributes of single data point are concerned with the accuracy of the individual, time-stamped measurements, while data set attributes relate to the accuracy and logical consistency of a group of data points or an entire set of PMU data. Data set attributes are related to the condition of the underlying communication network through which PMU data are transmitted. Based on these attribute levels, [20] divided PMU error sources into three categories, and shown in Table 2.1.

Table 2.1. Categorization of PMU error sources

Categories	Error Sources
Data point	Accuracy, noise, phase-error, harmonic distortion, estimation algorithms, asynchronous local behaviors (e.g. time-skew), instrument error
Dataset	Status code error, improperly configured PMUs, abnormal or loss of PDC configuration, frequency calculation discrepancies, mislabeling due to erroneous timestamps, CRC error, invalid timestamp
Data stream	Network limitations - Data loss or drop-outs, network latency; increase in endpoint applications

### 2.2 PMU Error Mechanisms

The unique time-synchronization aspect of PMU operation requires a prior knowledge of the operation mechanisms associated with data errors before prototype synthetic errors can be generated. Based on the developed models, the appropriate modifications are effected on bus phasor values (magnitude or/and angle). This is in addition to other no-time based errors (e.g., noise, repeated values and dropped data frames).

#### 2.2.1 Time Errors and Error Propagation Models

A loss of synchronism between a reference coordinated universal time (UTC) signal, obtained via the use of a global positioning system (GPS) receiver, and a PMU device internal sampling clock

causes time-skew errors [6, 21], and have been observed to manifest as phasor angle biases in reported measurements. However, they are observed not to affect the phasor magnitude [21]. Assuming an off-nominal, system frequency of  $f_i$  Hz, the phase angle deviation  $\Delta\delta_\varepsilon$  due to a time error  $\Delta t_\varepsilon$ , is computed as,

$$\Delta\delta_\varepsilon = 360\Delta t_\varepsilon f_i \quad (2.1)$$

where  $f_i = f_o + \Delta\varepsilon$ ,  $f_o$  is the nominal frequency and  $\Delta\varepsilon$  is the deviation from  $f_o$ . The component of  $\Delta\delta_\varepsilon$  due to  $\Delta\varepsilon$  is  $360\Delta t_\varepsilon \Delta\varepsilon$ .  $\Delta t_\varepsilon$  is in the order of microseconds, and in normal operating conditions,  $\Delta\varepsilon \in (0, 0.05)$ . Ignoring  $\Delta\delta_{\Delta\varepsilon}$ , the updated equation becomes,

$$\Delta\delta_\varepsilon = 360\Delta t_\varepsilon f_o \quad (2.2)$$

A corresponding phase angle error due to an observed time difference at each reported sample, however is dependent on the source of timing error. Thus, the instantaneous phase angle error introduced in any reported sample at time,  $t$  from the moment of error initiation is given by a generalized error propagation model,

$$\Delta\delta_\varepsilon(t) = 360\Delta t_\varepsilon(t) f_o \quad (2.3)$$

$\Delta t_\varepsilon(t)$  is the instantaneous, accumulated time drift (or time-skew) at time  $t$ .

PMUs report equal time-interval samples of data measurements in cycles, such that the number of data samples reported at any cycle is known as the report rate. The accumulated time drift at any sample point is dependent on the source of error.

#### 1. Clock drift

Here, the internal clock of a PMU is observed to gradually drift away in time due to a delay, which then causes an uneven, accumulating time-interval between samples within a report cycle. A periodic, re-synchronization attempt with a GPS pulse per second (PPS) signal only resets the synchronization status of the first data sample in the next report cycle before the clock drift begins all over again. The error propagation model for this time error behavior is given as,

$$\Delta t_{\varepsilon,i}(t) = (i - 1)\Delta t_\varepsilon, i = 1, 2 \dots n \quad (2.4)$$

where  $n$  is the reporting rate of the PMU.

#### 2. Intermittent GPS Signal

Due to issues, such as loose wiring or incorrect placement of PMU GPS receiver, the device loses connection to the GPS reference signal. A time error, due to a delay, is observed to appear uniformly on subsequent data samples. The time error is observed to appear randomly on consecutive sets of data samples when GPS connectivity is intermittent (e.g. due to loose wiring), and an accumulating time error observed on all samples during a total GPS signal loss (e.g. due to

improper placement or malfunctioning of device). The models for the intermittent and total GPS signal loss (GSL) time error behaviors are states respectively as,

$$\Delta t_{\varepsilon}(t) = \Delta t_{\varepsilon} \quad (2.5)$$

$$\Delta t_{\varepsilon}(t) = t\Delta t_{\varepsilon} \quad (2.6)$$

### 3. Spoofing of GPS receiver signal

Here, an attacker initially acts as an authentic source of correct external reference signal to the PMU, and then attacks the device by gradually leading its signal away from the authentic GPS signal mode. The attack model is given as,

$$\Delta t_{\varepsilon}(t) = \Delta t_{\varepsilon, capture} + tdt \quad (2.7)$$

$\Delta t_{\varepsilon, capture}$  is a time error at the instance when an attacker completely captures the device receiver, and  $dt$  is the rate of time signal divergence induced by the attacker.

#### 2.2.2 Non-Time Errors

Similar to data measurements obtained from other grid-installed sensors, PMU data are prone to the effects of unwanted noisy signals, data drops due to communication issues which affect network data streaming ability and repeated measurement values.

Noise in data measurements is modeled as an additive, Gaussian distributed signal, which is parameterized by a zero-mean and finite variance ( $\sigma^2$ ). The standard deviation ( $\sigma$ ), associated with each of the measurement time points, is obtained from a Signal-Noise Ratio, (SNR, which is in decibels),

$$\sigma = 10^{-SNR/20} \quad (2.8)$$

Data drop is measured by a drop-out rate attribute, and defines the rate at which packets are lost in a data stream [19]. No data is reported at time points during which packets are lost or delayed, and [22] suggests the use of NaN (not a number) or 0x8000 (-32768)- corresponding to zero values - as filler data, which are not used in actual computation.

#### 2.2.3 Updating Derived Measurements (Frequency and ROCOF)

Depending on the type of synthetic data error that is prototyped, a re-computation of the frequency and ROCOF signals is required. Currently, no specific estimation technique for these quantities has been defined by the IEEE reference documentation [22]. Based on the implicit definition of frequency as the rate of change of phasor angle, the derived measurements can be computed in the frequency domain as,

$$f = \frac{s}{1 + sT} \theta \quad (2.9)$$

$$ROCOF = \frac{s}{1 + sT} f \quad (2.10)$$

where  $T \sim 0.2$  second is a time-delay used to capture a window of data samples.

### 2.3 Synthetic Networks

Confidentiality issues associated with obtaining actual field data poses a challenge to research activities, and thus prompts the use of artificially-generated data for study and research purposes through the design of synthetic networks.

Synthetic grids are fictitious, but realistic, models of power grids [23-26]. They are statistically similar to real power grids since they are designed with respect to publicly available data e.g. size and locations of generators, population density, etc. Thus, they do not contain any critical energy infrastructure information (CEII) and can be freely shared, used in project publications and freely provided to other researchers [27].

Fig. 2.1. shows a synthetic 2,000-bus network spread out over the geographic region of Texas, and with a system operating frequency of 60-Hz.

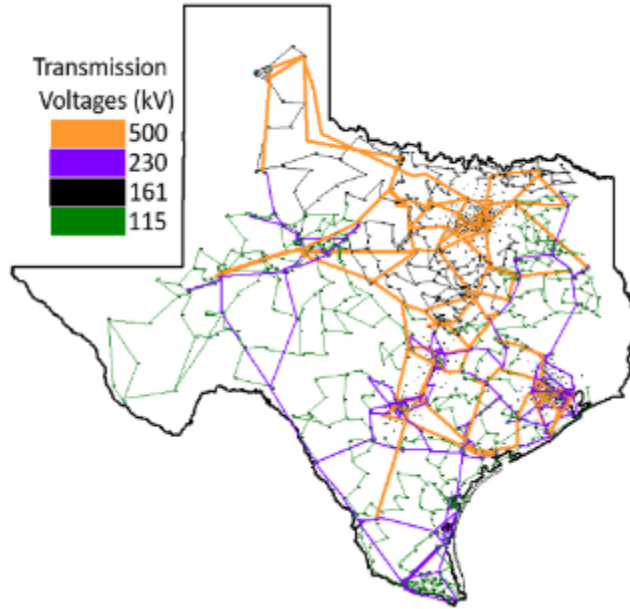


Fig. 2.1. A 2,000-bus synthetic network

Comprising of 1,250 substations, 432 generators, 3,209 transmission lines and different component dynamics set up in the system, the network is designed to simulate the operation of an actual power grid. More details on this, and a 10,000-bus system used in this work are presented in Appendix A.

## 2.4 PMU Data Prototypes for Time Errors

Figs. 2.2 and 2.3 illustrate voltage angle (VA) profiles based on the time propagation models in (4) – (7). Four different PMU time error prototypes were generated using original data from a test bus in the 2,000-bus network after a 30 second simulation. Error injection is initiated at the 5<sup>th</sup> second, and exists for 20 seconds. The report rate of the PMU is 30 samples per second.

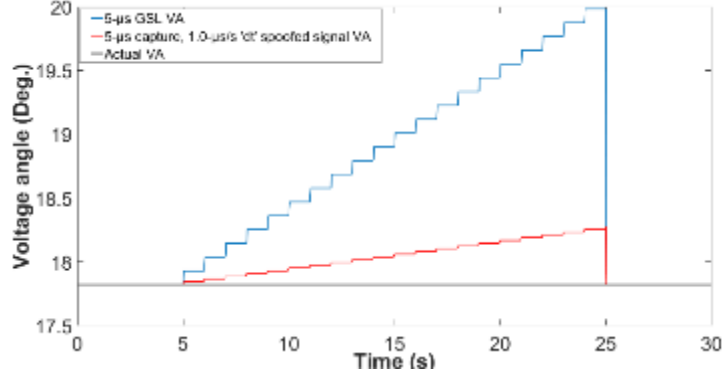


Fig.2.2. Prototype voltage angles for GSL and signal spoof

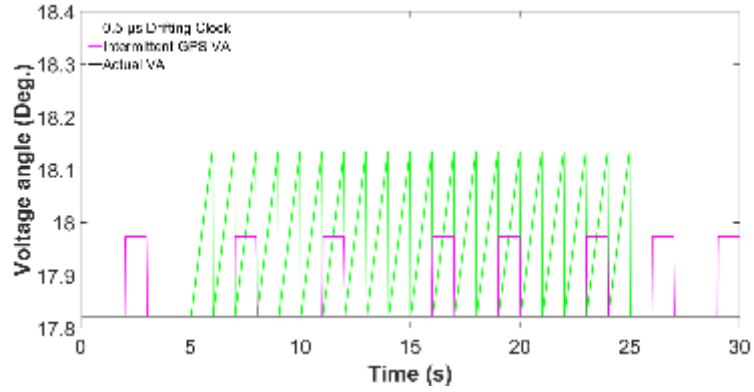


Fig.2.3. Prototype voltage angles for clock drift and intermittent GPS

In Fig. 2.2, the VA waveforms of the GPS signal loss (GSL) event and a spoofed-GPS time signal are shown. The black horizontal line is the original, steady state VA. The blue-colored GSL event has a pulse per second (PPS) time error ( $\Delta t_e$ ) of  $5 \mu s$ , and the red-colored spoofed signal event has a time error divergence rate ( $dt$ ) of  $1 \mu s/s$ . For each of the events, the phase angle error  $\Delta \delta_e(t)$  is applied uniformly on all 30 samples in a one-second reporting period prior to the next set of reported samples.

Fig 2.3. illustrates VA profiles due to two different causes of PMU clock time offsets – a constant  $0.5 \mu s$  time error due to a drifting internal clock, and a  $1.0 \mu s$  error due to intermittent GPS clock signals received by the PMU device. The green-colored ramp for the clock drift error is indicative of the accumulating time error at each sample. In contrast, a uniform time error is observed for all samples in the case of intermittent GPS signal.

PMUs report ROCOF data which can also be used to monitor phasor angle changes. The derived ROCOF data for the voltage angle errors are shown in Fig. 2.4 and 2.5.

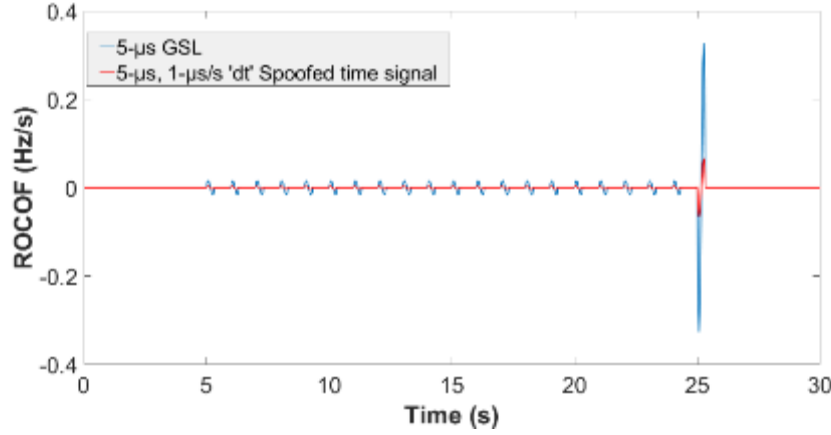


Fig.2.4. Derived ROCOF data for prototyped PMU voltage angles in Fig. (2.2)

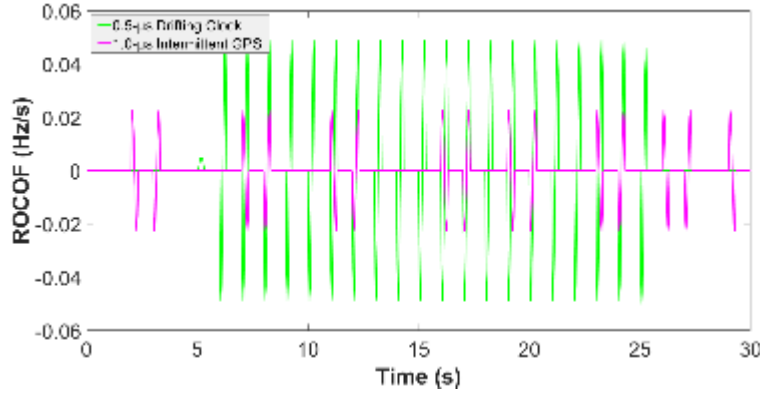


Fig.2.5. Derived ROCOF data for prototyped PMU voltage angles in Fig. (2.3)

Periodic ripples observed in Fig. 2.4 for both GSL and spoofed GPS signal are attributed to the small jumps in voltage angles due to the incremental time errors. However, at the point of error removal, the accumulated voltage angle deviation results in a sudden spike in the ROCOF. We observe that the GSL event generates a significant spike (0.33 Hz/sec) which is due to the large angle deviation as compared to the case of the spoofed time signal.

In Fig. 2.5, the observed uniform ROCOF measurements for a PMU internal clock offset is consistent with the periodic VA ramp-and-reset observed in Fig. 2.3. With an intermittent GPS signal, we observe a pairwise formation of positive and negative edges of ROCOF measurements.

### 3. Large-Scale System Data Error Analysis for PMU Synchrophasor Data

---

In this chapter, a distributed, error analysis technique is proposed to evaluate data segments of time-series measurements for errors using bus data obtained from a large-scale system. This constitutes the PMU data error analysis (PDA) block in the proposed framework of Fig. 1.1.

#### 3.1 Distributed Application of a Local Outlier Factor Analysis Method

Given a dataset  $X$ , composed of different time series measurements obtained from  $n$  number of PMU nodes, the aim is to be able to identify inconsistent data segments within any of the  $n$  measurements.

$$X = \{x_1^t, x_2^t, \dots, x_n^t\}; x_i = \{x_{i1}, x_{i2}, \dots, x_{ip}\} \quad (3.1)$$

$x_i$  is the data time series obtained from the  $i^{\text{th}}$  PMU device, and consists of  $p$  data points.

In previous works [28, 29], a local outlier factor (LOF) method was implemented to compute degrees of correlation of all measurements relative to a PMU dataset, from which computed error metric were used to identify data measurements considered to deviate from the dataset. The LOF technique is an unsupervised outlier detection algorithm which is based on the density of the  $k$ -nearest neighborhood of each object [30]. By comparing the relative densities of each neighbor, and computing an LOF value, it is able to detect an outlying object by identifying the largest-value LOF, and which is also most distinct from other LOF values in the set. A summary of the procedures for computing LOF values are given in appendix B.

In this work, a windowing technique which searches for erroneous data segments across all time-series measurements obtained from a large-scale system is implemented. It is observed that in a large system where buses are separated by large geographical and electrical distances, wide-area variations in bus signal trends during system events can mask out bad data due to wrongly-computed LOF values. In addition, it is observed that a direct implementation of the LOF method in a large system is computationally intensive since the  $k$ -nearest neighborhood of a measurement can be very large.

Figure 3.1 shows eleven locations in the grid from which voltage measurements were obtained after the contingency outage of a 230-kV line in the 2,000-bus synthetic grid. The simulation was run for 3-seconds, and the report rate of all PMUs set to 30 samples per second.

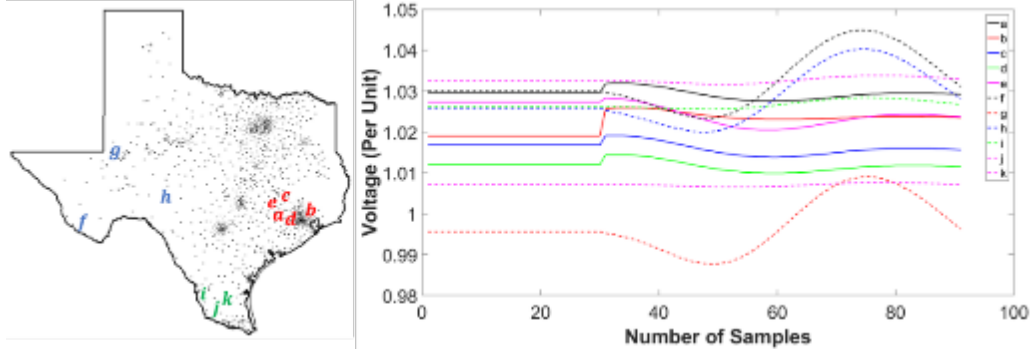


Fig. 3.1. 3-second voltage measurement

Using all signals in an LOF-based data error analysis, the computed error metrics for the eleven different bus signals are given in Table 3.1.

Table 3.1. LOF results for all 11 signals

Bus	<i>a</i>	<i>b</i>	<i>c</i>	<i>d</i>	<i>e</i>	<i>f</i>	<i>g</i>	<i>h</i>	<i>i</i>	<i>j</i>	<i>k</i>
LOF	1.000	4.342	1.000	1.000	4.590	4.937	5.069	4.891	1.000	1.000	1.000

The dis-similar signal trends in the selected bus measurements are adequately captured by the computed LOF values. Though the non-uniform LOF value metrics is solely caused by the grid event, this pre-existing state sets a condition that easily distorts true LOF computation and error identification in the event that actual measurement errors indeed exist in the system. In addition, considering all 2,000 input grid signals in the error analysis process, runtime for computing the LOF value for each of the bus measurement can be prohibitively high.

To address these limitations, a distributed computation method, which takes into consideration local signal variations in the wide-area network is proposed. Table 3.2 show computed LOFs when the signals are aggregated into two different, naïve clustering formations: A -  $\{a, b, c, d, e\}, \{f, g, h\}, \{i, j, k\}$ ; and B -  $\{b, e\}, \{a, c, d\}, \{f, g, h\}, \{i, j, k\}$  respectively.

Table 3.2. LOF results for all 11 signals using two sets of clustering

Bus	<i>a</i>	<i>b</i>	<i>c</i>	<i>d</i>	<i>e</i>	<i>f</i>	<i>g</i>	<i>h</i>	<i>i</i>	<i>j</i>	<i>k</i>
LOF-A	1.000	4.342	1.000	1.000	4.590	1.000	1.000	1.000	1.000	1.000	1.000
LOF-B	1.000	1.000	1.000	1.000	1.000	1.000	1.000	1.000	1.000	1.000	1.000

A uniform set of computed error metrics observed at all bus locations for *B*-cluster formation provides a base condition for which the true presence of data errors can be detected if they exist in the system.

### 3.2 Procedures in a Distributed Error Analysis

The flowchart for the proposed distributed LOF error analysis for the measurements obtained from the large system is illustrated in Fig. 3.2.

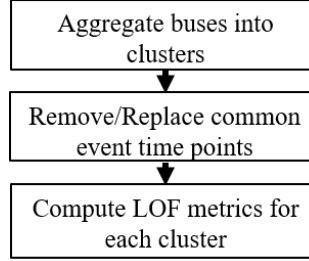


Fig. 3.2. Wide-area search for data errors

#### 3.2.1 Bus Aggregation

The method used to partition the system into smaller and local groups is governed by the concept of voltage control areas i.e. groups of buses exhibiting strong electrical coupling among each other. Augmented local bus information – bus geographical location and derived information from bus voltage measurement – are used to determine bus clusters. Integration of bus geography with voltage information ensures that generated bus clusters are able to track the dynamic response of the system rather than a sole use of fixed, bus geography coordinates (longitude and latitude) which are devoid of any electrical information.

Principal component analysis (PCA) method is used to extract true voltage information pertaining to individual buses. The PCA technique re-expresses the data set  $\mathbf{X}$  into its most meaningful set of basis [31], and for which an orthonormal matrix,  $\mathbf{P}$  (the basis) is known to diagonalize a covariance matrix,  $\mathbf{S}_Y (= \frac{1}{n-1} \mathbf{Y}\mathbf{Y}^T)$ , such that  $\mathbf{Y} = \mathbf{P}^T \mathbf{X}$ . The eigen-decomposition of  $\mathbf{S}_Y$  yields the ordered eigenvalues and eigenvectors,

$$\begin{aligned} \lambda &= \{\lambda_1, \lambda_2, \dots, \lambda_m\}; \lambda_1 \geq \lambda_2 \dots \geq \lambda_m \\ \mathbf{P} &= \{\mathbf{PC}_1, \mathbf{PC}_2, \dots, \mathbf{PC}_m\}; \mathbf{PC}_i \in \mathbb{R}^n \end{aligned} \quad (3.2)$$

The order of importance of the principal component vectors in  $\mathbf{P}$ , which is given as  $\mathbf{PC}_1 > \mathbf{PC}_2 > \dots > \mathbf{PC}_m$ , is then based on the order of the largest to the smallest-sized eigenvalues.

Figure 3.3 shows plots of the first eight principal vector components, and the corresponding eigenvalues, after performing PCA technique on voltage data set obtained from the synthetic 2,000-bus system after a generator outage at bus 1506, however with noise signals injected at buses 1 and 2. Table 3.3 gives the variance percentage for each of the components.

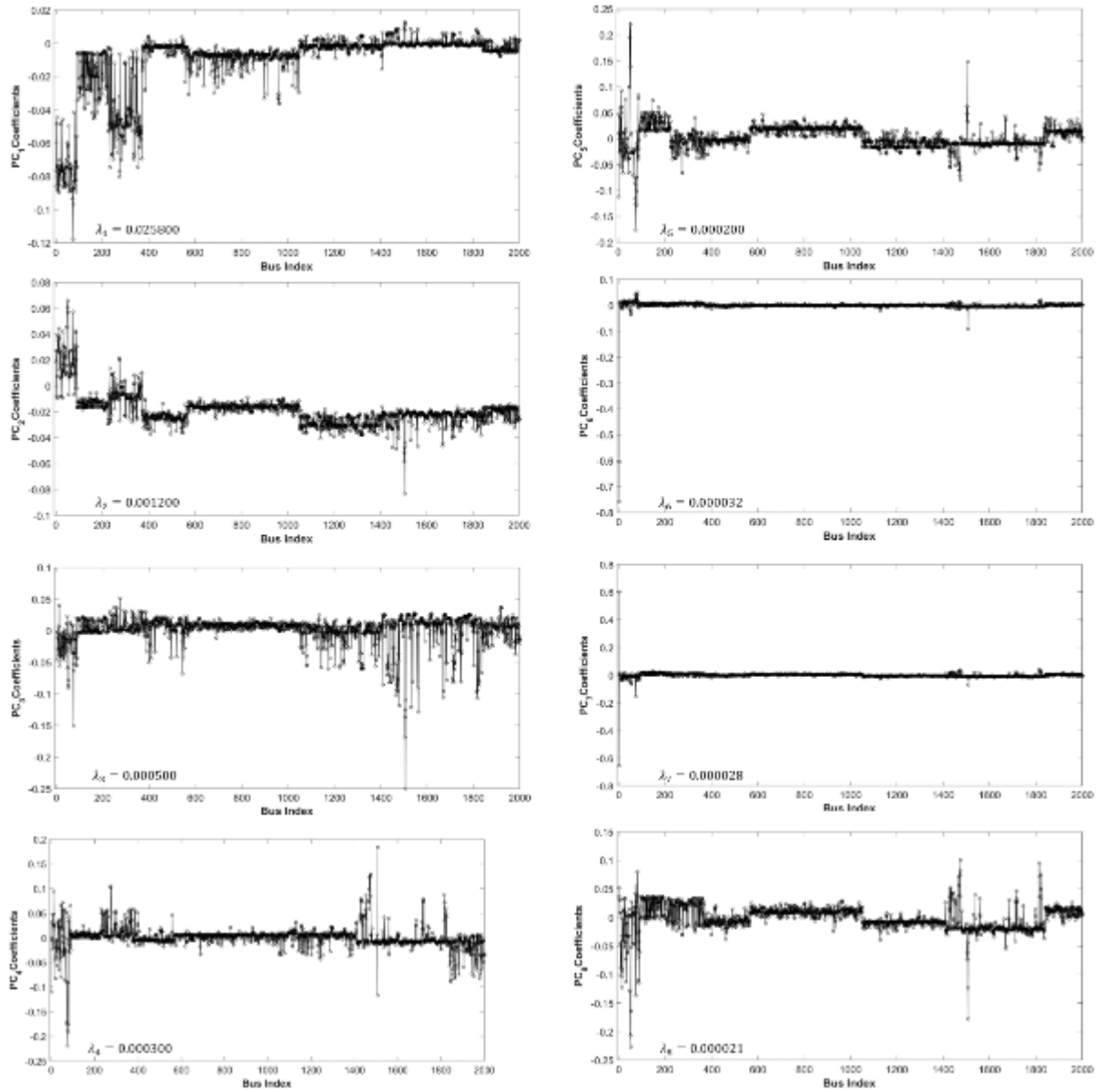


Fig. 3.3. First eight principal component vectors

Table 3.3. Variance percentage of principal components -  $(PC_i / \sum PC_i) \times 100\%$

Principal Component	$PC_1$	$PC_2$	$PC_3$	$PC_4$	$PC_5$	$PC_6$	$PC_7$	$PC_8$
Variance %	91.880	4.270	1.780	1.068	0.712	0.114	0.0997	0.075

The extent of activity of any  $i^{th}$  bus is indicated by the absolute value of its coefficient in the component vector. As expected, the variance percentage for  $PC_1$  (i.e., 91.88%) is observed to be dominant since it bears most of the voltage information in the system. True system information is embedded in the first few components after which the effect of system noise and data errors become more dominant as observed by the bus coefficients in  $PC_6$  and  $PC_7$ .

A hybrid, data-driven approach implemented for the purpose of clustering, thus augments every bus geography information with its principal vector coefficient(s).

$$\mathbf{X}_i = [\text{Geo}_{lat,i}, \text{Geo}_{long,i}, \mathbf{PC}_{1,i}, \dots, \mathbf{PC}_{n,i}] \quad (3.3)$$

$\mathbf{X}_i$  is an hybrid vector for the  $i^{th}$  bus, which entries are made up of latitude and longitude coordinates,  $\text{Geo}_{lat,i}$  and  $\text{Geo}_{long,i}$ , and bus entries in the  $n$  significant principal components  $\mathbf{PC}_{1,i}, \dots, \mathbf{PC}_{n,i}$ .

An aggregation of the bus vectors in (3.3) is carried out using  $k$ -means algorithm [32] - a simple and fast clustering technique. Furthermore, a pre-processing step prior to the detection of bus or PMU locations reporting data errors is to identify and isolate actual system disturbance data.

### 3.2.2 Error Assessment of Bus Measurements

A distributed LOF computation is performed cluster-wise on the grid. Using a sliding window, defined by  $\tau$ - width and  $\tau_s$ -sliding time, the bus signals are individually assessed for errors by computing error metric for  $m$  segments in the time-series data.

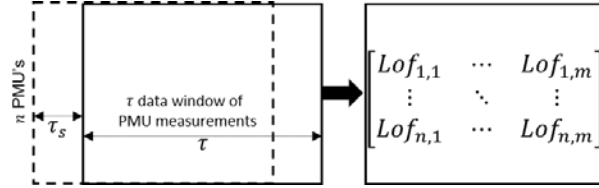


Fig. 3.4. Window technique for assessing error level in data segments

**Note:** A phasor measurement consists of a magnitude and angle component. Because PMU errors affect either or both components, it is important to specify the measurement component being assessed for errors. If the focus is magnitude (or angle), the input data to the LOF routine is phasor magnitude (or ROCOF). Absolute values of voltage angles do not convey much information, and cannot be used to adequately monitor PMU time errors. On the other hand, ROCOF measurements provide a good indication of voltage angle dynamics with an added ability of being able to detect small and sudden changes in voltage angles. Consequently, ROCOF qualifies as a good parameter to monitor time errors in PMU devices.

### 3.3 Simulation and Results

A 10-second simulation is carried out on the 2,000 bus network during which one of the 115-kV transmission lines is disconnected after 3 seconds. A data error analysis is carried out on the voltage measurements obtained from the system. Considering only the contingency event (a 115-kV line outage), Table 3.4 gives a summary of the computed error metrics for different system configurations.

Table 3.4. Summary of computed phasor magnitude LOFs (event only)

# Control areas /clusters	Event points removed?	Highest LOF(s)	Bus Index
1	Y	[16.69,8.355,8.358,8.355]	[6276,4174,6128,6015]
	N	[16.69,8.355,8.358,8.355]	[6276,4174,6128,6015]
5	Y	8.360	6015, 6128
	N	8.360	6015, 6128
20	Y	1.000	ALL
	N	8.360	6128
1	Y *	5.060	6276

\* Event time points removed separately for individual bus measurements

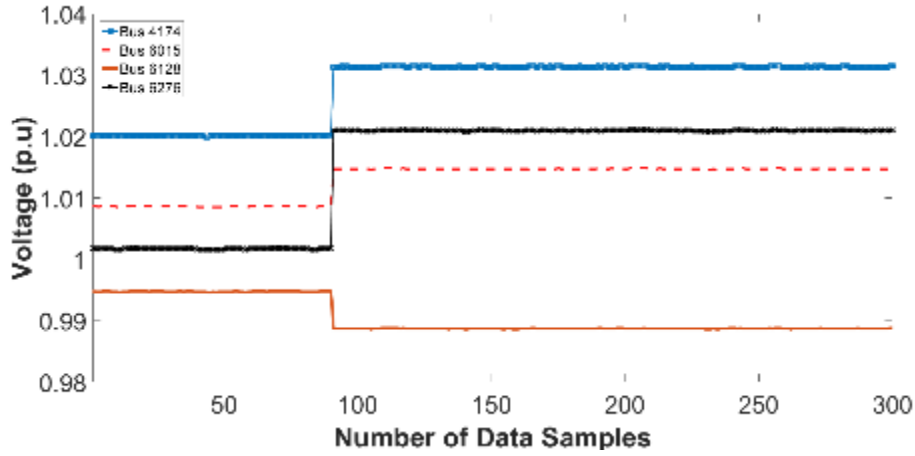


Fig. 3.5. Voltage magnitude measurements at event bus locations

According to the direct LOF computation method, false data error notifications are observed at buses (IDs: 6276, 4174, 6128, 6015) where the event is most significant, even though the disturbance has little impact on the system. Regardless of the removal of event points, LOF analysis is not able to distinguish the event from instances of data errors, and thus mis-identifies event buses as locations with the largest system LOFs. The proposed distributed method applied to a 5-cluster system aggregates bus IDs 4174 and 6276 into a cluster where a high voltage correlation results in smaller LOF values. However, a false identification of bus IDs 6015 and 6128 with LOF values 8.36 is due to both buses belonging to separate clusters with disparities in their voltage patterns.

Using a 20-cluster system, more groups containing buses with similar, dynamic voltage response are generated. Fig. 3.6 shows re-allocation of the event buses to cluster 2, 5 and 17 such that computed LOF value is 1.0 at all buses, thus isolating the impact of the event.

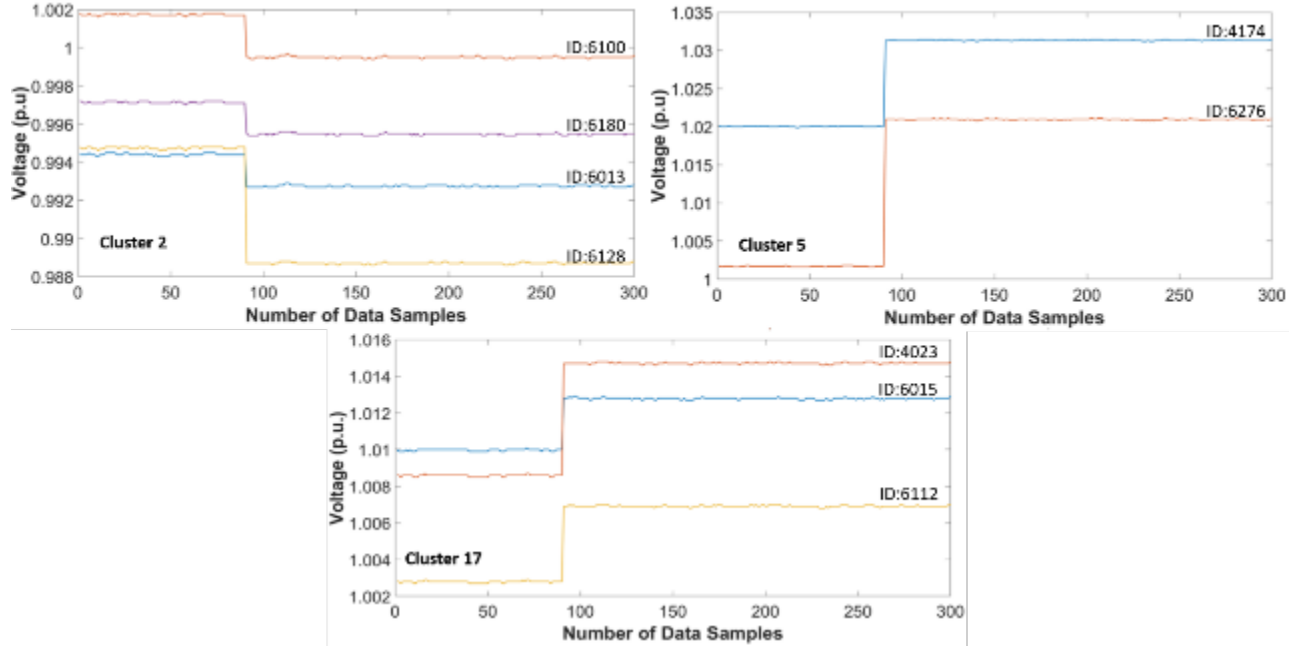


Fig. 3.6. Event buses re-distributed to three clusters

**Error 1:** In this scenario, 45-dB of noise signal is injected in the phasor voltage measurements reported by the PMU located at substation ID 1250. Table 3.5 provides a summary of the computed LOFs.

Table 3.5. Summary of computed phasor magnitude LOFs (event and noise error)

# Control areas /clusters	Event points removed?	Highest LOF(s)	Bus Index
1	Y	[16.69,8.355,8.358,8.355]	[6276,4174,6128,6015]
	N	[16.69,8.355,8.358,8.355]	[6276,4174,6128,6015]
5	Y	[8.358,8.358,2.941,3.263,2.941]	[6015,6128,8158,8159,8160]
	N	[8.358,8.358,2.941,3.263,2.941]	[6015,6128,8158,8159,8160]
20	Y	[2.941,3.263,2.941]	[8158,8159,8160]**
	N	[8.360,2.941,3.263,2.941]	[6128,8158,8159,8160]
1	Y *	5.060	6276

\* Event time points removed for individual bus measurements, \*\* PMU 1250 reports measurements for buses 8158-8160

Based on the large LOF values observed at the event buses, the direct LOF computation mis-identifies these locations as sources of erroneous measurements even though data errors are reported by another PMU set of phasor measurements. A distributed error analysis on the 5-cluster system identifies all three erroneous measurements, with LOF values 2.941, 3.263 and 2.941, in

addition to two event bus measurements (bus IDs 6015 and 6128). Finally, with a 20-cluster system, all event buses are isolated, and thus correctly identifying only the measurements with true data errors. Table 3.6 shows bus allocations in four groups within the 20-cluster system.

Table 3.6. Cluster formation

Cluster 2	[6013,6100,6128,6180]
Cluster 5	[4174,6276]
Cluster 16	[8158,8159,8160, ...]
Cluster 17	[4023, 6015, 6112]

Error 2: In addition to the actual system event and scenario of Error 1, time errors were incorporated into the phasor measurements reported by the PMUs located at substation IDs 4, 538 and 764. Time error details and the voltage angles for the affected measurements are shown in Table 3.7 and Fig. 3.7 respectively.

Table 3.7. Simulated time errors

SS/PM U ID	# buses	Error Type (T)	Error	Parameters	Duration
4	2	T-2	Clock drift	Skew: 1- $\mu$ s	7-sec
538	1	T-2	Clock drift	Skew: 0.5- $\mu$ s	10-sec
764	1	T-1	Int. GPS	Skew: 10- $\mu$ s, 5 instances	1-sec/instance

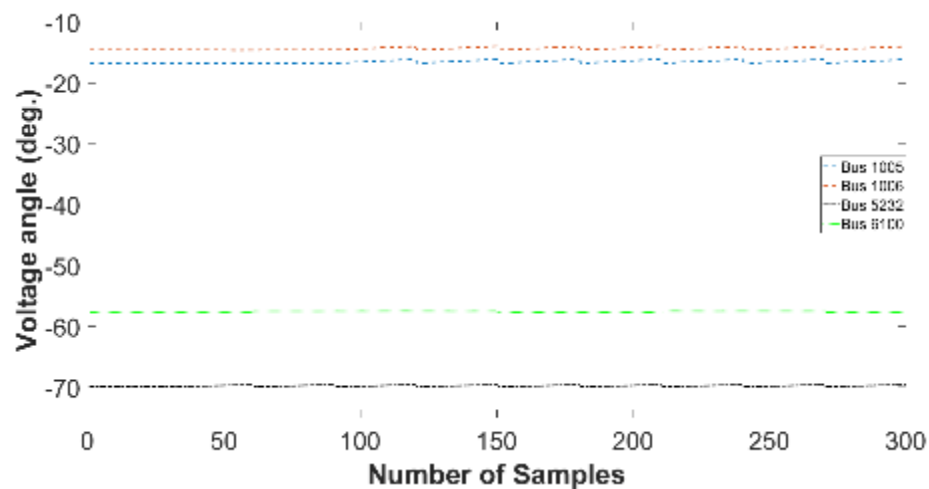


Fig. 3.7. Voltage angle measurements at time-error bus locations

The effects of both data errors are observed in the ROCOF data, and thus used as the input data source in the error analysis. Table 3.8 summarizes the results.

Table 3.8. Summary of computed phasor angle LOFs (event, noise and time errors)

# Control areas /clusters	Event points removed?	Highest LOF(s)	Bus Index
1	Y	[522,522,325,200,58,248,253,291]	[1005,1006,5232,6100,6276,8158,8159,8160]
	N	[522,522,325,200,58,248,253,291]	[1005,1006,5232,6100,6276,8158,8159,8160]
20	Y	[297,192,192,41,248,253,132]	[5232,1005,1006,6100,8158,8159,8160]

Similar to the previous scenario, the distributed method is able to detect all bus/PMU locations where data errors were reported while isolating the event bus locations.

Table 3.9 shows error analysis computation times for the single area, 5-cluster, and 20-cluster system configuration which was carried out on 10-second data on a 3.6 GHz processor, windows-based system.

Table 3.9. LOF execution time for different system configurations

# Control areas /clusters	1	5	20
Time (sec)	284	70	21

A notable processing time for the single area can be attributed largely to the several executions of some of the LOF analysis steps carried out within the large  $k$ -neighborhood of each of the 2,000 measurements. This is not the case with the clustered configurations, and it is assumed that with parallel computation, the running time for clustered systems can be much reduced.

### *Windowing Scheme*

A distributed LOF computation for the windowing scheme in Fig. 3.4 is applied on the 10-sec data obtained for error cases 1 and 2, using time window and time step of 1-sec and 0.5-sec respectively. The derived error values for each segment in all 2,000 measurements for both data error cases is shown in Fig. 3.8 and 3.9.

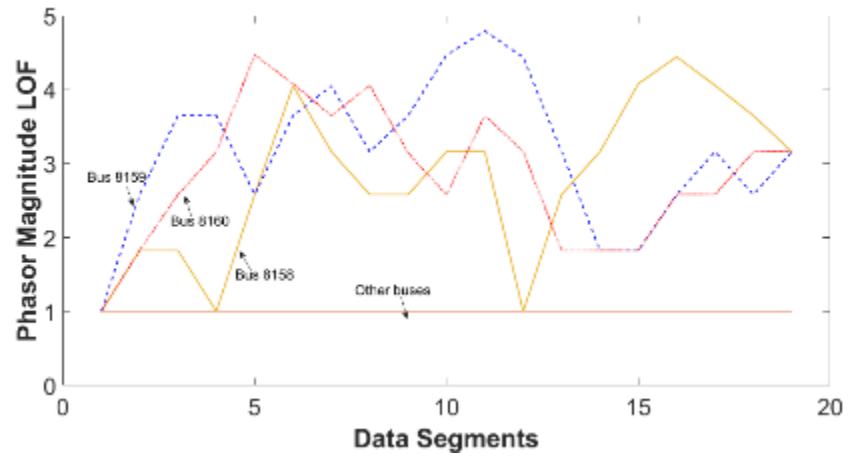


Fig. 3.8. Data segment errors in all 2,000 voltage magnitude measurements for error case #1

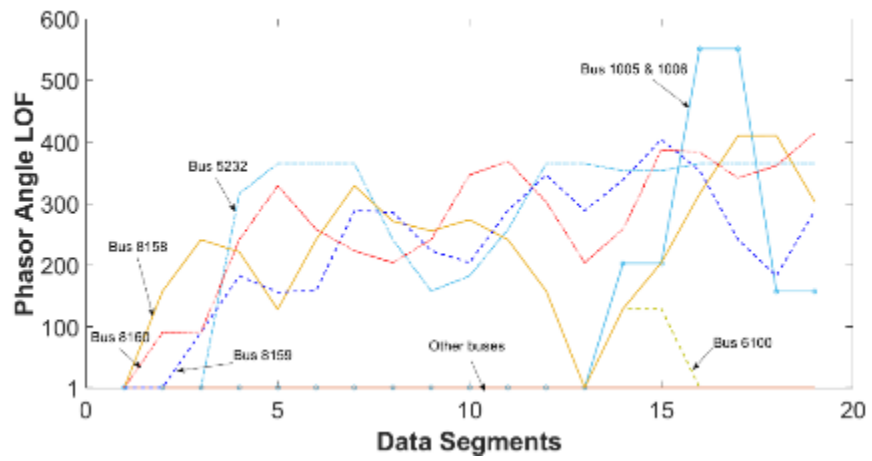


Fig. 3.9. Data segment errors in all 2,000 voltage angle measurements for error case #2

## 4. Presenting Computed Data Error Results of Large-Scale System through Multidimensional Scaling Visualization

---

In this chapter, error metrics computed for the different measurements in a large-scale system (here, the 2000-bus synthetic network) and PMU device information about the synchronization status of each data sample are presented in visual form. This constitutes the PMU data visualization (PDV) block in the proposed framework of Fig. 1.1. An overview of the multidimensional scaling technique, and how it was applied in this work to the error cases in the previous chapter are presented.

### 4.1 Data Error Visualization Using Multidimensional Scaling

Depending on the number of data segments assessed for errors, the computed time-series, LOF values for each PMU measurement can generate vectors of high dimensions. The method which has been adopted for visualizing errors in this work relies on observing correlations among different bus measurements for any given data error type, and visually displaying them as dissimilarities in a two dimension chart. The different charts generated are based on the use of the multidimensional scaling (MDS) which can be a useful method for representing power system information [33, 34].

MDS is used to represent measurements of similarity or dissimilarity among pairs of objects as distances between points of a low-dimensional, multidimensional space [35]. Given the time-series error values ( $\mathbf{LOF}_{orig}$ ) computed at  $m$  different data segments for  $n$  PMU measurements, and a pairwise, proximity matrix ( $\delta$ ) between them in (1) and (2) respectively.

$$\mathbf{LOF}_{orig} = \begin{bmatrix} Lof_{1,1} & \dots & Lof_{1,m} \\ \vdots & \ddots & \vdots \\ Lof_{n,1} & \dots & Lof_{n,m} \end{bmatrix} \quad (4.1)$$

$$\delta = \begin{bmatrix} \delta_{11} & \dots & \delta_{1n} \\ \vdots & \ddots & \vdots \\ \delta_{n1} & \dots & \delta_{nn} \end{bmatrix}, \delta_{ij} = \begin{cases} dissim(Lof_i, Lof_j); & i \neq j \\ 0; & i = j \\ i, j = 1, 2, \dots, n \end{cases} \quad (4.2)$$

The output of the MDS algorithm is a set of  $n$  coordinates,  $\mathbf{LOF}_{coord}$  in two dimensions, which re-represents  $\mathbf{LOF}_{orig}$ , and preserves or approximates the pairwise proximities in  $\delta$ . That is,

$$\mathbf{LOF}_{coord} = \begin{bmatrix} l_{1,1} & l_{1,2} \\ \vdots & \vdots \\ l_{n,1} & l_{n,2} \end{bmatrix} \quad (4.3)$$

$$\mathbf{d} = \begin{bmatrix} d_{11} & \dots & d_{1n} \\ \vdots & \ddots & \vdots \\ d_{n1} & \dots & d_{nn} \end{bmatrix}, d_{i\Box} = \begin{cases} dissim(i, j); & i \neq j \\ 0; & i = j \end{cases} \quad (4.4)$$

The MDS optimization problem is then to identify the optimal set of coordinates in  $\mathbf{LOF}_{coord}$  which minimizes a stress function which corresponds to a sum of squared errors.

$$\sigma = (l_{1,1}, l_{1,2}), \dots, (l_{n,1}, l_{n,2}), \arg \min \sum_{i=1}^{n-1} \sum_{j=i+1}^n (d_{ij} - \delta_{ij})^2 \quad (4.5)$$

#### Computation of $\mathbf{LOF}_{coord}$

The choice of classical MDS [36] for this work is due to it being a non-iterative technique, and generating analytical solutions within a fast computation time. Classical MDS assumes the proximity matrix,  $\delta$  as a distance matrix, and finds the coordinate matrix,  $\mathbf{LOF}_{coord}$  comprising of the two leading eigenvectors obtained from the eigen-decomposition of the normalized proximity matrix.

## 4.2 Generating Data Error, Hybrid Correlation Charts

For this work, the MDS is used to facilitate the display of the system structure by observing all PMU similarities using smaller LOF dimensions. It is used to transform the dissimilarities observed within a given dataset into a 2-D graphical representation. The benefit lies in visually displaying the dynamic electrical parameters (e.g. voltage magnitude and angle, frequency and ROCOF), and providing a better means of conveying the measurement errors.

#### Proximity Matrices

The multidimensional matrix,  $\mathbf{LOF}_{orig}$  is used to compute the entries in the proximity matrix,  $\delta$  in (4.2), which are defined as Euclidean distances i.e.,

$$dissim(LoF_i, LoF_j) = \sqrt{\sum_{p=1}^m (LoF_{i,p} - LoF_{j,p})^2} \quad (4.6)$$

When the choice is on visualization of the similarities among the synchronization status of all PMUs, which is based on their sync bits, the pairwise, binary-based distances, in the proximity matrix,  $\delta_{sync}$  are computed using the Rogers & Tanimoto binary similarity measure [35, 37], given as,

$$dissim(Pmu_i, Pmu_j) = \frac{a + d}{a + d + 2(b + c)} \quad (4.7)$$

Each of  $Pmu_i, Pmu_j$  is a binary string formed by cascading all data frame sync bits in a given PMU measurement;  $a, b, c$  and  $d$  are obtained from Table 4.1.

Table 4.1. Expression of binary instances

		Object B	
		1	0
Object A	1	a	b
	0	c	d

$a$  is the number of times elements in Object A and B are simultaneous bit-1;  
 $d$  is the number of times elements in Object A and B are simultaneous bit-0  
 $b$  is the number of times elements in Object A are bit-1, and elements in B are bit-0; and  
 $c$  is the number of times elements in Object A are bit-0, and elements in B are bit-1

The choice of selection of this binary similarity measure is based on the need to emphasize bit differences and similarities between PMUs. In addition, computed dis-similarity values always lies between 0 and 1.

### *Selecting MDS axis for plotting*

Time-series phasor measurements, obtained from PMUs, comprise of two aspects – magnitude and angle – which are both affected differently depending on the type of error. Therefore, we propose to visualize the wide-area similarity in all measurements using the relevant aspect when an error type is specified.

1. Noise Errors: Noisy signals are observed in both aspects of phasor measurements. As a result, significant noise levels are identified by visualizing the coordinate matrices of both magnitude-based and angle-based **LOF** matrices.

Input: Proximity matrix ( $\delta_{M,LOF}$ ) corresponding to magnitude-based **LOF**; and proximity matrix ( $\delta_{R,LOF}$ ) corresponding to angle-based **LOF**.

Output: First dimension of coordinate matrix,  $X_M$ ; and first dimension of coordinate matrix,  $X_R$

2. Timing Errors (GPS vs Clock drift): Timing errors reflect in the phasor angles. In addition, the PMU Sync bit (bit 13 in the STAT field) is flagged to ‘1’ once time-issues are observed to have occurred. Thus, we visualize the coordinate matrices of both angle-based **LOF** and sync status.

Input: Proximity matrix ( $\delta_{R,LOF}$ ) corresponding to angle-based **LOF**; and proximity matrix ( $\delta_{sync}$ )

Output: First dimension of coordinate matrix,  $X_R$ ; and first dimension of coordinate matrix,  $X_{sync}$

## **4.3 Simulation and Results**

The simulation case involves the outage of one of the 115-kV lines during a 10-second simulation, and the information being used are obtained from the error injection case which was previously described in chapter 3 i.e. an integration of the original event measurements with noisy signals at PMU 1250 and time errors signals at PMUs 4,538 and 764. Based on these different types of errors (noise and time errors) which are present in the data, two different MDS visualization options are used for this purpose.

Given the occurrence of clock drift and intermittent GPS time errors as described in Table 4.4, the flag bit values indicating the status of each sample synchronization (PMU Sync bit 13) are demonstrated in Fig. 4.1 and 4.2. A bit value of zero (or OFF) indicates a synchronized sample, and a bit value of one (or ON) is a sample that is out of sync.

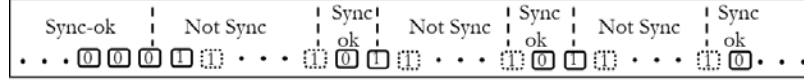


Fig. 4.1. Bit flag updates for clock drift error

The clock drift is an alternating sequence of bit changes. Prior to time issues, bit 13 is 0 (Sync ok) until the moment the drifting begins with the first data sample, when bit 13 changes to 1 (Not Sync). For a reporting period, it remains out of sync, and all sample bit status is preserved as value 1. An attempt at re-synchronizing first sample in the next report cycle sets bit 13 to 0 momentarily, after which drifting continues with the second sample. Bit 13 is set back to 1 for the reporting period. The cycle is repeated for as long as the PMU clock issue exists.

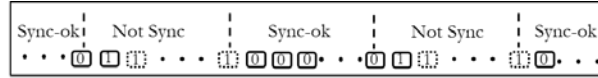


Fig. 4.2. Bit flag updates for intermittent GPS error

Sequencing of bit changes in the case of intermittent GPS is to a lesser degree than the clock drift, and depends on the frequency and duration of signal loss. Hence, the non-periodic sequencing of bit changes in Fig. 4.2. A period of bit-OFF (Sync-ok, and bit value is 0), followed by another equal- or non-equal duration of bit-ON (Not Sync, and bit value is 1).

### *Generation of MDS Correlation Graphs*

Based on figures 4.1 and 4.2, bit adjustments due to clock drifts and intermittent GPS signal reception are performed on the bus measurements of PMUs 4, 538, and PMU 764 respectively. Execution of MDS procedures on the proximity matrices –  $\delta_{M,LOF}$ ,  $\delta_{R,LOF}$  and  $\delta_{sync}$  – across all 2,000 buses generates the reduced two-dimension coordinate matrices,  $X_M$ ,  $X_R$  and  $X_{sync}$  respectively. Table 4.2 shows the normalized coordinates for each bus in the  $X_M$ ,  $X_R$  and  $X_{sync}$  matrices

Table. 4.2 MDS coordinates for PMU bit-13 status flag and phasor angle error

PMU ID	Bus IDs	$X_{M,1}$	$X_{M,2}$	$X_{R,1}$	$X_{R,2}$	$X_{sync,1}$	$X_{sync,2}$
4	1005	0.001	0.000	-0.251	0.657	-0.512	-0.323
	1006	0.001	0.000	-0.251	0.657	-0.512	-0.323
538	5232	0.001	0.000	-0.517	-0.240	-0.591	0.031
764	6100	0.001	0.000	-0.028	0.012	-0.352	0.889
1250	8158	-0.526	0.864	-0.414	-0.070	0.001	0.000
	8159	-0.639	-0.495	-0.428	-0.190	0.001	0.000
	8160	-0.560	-0.225	-0.499	-0.193	0.001	0.000
Others	Others	0.001	0.000	0.001	0.000	0.001	0.000

In the absence of errors, the coordinates of all buses in either of the three coordinate matrices should approximately lie close to an origin i.e. (0, 0). However, isolated bus coordinates exhibiting significant deviations from this point is an indication of the presence of anomaly in the reported measurement. The hybrid-MDS graph in Fig. 4.3 is obtained by plotting  $X_{R,1}$  and  $X_{sync,1}$ , and provides a method to visualize the correlations among PMU measurements when time errors are present.

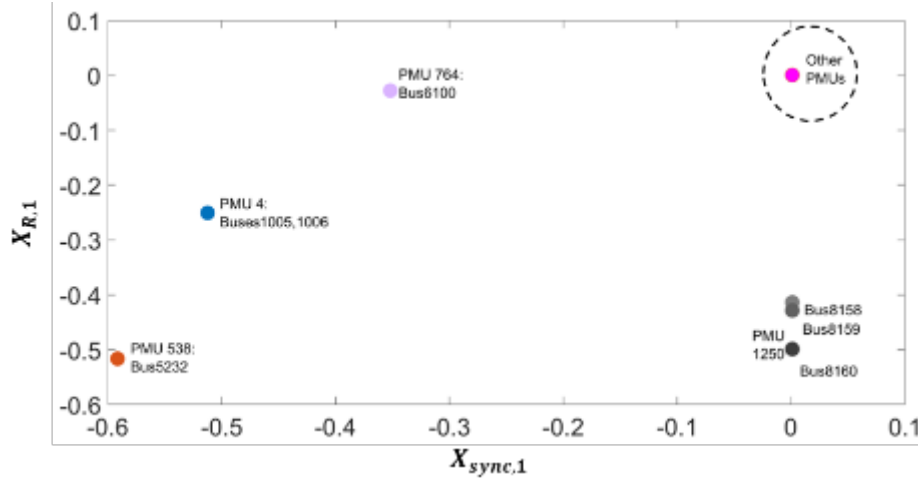


Fig. 4.3. Hybrid-MDS spatial representation of noise and time errors in PMU data

The diagonal distances spanned across both sync and phasor angle correlation axis from majority of other PMU measurements is indicative of actual time errors present in some of the reported measurements. The most severe cases are observed to occur in measurements obtained from PMUs 4 and 538 where the clock drift error had occurred for the most part of the simulation (i.e. 7 and 9 seconds respectively) followed by the five instances of intermittent, external time synchronization in PMU device 764. The vertical distance between PMU ID 1250 and ‘other PMUs’, however does not necessarily indicate a time error as the device is correlated in the sync axis with ‘other PMUs’. Further investigations, by updating the graph to a plot of  $X_{R,1}$  and  $X_{M,1}$  in Fig. 4.4, reveal the large deviation of PMU 1250 with respect to the other PMUs along the phasor magnitude correlation axis. The data error can be attributed to other causes which simultaneously impact on both components of phasor measurements, and in this case, the effect of noisy signals.

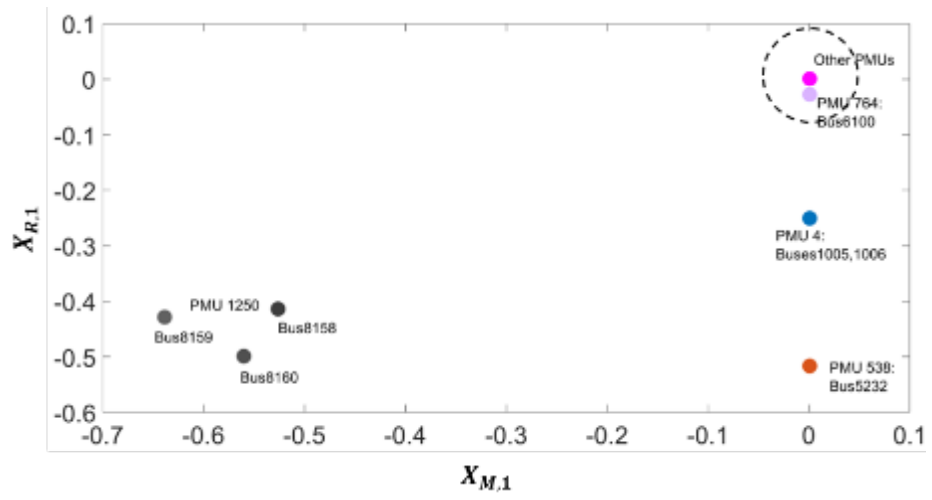


Fig. 4.4. Hybrid-MDS spatial representation of errors in PMU magnitude and angle data

## 5. Wide-Area Visualization of Large-Scale, Grid Oscillation Results Obtained from the Analysis of Synchrophasor Data

---

In this chapter, wide-area visualization methods are used to present results of low-frequency disturbance modes obtained from the analysis of synchrophasor data obtained from large-scale grids. Information pertaining to mode estimation quality, oscillation mode activities and source of oscillations are presented in a wide-area perspective in order to capture the holistic, underlying state of the system.

### 5.1 Oscillation Monitoring

A critical activity in preserving the safe operation of the power grid, the objective of oscillation analysis, monitoring and control is to search for sources of low-frequency oscillation disturbances that may threaten the stability of the system in order to eliminate them [15, 38]. This is achieved through the technique of modal analysis whose goal is to obtain a re-constructed signal,  $\hat{y}(t)$  that is a sum of un(damped) sinusoids and considered to be a close approximate of an original signal  $y(t)$ . The observations not fully captured by the reconstructed signal often constitutes an error signal,  $e(t)$ .

$$\hat{y}(t) = \sum_{j=1}^q A_j e^{\sigma_j t} \cos(\omega_j t + \phi_j) \quad (5.1)$$

$$e(t) = \sum_{j=1}^q \|y(t_j) - \hat{y}(t_j)\|_2^2 \quad (5.2)$$

An identified  $j^{th}$  low-frequency signal (or mode) is characterized by its modal parameters: damping factor ( $\sigma_j$ ), frequency ( $\omega_j$ ) and mode shape consisting of amplitude ( $A_j$ ) and phase ( $\phi_j$ ).  $q$  is the number of dominant low-frequency modes captured by the analysis.

Different modal analysis techniques are used in power systems to reveal underlying low frequency signals intrinsic to power system measurements [39-43]. The traditional Prony analysis computes the roots of a polynomial to determine the modal frequencies of a signal. These characteristic polynomials are associated with a discrete linear prediction model (LPM) which are used to fit the observed measurements. In the matrix pencil technique, a singular value decomposition is performed on a Hankel matrix, after which the eigenvalues and other modal parameters are obtained. One of the advantages of this method is its tolerance to the presence of noise in the observed measurements. A nonlinear least squares optimization method, which encapsulates the linear variables into nonlinear variables, is used by the variable projection method (VPM) to simultaneously estimate all the modal parameters. However, [44] showed that the initial modes provided by the matrix pencil method are usually sufficient. Also, a fast method of dynamic mode decomposition was proposed in [43] for off-line and on-line simultaneous processing of multiple time-series signals.

Though the above-mentioned modal techniques are able to estimate the modal contents of power system oscillatory disturbance data, the focus of this work is not to dwell on the chosen method used to identify these low frequency signals in power system measurements. Rather, the objective of this work is to demonstrate how wide-area visualizations, different from other visualization techniques [45-49], can be used to convey holistic system dynamics to control center personnel. A power systems simulation software, PowerWorld simulator, is used to demonstrate the proposed wide area visualization techniques.

## **5.2 Wide-Area Visualization of Modal Information**

Synthetic networks on which oscillation results are presented are based on pre-existing, one-line diagrams which have been overlaid on a geographical map of the United States. In addition to the use of contour plots, dynamic data are visualized using geographical data views (GDVs), which are implemented as part of an information layering technique to present large amounts of data [50-52].

### **5.2.1 Quality Estimation of Modal Analysis Technique**

The desire is to approximate as closely as possible each original signal using the signals from (5.1). However, the few dominant system modes are not sufficient to fully represent the original signal and other dynamics in the system. The quality of the mode estimation process is thus measured in terms of the difference between the original and reconstructed signal.

Fig. 5.1 shows the actual (blue), reproduced (red) frequency signals and the CFs (cost functions or mismatch errors,  $\epsilon$ ) at nine different buses in a 2,000-bus network. Here, the case involves a 10-second transient stability simulation of the system during which two generators are disconnected after one second.

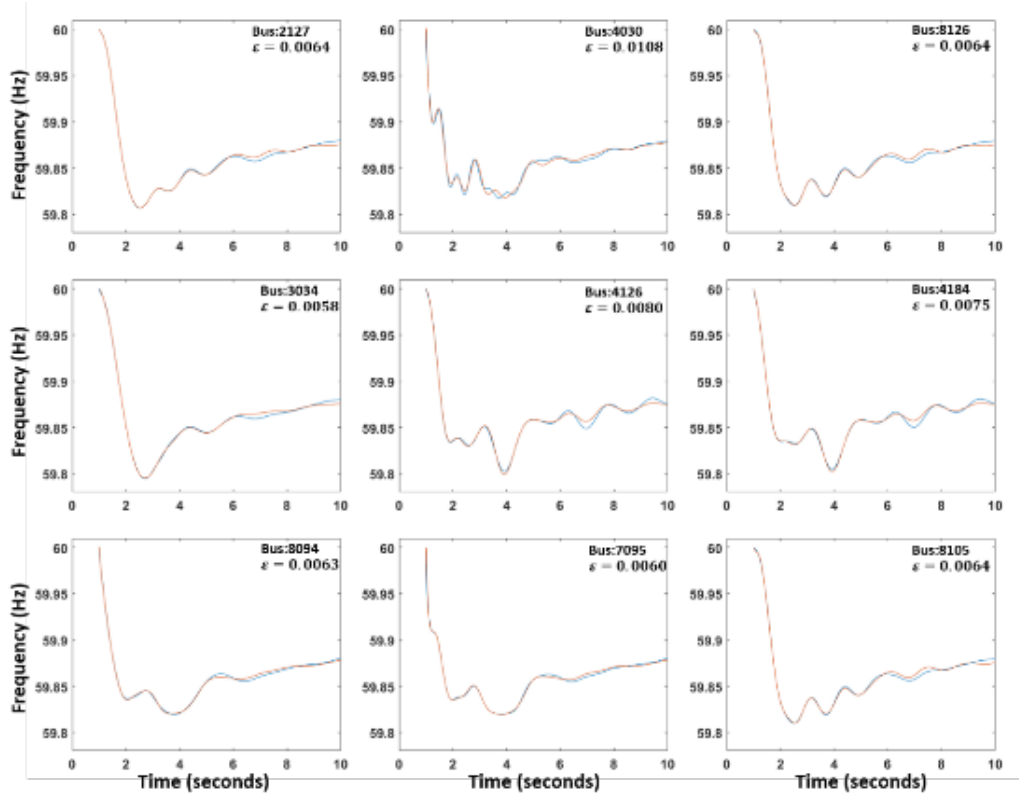


Fig. 5.1. The cost functions, actual and reproduced frequency signals at 9 locations

Using the definition in (5.2), the computed best and worst case cost functions are 0.0058 and 0.0108 respectively, and which were observed at bus IDs, 3034 and 4030, respectively. However, relatively low values of the extreme CF quantities indicate the good matching ability of the proposed technique. The wide-area trend of the CF is shown in Fig. 5.2.

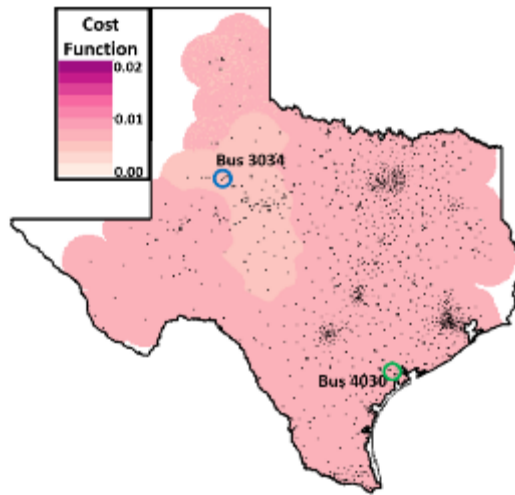


Fig. 5.2. Wide-area system cost function

A color scale has been set arbitrarily  $[0, 0.02]$  to indicate the best and worst case matching errors while the signal buses 3034 and 4030 are enclosed by blue and green circles respectively. The uniform variation of the cost function is largely indicative of the global pattern of system frequency, and good quality of the modal technique used for this purpose.

Fig. 5.3 (a) shows the wide-area trend of the CF when modal decomposition was applied on the voltage measurements.

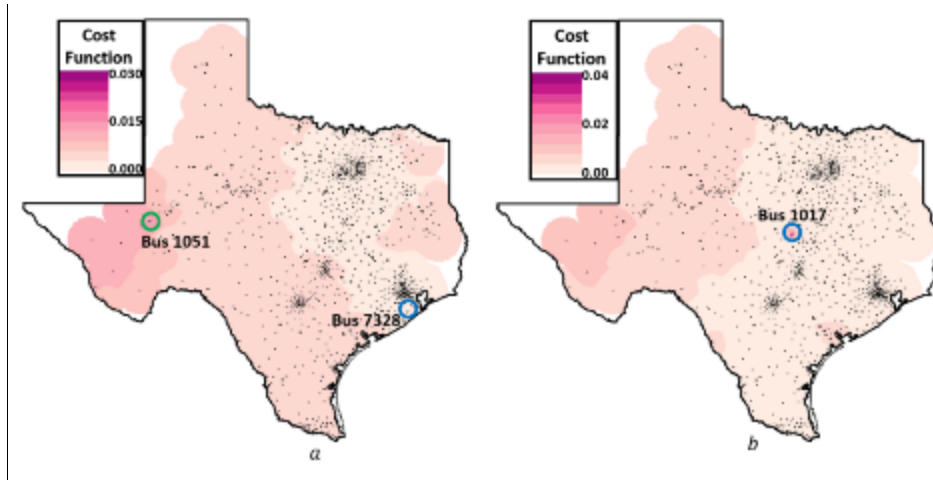


Fig. 5.3. (a) Wide-area cost function using voltage measurements; (b) with noise signal at bus 1017

A wider CF range,  $[0.0014 \ 0.028]$  at bus IDs 7328 and 1051 respectively, and more variation in all bus CFs are indicative of the local action of voltage trends observed in the system after the contingent generator outage. This can be attributed to the fact that fewer frequency modes could be prevalent at different bus locations, however they remain invisible to the system. Hence, they are not captured during signal reconstruction.

Another unique case of CF variation that could point to an event, and thus assist operators in understanding the system is when locations report erroneous data deemed to be inconsistent with the actual system trend. Fig. 5.3(b) is the wide-area CF when noisy data is reported by a PMU device at bus location 1017. High CF at an isolated bus location indicates a prevailing, anomaly condition, and especially when nearby buses have much lower CF values.

## 5.2.2 Oscillation Modes

The mode shape describes the relative activity of the state within an oscillation mode. Comprising of both magnitude and angle information, this vectoral attribute can be a distraction source when visualizing individual signal mode shape information in a wide area network.

Fig. 5.4 shows the current phasor technique used to view mode shapes in different sections of the power system [15, 49, 53]. Mode shapes at twenty different bus locations ( $a$  to  $t$ ) are currently being displayed.

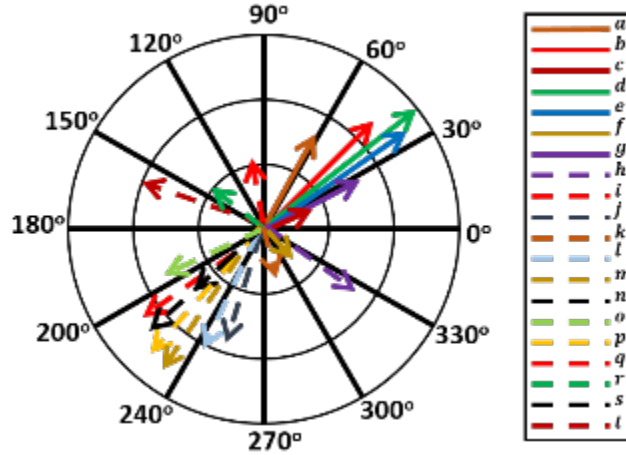


Fig. 5.4 Phasor vector plot of mode shapes at 20 bus locations

Using this method, the figure is able to capture the relative magnitudes and angles at the different buses. However, as mode vectors align in the same direction, and vector magnitudes become equal, the occurrence of significant vector overlaps result in the inability to distinguish among the mode shapes at the different buses. Most importantly, extracting the underlying system dynamics information from the phasor diagram is challenging without the use of an actual geographic map.

#### *Vector Field Visualization*

The vectoral characteristics of all bus mode shape information makes them amenable to being represented as two-dimension (2D) vector fields on geographical-based, one-line diagram of the system [50, 54, 55]. Among the different forms for vector field visualization in 2D surfaces, the choice of using arrow icons on a rectangular grid (GRID) vector field visualization is predicated on its ability to convey a sense of bus swing direction at any of the grid regions. This information is more critical to an operator rather than, for example, the short time it may take an operator to identify a critical point on the vector field if line-integral convolution (LIC) were used [55]. In addition, the GRID method has the ability to help users identify critical points within local neighborhoods on the vector field, which could indicate locations in need of attention. For example, the arrows forming the boundary of the green-colored, contour region of the grid indicates the extent of bus inclusions in the two-area swing of the system.

Based on the highlighted benefits of using 2D vector fields, a more effective, wide-area visualization is implemented to address the challenges faced by the phasor plot. This technique makes use of the attributes of glyph objects (phasor arrows) which are geographically-distributed on the one-line diagram to capture mode activities at all the individual buses. As a layering option, contour plots which encode other bus or area information (e.g. the direction of swing) are set in the background to provide more system dynamics that might not be fully captured by the mode vectors. Fig. 5.5(a) and (b) show mode shape information for an inter-area mode (0.541 Hz) and a local mode (3.576 Hz) using the frequency measurements obtained from the 2,000-bus case during two different simulations. All signal amplitudes have been scaled by their standard deviation values.

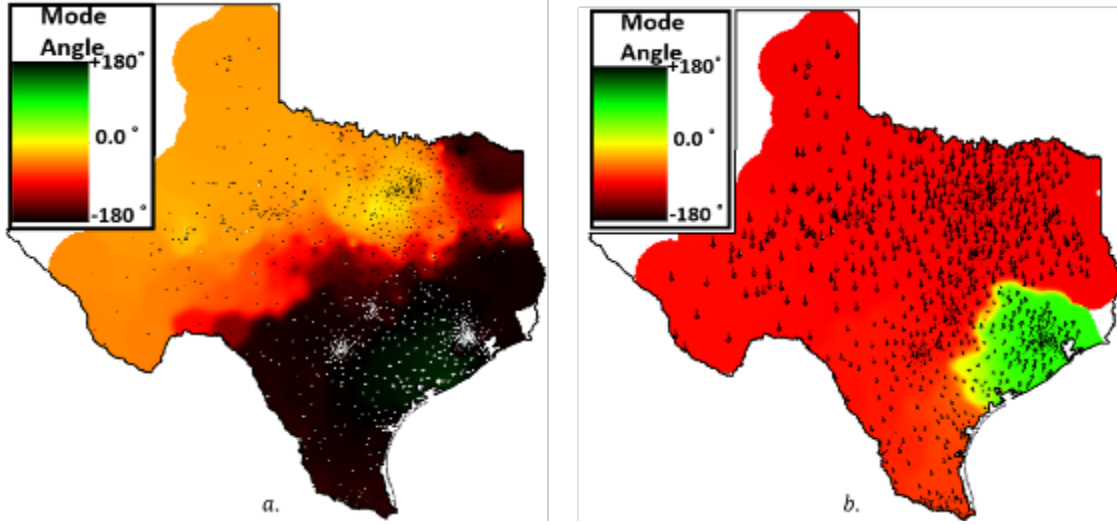


Fig. 5.5. Frequency mode shape for (a) local, and (b) inter-area modes

Abrupt change in colored contours between angle limits,  $-180^\circ$  and  $180^\circ$ , are often misleading since in actual geometry both angles are exact. To avoid this sudden color change, a circular (or cyclic) color map, which assigns the same or similar colors to angular values close to these limits, has been used. The color map used to highlight the mode angles at different signal bus locations provides a user with a wide-area summary of the swing direction at the different buses. Individual bus signal amplitude and angle are encoded in the size and orientation of the phasor arrow relative to the positive x-axis respectively. The geographical information of each bus is used to set the location of its GDV-based arrow. The inter-area oscillation in Fig. 5.5(b) shows two marked distinct areas, such that buses in these regions have a similar direction of swing for the oscillation mode. A comparison of the arrow lengths indicates the lower level of mode activity in the local mode of Fig. 5.5(a) than the inter-area oscillation in Fig. 5.5(b).

### 5.3 Visualization of Oscillation Sources

Sustained oscillations pose a threat to the safe and secure state of the system, and it is important to identify oscillation sources in order to eliminate them. An energy-based method [56, 57] is used for locating the source of oscillation by computing several dissipating energy (DE) coefficients associated with oscillation energy flowing across different transmission lines in the network. In large, inter-connected systems, a wide-area visualization of branch energy flows becomes critical for users to reliably point to disturbance sources by tracking the directions and magnitudes of DE flow arrows. The derivations of the  $DE_{ij}$  factor for any transmission line connecting bus  $i$  and  $j$ , are given in [56, 57].

The direction of oscillation is dictated by the sign of  $DE_{ij}$  – negative sign indicating energy production from a source to the network element dissipating the energy. In a wide-area visualization sense, computed  $DE$  coefficients can then be aggregated at each bus to show the net contribution to oscillation energy in the network.

A demonstration of the oscillation energy flow in the detection of an oscillation source is carried out for a 2,000-bus case, whereby one of the system generators is set to negative damping and a 500-kV line is outaged. A 3.576 Hz local mode, with a negative damping of -0.06, is identified in the system, and indicative of a sustained system oscillation. Using the measurements (frequency and voltage at all buses, and real and imaginary power flows across all transmission lines) obtained for this mode, the energy-based approach is used to track the source of disturbance in the system.

Fig. 5.6 shows the time-evolution oscillation energy and computed  $DE$  coefficient for all branches in the network.

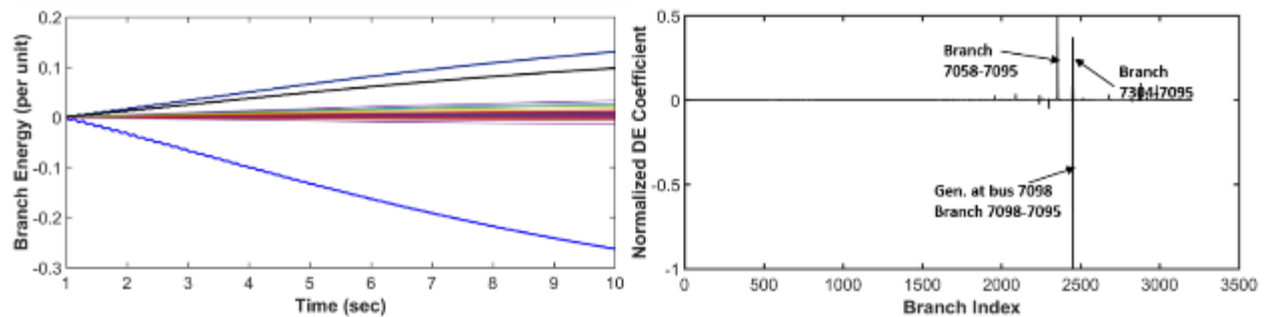


Fig. 5.6. Local oscillation - All branch oscillation energies and dissipating energy ( $DE$ ) coefficients

The increasing, outward flow of oscillation energy on the branch connected to bus 7098 is due to the negative damped response of the generator at the node, which is supported by the computed  $DE$  value. Relatively few transmission lines are involved in the flow of oscillation energy. Using size and color attributes of GDV-based, ovals to encode bus  $DE$  magnitude and direction of flow of the oscillation energy respectively, Fig. 5.7 is able to quickly convey to a user the source of oscillation. Constant generation of oscillation energy is a result of the negative damping which was set on the generator machine. An informed, control decision (e.g. disconnect the generator from the system) can then be taken.

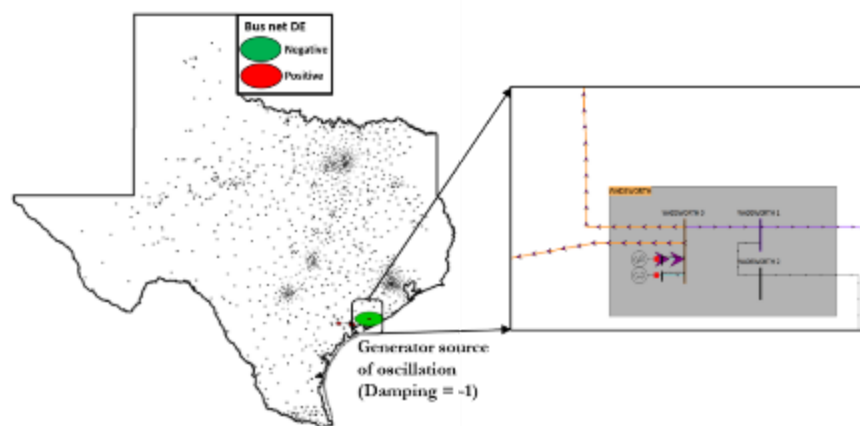


Fig. 5.7. Local oscillation - Oscillation source and branch  $DE$  flow

Inter-area oscillations are more complex than local oscillations, as it involves a higher participation of majority of the system transmission lines, buses and substations. Several research works are still being performed to understand this type of oscillation. An example wide-area visualization of an inter-area mode is shown in Fig. 5.8, and is based on the computed oscillation energies and branch DE values in Fig. 5.9.

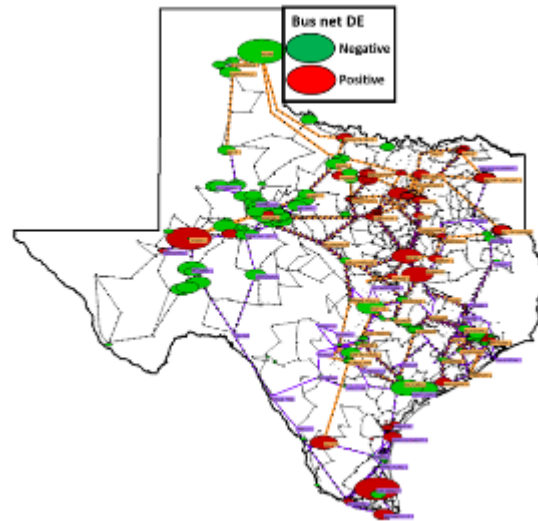


Fig. 5.8. Inter-area oscillation - Oscillation source and branch *DE* flow

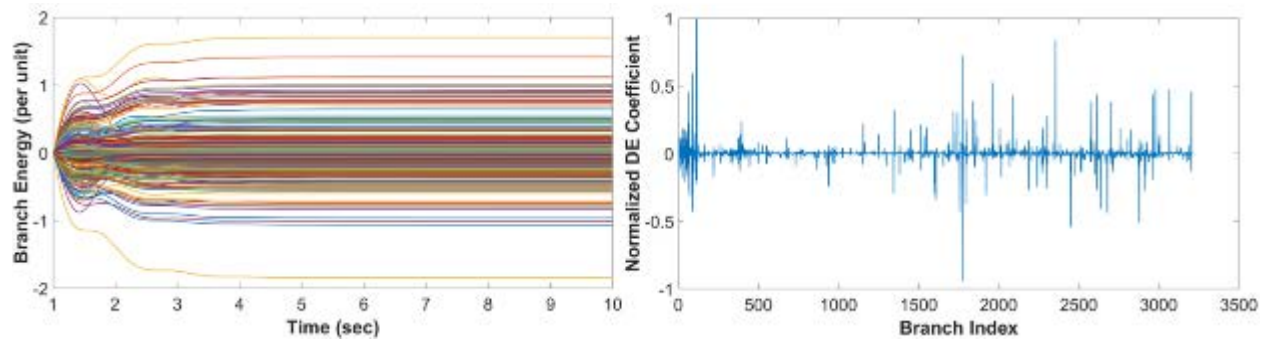


Fig. 5.9. Inter-area oscillation - All branch oscillation energies and dissipating energy (*DE*) coefficients

## 6. Conclusions

---

In this report, data errors in PMU and other synchrophasor devices which cause some of the data quality issues associated with synchrophasor data are discussed. Error mechanisms pertaining to the unique time stamping and synchronization operation of the devices are presented as time error propagation models in order to understand the evolution of different time errors. Furthermore, prototype data errors which manifest these timing inconsistencies are then synthesized.

As power systems increase in scale and components, spatio-temporal correlations among bus measurements become more complex. A distributed analysis technique, supported by density-based clustering technique, is proposed for use in the error assessment of phasor data measurements obtained from buses in a 2,000-bus, large-scale synthetic network. Generated results are observed to better reflect the true quality state of grid phasor measurements than when a central error analysis, which considers all the measurements, is performed.

Given that large amounts of data are generated and transmitted to control centers, a method to present computed error metrics information for a large-scale system using multidimensional analysis scaling visualization is proposed. The method provides a visual, comparative assessment of measurement errors at different buses in the system.

Finally, as a demonstration of some of the new techniques that are currently being implemented in PowerWorld simulator, wide area visualization methods are used to show how system-based, large-scale grid oscillation results can be presented to Engineers in a holistic manner. These methods are used to capture overall system state and dynamics for improved decision making.

## Appendix A

### Synthetic 2000-bus Texas Network

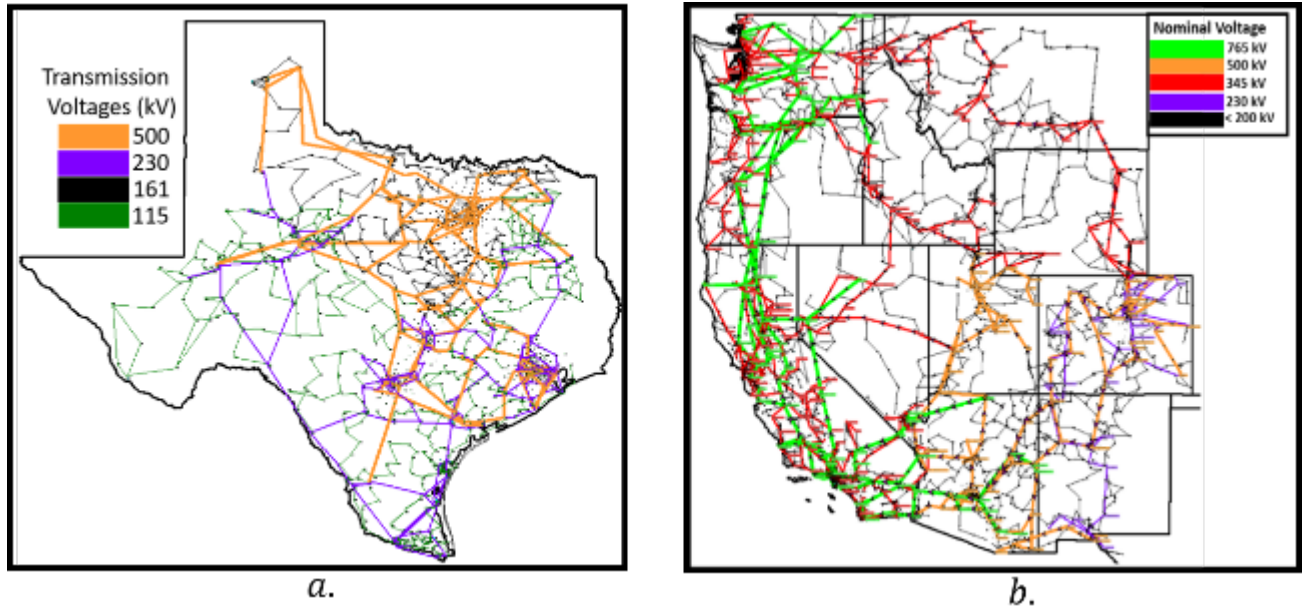


Fig. A-1. (a) 2,000-bus network (b) 10,000-bus network

The 2,000- and 10,000-bus networks are artificially-created grids covering the geographical space of the state of Texas, and the interconnected grid of Western U.S. respectively. Relevant details used for this work are shown in Table A-1.

Table A-1. Network Information

	2,000-bus	10,000-bus
# of substations	1,250	4,762
# of generators	432	1,937
# of transmission lines	3,209	12,706
Operating frequency	60 Hz	
PMU report rate	30 samples/ second	

## Appendix B

---

### Computing Local Outlier Factor (LOF)

Given objects  $p, o \in D, o' \in D \setminus \{p\}$ ;  $D$  = Total space;  $p$  = Object of interest ;  $k, MinPts > 0$

Step 1. Compute  $k$ -distance,  $k\text{-dist}(p)$

$$k\text{-dist}(p) = d(p, o); \begin{cases} d(p, o') \leq d(p, o); \text{ for at least } k \text{ objects} \\ d(p, o') \leq d(p, o); \text{ for at most } (k - 1) \text{ objects} \end{cases}$$

Step 2. Compile  $k$ -nearest neighbors,  $N_{k\text{-dist}}(p)$

$$N_{k\text{-dist}}(p) = \{ o \in D \setminus \{p\}; d(p, o) \leq k\text{-dist}(p) \}$$

Step 3. Compute reachability distance,  $\text{reach-dist}_k(p, o)$

$$\text{reach-dist}_k(p, o) = \max(k - \text{dist}(o), d(p, o))$$

Step 4. Compute reachability density ,  $\text{lrd}_{MinPts}(p)$

$$\text{lrd}_{MinPts}(p) = 1 / \left[ \frac{\sum_{o \in N_{MinPts}(p)} \text{reach-dist}_{MinPts}(p, o)}{|N_{MinPts}(p)|} \right]$$

Step 5. Compute local outlier factor,  $\text{LOF}_{MinPts}(p)$

$$\text{LOF}_{MinPts}(p) = \frac{\text{lrd}_{MinPts}(p)}{\min_{q \in N_{MinPts}(p)} \text{lrd}_{MinPts}(q)}$$

A small LOF value ( $\sim 1.0$ ) is indicative of a high density neighborhood around an object. Large LOF values are associated with a sparse neighborhood, and typical of an outlier object [10]. For this work,  $k$  and  $MinPts$  parameters are set to both equal 50% of the total measurements (or objects) in the dataset being considered.

## References

---

- [1] A. Silverstein. Synchrophasors and the grid [Online]. Available: [https://www.energy.gov/sites/prod/files/2017/09/f36/2\\_Modern%20Grid-networked%20Measurement%20and%20Monitoring%20Panel%20-%20Alison%20Silverstein%2C%20NASPI.pdf](https://www.energy.gov/sites/prod/files/2017/09/f36/2_Modern%20Grid-networked%20Measurement%20and%20Monitoring%20Panel%20-%20Alison%20Silverstein%2C%20NASPI.pdf)
- [2] A. G. Phadke, "Synchronized phasor measurements in power systems," *IEEE Computer Applications in Power*, vol. 6, no. 2, pp. 10-15, 1993.
- [3] J. Zhao, L. Zhan, Y. Liu, H. Qi, J. R. Garcia, and P. D. Ewing, "Measurement accuracy limitation analysis on synchrophasors," in *2015 IEEE Power & Energy Society General Meeting*, 2015, pp. 1-5.
- [4] M. Brown, M. Biswal, S. Brahma, S. J. Ranade, and H. Cao, "Characterizing and quantifying noise in PMU data," in *2016 IEEE Power and Energy Society General Meeting (PESGM)*, 2016, pp. 1-5.
- [5] D. Macii, D. Fontanelli, G. Barchi, and D. Petri, "Impact of Acquisition Wideband Noise on Synchrophasor Measurements: A Design Perspective," *IEEE Transactions on Instrumentation and Measurement*, vol. 65, no. 10, pp. 2244-2253, 2016.
- [6] Q. Zhang, V. Vittal, G. Heydt, Y. Chakhchoukh, N. Logic, and S. Sturgill, "The time skew problem in PMU measurements," in *2012 IEEE Power and Energy Society General Meeting*, 2012, pp. 1-6.
- [7] T. Bi, J. Guo, K. Xu, L. Zhang, and Q. Yang, "The Impact of Time Synchronization Deviation on the Performance of Synchrophasor Measurements and Wide Area Damping Control," *IEEE Transactions on Smart Grid*, vol. 8, no. 4, pp. 1545-1552, 2017.
- [8] D. P. Shepard, T. E. Humphreys, and A. A. Fansler, "Evaluation of the vulnerability of phasor measurement units to GPS spoofing attacks," *International Journal of Critical Infrastructure Protection*, vol. 5, no. 3-4, pp. 146-153, 2012.
- [9] X. Jiang, J. Zhang, B. J. Harding, J. J. Makela, and A. D. Domínguez-García, "Spoofing GPS Receiver Clock Offset of Phasor Measurement Units," *IEEE Transactions on Power Systems*, vol. 28, no. 3, pp. 3253-3262, 2013.
- [10] C. Huang *et al.*, "Data quality issues for synchrophasor applications Part I: a review," *Journal of Modern Power Systems and Clean Energy*, vol. 4, no. 3, pp. 342-352, 2016.
- [11] P. Kansal and A. Bose, "Bandwidth and latency requirements for smart transmission grid applications," in *2013 IEEE Power & Energy Society General Meeting*, 2013, pp. 1-1.
- [12] M. Asprou and E. Kyriakides, "The effect of time-delayed measurements on a PMU-based state estimator," in *2015 IEEE Eindhoven PowerTech*, 2015, pp. 1-6.
- [13] J. D. Taft, "Grid architecture 2," Pacific Northwest National Laboratory (PNNL), Richland, WA (United States)2016.
- [14] D. Novosel, V. Madani, B. Bhargave, K. Vu, and J. Cole, "Dawn of the grid synchronization," *IEEE Power and Energy Magazine*, vol. 6, no. 1, pp. 49-60, 2008.
- [15] D. Trudnowski. Properties of the Dominant Inter-Area Modes in the WECC Interconnect [Online]. Available: <https://www.wecc.biz/Reliability/WECCmodesPaper130113Trudnowski.pdf>
- [16] NERC, "Reliability guideline - forced oscillation monitoring & mitigation," 2017.
- [17] E. National Academies of Sciences and Medicine, *Enhancing the Resilience of the Nation's Electricity System*. National Academies Press, 2017.
- [18] P. Simulator, "PowerWorld Corporation," ed: October, 2005.

- [19] P. NASPI, "PMU Data Quality: A Framework for the Attributes of PMU Data Quality and Quality Impacts to Synchrophasor Applications," 2017.
- [20] I. Idehen, Z. Mao, and T. Overbye, "An emulation environment for prototyping PMU data errors," in *2016 North American Power Symposium (NAPS)*, 2016, pp. 1-6.
- [21] Q. F. Zhang and V. M. Venkatasubramanian, "Synchrophasor time skew: Formulation, detection and correction," in *2014 North American Power Symposium (NAPS)*, 2014, pp. 1-6.
- [22] "IEEE Standard for Synchrophasor Data Transfer for Power Systems," *IEEE Std C37.118.2-2011 (Revision of IEEE Std C37.118-2005)*, pp. 1-53, 2011.
- [23] A. B. Birchfield, T. Xu, and T. J. Overbye, "Power Flow Convergence and Reactive Power Planning in the Creation of Large Synthetic Grids," *IEEE Transactions on Power Systems*, pp. 1-1, 2018.
- [24] Z. Wang, A. Scaglione, and R. J. Thomas, "Generating Statistically Correct Random Topologies for Testing Smart Grid Communication and Control Networks," *IEEE Transactions on Smart Grid*, vol. 1, no. 1, pp. 28-39, 2010.
- [25] E. Cotilla-Sanchez, P. D. H. Hines, C. Barrows, and S. Blumsack, "Comparing the Topological and Electrical Structure of the North American Electric Power Infrastructure," *IEEE Systems Journal*, vol. 6, no. 4, pp. 616-626, 2012.
- [26] G. A. Pagani and M. Aiello, "The power grid as a complex network: a survey," *Physica A: Statistical Mechanics and its Applications*, vol. 392, no. 11, pp. 2688-2700, 2013.
- [27] ECEN. Electric Grid Test Case Repository [Online]. Available: <https://electricgrids.engr.tamu.edu/electric-grid-test-cases/>
- [28] M. Wu and L. Xie, "Online Detection of Low-Quality Synchrophasor Measurements: A Data-Driven Approach," *IEEE Transactions on Power Systems*, vol. 32, no. 4, pp. 2817-2827, 2017.
- [29] I. Idehen and T. Overbye, "A similarity-based PMU error detection technique," in *2017 19th International Conference on Intelligent System Application to Power Systems (ISAP)*, 2017, pp. 1-6.
- [30] M. M. Breunig, H.-P. Kriegel, R. T. Ng, and J. Sander, "LOF: identifying density-based local outliers," in *ACM sigmod record*, 2000, vol. 29, no. 2, pp. 93-104: ACM.
- [31] J. Shlens, "A tutorial on principal component analysis," *arXiv preprint arXiv:1404.1100*, 2014.
- [32] J. MacQueen, "Some methods for classification and analysis of multivariate observations," in *Proceedings of the fifth Berkeley symposium on mathematical statistics and probability*, 1967, vol. 1, no. 14, pp. 281-297: Oakland, CA, USA.
- [33] F. Belmudes, D. Ernst, and L. Wehenkel, "Pseudo-Geographical Representations of Power System Buses by Multidimensional Scaling," in *2009 15th International Conference on Intelligent System Applications to Power Systems*, 2009, pp. 1-6.
- [34] P. Cuffe and A. Keane, "Visualizing the Electrical Structure of Power Systems," *IEEE Systems Journal*, vol. 11, no. 3, pp. 1810-1821, 2017.
- [35] C.-h. Chen, W. K. Härdle, and A. Unwin, *Handbook of data visualization*. Springer Science & Business Media, 2007.
- [36] Togerson's Classical MDS Derivation [Online]. Available: <http://forrest.psych.unc.edu/teaching/p230/Torgerson.pdf>

- [37] S.-S. Choi, S.-H. Cha, and C. C. Tappert, "A survey of binary similarity and distance measures," *Journal of Systemics, Cybernetics and Informatics*, vol. 8, no. 1, pp. 43-48, 2010.
- [38] NERC. 1996 System Disturbances [Online]. Available: <https://www.nerc.com/pa/rrm/ea/System%20Disturbance%20Reports%20DL/1996SystemDisturbance.pdf>
- [39] J. F. Hauer, "Application of Prony analysis to the determination of modal content and equivalent models for measured power system response," *IEEE Transactions on Power Systems*, vol. 6, no. 3, pp. 1062-1068, 1991.
- [40] Y. Hua and T. K. Sarkar, "Matrix pencil method for estimating parameters of exponentially damped/undamped sinusoids in noise," *IEEE Transactions on Acoustics, Speech, and Signal Processing*, vol. 38, no. 5, pp. 814-824, 1990.
- [41] L. L. Grant and M. L. Crow, "Comparison of Matrix Pencil and Prony methods for power system modal analysis of noisy signals," in *2011 North American Power Symposium*, 2011, pp. 1-7.
- [42] A. R. Borden and B. C. Lesieutre, "Variable Projection Method for Power System Modal Identification," *IEEE Transactions on Power Systems*, vol. 29, no. 6, pp. 2613-2620, 2014.
- [43] S. Mohapatra and T. J. Overbye, "Fast modal identification, monitoring, and visualization for large-scale power systems using Dynamic Mode Decomposition," in *2016 Power Systems Computation Conference (PSCC)*, 2016, pp. 1-7.
- [44] A. B. Birchfield and T. J. Overbye, "Convergence characteristics of the variable projection method for mode extraction," in *2017 IEEE Texas Power and Energy Conference (TPEC)*, 2017, pp. 1-6.
- [45] R. A. Becker, S. G. Eick, and A. R. Wilks, "Visualizing network data," *IEEE Transactions on Visualization and Computer Graphics*, vol. 1, no. 1, pp. 16-28, 1995.
- [46] M. J. Laufenberg, "Visualization approaches integrating real-time market data," in *IEEE PES Power Systems Conference and Exposition, 2004.*, 2004, pp. 1550-1555 vol.3.
- [47] S. Yan and T. J. Overbye, "Visualizations for power system contingency analysis data," *IEEE Transactions on Power Systems*, vol. 19, no. 4, pp. 1859-1866, 2004.
- [48] Y. Zhang *et al.*, "Visualization of wide area measurement information from the FNET system," in *2011 IEEE Power and Energy Society General Meeting*, 2011, pp. 1-8.
- [49] J. N. Bank, O. A. Omitaomu, S. J. Fernandez, and Y. Liu, "Extraction and visualization of power system interarea oscillatory modes," in *IEEE PES General Meeting*, 2010, pp. 1-7.
- [50] C. Ware, *Information visualization: perception for design*. Elsevier, 2012.
- [51] E. R. Tufte, *Envisioning information*. Graphics Press, 1990.
- [52] T. J. Overbye, E. M. Rantanen, and S. Judd, "Electric power control center visualization using Geographic Data Views," in *2007 iREP Symposium - Bulk Power System Dynamics and Control - VII. Revitalizing Operational Reliability*, 2007, pp. 1-8.
- [53] R. M. Gardner, G. B. Jordan, and Y. Liu, "Wide-Area mode visualization strategy based on FNET measurements," in *2009 IEEE Power & Energy Society General Meeting*, 2009, pp. 1-6.
- [54] D. Weiskopf, *Vector Field Visualization*. Springer, 2007.
- [55] D. H. Laidlaw *et al.*, "Comparing 2D vector field visualization methods: a user study," *IEEE Transactions on Visualization and Computer Graphics*, vol. 11, no. 1, pp. 59-70, 2005.

- [56] L. Chen, Y. Min, and W. Hu, "An energy-based method for location of power system oscillation source," *IEEE Transactions on Power Systems*, vol. 28, no. 2, pp. 828-836, 2013.
- [57] S. Maslennikov, B. Wang, and E. Litvinov, "Locating the source of sustained oscillations by using PMU measurements," in *2017 IEEE Power & Energy Society General Meeting*, 2017, pp. 1-5.